

**MECHANISTIC STUDY AND LIGAND OPTIMIZATION OF THE
COPPER(I)-CATALYZED AZIDE-ALKYNE CYCLOADDITION
(CUAAC) REACTION**

A Dissertation Presented to
the Faculty of the Department of Chemistry
University of Houston

In Partial Fulfillment
of the Requirements for the Degree
Doctor of Philosophy

By

Haoqing Chen

December 2016

**MECHANISTIC STUDY AND LIGAND OPTIMIZATION OF THE
COPPER(I)-CATALYZED AZIDE-ALKYNE CYCLOADDITION
(CUAAC) REACTION**

Haoqing Chen

APPROVED:

Dr. Chengzhi Cai, Chairman

Dr. Olafs Daugulis

Dr. Randolph Thummel

Dr. Vassiliy Lubchenko

Dr. Yuhong Wang

**Dean, College of Natural Science and
Mathematics**

ACKNOWLEDGEMENT

First, I want to express my appreciation and gratitude to my advisor Dr. Chengzhi Cai. He offered me the opportunity for studying abroad. In the past years, he spent a lot of time, energy and patience in guiding me to be a junior investigator in chemistry. He is a hard-working, optimistic, confident, and good-tempered person. I would like to follow his example in the future.

I want to thank Dr. Olafs Daugulis, Dr. Randolph Thummel, Dr. Vassiliy Lubchenko and Dr. Yuhong Wang for being my committee members. They are excellent teachers who imparted their knowledge of chemical and biological sciences to me. I appreciate their time and attention devoted to my study and research projects.

I'd like to thank my group members, especially Dr. Siheng Li, Zhiling Zhu, Bin Yang, Fei Yu, Yongkai Huang, Yuyu Long, and Srujana Lam. They gave me a memorable time in Dr. Cai's lab. My appreciation also goes to all the faculty, staff and students in the Department of Chemistry.

Last but not least, I'd like to say thank you to my family members, especially my parents and my husband Yong, they are great person who guided me in the right way with their love and support.

**MECHANISTIC STUDY AND LIGAND OPTIMIZATION OF THE
COPPER(I)-CATALYZED AZIDE-ALKYNE CYCLOADDITION
(CUAAC) REACTION**

An Abstract of Dissertation Presented to
the Faculty of the Department of Chemistry
University of Houston

In Partial Fulfillment
of the Requirements for the Degree
Doctor of Philosophy

By

Haoqing Chen

December 2016

ABSTRACT

The copper(I)-catalyzed azide-alkyne cycloaddition (CuAAC) reaction is a prime example of “click reaction” that has been widely applied in diverse fields. The mechanism of this reaction has been proposed involving di-copper complexes as the kinetically favored active species, which are difficult to detect due to the multiple fast equilibria between the copper complexes and the instability of copper(I) to disproportionation and aggregation.

We first investigated the intermediates in CuAAC reaction with the widely used tris(triazolylmethyl)amine ligand. Using electrospray ionization mass spectrometry (ESI-MS), we detected unprecedented tri-copper(I) acetylide and triazolide intermediates. By linking an alkyne with the ligand, we enriched the di- and tri-copper(I) acetylides in aqueous solutions, and quantitatively analyzed the reactivity under stoichiometric and catalytic conditions. The di-copper(I) reaction mechanism was energetically preferred under stoichiometric conditions, while the tri-copper(I) intermediates are more stable and the reaction can go through both pathways under catalytic conditions. We obtained the single crystal X-ray diffraction structure of the tri-copper(I) acetylide intermediate bearing one tris(triazolylmethyl)amine ligand, which displayed high catalytic activity in CuAAC reaction.

Based on the ESI-MS results and the crystal structure, we proposed the tri-copper(I) CuAAC reaction mechanism. Under stoichiometric condition, the tri-copper(I) acetylide directly coordinates with azide and generates an azide-acetylide adduct to form the triazole ring. Under catalytic condition, the reaction could involve an internal copper(I)

dissociation from the acetylide to reduce the steric hindrance. The activation energy of the proposed di-copper(I) pathway was calculated 2 kcal/mol lower than the tri-copper(I) pathway.

To study the ligand effect on the oxidative side reaction of CuAAC that caused significant damage to biomolecules, we synthesized a series of tripodal amine ligands bearing triazole or phenyl substitution groups, which can coordinate to copper(I) with five- or six-membered chelating arm length. The best copper(I) ligand in CuAAC reaction were screened.

In addition, we designed a platform for high throughput screening of copper(I) catalyst exhibiting high CuAAC activity and high stability. The lead catalyst first generating the product upon addition of a low concentration of azide to the library can be identified by ESI-MS. The feasibility of this approach was studied using the tris(triazolylmethyl)amine ligand.

TABLE OF CONTENTS

Chapter 1 Literature Review	1
1.1 Introduction to CuAAC Reaction	1
1.1.1 Discovery	1
1.1.2 Applications of CuAAC Reaction.....	2
1.1.3 Reagents and Catalysts: Properties and Side Reactions.....	3
1.1.3.1 Terminal Alkynes.....	3
1.1.3.2 Organic Azides.....	4
1.1.3.3 Copper(I).....	4
1.2 Mechanistic Studies on CuAAC Reaction	5
1.2.1 Early Mechanistic Studies: the “Mono-copper” Catalytic Cycle.....	5
1.2.2 The “Di-copper” Model	6
1.2.3 Reaction Orders in Reagents and Catalysts by Initial Rate Studies	7
1.2.3.1 Azide	7
1.2.3.2 Alkyne.....	7
1.2.3.3 Copper(I) and Copper(I) Complexes	8
1.2.4 Theoretically Optimized Intermediate Structures and Activation Barriers.....	9
1.2.5 Structure of Isolated Intermediates	11
1.2.5.1 Copper(I) Acetylides.....	11
1.2.5.2 Copper(I) Triazolides.....	14
1.2.6 Real-time Monitoring of Reaction Process	15
1.2.6.1 Detection of Reactive Intermediates during CuAAC Reaction by Mass Spectrometry	15
1.2.6.2 Experimental Proof of Stepwise Mechanism by Time-resolved Online ATR-FTIR	16
1.2.7 Direct Evidence of Di-copper(I) Mechanism from Isotopic Crossover Studies	17
1.2.8 Factors Influencing Reaction Rate	18
1.2.8.1 Solvent Effects	18
1.2.8.2 The Structure of Reagents.....	19
1.2.8.3 Counteranions	21
1.2.8.4 Ancillary ligands	22
1.3 Ancillary Ligands in CuAAC Reaction	22
1.3.1 Common Ligands Employed in CuAAC Reaction	22

1.3.1.1	Nitrogen Donors.....	22
1.3.1.2	Carbon Donors	24
1.3.1.3	Heavier Atom Donors	25
1.3.1.4	Polymeric Ligands	26
1.3.2	The Nature of Bonding in Copper(I) Acetylide Complexes	26
1.3.2.1	Cuprophilic Interactions.....	26
1.3.2.2	Copper(I)-alkyne and Copper(I)-acetylide Interactions.....	27
1.3.3	The Nature of Bonding in Key Ancillary Ligands in CuAAC Reaction	28
1.3.3.1	Phosphine Ligands	28
1.3.3.2	Unsaturated Nitrogen Donors	29
1.3.3.3	N-heterocyclic carbene (NHC)	30
1.3.4	Ligands Preventing Copper(I) from Oxidation	30
1.3.4.1	Mechanism of Copper(I) Oxidation.....	30
1.3.4.2	Ligand Effect on Copper-dioxygen Reactivity	31
Chapter 2 Hypothesis and Specific Aims		34
2.1	Overall Goal and Hypothesis	34
2.2	Specific Aims.....	35
2.2.1	Aim 1	35
2.2.2	Aim 2	35
Chapter 3 Mechanistic Investigations on Tris(triazolylmethyl)amine Ligand-accelerated CuAAC Reaction in Aqueous Solutions.....		37
3.1	Introduction.....	37
3.1.1	Tris(triazolylmethyl)amine Ligands: Activity and Applications	37
3.1.2	Previous Mechanistic Investigations on Tris(triazolylmethyl)amine Ligands.....	38
3.1.3	Electron Spray Ionization Mass Spectrometry for Detection of Reaction Intermediates.....	39
3.2	Mechanistic Studies in Aqueous Solutions under Stoichiometric Condition	40
3.2.1	Ligand Design.....	40
3.2.2	Intermediate Detection and Characterization.....	41
3.2.2.1	Visible Comparison of copper(I) Chelating Ability of Ligand 1 and TL	41
3.2.2.2	Ligand 1 -copper(I) Complexes Solution Equilibria.....	43
3.2.2.3	Monitoring the Reaction Between the Ligand 1 -copper(I) Complexes and Azide	52

3.2.3	Quantitative Analysis of CuAAC Reactivity of Di-copper(I) and Tri-copper(I) Acetylide	62
3.3	Mechanistic Studies in Aqueous Solutions under Catalytic Condition.....	66
3.3.1	Ligand Design.....	66
3.3.2	Intermediate Detection and Characterization.....	66
3.3.2.1	Copper(I)-acetylide Complexes Solution Equilibria.....	66
3.3.2.2	Intermediate Detection in the Reaction Between the 3 -copper(I) Complexes and Azide	68
3.3.3	Quantitative Analysis of CuAAC Reactivity of Di-copper(I) and Tri-copper(I) Acetylide Under Catalytic Condition.....	69
3.4	Comparison of Copper(I)-Chelating Ability of Tris-, Bis-, and Mono-(triazolylmethyl)amine Ligands in Aqueous Solutions.....	74
3.5	Conclusions.....	76
3.6	Experimental Section	77
3.6.1	General Methods	77
3.6.2	Supplementary Figures	78
3.6.3	UV-Vis Spectra of 1 -copper(I) Complexes at Various Cu/ 1 Ratio.....	85
3.6.4	Experimental Details.....	86
3.6.4.1	Visible Comparison of copper(I) Chelating Ability of Ligand 1 and TL (Figure 3-1)	86
3.6.4.2	ESI-MS Spectra of TL -Cu _n Complexes in Deoxygenated Water (Figure 3-2). 86	
3.6.4.3	ESI-MS analysis for intermediate solution equilibria in Cu ^I 1 solutions w/ or w/o N ₃ EG ₄ (Figure 3-3 & Figure 3-14).....	86
3.6.4.4	NMR Spectra of Cu/ 1 1:1 – 3:1 Mixtures in Deoxygenated D ₂ O (Figure 3-6) .87	
3.6.4.5	Kinetic studies for reaction between 1 and N ₃ EG ₄ (Figure 3-16).....	88
3.6.4.6	Kinetic studies for reaction between 1 and 2-azidoethanol (Figure 3-17).....	89
3.6.4.7	ESI-MS analysis for intermediate solution equilibria in Cu ^I 3 solutions (Figure 3-18A, Figure 3-21)	90
3.6.4.8	Kinetic studies for reaction between 3 and N ₃ EG ₄ with various amount of copper(I) (Figure 3-18B).....	90
3.6.4.9	Kinetic studies for reaction between 3 and N ₃ EG ₄ with catalytic amount of copper(I) (Figure 3-22)	91
3.6.4.10	Intermediate detection for reaction between 3 and N ₃ EG ₄ at 3 /Cu 10:6 (Figure 3-19)	92
3.6.5	Calculations.....	93
3.6.5.1	Second-order rate constants <i>k</i> _{obs} (Figure 3-16B).....	93

3.6.5.2	Second-order rate constants k_{obs} (Figure 3-17).....	93
3.6.5.3	Calculation of k_{obs} of reaction between 3 and N_3EG_4	93
3.6.6	Synthetic Procedure and Compound Characterizations	95
Chapter 4	Mechanistic Investigations on Tris(triazolymethyl)amine Ligand-accelerated CuAAC Reaction in Organic Solvents	105
4.1	Introduction.....	105
4.2	Isolation of Tri-copper(I) Acetylide Complex Bearing Tris(triazolymethyl)amine Ligand	106
4.2.1	Ligand Design and Single Crystal Growth	106
4.2.2	Characterization of Single Crystal of Tri-copper(I) Acetylide Complex 4-1 : X-ray Structure, ESI-MS, NMR and FT-IR Spectra.....	109
4.3	Activity Studies.....	116
4.3.1	CuAAC Reaction in Nitrogen Atmosphere	116
4.3.2	Reaction in Air	118
4.4	Mechanism Proposal.....	119
4.5	Conclusions.....	121
4.6	Experimental Section	121
4.6.1	General Methods	121
4.6.2	Experimental Details.....	121
4.6.2.1	Synthesis of Complex 4-1	121
4.6.2.2	NMR Spectroscopy of Complex 4-1	122
4.6.2.3	Elemental Analysis of Complex 4-1	125
4.6.2.4	UV-Vis Spectrum of Complex 4-1	126
4.6.2.5	Single Crystal X-ray Diffraction Analysis of Complex 4-1	127
4.6.2.6	ESI-MS Spectra of CuAAC Intermediates between Complex 4-1 and Benzyl Azide	127
4.6.2.7	Comparison of Reaction Yield in Anaerobic Chamber	128
4.6.2.8	Comparison of Reaction Yield in Air	128
4.6.3	Crystal Data for Complex $[\text{Cu}_6(\text{TATA})_2(\mu_3\text{-}\eta^1, \eta^1, \eta^2\text{-C}\equiv\text{CR})_2]^{4+}$	130
4.6.4	Compound Synthesis Procedure	133
Chapter 5	DFT Calculations on Tri-copper(I) and Di-copper(I) CuAAC Reaction Pathways	138
5.1	Introduction.....	138
5.2	Results and Discussion	139

5.2.1	Geometric Optimization and Energy Calculations of Intermediates in Di-Copper(I) and Tri-Copper(I) Reaction Pathways	139
5.2.2	Optimization of Crystal Structure for Orbital Explanation.....	140
5.3	Conclusions.....	142
5.4	Experimental Section.....	142
5.4.1	The Gas- and Solution-phase Energetics for the Reaction of Di-Cu / Tri-Cu Propynide with Methyl Azide.....	142
Chapter 6 Study of the Ligand Effects on CuAAC Reactivity and Antioxidation Ability		143
6.1	Introduction.....	143
6.2	Results and Discussion	144
6.2.1	Ligand Design.....	144
6.2.2	Kinetic Studies on CuAAC Reaction.....	145
6.2.3	Inhibiting Effect of Excess Ligands.....	147
6.2.4	Oxidation Rate of Copper(I) Complexes bearing Anti-oxidation Ligands	150
6.3	Conclusions.....	151
6.4	Experimental Section.....	152
6.4.1	Experimental Details.....	152
6.4.1.1	General Procedure for Kinetic Studies for CuAAC Activity of Selected Ligands	152
6.4.1.2	Oxidation Rate of Copper(I) Complexes bearing Anti-oxidation Ligands	153
6.4.2	Supplementary Figures	153
6.4.3	Compound Synthesis Procedure	154
Chapter 7 Feasibility Study on a Mass-Spectrometry-Based Method for High-Throughput Screening of Ligands for CuAAC Reaction.....		165
7.1	Introduction.....	165
7.2	Reaction Condition Optimization and Reactor Design.....	166
7.2.1	Contamination Control.....	166
7.2.2	Purification and Concentration of Reaction Products.....	167
7.2.3	Oxygen Control.....	168
7.3	Method Validation using CuAAC Reaction of Ligand 1	169
7.4	Conclusions.....	171
7.5	Experimental Section.....	172
7.5.1	Preparation of Trace Metal Clean Reaction Containers.....	172
7.5.2	Preparation of Deoxygenated Water	172

7.5.3	ICP-MS Detection of Copper Concentration in Selected Solutions	172
7.5.4	Kinetic Studies for CuAAC Reaction of Ligand 1 at 10 nM Concentration.....	173
7.5.4.1	Rate Order in Copper(I)	173
7.5.4.2	Rate Order in Azide	174
7.5.4.3	Rate Order in Ascorbate.....	174
7.5.4.4	CuAAC Reaction in Alkyne 1 & Alkyne 7-1 Mixture	174
7.5.5	Synthesis Procedure and NMR Spectra	174
Chapter 8 Summary		176
References		180
Appendix A: NMR Spectra		191
Appendix B: Coordinates and Energies for Ground State and Transition State Geometries (in Chapter 5)		221

LIST OF FIGURES

Figure 1-1.....	13
Figure 3-1.....	41
Figure 3-2.....	42
Figure 3-3.....	44
Figure 3-4.....	45
Figure 3-5.....	47
Figure 3-6.....	48
Figure 3-7.....	50
Figure 3-8.....	52
Figure 3-9.....	53
Figure 3-10.....	54
Figure 3-11.....	55
Figure 3-12.....	56
Figure 3-13.....	58
Figure 3-14.....	59
Figure 3-15.....	62
Figure 3-16.....	64
Figure 3-17.....	65
Figure 3-18.....	67
Figure 3-19.....	69
Figure 3-20.....	70
Figure 3-21.....	72
Figure 3-22.....	73

Figure 3-23	75
Figure 3-24	75
Figure 3-25	78
Figure 3-26	79
Figure 3-27	82
Figure 3-28	83
Figure 3-29	84
Figure 3-30	85
Figure 4-1	106
Figure 4-2	109
Figure 4-3	110
Figure 4-4	112
Figure 4-5	113
Figure 4-6	114
Figure 4-7	115
Figure 4-8	116
Figure 4-9	117
Figure 4-10	118
Figure 4-11	123
Figure 4-12	124
Figure 4-13	125
Figure 4-14	126
Figure 5-1	141
Figure 6-1	146
Figure 6-2	149

Figure 6-3	150
Figure 6-4	151
Figure 6-5	153
Figure 7-1	167
Figure 7-2	168
Figure 7-3	171

LIST OF SCHEMES

Scheme 1-1	1
Scheme 1-2	6
Scheme 1-3	28
Scheme 1-4	31
Scheme 3-1	40
Scheme 3-2	46
Scheme 3-3	56
Scheme 3-4	57
Scheme 3-5	60
Scheme 3-6	63
Scheme 3-7	65
Scheme 3-8	68
Scheme 3-9	81
Scheme 4-1	108
Scheme 4-2	120
Scheme 5-1	140

Scheme 6-1	143
Scheme 7-1	165
Scheme 7-2	170

LIST OF TABLES

Table 3-1	63
Table 3-2	67
Table 3-3	71
Table 3-4	73
Table 4-1	131
Table 4-2	132
Table 4-3	132
Table 5-1	142
Table 5-2	142

LIST OF CHARTS

Chart 1-1	8
Chart 1-2	25
Chart 1-3	31
Chart 1-4	33
Chart 3-1	74
Chart 4-1	107
Chart 5-1	141
Chart 6-1	144

LIST OF ABBREVIATIONS

ATR-FTIR	Attenuated total reflection Fourier transform infrared spectroscopy
(Bim) ₃	Tris(2-benzimidazolylmethyl)amine
(Bim)(Py) ₂	Mono(benzimidazole)-bis(pyridine)
BTMSA	Bis(trimethylsilyl)acetylene
BTAA	2-[4-((Bis[(1-tert-butyl-1H-1,2,3-triazol-4-yl)methyl]amino)methyl)-1H-1,2,3-triazol-1-yl]acetic acid
BTES	2-[4-((Bis[(1-tert-butyl-1H-1,2,3-triazol-4-yl)methyl]amino)-methyl)-1H-1,2,3-triazol-1-yl]ethyl hydrogen sulfate
BTTP	3-[4-((Bis[(1-tert-butyl-1H-1,2,3-triazol-4-yl)methyl]amino)methyl)-1H-1,2,3-triazol-1-yl]propanol
BTTPS	3-[4-((Bis[(1-tert-butyl-1H-1,2,3-triazol-4-yl)methyl]amino)methyl)-1H-1,2,3-triazol-1-yl]propyl hydrogen sulfate
CAAC	Cyclic (alkyl)(amino) carbene
CID	Collision induced dissociation
CuAAC	Copper(I)-catalyzed azide-alkyne cycloaddition
DFT	Density functional theory
DIPEA	N,N-Diisopropylethylamine
DMF	Dimethylformamide
DMSO	Dimethylsulfoxide
DNA	Deoxyribonucleic acid
Dppm	1,1-Bis(diphenylphosphino)methane (Ph ₂ PCH ₂ PPh ₂)
DTPA	Diethylenetriaminepentaacetic acid
<i>E.coli</i>	<i>Escherichia coli</i>
ESI	Electrospray ionization
HPLC	High performance liquid chromatography
HRMS	High-resolution mass spectrometry
ICP-MS	Inductively coupled plasma mass spectrometry
KIE	Kinetic isotopic effect
LDPE	Low-density polyethylene
MS/MS	Tandem mass spectrometry

m/z	Mass-to-charge ratio
NA	5,7-Dimethyl-1,8-naphthyridin-2-amine
NAN	Bis(5,7-dimethyl-1,8-naphthyridin-2-yl)amine
NBO	Natural bond orbital
NHC	N-heterocyclic carbene
NMP	N-Methyl-2-pyrrolidone
NMR	Nuclear magnetic resonance
PBS	Phosphate-buffered saline
PE	Polyethylene
PMDETA	<i>N,N,N',N',N''</i> -Pentamethyldiethylenetriamine
PP	Polypropylene
PTFE	Polytetrafluoroethylene
RNA	Ribonucleic acid
ROS	Reactive oxygen species
TATA	Tris[(1-adamantyl-1 <i>H</i> -1,2,3-triazol-4-yl)methyl] amine
TBTA	Tris((1-benzyl-1 <i>H</i> -1,2,3-triazol-4-yl)methyl)amine
TEPA	Tris[2-(2-pyridyl)ethyl]amine
THF	Tetrahydrofuran
THPTA	Tris[(1-hydroxypropyl-1 <i>H</i> -1,2,3-triazol-4-yl)methyl]amine
TL	Tris(triazolylmethyl)amine ligand
TMPA	Tris[(2-pyridyl)methyl]amine
Tren	Tris(2-aminoethyl)amine
UV-Vis	Ultraviolet–visible spectroscopy

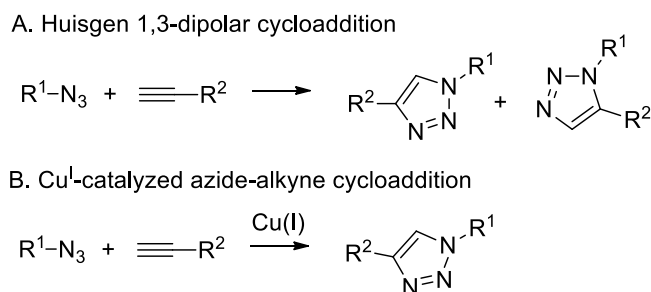
Chapter 1 Literature Review

1.1 Introduction to CuAAC Reaction

1.1.1 Discovery

The Thermal Reaction

The 1,3-dipolar cycloaddition reactions between a 1,3-dipole and a dipolarophile to form a five-membered ring, such as an organic azides and an alkyne to form a 1,2,3-triazole, were first termed by Rolf Huisgen in the 1960s.¹⁻² They are generally referred as the “Huisgen cycloaddition”. The thermal Huisgen reaction for azide-alkyne cycloaddition is highly exothermic but exhibiting high activation barrier that requires elevated temperature to proceed. In addition, the reaction is not regioselective and statistically produces a mixture of 1,4 and 1,5 disubstituted 1,2,3-triazoles (Scheme 1-1A).³



Scheme 1-1 The Huisgen cycloaddition and the copper(I)-catalyzed azide-alkyne cycloaddition

The Copper(I)-Catalyzed Azide-alkyne Cycloaddition Reaction

In 1984, L'abbé discovered the catalytic effect of copper(I) in Huisgen cycloaddition that allowed the reaction to proceed at a low temperature with a low reaction yield.⁴ After almost twenty years, the Meldal⁵ and Sharpless⁶ groups independently reported the copper(I)-catalyzed azide-alkyne

cycloaddition (CuAAC) reactions. The former group employed copper(I) iodide in organic solvents for solid phase synthesis of peptidotriazoles, and the latter group conducted the reaction in aqueous solutions using *in situ* reduced copper(I) salts as homogeneous catalysts. The main advantages of the copper(I)-catalyzed reaction are the high yield and regioselectivity that exclusively produces the 1,4-disubstituted 1,2,3-triazoles with little by-products, the mild reaction condition, and the reaction's high compatibility with most functional groups such as ester, ether, amide and thioether. The reactions featuring these unique properties were given the term "Click Chemistry" by Sharpless⁷, which also includes the Diels-Alder addition, nitrile oxide cycloaddition, tetrazole cycloaddition, thiol-click reaction (thiol-ene, thiol-yne, thiol-isocyanate additions), non-Aldol carbonyl reactions (hydrazone/oxime ether formation, amide/isourea formation), and other 1,3-dipolar cycloadditions (metal-catalyzed azide-alkyne cycloadditions, strain promoted 1,3-dipolar cycloadditions).⁸⁻¹⁰

1.1.2 Applications of CuAAC Reaction

The excellent stability of the 1,4-disubstituted 1,2,3-triazole product under acid/basic and reductive/oxidative conditions makes it an ideal linkage in organic synthesis. In biological system, the triazole moiety is resistant to metabolic degradation and acts as a potential mimic of the Z-amide bond in peptide.¹¹ Besides, the large dipole moment of this heterocycle gives it good activity in supramolecular interactions particularly in hydrogen bonding and metal coordination.¹² Therefore, the CuAAC reaction has become a powerful synthetic tool in many fields,¹³ such as drug discovery, bioconjugation and materials science.

The CuAAC reaction has been used for generating triazole scaffolds in biologically active compounds such as antimicrobial drugs and enzyme inhibitors.¹⁰⁻¹¹ These drug candidates were mainly obtained through high-throughput screening and fragment-based drug discovery.¹⁴

Chemical reactions that are orthogonal to the functional groups in biological systems are required for modification and labeling of specific biomolecules to elucidate the complex biological processes in living system.¹⁵ Regardless of the oxidative side reaction and the toxicity issue of copper catalyst, CuAAC reaction is an ideal tool for bioorthogonal applications since the alkynes and azides are rare in nature, and they are relatively easy to be incorporated to biomolecules.¹⁶ The reaction has now been employed in a wide range of biomolecules, including peptides,¹⁷⁻¹⁸ proteins,¹⁹ glycans,²⁰⁻²² lipids, DNAs²³ and RNAs.¹⁴

The CuAAC reaction has also been extensively employed in synthesis and modification of polymer and nanoparticle; surface modification, patterning, and lithography; and responsive materials self-assembly.^{8, 24}

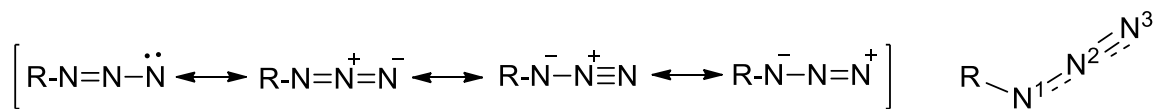
1.1.3 Reagents and Catalysts: Properties and Side Reactions

Three essential components are required for CuAAC reaction: the terminal alkyne, organic azide, and the copper(I) catalyst.

1.1.3.1 Terminal Alkynes

Terminal alkynes are more acidic than alkenes and alkanes with a pK_a values of around 25 for methylacetylene. The π -coordination of a copper(I) decreases the pK_a of the terminal alkyne by ~9.8 units, giving sufficient acidity of the alkynyl proton to be removed by water as a weak base.²⁵ The Cu-catalyzed oxidative coupling of terminal alkynes (Eglinton variation of Glaser coupling)²⁶ is one of the major side reactions of CuAAC in absence of reducing agents, in which the terminal alkynes were oxidized by dioxygen catalyzed by the Cu(II)/Cu(I)/O₂ redox cycle to generate diacetylenes.²⁷ In many cases this reaction was used for *in situ* generation of copper(I) source.²⁸⁻³⁰

1.1.3.2 Organic Azides



Organic azides can be stabilized by a series of resonance structures, among which the most stable structure calculated (shown on the right) bears three near-linear arranged nitrogens ($\angle \text{N}^1-\text{N}^2-\text{N}^3$ 172.5°) and a bent $\text{R}-\text{N}^1-\text{N}^2$ angle (115.2°), indicating a bond order of 2.5 between N^2 and N^3 and 1.5 between N^2 and N^1 .³¹ Natural Bond Orbital (NBO) analysis revealed three N^3-N orbitals with -0.05 charge on N^3 , and one N^1-N orbital with -0.54 charge on N^1 .³² Therefore, the organic azides can easily undergo reaction with electrophiles by the Lewis basic alkylated nitrogen (N^1) and with nucleophiles by the terminal nitrogen (N^3).³³

The Staudinger reaction is the major competing reaction in CuAAC when using phosphine ligand. The phosphine ligand can attack the electrophilic terminal nitrogen and form a linear phosphazide, which undergoes intramolecular rearrangement to generate intermediate aza-ylide that hydrolyzed by water to yield amine and phosphine oxide.³⁴

Organic azides are thermally decomposable and explosive substances that release N_2 upon heating, external impact or pressure, especially when the number of carbon is less than that of nitrogen atoms.

1.1.3.3 Copper(I)

A number of protocols for generating the copper(I) oxidation state have been developed, including the direct use of copper(I) salts in organic solvents,⁵ preformed copper(I)-complexes³⁵ and polymeric structures,³⁶ copper(0) metals and nanoclusters,³⁷⁻³⁸ and the by far most frequently used *in situ* generation of copper(I) by reducing copper(II) (CuSO_4 or $\text{Cu}(\text{OAc})_2$) with a

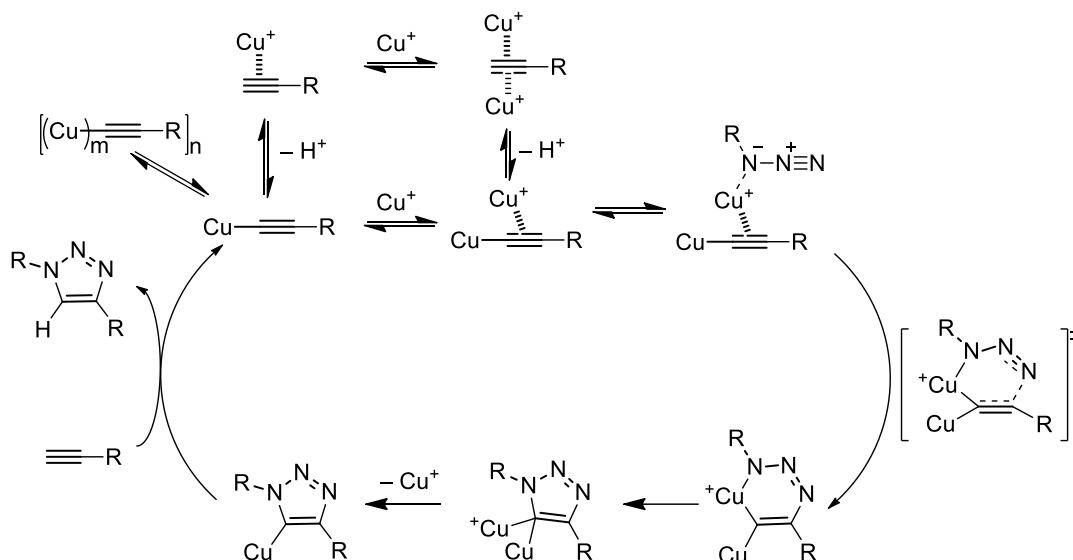
sacrificial reducing agent (*e.g.*, sodium ascorbate), which was first introduced by the Sharpless and Fokin group.^{6, 39} Maintaining the copper(I) oxidation state in air and aqueous solutions is challenging, due to the high sensitivity of cuprous ion to oxygen and the propensity of copper(I) to disproportionate. The copper(I) catalyst can generate a series of off-cycle inactive species including copper(II) (by oxidation), copper(0) (by disproportionation), and multi-copper aggregates. Ancillary ligands have been developed to stabilize the copper(I) catalyst in active form.

1.2 Mechanistic Studies on CuAAC Reaction

1.2.1 Early Mechanistic Studies: the “Mono-copper” Catalytic Cycle

The mechanism of CuAAC reaction was first proposed by the Fokin group in 2004 from a Density Functional Theory (DFT) calculation comparing the thermal and copper(I)-catalyzed azide-alkyne cycloaddition.²⁵ The thermal reaction is a concerted process. Activation energies (≈ 26 kcal/mol) are similar for forming 1,4- and 1,5-regioisomers of 1,2,3- triazole. The copper(I)-catalyzed cycloaddition was proposed as a stepwise process, starting from the formation of mono-copper azide-acetylide precursor complex (-2.0 kcal/mol), followed by the connection of the first N–C bond in the 1,4-disubstituted triazole, generating a six-membered copper(III) metallacycle intermediate that undergoes exergonic ring contraction, reductively eliminating the copper through a low activation barrier (3.2 kcal/mol). The first N–C bond formation step has an activation energy of 18.7 kcal/mol, which is 7 kcal/mol lower than the thermal reaction, in agreement with the 7-to-8-orders-of-magnitude rate acceleration in the copper(I)-catalyzed process.

1.2.2 The “Di-copper” Model



Scheme 1-2 General di-copper catalytic cycle in CuAAC reaction

In the general scheme, the overall rate of a stepwise reaction is determined by the rate of the slowest step rather than the sum of velocity of each elementary steps. Regardless of the influence of product during the initial stage, the rate order of reaction (the relationship between the reaction rate and concentration) with respect to reagents and catalysts is determined by the molecularities of active species in the rate-limiting step(s).

The rate-limiting step for converting alkyne and azide to triazole was first experimentally investigated by Rodionov *et al.* who studied the reaction kinetics without ancillary ligands.⁴⁰ With *in situ* generated copper(I) (from CuSO_4 and sodium ascorbate) in 80% DMSO and 20% water, the reaction rate law is first order in azide, between first- and second-order in alkyne, and second-order in copper(I) (under catalytic condition with addition of trace amount of triazole ligand). A rational di-copper(I) catalytic cycle was proposed (Scheme 1-2) based on these findings and the mono-copper(I) model. The reaction goes through the deprotonation of alkyne to form di-copper

acetylide, generation of azide-alkyne-copper precursor complex, nucleophilic attack from the acetylide to the terminal nitrogen of azide that generates the metallacycle intermediate, and elimination of one copper to form a copper-triazolide, followed by protonation to yield the product and regenerate the Cu catalyst. The CuAAC reaction involving ancillary ligands was investigated in the later studies.

1.2.3 Reaction Orders in Reagents and Catalysts by Initial Rate Studies

1.2.3.1 Azide

The coordination of azide with copper(I) to form the azide-acetylide precursor complex is a fast process in some cases that reaches pre-equilibrium before the rate-limiting step(s). For example, when the reaction was performed in water⁴¹ or using a copper(I)-chelating azide,³⁰ a zero-order kinetics in azide was observed. However, the azide-coordination step can be rate-limiting in the presence of competing ligands (*e.g.*, PPh₃, Cl⁻), in which first-order rate dependence on the concentration of azide was observed.⁴¹⁻⁴²

1.2.3.2 Alkyne

In presence of strong-coordinating ancillary ligands or solvents that inhibit the alkyne-copper(I) binding, formation of the copper(I)-alkyne complex or the following deprotonation step turns to a rate-limiting step. Strong copper(I) ligands such as tris(2-benzimidazolylmethyl)amine ((**Bim**)₃, Chart 1-1) showed first order in alkyne in Tris buffer (containing Tris base and Cl⁻) and 0.6 order in water or KCl solution,⁴¹ and strong coordinating solvents such as acetonitrile turned the alkyne into second-order, indicating two alkyne molecules taking part in the rate-determining step.³⁰ Weakly coordinating ligands such as tris((1-benzyl-1H-1,2,3-triazol-4-yl)methyl)amine (**TBTA**, Chart 1-1) gave a negative order in alkyne in water,⁴¹ while weakly coordinating solvent chloroform turned the alkyne to zero order.⁴² These phenomena can be explained by the fast pre-

equilibrium between the excessive alkyne and copper(I)-acetylide, which was reached before the rate-limiting step in absence of a strong competing ligand. The extra alkyne may inhibit the azide-coordination that result in a negative order in alkyne concentration.

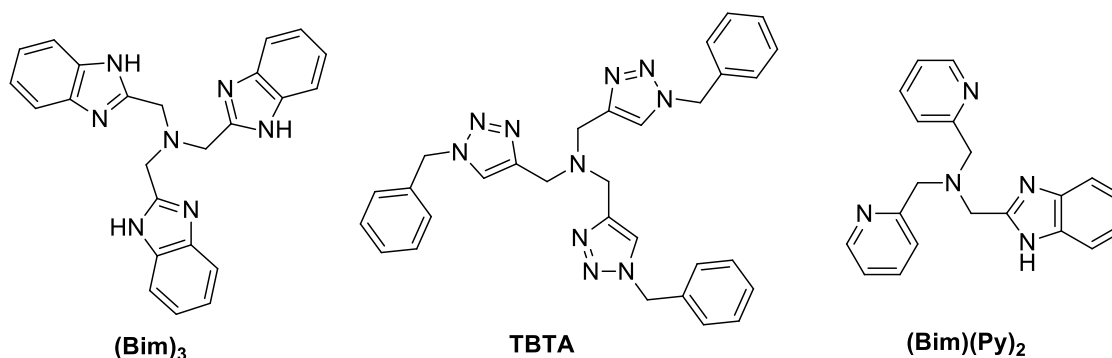


Chart 1-1 Structure of selected multi-dentate copper(I) ligands

1.2.3.3 Copper(I) and Copper(I) Complexes

A second-order dependence in copper(I) concentration was generally observed in solution containing highly diluted copper(I), *e.g.*, with $\text{Cu}(\text{OAc})_2$ at 0.2%–6% loadings in MeCN and MeOH.³⁰ However, the increase in Cu concentration can alter the rate order in copper(I). In the first kinetic studies performed by Rodionov *et al.*, the rate order in copper(I) dropped from 2.0 at low Cu loading to 0.6 at high Cu loading.⁴⁰ In chloroform using $(\text{PPh}_3)_2\text{Cu}(\text{OAc})$ as catalyst, the rate order was 1.7 at $[\text{Cu}]$ 0.003–0.009 mol%, 0.6 at $[\text{Cu}]$ 0.6–1.3 mol% and 0.2 at $[\text{Cu}]$ 3–13 mol%.⁴² The decreased rate order can be attributed to the increased aggregation of copper(I) species at higher concentrations, which generated a larger portion of catalytic inactive species that not participate in the catalytic cycle.

Coordinating strength of copper(I) ligands and solvents can also influence the rate orders in $[\text{Cu}]$. Coordinating solvents often resulted in higher order in copper(I) complexes, *e.g.*, 2.3 order in $[\text{Cu}((\text{Bim})_3)_2]$ in Tris buffer (w/ cat. $[\text{Cu}]$)⁴¹ and third order in $[\text{Cu}((\text{Bim})(\text{Py})_2)]$ ($(\text{Bim})(\text{Py})_2$:

mono(benzimidazole)-bis(pyridine), Chart 1-1) in 80% DMSO (w/ 0.1–1 equiv. Cu),⁴³ because the dissociation of Cu complex in these solvents made the reaction depend on both the molecularity of copper(I) and ligands in the complex ($R = k[\text{Cu}]^2[\text{L}]^1$). Stronger coordinating copper(I) ligands vs. solvents can generate intact active multi-copper(I) complexes during the reaction, resulting in kinetics of less than second-order, for example, first order in $[\text{Cu}(\text{Bim})(\text{Py})_2]$ or $[\text{Cu}_2(\text{Bim})(\text{Py})_2]$ in 90% H₂O (w/ 0.1–1 equiv. Cu),⁴³ first order in $[\text{Cu}(\text{TBTA})_2]$ in water (w/ cat. [Cu]),⁴¹ 1.3 order in $[\text{CuSO}_4]$ with “chelating” azide (*vide infra*),⁴⁴ and first order in $[\text{Cu}_2(\text{NAN})_2]$ (NAN: bis(5,7-dimethyl-1,8-naphthyridin-2-yl)amine) or 1.5 order in $[\text{Cu}_4(\text{NAN})_2(\text{NA})_2]$ (NA: 5,7-dimethyl-1,8-naphthyridin-2-amine) in THF (w/ cat. [Cu]).⁴⁵ If the ligand was insufficient to maintain a high level of active copper(I) species that controlled the overall reaction kinetics, fractional or near-zero orders could also be observed, for example negative order in $[\text{Cu}_2(\text{TBTA})]$, 0.1 order in $[\text{Cu}(\text{TBTA})]$, and 0.6 order in $[\text{Cu}(\text{TBTA})_2]$ in 90% H₂O in air (w/ 0.1–1 equiv. Cu).⁴³

1.2.4 Theoretically Optimized Intermediate Structures and Activation Barriers

After the realization of second-order rate dependence on [Cu], a number of computational calculations were performed to obtain the energies and properties of proposed intermediates and transition state structures. Despite the difference in calculation methods, almost all calculated energy barriers in the di-Cu pathway were lower than the mono-Cu pathway due to the ring strain of the mono-Cu alkenylidene structure.

The highest energy consuming step, the first N-C bond formation, was first compared in the two reaction pathways in water.⁴⁶ Participation of the second copper decreased the activation barrier to 12.9 or 10.5 kcal/mol (with acetylide or chloride as ligand, respectively), which was 5–7 kcal/mol lower than the mono-copper pathway. The optimized transition state included one Cu

linking the acetylide with the alkylated nitrogen of azide, while another Cu coordinated only to the acetylide.

The stepwise mechanism of the reaction was confirmed by topological evolution,⁴⁷ and the whole range of reaction was first investigated using a bridged tetra-nuclear μ -Cu-acetylide aggregate substrate.⁴⁸⁻⁵⁰ Generation of the azide-acetylide precursor complex was endothermic (7.4 kcal/mol in gas phase,⁴⁸ and 10.5 kcal/mol⁴⁹ or 8.5 kcal/mol⁵⁰ in water), and formation of the first N-C bond required activation barrier of 13.3 kcal/mol in gas phase,⁴⁸ and 18.5 kcal/mol⁴⁹ or 16.7 kcal/mol⁵⁰ in water, which is 8⁴⁸ to 8.6⁴⁹ kcal/mol lower than the barrier in mono-Cu pathway, and 17.5 kcal/mol lower than the thermal cycloaddition for both regioisomers.⁴⁹ Using an accelerating ligand phenanthroline, the transition state barrier further dropped by 2 kcal/mol, in accordance with the two folds of magnitude faster rate of ligand-accelerated reaction.⁴⁸ While using a σ -coordinated di-copper acetylide that was less stable than the tetra-nuclear μ -Cu-acetylide,⁵⁰ generation of the first N-C bond from azide-acetylide precursor complex required less energy (16.0 kcal/mol), which was 4.4 kcal/mol lower than generating the 1,5-isomer.⁴⁹

In aprotic solvent (CH_2Cl_2), the deprotonation of alkyne is endothermic (6.7 kcal/mol) and requires a high activation energy (11.1 kcal/mol) that was comparable to the formation of N-C bond (13.5 kcal/mol).⁴² The key di-copper acetylide intermediate was preferentially formed from mono-copper acetylide ($\Delta G^\ddagger = 11.1$ kcal/mol) instead of directly from alkyne ($\Delta G^\ddagger = 16.1$ kcal/mol). In gas phase the deprotonation of alkyne by a mono-copper complex $[\text{Cu}(\text{hexabenzyl})\text{tren}][\text{Br}]$ (**tren** = tris(2-aminoethyl)amine) also required a high energy barrier of 14.4 kcal/mol.⁵¹

To understand the possible pathway generating the isolated di-copper triazolide intermediate (Figure 1D, *vide infra*),⁵² an alternative pathway was proposed with a transition-state structure involving two coppers of completely different coordination environment.⁵³ One copper σ -

coordinated to the acetylide and interacted with the alkylated nitrogen of azide, while the other copper π -coordinated to the acetylide and bound to the terminal nitrogen of azide. However, this pathway was refuted by the remarkably high activation barrier (38.8 kcal/mol) calculated.

Natural Bond Orbital (NBO) calculations revealed the distribution of electron density in intermediates. Initially, the di-copper acetylide mostly adopted a $\mu_2, \eta^{1,2}$ coordination mode, but the coordination of azide with copper(I) weakened the π -interaction between copper(I) and acetylide, generating a more symmetric $\mu_2, \eta^{1,1}$ coordination mode.^{47, 53} Increased positive charge on copper(I) and negative charge on the alkylated nitrogen of azide was observed,⁵⁰ indicating back-donation of electrons from copper(I) to azide. Although topology investigation indicated electrophilic property of the alkylated carbon of acetylide,⁴⁷ NBO calculations showed large electron transfer interactions from the n orbital of terminal carbon to the n* orbital of alkylated carbon that finally donated to the π^* orbital of terminal nitrogen of azide for generating the first N–C bond.⁵³ The Cu(I)-ligand bond maintained ionic character throughout the reaction catalyzed by the mono-copper complex [Cu(hexabenzyl)tren][Br].⁵¹

1.2.5 Structure of Isolated Intermediates

Isolation of the proposed intermediates from the catalytic cycle can help understanding the coordination structure and comparing the reactivity of these active species.

1.2.5.1 *Copper(I) Acetylides*

Efforts have been made to isolate the key active species copper(I) acetylides in order to obtain their reactivity. Although the copper(I) acetylides have been extensively studied during the past two decades,⁵⁴⁻⁵⁶ the indiscriminate aggregation of copper(I) acetylides remains a major obstacle in preparing and isolating well-characterized low-nuclearity [C \equiv CCu(I)] compounds. The propensity of forming polymeric poorly-soluble aggregates was primarily attributed to the weak

metal-metal interactions between the d^{10} orbitals of monovalent copper(I).⁵⁷ In the absence of a bulky ligand, only highly aggregated Cu-acetylide clusters were isolated, such as the t-butyl acetylide-bridged Cu_{20} clusters,⁵⁷ the 1,1,1,5,5,5-hexafluoroacetylacetonate stabilized Cu_{10-26} clusters,⁵⁸⁻⁶⁰ and the 4-aminopyridinium stabilized Cu_9 cluster.⁶¹ Four types of coordination modes were observed in these clusters, including $\mu_2, \eta^{1,1}-(\text{C}\equiv\text{C})\rightarrow\text{Cu}_2$, $\mu_2, \eta^{1,2}-(\text{C}\equiv\text{C})\rightarrow\text{Cu}_2$, $\mu_3, \eta^{1,1,2}-(\text{C}\equiv\text{C})\rightarrow\text{Cu}_3$, and $\mu_4, \eta^{1,1,1,2}-(\text{C}\equiv\text{C})\rightarrow\text{Cu}_4$. The multi-copper coordination on each acetylide unit results in noticeable bending (up to 152°) and lengthening (up to 1.27 \AA) of the $\text{C}\equiv\text{C}$ bonds.

To reduce the nuclearity of copper(I)-acetylides, sterically encumbered ligands and remote bulky aromatic substituent(s) on the acetylide can be incorporated to “cap” the metal coordinating surfaces.^{58, 62} Many oligomeric or monomeric copper(I) acetylides have been successfully isolated. Tri-nuclear $\mu_3, \eta^1-\text{Cu}_3(\text{C}\equiv\text{CR})_{1-2}$ complexes⁶³⁻⁷⁰ and tetra-nuclear $\mu_4, \eta^{1,1,2,2}-\text{Cu}_2(\text{C}\equiv\text{C})\text{Cu}_2$ complex⁷¹ were synthesized using diphosphine ligands such as dppe ($\text{Ph}_2\text{PCH}_2\text{PPh}_2$). Tetra-nuclear $\mu_3-\text{Cu}_4(\text{C}\equiv\text{CR})_4$ open-cube complexes⁷²⁻⁷⁴ were synthesized using aromatic monophosphine ligands. The thiophenolate ligand bearing amine substituent can also bridge three copper(I) in $\mu_3, \eta^1-\text{Cu}_3\text{L}_2(\text{C}\equiv\text{CR})_2$ complexes.⁷⁵ A tetra-imino macrocyclic ligand encapsulates copper(I) in a unique tetra-copper mono-acetylide complex, in which the copper(I) adopts $\mu_4, \eta^{1,1,2,2}-(\text{C}\equiv\text{C})$ coordination mode, causing extensive elongation (1.38 \AA) and bending (145.7°) of the $\text{C}\equiv\text{C}$ bond.⁷⁶

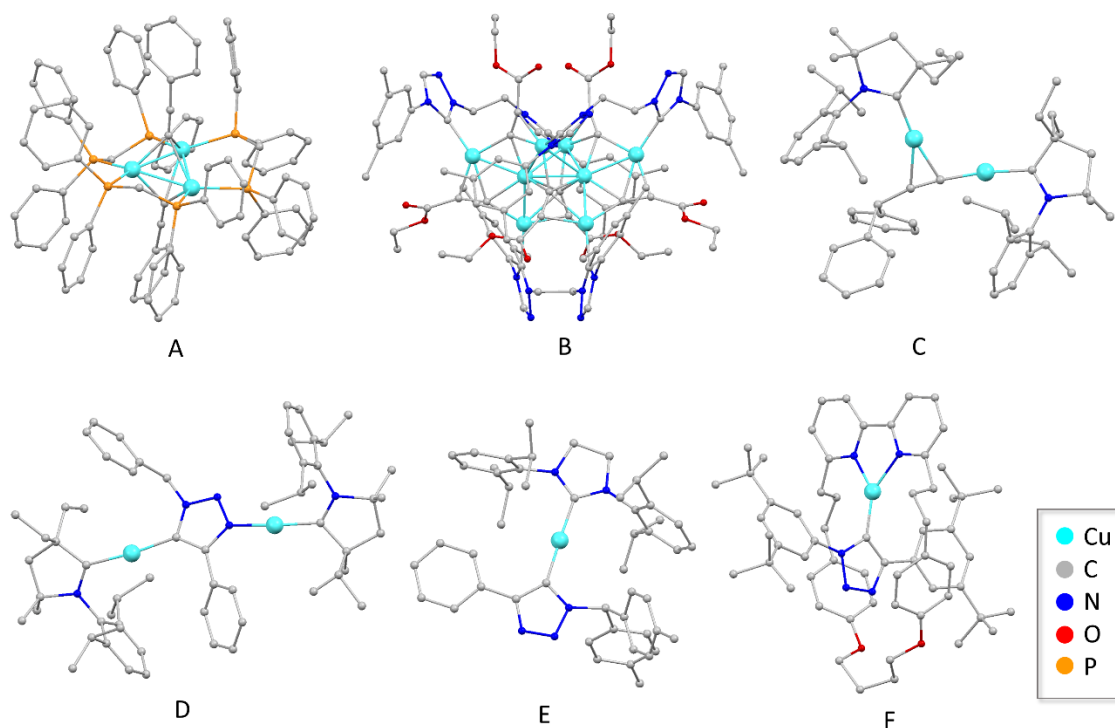


Figure 1-1 Single crystal X-ray structure of isolated key intermediates in CuAAC reaction. Hydrogen atoms were omitted for clarity.

Among these molecularly defined multi-nuclear copper(I)-acetylides, the tri-nuclear $[\text{Cu}_3(\mu_3\text{-}\eta^1\text{-C}\equiv\text{CPh})_2(\mu\text{-dppm})_3]^+$ (Figure 1-1A, Cu/acetylide = 3:2)⁷⁷ was first examined in CuAAC reaction, which gave only 50% yield with respect to total alkyne upon addition of excess benzyl azide at room temperature.⁴⁰ The first catalytically active multi-Cu acetylide complex was isolated by the Straub group.⁷⁸ By reacting an alkyne with a di-copper complex bearing bidentate N-heterocyclic carbene (NHC) ligand (ethylenebis-1,2,4-triazol-5-ylidene), they generated an octacopper hexaacylide cluster that was air stable in solid state (Figure 1-1B). Apart from the weak cuprophilic interactions (Cu–Cu: 2.44–2.68 Å), the two coppers in the center (18e) were stabilized by four acetylides and the other six coppers (16e) were stabilized by two acetylides and one NHC ligand. Each acetylide was coordinated by 3–4 coppers in $\mu_3, \eta^{1,1,2}$ or $\mu_4, \eta^{1,1,1,2}$ mode. Compared to the di-copper NHC complex, the cluster displayed only 1/3 catalytic efficiency in

CuAAC reaction due to the aggregation of copper, but still faster than Cu(OAc). Upon addition of acetic acid, the reaction completed within 5 min at 27°C, which was attributed to the rapid dissociation of octacopper cluster to monomers.

To obtain a copper(I)-acetylide monomer, the Bertrand group employed a sterically hindered and strong σ -donating cyclic (alkyl)(amino) carbene (CAAC) ligand to cap the coppers, and isolated the first reactive di-copper acetylide monomer in CuAAC reaction (Figure 1-1C).⁵² Structurally, the two copper(I) $\mu_2, \eta^{1,2}$ coordinated to the acetylide without evidenced interaction (Cu–Cu: 2.94 Å), but the difference in σ, π -coordination mode disappeared in solution. Compared to the mono-copper acetylide, the di-copper acetylide exhibited superior activity in the reaction with benzyl azide in dichloromethane, although the reaction rate of both were slow due to the hindrance of CAAC ligand. The reaction with di-copper acetylide generated an air- and moisture-stable di-copper triazolide intermediate (Figure 1-1D) that can be protonated by phenyl acetylene and complete the turnover of catalytic cycle.

1.2.5.2 *Copper(I) Triazolides*

Copper(I) triazolide is highly susceptible of protonation, thus sterically congested environment is need for protecting this otherwise short-lived species. The first triazolide intermediate was isolated from the reaction between a sterically demanding azide and NHC-stabilized mono-copper acetylide in aprotic solvent toluene.⁷⁹ The copper(I) is linearly coordinated by the triazolide and NHC ligand (Figure 1E). Aggregation of copper(I)-acetylides and protonation of triazolide is prevented by the relative hindered and stable coordination of NHC ligand. A later study using a 2,2'-bipyridinyl macrocycle in the CuAAC reaction between bulky azide and acetylene gave a copper(I) triazolide mechanically interlocked in a rotaxane-like structure (Figure 1-1F).⁸⁰ Although the triazolide complex was isolated from aprotic solvent Et₂O, it was also

stable against protonation in alcoholic and aqueous solutions, even in presence of strong proton donor such as carboxylic acids.

A di-copper triazolide intermediate (Figure 1-1D) in CuAAC reaction was isolated and characterized by the Bertrand group from the CAAC-stabilized di-copper acetylide (*vide supra*).⁵² The two copper(I) ions coordinates to the N³ and C⁵ of triazolide, respectively, showing non-equivalent environment in solid state and also in solution (confirmed by NMR). However, the structure of the isolated copper(I) complexes may also depend on crystallization conditions and other factors, which cannot confidently represent the structure of the triazolide generated immediately after the CuAAC ring-contraction step (Scheme 1-2). In fact, DFT optimized di-copper triazolides showed that the C⁵ of triazolide simultaneously connected to two coppers that were perpendicular to the triazolide plane.^{42, 50, 53} Besides, the symmetrical three-center-two-electron (3c-2e) bonding mode is not uncommon in organocopper complexes, *e.g.*, in the isolated dimer of “Rind” complexes, the two Cu atoms were perpendicularly bridged by the ligands.⁸¹

1.2.6 Real-time Monitoring of Reaction Process

1.2.6.1 *Detection of Reactive Intermediates during CuAAC Reaction by Mass Spectrometry*

Although the long-lived intermediates can be isolated by crystallization under specific conditions, most reactive intermediates are high-energy, short-lived species, existing in low concentration and in equilibrium with other intermediates in solution. In this case, mass spectrometry can be used for direct investigation of these elusive species since it provides crucial information on the real-time distribution of intermediates by feasible simultaneous detection and quantification of ionizable species in solution, which is not possibly gained by isolation method. The “soft” ionization method Electrospray Ionization (ESI) can efficiently transfer ion from solution to gas

phase with minimum fragmentation, giving accurate mass and isotopic distributions of mostly unaltered intermediates under sub-millimolar concentration.⁸²⁻⁸⁴

Using electrospray ionization mass spectrometry, the Angelis group detected all the proposed copper(I)-containing intermediates in the CuAAC catalytic cycle.⁸⁵ The cycloaddition catalyzed by 5% [Cu(PPh₃)₂(OTf)] in dichloromethane showed major peaks of Cu-PPh₃ complexes and tiny amount of intermediates including di-copper alkyne (3 %), di-copper acetylide (< 0.1%), di-copper triazolide and the triazole product (< 0.1%). To reduce the charge-induced copper(I) dissociation from reactive intermediates, the authors incorporated an imidazolium salt as a “charge tag” on the peripheral side arm of the acetylide. The azide-alkyne precursor complex (< 0.2%) of low intensity was detected and confirmed by tandem mass spectrometry (MS/MS) through Collision Induced Dissociation (CID). Recently the same group further investigated the CuAAC reaction in gas phase,⁸⁶ in which the mono-copper acetylide was found unreactive toward the azide, while the di-copper acetylide needs to be stabilized by at least one ancillary ligand for the cycloaddition step to occur.

Besides ESI-MS, Inductively Coupled Plasma Mass Spectrometry (ICP-MS) was also employed to detect the short-lived intermediates in CuAAC reaction.⁸⁷ Cu²⁺ ions was introduced into the instrument to produce continuous and stable Cu⁺, while the ligands and reactants were mixed directly at the collision reaction cell of the mass analyzer. Mono-copper alkyne and acetylide as well as a small amount of di-copper acetylide were observed. Mono-copper triazolide (or azide-acetylide precursor complex) was observed but not distinguished.

1.2.6.2 Experimental Proof of Stepwise Mechanism by Time-resolved Online ATR-FTIR

Real-time monitoring of the stepwise process of CuAAC reaction was achieved by time-resolved online Attenuated Total Reflection Fourier Transform Infrared Spectroscopy (ATR-FTIR) that

directly responds to all reacting intermediates with little time delay.⁸⁸ The cycloaddition catalyzed by CuBr and *N,N,N',N',N''*-pentamethyldiethylenetriamine ligand (PMDETA) revealed earlier consumption of alkyne than azide, which was prior to the formation of triazole. The azide-acetylide precursor complex was first accumulated to a considerable amount, remain unchanged, then decreased after consumption of all reagent. In this case, the rate-limiting step was assigned to the transition of the precursor complex to the triazole product.

1.2.7 Direct Evidence of Di-copper(I) Mechanism from Isotopic Crossover Studies

The Fokin group performed a convincing study for demonstrating the involvement of two copper(I) atoms in the triazole-formation step.⁸⁹ Addition of catalytic amount of copper(I) into the mixture of benzyl azide and a pre-formed, σ -bound mono-copper acetylide (stabilized by NHC ligand) rapidly generated the triazole product that cannot be produced by the inactive mono-copper acetylide itself. When reacting benzyl azide with the mono-copper acetylide (⁶³Cu:⁶⁵Cu = 69:31) in presence of one equivalent of isotopically pure [⁶³Cu(MeCN)₄PF₆], the yielded NHC-stabilized mono-copper triazolide showed a 50% enrichment of ⁶³Cu (⁶³Cu:⁶⁵Cu = 85:15). The enrichment could only be caused by the coordination of the terminal carbon of acetylide to the extra ⁶³Cu that subsequently bound to the NHC ligand via ligand exchange before the ring contraction step. Since the enrichment never happened with pure acetylide or triazolide, the ligand exchange could only proceed from the azide-acetylide precursor complex or from the metallacycle intermediate. Theoretical calculations showed a higher possibility of the latter, although it still requires a relatively high activation barrier of 11.9 kcal/mol.⁵³

1.2.8 Factors Influencing Reaction Rate

The overall reaction rate is associated with the entropy and enthalpy of reagents, intermediates, transition states and products, which can be affected by many factors including solvents, structure of reagents, counteranions, and ancillary ligands.

1.2.8.1 Solvent Effects

Solvation can lead to significant changes of the structure and concentration of the active species in CuAAC reaction compared to the isolated molecules in gas phase.

Coordination Strength

In general, solvents can be categorized by coordination ability following the order of dimethylsulfoxide (DMSO) > water > dimethylformamide (DMF) \approx acetonitrile > tetrahydrofuran (THF) > methanol \approx *t*-butanol > acetone > toluene > diethyl ether > dichloromethane > n-hexane.⁹⁰ In the absence of an ancillary ligand, the copper catalysts exhibited a higher activity in stronger coordinating solvents such as DMSO, water, DMF, and N-Methyl-2-pyrrolidone (NMP) compared to THF, alcohols, and acetone.⁴³ Acetonitrile is an exception that inhibits the reaction due to its strong coordination with copper(I)^{53, 91} originated from the molecule's small size, favorable rod-like shape, and π -accepting ability.^{53, 92} Strong coordinating solvents such as DMSO, DMF and NMP can also prevent the formation of inhibitory copper(I) complexes generated by excessive strong chelating ligand such as **(Bim)(Py)₂** (Chart 1-1).

Aprotic and Protic Solvents

Although the rate-limiting step in CuAAC reaction has been assigned to the formation of first N-C bond of the triazole ring that requires the highest activation energy (*vide supra*), the

calculated energy barrier for the deprotonation of alkyne is considerably high in dichloromethane⁴² and in gas phase.⁵¹ Consistently, experimental observations also revealed the deprotonation of alkyne as rate-limiting step in dichloromethane, because the formation of copper(I)-acetylide from mono- or di-copper triazolide (turnover step) was slower than the formation of di-copper triazolide.⁵² Besides, when using copper(I) complex as catalyst, a long induction period for generating di-copper acetylide was observed before the formation of the di-copper triazolide.

Compared to aprotic solvents, the deprotonation of alkyne in protic solvents was much faster.³⁰ With deuterium labeled alkyne, an induction period and a primary Kinetic Isotopic Effect (KIE, k_H/k_D) of 2.3 were observed in acetonitrile, suggesting the rate-limiting deprotonation of alkyne. By contrast, the reaction in methanol proceeded immediately upon mixing with a normal KIE. High efficiency of alkyne deprotonation was commonly observed in water, in which the hydroxide anion can act as a base to remove the proton from copper(I) π -coordinated terminal alkyne that exhibits a decreased pK_a (≈ 15).⁹³

1.2.8.2 The Structure of Reagents

Chelating Azides

Early experimental studies have already revealed the weak binding of copper(I) with azide in CuAAC reactions that can be facilitated by linking the azide at the proximal position of copper(I) complexes.^{40, 94} Calculations also suggested non-neglectable energy demands for the formation of the azide-acetylide precursor complex.^{48-50, 53} It was found in the isolated copper(I)-azide complex³² that the copper(I) center preferred to bind the terminal nitrogen (N^3) of azide (similar to a tantalum(III) azido complex⁹⁵) instead of the negatively charged alkylated nitrogen (N^1) of azide as proposed in CuAAC reaction. The preference was not because of steric hindrance, since

a silver(I) analogous complex of the same azide adopted Ag(I)-N¹ coordination. Compared to N¹, the π -accepting N³ can receive extra electron density from the electron-rich d¹⁰ copper(I) that enabled stronger coordination by π -back bonding. Calculations also showed a larger electron density drop in copper(I) compared to silver(I) upon binding to N³. However, the copper(I)-azide coordination is very weak and the bond lengths and angles in azide did not alter much compared to the free aliphatic azides. Thus, an auxiliary ligand is needed for stabilizing the copper(I) at the alkylated nitrogen of azide to facilitate the reaction.

Azides carrying adjacent N-donor ligands (*e.g.*, pyrazole or pyridine) have been applied in “Cu(II)” catalyzed CuAAC reaction, in which the copper(I) was generated *in situ* from Cu(II)-azide complexes.^{28-30, 96} The Lewis acidic Cu(II) prefers to interact with the alkylated nitrogen (N¹) of azide and often adopts a Jahn–Teller distorted octahedral geometry, in which the chloride or nitrile ligands coordinates at the apical position and the “chelating” azides coordinates at the equatorial position of copper(II).^{28-29, 97-98} When using a carbonyl stabilizing group (acetate or hexafluoroacetylacetonate), the azide prefers to coordinate at the apical position without participation of chelating arms.^{30, 99} The interaction between copper cations and azide has been summarized by Zhu.¹⁰⁰

The introduction of “chelating” azides in CuAAC reaction largely accelerated the overall rate^{28-30, 101} and switched the rate-limiting step from azide-coordination⁴² to alkyne deprotonation³⁰ (reflected by KIE). Electron-donating substituents on the chelating arms further increase the reaction rate,¹⁰¹ and the multi-dentate chelating azides bearing triazole groups undergo ultra-fast CuAAC reaction under micromolar concentration with a half-completion time of less than 40 s.⁴⁴ The enhanced binding affinity with copper(I) also enabled the azide to compete with strong chelating proteins and peptides in the complex biological systems and reduced the cytotoxicity of

copper(I) (*vide infra*), making the reaction efficiently applied in bioorthogonal bioconjugation even inside living cells.⁴⁴

Electron-deficient Alkynes

In the thermal Huisgen cycloaddition, the use of electron-deficient terminal alkynes affords only 1,4-regioisomers.¹⁰² In the copper-catalyzed reaction, electron-deficient alkynes can further increase the reaction rate.¹⁰³⁻¹⁰⁵ Systematic studies revealed that alkynes with adjacent carbonyl groups reacted the fastest, followed by propargyl alcohol, ethers or amines. Alkynes bearing alkyl or aryl group showed the lowest activity, but the difference between various type of alkyne is not so significant compared to the modifications on azide.¹⁰³ The electron deficiency in alkynes could increase the copper to alkyne π -back bonding to strengthen the di-copper acetylide structure for the cycloaddition to occur.⁸⁶

1.2.8.3 Counteranions

Counteranions such as phenolate (PhO^-), acetate (CH_3COO^-), chloride (Cl^-), triflate (CF_3SO_3^-), tetrafluoroborate (BF_4^-), and hexafluorophosphate (PF_6^-) can be inevitably introduced into the CuAAC reaction from the copper(I) salts. These weakly coordinating anions may act as a base, or as labile ligands to modulate the vacant coordination sites of copper(I) center, or interference with the copper(I)-alkyne and copper(I)-azide interaction.

Counteranion effect has been systematically investigated by Bertrand group using the strong CAAC ligand that allowed the differentiation of intermediates from each step.¹⁰⁶ In aprotic solvent dichloromethane with 5% copper(I) catalyst, the easiness of deprotonation of alkyne largely depend on the basicity of counteranions following the order of $\text{tBuO}^- > \text{PhO}^- > \text{CH}_3\text{COO}^- \gg \text{Cl}^- \approx \text{CF}_3\text{SO}_3^-$. The rate for generating di-copper(I) acetylide from the mono-copper(I) acetylide followed the order of $\text{CF}_3\text{SO}_3^- \gg \text{Cl}^- > \text{CH}_3\text{COO}^- > \text{PhO}^-$, which was inversely related

to the coordination strength of these counteranions.⁹⁰ Proto-demetalation of the triazolide was over two orders of magnitude faster with the help of CH_3COO^- than other counteranions, and inhibited by phenolate.

1.2.8.4 Ancillary ligands

Ancillary ligands are important components in the CuAAC reaction, which can enormously speed up the reaction in many ways such as increasing the solubility of copper(I) in solution, maintaining the copper(I) oxidation state by preventing oxidation and disproportionation, or generating the reactive multi-copper(I) intermediates.⁸⁶ On the other hand, strong coordinating ligands may inhibit the reaction by competing with alkynes or azides in copper(I) coordination.⁴² The detailed analysis of these ancillary ligands will be discussed below.

1.3 Ancillary Ligands in CuAAC Reaction

1.3.1 Common Ligands Employed in CuAAC Reaction

N, C, P, S donors are the most-frequently employed ligands for accelerating the CuAAC reaction.¹⁰⁷

1.3.1.1 Nitrogen Donors

Inspired from the copper(I) ions in biological system that are often chelated by histidine residues, nitrogen donor ligands such as pyridines, triazoles, imidazoles, and alkyl amines are widely used for stabilizing copper(I) ion in CuAAC reaction.

Neutral Unsaturated Nitrogen Donors

Triazoles, the product of CuAAC reaction, have been extensively used as transition metal ligands in a large variety of application,¹⁰⁸ but only the polydentate triazoles were found promising in

accelerating the CuAAC reaction.¹⁰⁹ The tripodal tetradentate ligand tris[(1-benzyl-1H-1,2,3-triazol-4-yl)methyl]amine (**TBTA**, Chart 1-2) was found to significantly enhance the reaction rate and maintain the copper(I) oxidation state in air.¹¹⁰ A series of water-soluble derivatives of **TBTA** have been developed to facilitate the reaction in aqueous solution for applications in bioconjugation, including the ligands **THPTA**,¹¹¹⁻¹¹² **BTAA**,¹¹³ **BTES**,¹¹⁴ **BTPS**,¹¹⁵ **BTTP**,¹¹⁶ **TL**,¹¹⁷ *etc.* (Chart 1-2), which let the reaction finish within 20 min under sub-millimolar concentration.

Another important polydentate triazole ligand, the water-soluble tripodal tris(triazolyl)methanol (Chart 1-2), was complexed with copper(I) and acted as an efficient catalyst in CuAAC reaction with 0.5% catalyst loading in water or neat conditions.¹¹⁸ The copper(I) complex can be ligated with a resin to generate an air-stable and reusable heterogeneous catalyst.¹¹⁹ Its catalytic activity can be tuned by adding electron-withdrawing or electron-donating groups on the triazole.¹²⁰

Ligands derived from the trimethylamine skeleton using pyridyl, imidazolyl and thiazolyl coordinating arms have been developed.^{43, 121} These stronger chelating ligands exhibited higher activity in coordinating solvent such as DMSO compared to the tris((triazolyl)methyl)amine ligands, but a significant drawback is that the excessive ligands could block the coordination sites of copper(I) and inhibit the reaction.

Rigid aromatic amines such as bipyridines and 1,10-phenanthrolines can also afford significant improvement on reaction efficiency³⁹ and protocols have been developed for application in bioconjugation.¹²² However, the acute air sensitivity of 1,10-phenanthrolines copper(I) complexes requires anaerobic operations that is hard to execute.¹²³

Neutral Saturated Nitrogen Donors

Besides the common bases such as DIPEA (N,N-Diisopropylethylamine) and Et₃N (trimethylamine), the tripodal tris(2-aminoethyl)amine (“tren”, Chart 1-2) derivatives bearing sterically hindered alkyl (C18)¹²⁴ or aryl (benzylic)¹²⁵ substitution groups were successfully complexed with CuBr and applied as pre-formed and recyclable copper(I) catalysts in organic solvents and in water.

1.3.1.2 Carbon Donors

N-Heterocyclic carbene (NHC) ligands (Chart 1-2) have showed remarkable activity in CuAAC reaction. The NHC-copper(I) complexes feature low catalyst loading, high stability, and antioxidation ability,¹²⁶⁻¹²⁸ which makes it a good candidate for bioconjugation with water-soluble substituents.¹²⁹ Since each NHC ligand can form a dative bond with one copper(I), methods have been developed to generate the active multi-nuclear copper(I) complexes by linking two NHC ligands together³⁵ or linking the NHC ligands with other aromatic nitrogen donors, which were able to reduce the activation energy and further enhance catalytic activity.¹³⁰⁻¹³²

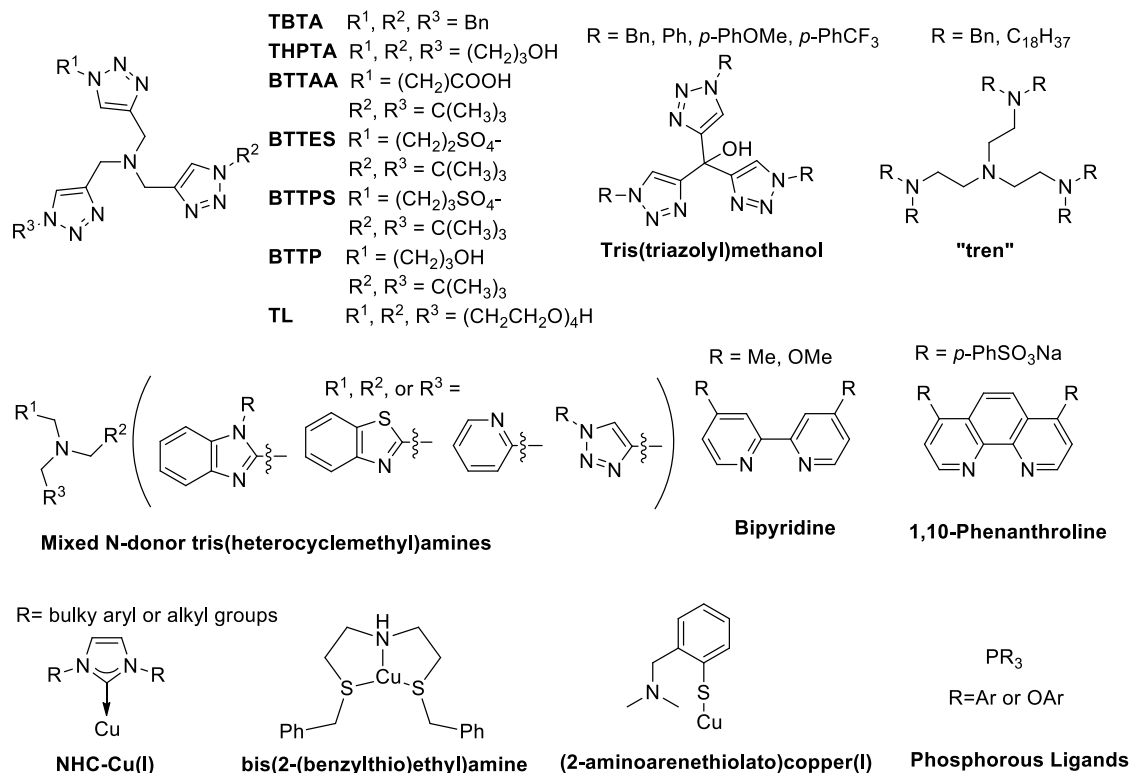


Chart 1-2 Commonly Used CuAAC Ancillary Ligands

1.3.1.3 Heavier Atom Donors

Phosphine Ligands

Commercial available phosphorous ligands such as triphenylphosphine were first used as CuAAC ligands to increase the solubility of copper(I) salt in organic solvents.¹³³ The easy preparation, air-stability, and low catalyst loading give organo-phosphorous copper(I) complexes wide application in CuAAC reaction.¹³⁴ Phosphinite and phosphonite copper(I) complexes were also used for reaction in aqueous solutions that reached completion within hours with 0.5% catalyst loading.¹³⁵ In presence of phenanthroline additives, the reaction with 1% catalyst reached over 83% yield within 5 min.¹³⁶ Phosphines can also act as a reducing agent to convert copper(II) to the active copper(I) in non-polar aprotic solvent (*e.g.*, toluene).¹³⁷

Sulfur Ligands

Commercial available sulfur ligands have been tested in CuAAC reaction,¹³⁸ but they were less efficient and usually need to be combined with nitrogen donors. Examples include the bidentate 2-aminoarenethiolato copper(I) complex that displayed good catalytic activity in aprotic solvent,¹³⁹ and the bis(2-(benzylthio)ethyl)amine copper(I) complex that showed facile catalytic activity in aqueous solutions.¹⁴⁰

1.3.1.4 Polymeric Ligands

Besides small molecules, polymeric ligands also showed high efficiency. An amphiphilic dendrimeric ligand bearing nine triazoles was complexed with nine equivalent of copper(I) ion and applied in the CuAAC reaction. With down to 4 ppm catalyst loading, the reaction reached completion within 24 h at 30°C.³⁶ Polyethylene glycol-ligated tris(triazolyl)methanol ligands were complexed with copper(I), generating nanoparticles carrying 40–44 copper(I) ions. The CuAAC reaction in water completed within 24 h using 20 ppm of copper(I) from the polytriazole copper(I) particles.¹⁴¹

1.3.2 The Nature of Bonding in Copper(I) Acetylide Complexes

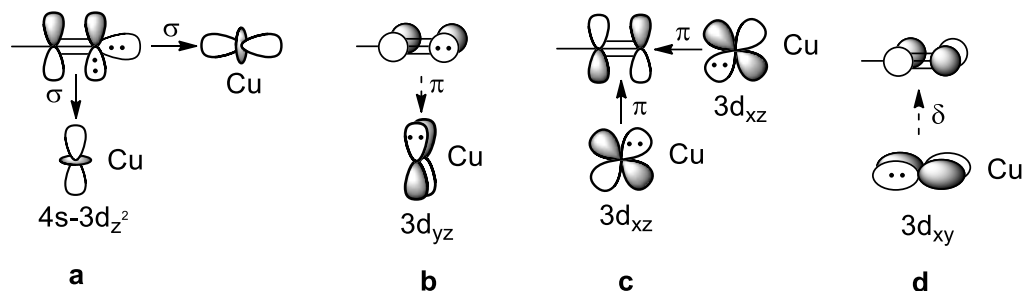
1.3.2.1 Cuprophilic Interactions

The copper(I) ion adopts a closed-shell configuration of Ar(3)d¹⁰. Unlike the copper(II) ion (d⁹) that can form localized covalent bonds through the unpaired electrons, theoretically, the highly occupied d-orbital in copper(I) generates repulsive interactions between two or more copper centers. Nonetheless, many multi-nuclear copper(I) complexes displayed weak but substantial attractive interactions between the copper(I) centers with notably shorter intermetallic distance (*e.g.*, Cu–Cu 2.45 Å¹⁴²) compared to the sum of van der Waals radius (2.8 Å)¹⁴³ and the separation in the copper metal (2.56 Å).¹⁴⁴ This attractive interaction was termed “cuprophilic

interaction” and the nature of which is still controversial.¹⁴⁵ Calculations revealed that it originated from the hybridization of the empty 4s and 4p orbitals of copper(I) into its 3d orbital.¹⁴⁶ The attractive energy of “cuprophilic interaction” was calculated as 4 kcal/mol (at Cu–Cu 2.6 Å), which is comparable to the strength of hydrogen bonds.¹⁴⁷ However, in some complexes with remarkably short Cu–Cu distance (Cu–Cu 2.35 Å¹⁴⁸), the direct copper-copper bonding was questioned and the metals were calculated to be brought together by the strong copper-ligand interaction and geometric constraints instead of covalent metal-metal bonding.¹⁴⁹ The shortest Cu–Cu distance (≈ 2.30 Å) was found in the μ -bridged copper(I) hydride clusters stabilized by strong donating NHC¹⁵⁰ or CAAC ligands.¹⁵¹ The interaction between the copper(I) centers was more specifically termed as a three-center two-electron interaction caused by the electron-deficiency of the complex with only 0.386 bond order calculated.¹⁵² Withdrawing the electron density from the 3d orbital of copper(I) by π -accepting ligands such as CO or CS can decrease the Pauli repulsion and strengthen the Cu-Cu interaction.¹⁴⁷

1.3.2.2 Copper(I)-alkyne and Copper(I)-acetylide Interactions

Compared to electrostatic attractions, the orbital contribution in π -mono-copper(I) acetylene was also much weaker. Coordination of a second copper(I) orthogonal to C \equiv C axis can increase the orbital interaction between alkyne and the first copper(I).¹⁵³ In bis(trimethylsilyl)acetylene (BTMSA) copper(I) complexes, using a β -diketimine ancillary ligand instead of β -diketone can increase the copper to alkyne π back-bonding.¹⁵⁴ Changing the nitrogen in β -diketimine to phosphine, or changing the oxygen in β -diketone to sulfur, will decrease the π back-bonding and slightly decrease the ligand to copper σ donation as well. The latter can be increased by adding electron-donating substitution next to the N donor of β -diketimine.¹⁵⁵



Scheme 1-3 Schematic representation of the key orbital interactions in copper(I)-acetylide complexes: (a) ligand to Cu(I) in-plane σ donation; (b) ligand to Cu(I) out-of-plane π_{\perp} donation; (c) Cu(I) to ligand in plane π_{\parallel} donation; (d) Cu(I) to ligand out-of-plane back-donation (δ and π).

Copper(I) ion is considered a poor π back-bonding metal compared to the isoelectronic Ni(0) complexes.¹⁵⁴ Comparing the group 11 metal in coordination with the Et-C \equiv C-Et stabilized by triazapentadienyl, the degree of π back-bonding followed the order of Au(I) > Cu(I) > Ag(I), reflected by bending of the triple bond and the decreasing in triple bond stretching frequency.¹⁵⁶

The σ lone pair on acetylide, which is analogous to the s orbital of a bridging hydride, makes it a good bridging ligand for multiple copper(I) ions.¹⁵⁷ The stability of a σ, π -di-copper(I) acetylide complex (with acetonitrile and NHC ligands) was predominantly contributed by the ligand to copper donation from the lone pair, and the alkyne π -orbital. Relatively weak cuprophilic interaction was found, but the copper to ligand σ^* or π^* back-bonding is neglectable.⁵³

1.3.3 The Nature of Bonding in Key Ancillary Ligands in CuAAC Reaction

1.3.3.1 Phosphine Ligands

The phosphine ligands are good σ donors comparable to imines.¹⁵⁸ Hybridization of the empty 3d orbital of phosphine makes it a fair π acceptor better than the neutral saturated nitrogen donor ligands but weaker than carbon monoxide.¹⁵⁹ The donor-acceptor ability can be adjusted by changing the substitution group on phosphine. Among the ligands PCl₃, PF₃, P(OCH₃)₃, PH₃,

PH_2CH_3 , $\text{PH}(\text{CH}_3)_2$, and $\text{P}(\text{CH}_3)_3$, $\text{P}(\text{CH}_3)_3$ is the best σ donor and PCl_3/PF_3 are the best π acceptors.¹⁶⁰

1.3.3.2 *Unsaturated Nitrogen Donors*

Phenanthroline

Substituted 2,2'-bipyridine or 1,10-phenanthroline ligands were one of the first studied additives in CuAAC reaction.³⁹ The phenanthroline ligands are both good σ donors and π acceptors. Similar to phosphines, electron-rich substituents can increase their σ donor ability and electron-withdrawing groups can increase their π acidity.¹⁶¹

Pyridine, Imidazole, and Triazole

Pyridine has an unsaturated nitrogen atom carrying an additional lone pair acting as a weak σ donor, and bearing occupied π orbitals acting as π donor and delocalized π^* antibonding orbitals as π acceptor.¹⁶² 1,2,3-Triazole has two effective neutral nitrogen donor atoms, the most basic N^3 and the weakly basic N^2 .¹² The N^3 is also a “pyridine” type nitrogen, but its π accepting ability is not as good as pyridine, since the better conjugation of pyridine’s π system allows more efficient delocalization of metal’s d electrons.¹⁶³ Imidazole mainly acts as a σ and π donor. The σ lone pair energy of nitrogen donor decreased from imidazole to pyridine, pyrazole and triazole. Among the three ligands (pyridine, imidazole, and triazole), triazole is the weakest donor and acceptor, compared to the strong π acceptor pyridine and the good σ/π donor imidazole.¹² However, the major interaction between copper(I) and imidazole is electrostatic attraction from the lone pair rather than a coordinative bond.¹⁶⁴

The π -accepting character of triazoles can be enhanced by adding electron-withdrawing substitution groups such as NO_2 ,¹⁶⁵ and other π accepting ligands such as CO can be employed to reduce the electron density of copper(I) and to strengthen the interaction between copper(I) and

weakly bound imidazole and triazole ligands.¹⁶⁶ The pyridine ligand, by contrast, is a good π acceptor that forming a stable structure with copper(I).¹⁶⁶

1.3.3.3 *N-heterocyclic carbene (NHC)*

Transition metal carbene complexes include the Fischer-type complexes bearing π -donors (*e.g.*, N, O) that bond to metals of low oxidation state, and the Schrock-type complexes bearing hydrogen/alkyl/aryl groups that bond to metals at a high oxidation state.¹⁵³ In contrast to the classical carbenes, the N-heterocyclic carbenes (NHC) exhibit an sp^2 -hybridized lone pair and an unoccupied p-orbital at the carbon (singlet state), which is stabilized by the σ -electron-withdrawing and π -electron-donating adjacent nitrogen atoms. Bulky substituents on the nitrogens can also help to stabilize the carbene carbon from dimerization.¹⁶⁷

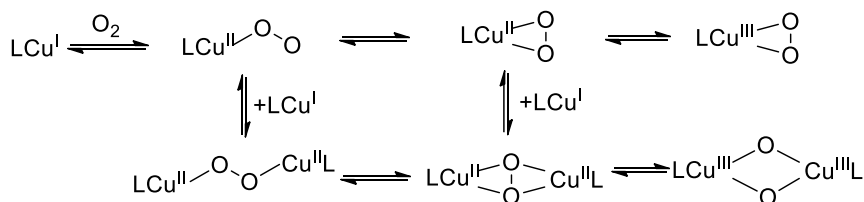
The copper(I)-ligand interaction in NHC-copper(I) complexes mainly comes from the Coulomb attraction between the positively charged copper(I) center and the σ lone pair of the carbene. Orbital interaction only contributes less than ¼ of the total stabilization energy, including a major ligand to metal σ donation and a minor metal to ligand π back-bonding, which is unfavored since the $p(\pi)$ orbital at the carbene carbon is highly filled by the strong nitrogen to carbon donation.¹⁶⁸⁻
¹⁶⁹ The π back-bonding was slightly higher in [(NHC)Cu]Cl complex than [(NHC)₂Cu]⁺ complex,¹⁷⁰ which has two structural isomers with perpendicular or coplanar arrangement of the ligands that are of similar energy.¹⁶⁹

1.3.4 Ligands Preventing Copper(I) from Oxidation

1.3.4.1 *Mechanism of Copper(I) Oxidation*

Copper-catalyzed oxidation of alcohols, amines, and alkanes has been extensively studied in many metalloenzymes in living systems. Most of these enzymes carry copper and organic cofactors or other metals. If copper is the only metal involved in these reactions, di-nuclear or

multi-nuclear copper centers are usually identified.¹⁷¹ Mechanistic studies revealed a stepwise oxidation process (Scheme 1-4). The first step is the activation of dioxygen via binding to copper(I) to form a 1:1 Cu/O₂ adduct. The mono-nuclear adduct prefers to react with a second copper(I) complex, generating the di-nuclear Cu₂O₂ complexes, which may further react with another copper(I) to give copper(II) complexes with higher-nuclearity.¹⁷²



Scheme 1-4 General Mechanism of Copper(I) Oxidation by Dioxygen

1.3.4.2 Ligand Effect on Copper-dioxygen Reactivity

Since the copper-dioxygen reaction is reversible, efforts have been made to develop new ligands that can prolong the lifetime of mono-copper(I) end-on superoxo complex or prevent its formation. The copper-dioxygen complexes have been isolated and extensively studied in literature.¹⁷³ Minor modifications on the chelating ring size, steric hindrance, and electronic properties of chelating ligands can significantly influence the redox chemistry of copper.

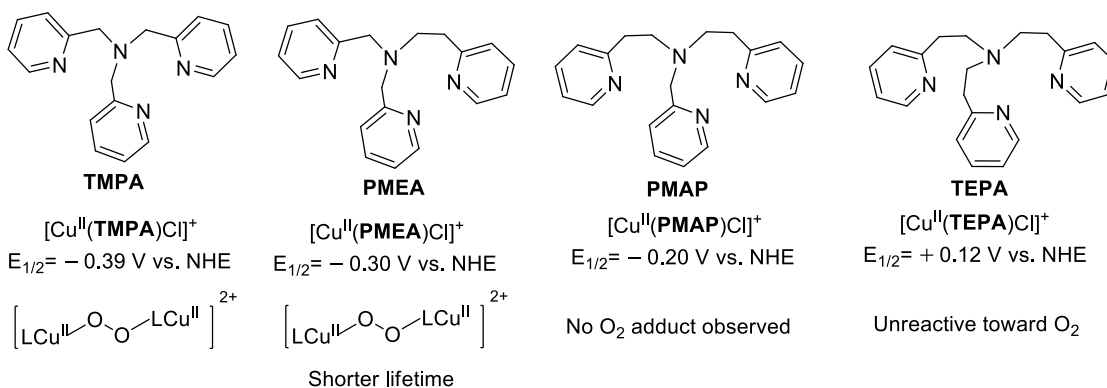


Chart 1-3 Increasing chelate ring size increased the redox potentials of copper complex.

Chelating Ring Size Effect

The copper(I)-chelating ring size is an important factor determining the copper-O₂ reactivity. For example, for the tripodal tetradentate pyridylamine ligands (Chart 1-3), insertion of one or two CH₂ groups between the central amine and the pyridine arm results in dramatic different redox potential of their copper(I) and copper(II) complexes, increased with the enlarged chelating ring size from five to six membered ring.¹⁷⁴ The enlarged N–Cu–N angle offers more protection for copper as indicated by the geometry of the copper(II) complex, *e.g.*, **TMPA** copper(II) complex (5,5,5) shows a trigonal bipyramidal geometry while the **TEPA** complex (6,6,6) displays a square pyramidal structure, thus suppressing or even preventing the reaction of copper with dioxygen. The reaction of [Cu^I(**TMPA**)(MeCN)] with O₂ initially formed a mono-copper(II)-superoxo compound that is unstable and reversible (Scheme 1-4), and then it readily react with another copper(I) complex, generating a stable dicopper(II) end-on peroxo compound. In comparison, the [Cu^I(**TEPA**)(MeCN)] is inert to O₂.

Electronic Effect

Increased electron donating ability on the chelating ligands leads to lower copper(I)/copper(II) redox potential and easier oxidation of the corresponding copper(I) complex. Higher electron density on ligands will increase the π -backbonding of copper(I) to a π -accepting ligand (*e.g.*, O₂), thus strengthen the mono-copper(I) dioxygen bond. The electronic effect mostly affected the second step of oxidation, *i.e.*, generating dicopper(II) end-on peroxide complex.¹⁷⁵

Ligand Denticity and Steric Effect

In general, tetradentate nitrogen-donor ligand-stabilized copper complex prefers to interact with one oxygen atom of the dioxygen forming “end-on” geometry, while the tridentate ligand-stabilized copper complex often adopts “side-on” peroxo or di-copper μ -oxo geometry. Bi-dentate

nitrogen-donor ligands readily react with dioxygen forming exclusively di-copper(III) μ -oxo compound. Addition of bulky substituents on the chelating arms can inhibit the oxidation reaction and generate more copper(II) or copper(I) complexes of lower oxidation state.¹⁷⁶

Phenyl group can also act as a chelating arm to reduce the copper(I)-dioxygen reactivity, which is enabled by the weak copper(I)- π interaction. The interaction with the aromatic ring can be enormously enhanced by adding a methyl group at the benzylic CH_2 to reduce the free rotation of phenyl ring (Chart 1-4). As a consequence, the stabilized complex is unreactive toward O_2 .¹⁷⁷

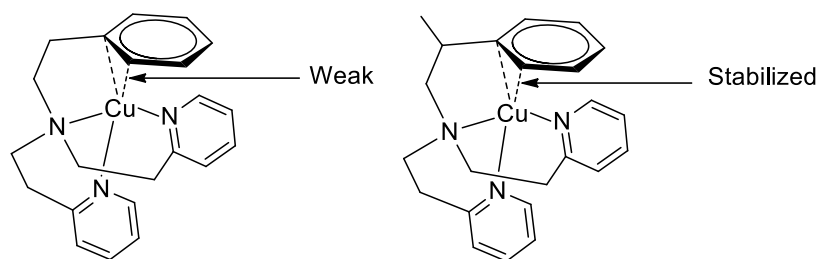


Chart 1-4 Influence of Cu(I)-phenyl interaction.

Chapter 2 Hypothesis and Specific Aims

2.1 Overall Goal and Hypothesis

The CuAAC reaction is an important method for bioconjugation, even in live cells. However, it is largely limited by the need of a relatively large amount (10–100 μM) of Cu(I), which causes various degree of cytotoxicity and oxidative side reactions. The long-term goal of this project is to develop highly efficient copper catalysts that are stable to oxidation and ligand exchange in biological environments. Realizing this goal may allow CuAAC reaction to be performed inside live cells, thus becoming a powerful tool for chemical biology research and development of novel biomaterials and drugs.

We hypothesize that the goal can be realized by developing strong Cu(I) ligands with a high CuAAC reactivity, which also can compete with the abundant and relatively weak biological ligands, such as GSH, which play a key role for intracellular Cu(I) trafficking. Such efficient ligands may allow us to perform intracellular CuAAC reaction using native cellular Cu(I), and eliminate the toxicity issue.

The most commonly utilized CuAAC ligands in bioconjugation are the tris(triazolylmethyl)amines. These ligands bear three chelating arms and one tertiary amine donor, forming three five-membered chelating ring with copper(I), which can offer modest protection for copper(I) against oxidation. These ligands by themselves can only generate mono-copper(I) complex, which is poorly active in CuAAC reaction. We hypothesize that the multi-dentate chelating structure is able to stabilize two or three copper(I) ions by interacting with the terminal alkyne, which is active towards the reaction with azide.

The CuAAC reaction has not been efficiently applied inside live cells, not only because of the cytotoxicity of copper(I), but also due to the competition of biological chelators such as copper chaperones and glutathione. The low copper(I) coordination strength of tris(triazolylmethyl)amines ligands leads to dissociation of copper(I), which will significantly decrease the catalytic efficacy and increase the generation of toxic reactive oxygen species. To apply the reaction inside live cells, the newly developed ligands should be able to stabilize multiple copper(I) ions in presence of the strong competing ligands.

2.2 Specific Aims

2.2.1 Aim 1

To investigate the detailed role of the tris(triazolylmethyl)amine ligands as an example to help understanding the mechanism of ligand-accelerated CuAAC reaction.

To achieve this aim, we will identify the active intermediates involved in the tris(triazolylmethyl)amine-accelerate CuAAC reactions, compare their activity, study the structure details of these intermediates, calculate the energy of active intermediates, and extract the most efficient reaction mechanism from the complicated reaction system. The elucidation of mechanism will be a guide for future ligand design.

2.2.2 Aim 2

To develop novel ancillary ligands that are both active in CuAAC reaction and exhibiting anti-oxidation property.

To achieve this aim, we will synthesize a series of structurally designed ligands with small modification on each ligand, compare their activity and anti-oxidation ability, and study the

hidden relationship between ligand structure and activity. We will screen a large library of multi-dentate ligands to obtain the most-efficient ligand.

Chapter 3 Mechanistic Investigations on

Tris(triazolymethyl)amine Ligand-accelerated CuAAC

Reaction in Aqueous Solutions

3.1 Introduction

3.1.1 Tris(triazolymethyl)amine Ligands: Activity and Applications

The polydentate triazole ligands tris(triazolymethyl)amines are among the most efficient and widely used ligands for CuAAC reaction.^{9, 16, 19} It was first discovered from an auto-catalytic phenomenon in the CuAAC reaction between benzyl azide and tripropargylamine.¹⁰⁹ The product tris[(1-benzyl-1H-1,2,3-triazol-4-yl)methyl]amine (**TBTA**, Chart 1-2) was isolated and used as a promising ligand to accelerate the reaction and protect the copper(I) from oxidation.¹¹⁰ Due to the poor water solubility of the benzyl side arms, a series of hydrophilic derivatives of **TBTA** have been developed for applications in aqueous solution, including **THPTA**,¹¹¹⁻¹¹² **BTTAA**,¹¹³ **BTTEs**,¹¹⁴ **BTTPS**,¹¹⁵ **BTTP**,¹¹⁶ **TL**,¹¹⁷ *etc.* (Chart 1-2). These water-soluble ligands were efficiently used for bioconjugation reactions, including conjugating fluorescent molecules on RNA,¹¹¹ coating the outer surface of the Q β virus-like particle with bovine serum albumin,¹¹¹ labeling the surface glycans on living mammalian cells^{115, 117} and zebrafish embryos,¹¹³ labeling surface proteins on living *E.coli* (*Escherichia coli*),^{112, 114-115} and labeling cytoplasmic proteins inside living *E.coli* cells.¹¹⁶

A typical bioconjugation reaction was conducted with 5–6 equivalents of ligand, which was sufficient to maintain the copper(I) oxidation state in air over a period of 20 hours.¹¹¹ Taking **THPTA** as an example, the reaction between 100 μ M alkyne and 50 μ M azide catalyzed by 50

μM copper(I) (*in situ* reduction of CuSO_4 by excessive sodium ascorbate) in potassium phosphate buffer reached completion within 60 min, and the time can be shortened to 20 min when using 100 μM copper(I). A noticeable but not significant rate drop was observed when increasing the ligand to copper(I) ratio from 1:1 to 6:1, due to the weak interaction between triazoles and copper(I). On the other hand, the catalytic efficiency of these complexes can be inhibited by excess alkyne as a competing ligand.¹¹¹

At ligand/copper(I) ratio of 5:1, the ligands bearing two t-butyl and one ionic carboxylic / sulfuric group (*e.g.*, **BTAA**, **BTPS**, and **BTES**) showed much higher activity than the ligands bearing three hydroxyl groups (*e.g.*, **THPTA**),¹¹³ but at ligand/copper(I) ratio of 2:1 the activity became similar (**BTAA** vs. **TL**, Chapter 6). The ionic tris(triazolylmethyl)amine ligands such as **BTAA** and **BTPS** is harder to penetrate cell membrane compared to the ligands with hydrophobic (**TBTA**) or hydroxyl (**BTTP**) substitutions, which enabled higher metal uptake in the cell cytoplasm for applications inside living cells.¹¹⁶

3.1.2 Previous Mechanistic Investigations on Tris(triazolylmethyl)amine Ligands

As discussed in Chapter 1, many ways can be employed to reduce the activation energy in the rate-limiting step(s) of CuAAC reaction, such as bringing two copper(I) ions together at the alkyne, reducing the electron density of alkyne, enhancing the copper(I)-azide interaction, and improving the deprotonation of alkyne. Kinetic studies have been performed to elucidate the complicated mechanism in CuAAC reaction with tris(triazolylmethyl)amine-copper(I) complexes. In the reaction between benzyl azide (1 mM) and phenylacetylene (1 mM) catalyzed by $\text{Cu}(\text{TBTA})_2$ (2–25%) in Tris buffer, the rate law with respect to copper(I) complex was first order.⁴¹ In solution containing 90% H_2O and 10% DMSO, the reaction between benzyl azide (100 μM) and phenylacetylene (200 μM) catalyzed by copper(I) (10, 50, 100, 200 μM) was -0.42 , 0.13 , 0.67 , 0.73 order in $\text{Cu}(\text{TBTA})_{1/2}$, $\text{Cu}(\text{TBTA})_1$, $\text{Cu}(\text{TBTA})_2$, $\text{Cu}(\text{TBTA})_4$, respectively.⁴³ The

author proposed that the active species $\text{Cu}_2(\text{TBTA})$ was formed during the reaction and remained intact throughout the reaction (Scheme 3-1A). However, the detection and isolation of these dinuclear species has not been reported.

3.1.3 Electron Spray Ionization Mass Spectrometry for Detection of Reaction Intermediates

Intermediate detection and isolation are the most direct methods to reveal the accelerating effect of a specific ligand in view of the complexity of CuAAC reaction mechanism. However, these reactive intermediates are difficult to be detected or isolated due to the presence of multiple fast equilibria between the organo-copper(I) species, the air-sensitivity of copper(I), and the tendency of disproportionation and aggregation of copper(I) in aqueous solution.⁵⁷ All of the successfully isolated CuAAC intermediates are stabilized by strong σ -donating and π -accepting copper(I) ligands such as NHC,^{79, 89} CAAC,⁵² and organophosphines.⁸⁵ In 2015, Iacobucci *et al.* detected the di-copper(I)-acetylide and di-copper(I)-triazolide intermediates stabilized by strong organophosphine ligands using ESI-MS.⁸⁵ In comparison, it is more challenging to study the intermediates of CuAAC reaction accelerated by weaker ligands such as tris(triazolylmethyl)amines since the triazole ligand as a weak donor and acceptor easily undergoes ligand dissociation, and the active species can be at low concentration.

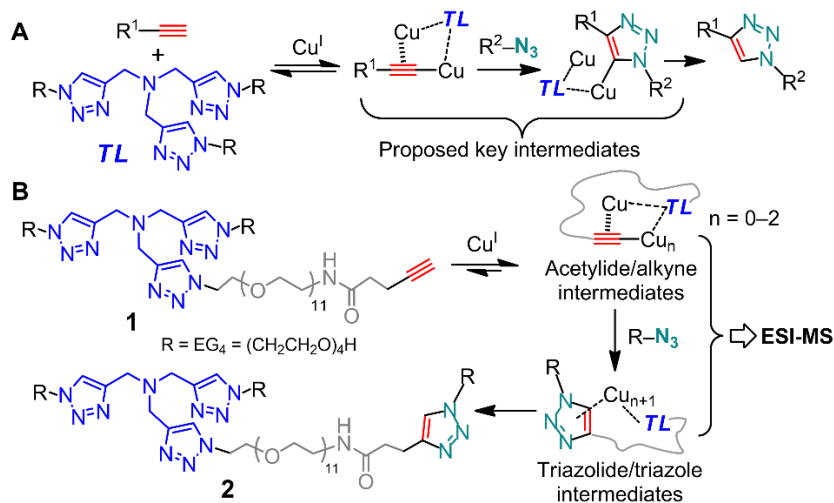
Electrospray ionization mass spectrometry (ESI-MS) has been widely used for investigation of organometallic reaction mechanisms,^{84, 178} detection of elusive reaction intermediates in solution,⁸² and studying the metal-ligand solution equilibria.^{83, 179} Since the ion transfer from solution to gas phase (desolvation) is not energy consuming, the non-covalent interactions in metal complex ions are assumed to be preserved in electrospray ionization (ESI) method.¹⁸⁰ The

desolvated ions in gas-phase detected by mass spectrometry are directly related to their concentration in solution phase, given by the “response factor” that is specific for each species.¹⁷⁹

3.2 Mechanistic Studies in Aqueous Solutions under Stoichiometric Condition

3.2.1 Ligand Design

We envisioned that the weakly bound copper(I)-ligand-acetylide complexes could be kinetically stabilized by conjugating the **TL** ligand and alkyne as **1** in Scheme 3-1B. A long oligo(ethylene glycol) (EG₁₁) chain was used as the linker to enhance water solubility. This design allowed us to directly monitor the elusive intermediates under low concentrations in aqueous solution (mimicking the general bioconjugation conditions). In this way, a series of multi-nuclear copper intermediates, including an unprecedented tri-copper-acetylide and a tri-copper-triazolide complex, were successfully intercepted by ESI-MS spectra, and the fate of these intermediates during the reaction with an azide was monitored.



Scheme 3-1 (A) Previously proposed di-copper intermediates involved in **TL**-accelerated CuAAC reaction,^{41, 43} and (B) our model system to facilitate interception of the intermediates.

3.2.2 Intermediate Detection and Characterization

3.2.2.1 Visible Comparison of copper(I) Chelating Ability of Ligand 1 and TL

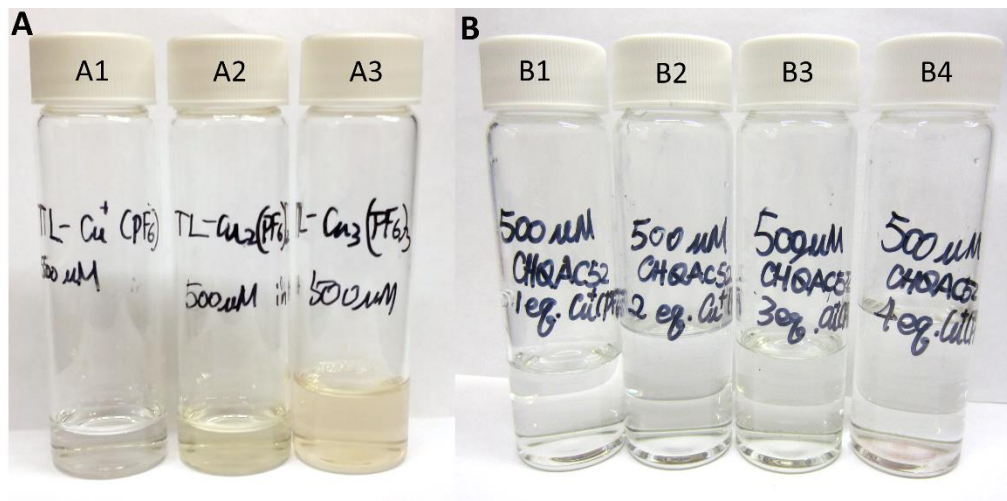


Figure 3-1 (A) Solutions of **TL** (0.5 mM) with 1–3 equiv. of copper(I) in deoxygenated water, picture taken right after mixing. (B) Solutions of **1** (0.5 mM) with 1–4 equiv. of copper(I) in deoxygenated water, picture taken after storage in an anaerobic chamber with <1 ppm oxygen for 4 months.

We first compared the stability of the Cu(I) complexes of **TL** and the alkyne-**TL** conjugate (**1**) at various copper/ligand ratio from 1:1 to 3:1. The samples were prepared by mixing the ligand with Cu(MeCN)₄PF₆ (1–3 equiv.) in MeCN, followed by lyophilizing the solution to completely remove MeCN. While all 1:1 mixtures of Cu/**TL** and Cu/**1** in water were stable as expected, we observed a marked difference when the Cu/ligand ratio was higher than 1:1. Upon dissolving in water, the Cu/**TL** 2:1 and 3:1 mixtures readily turned greenish-yellow and formed a red precipitate, indicating disproportionation of excess Cu(I) into Cu(II) and Cu(0) (Figure 3-1, A₂–A₃). ESI-MS confirmed the presence of mostly the mono-copper complex **TL**-Cu and only a small portion of the di-copper complex **TL**-Cu₂ (Figure 3-2), similar to previously reported result.⁴³ As shown in Figure 3-2, only a minor amount of dinuclear **TL**-Cu₂ ions were observed

in the solution with 2 and 3 equivalents of copper(I) and the spectra were less clean as compared to the one with 1 equivalent of copper(I). The spectra result is in consistency with observation (Figure 3-1) that without an alkyne, the multi-nuclear copper(I) complexes with tris((triazolyl)methyl)amine ligand were not stable.

By contrast, the solution of Cu/I 2:1 and 3:1 mixtures remained colorless and clear for more than 4 months when kept in closed vials in an anaerobic chamber (Figure 3-1, B₁ – B₃), although increasing the Cu/I ratio to 4:1 resulted in slow formation of Cu(0) (Figure 3-1, B₄). Thus, the presence of alkyne stabilizes the multi-nuclear **TL**-copper complexes in aqueous solution.

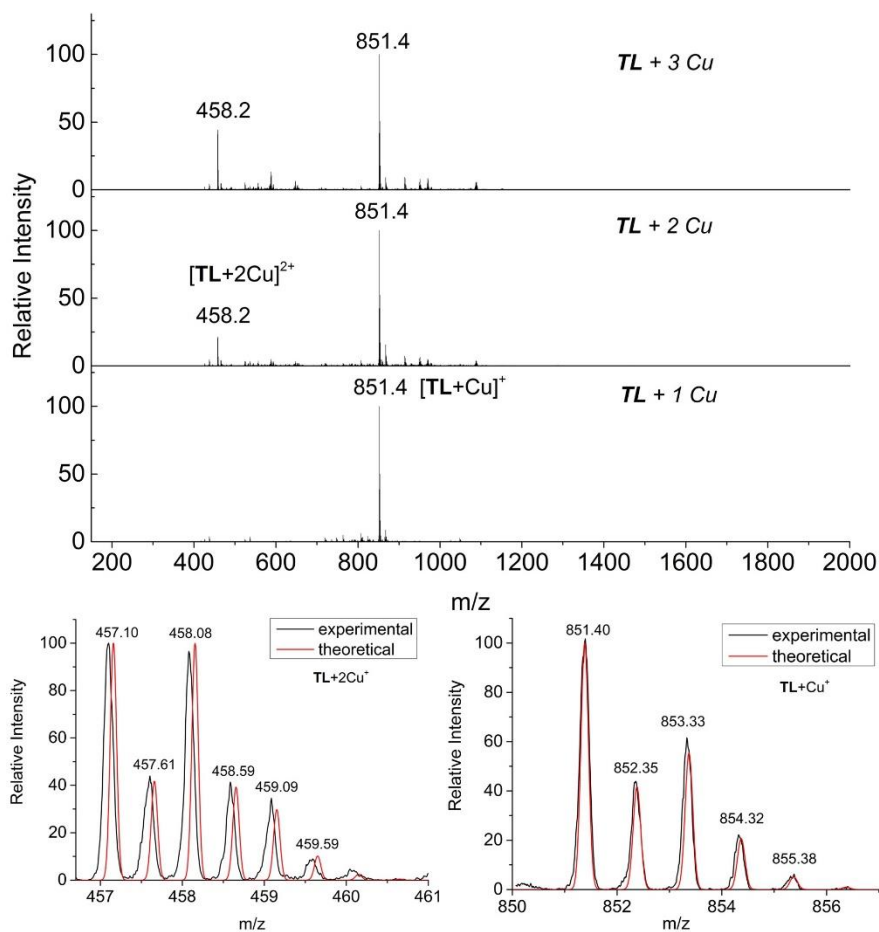


Figure 3-2 ESI-MS spectra of **TL**-Cu_n complexes in deoxygenated water.

3.2.2.2 *Ligand 1-copper(I) Complexes Solution Equilibria*

To probe the charged-copper species in the Cu/**1** mixtures, we infused a series of aqueous solutions of **1** (100 μM) with Cu(I) (1–3 equiv.) into the ESI mass spectrometer. The total ion spectra of the solutions are shown in Figure 3-3A. Each major peak in the spectra was assigned to a copper complex ion that matches the predicted m/z value and isotopic pattern (Figure 3-4, and inserts in Figure 3-3A for selected examples). The simplified coordination modes and equilibria of these copper complexes are proposed in Scheme 3-2.

The lack of pure samples of these unstable species precludes their accurate quantitation by ESI-MS. However, their relative abundance can be estimated by the peak intensities assuming that the ions have a similar ESI-MS response factor, since they consist of a water soluble ligand **1** and possess mostly two charges thereby a similar solvation energy.¹⁷⁹ In Figure 3-3A, the summary of MS intensity of all ligand **1**-containing species are similar in Cu/**1**=1:1, 2:1, and 3:1 conditions (1.5×10^9 , 1.3×10^9 , 1.5×10^9 , respectively), which indicates that the variation in MS response factor of **Ia**, **Ib**, **IIa**, **IIb** and **IIIa** are small and neglectable ($1.45 \pm 0.16 \times 10^7 \mu\text{M}^{-1}$). This assumption was further supported by the small variation of the total ion intensity throughout the reaction with an azide (Figure 3-5), although during which the concentrations of most intermediates varied over a large range.

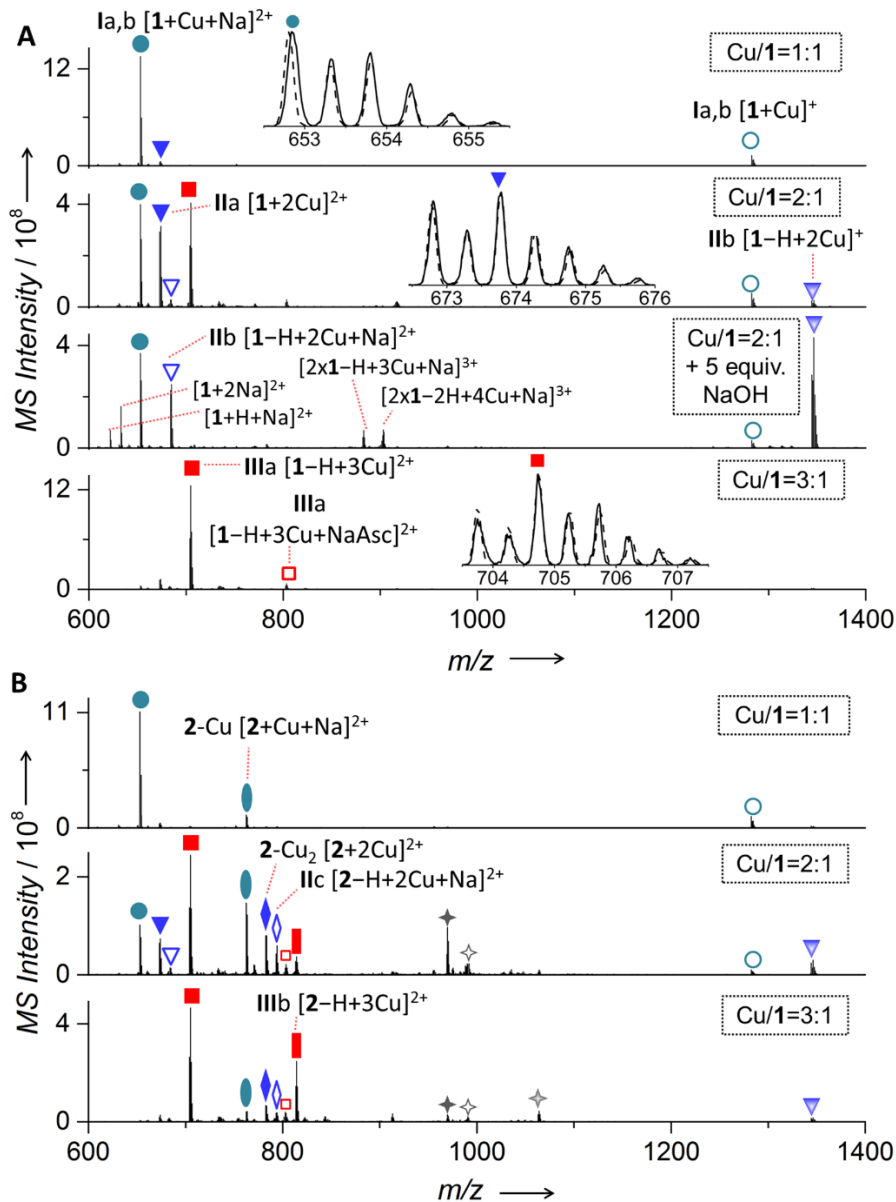


Figure 3-3 A) ESI-MS spectra for solutions of **1** (100 μM) and 1–3 equiv. of copper(I) generated from CuSO_4 (100–300 μM) and Na-Ascorbate (1 mM) in deoxygenated water. (B) Averaged ESI-MS spectra of the above solutions (without NaOH) taken between 4–6 min after addition of 1 equiv. of N_3EG_4 . All marked peaks are assigned and color-coded with cyan (circles) for mono-copper(I), blue (triangles) for di-copper(I) and red (squares) for tri-copper(I) species. The assignment is based on a good fit of the experimental (solid lines) and theoretical (dash line) isotopic patterns (Figures 3-4 & 3-9, selected examples are shown in inserts).

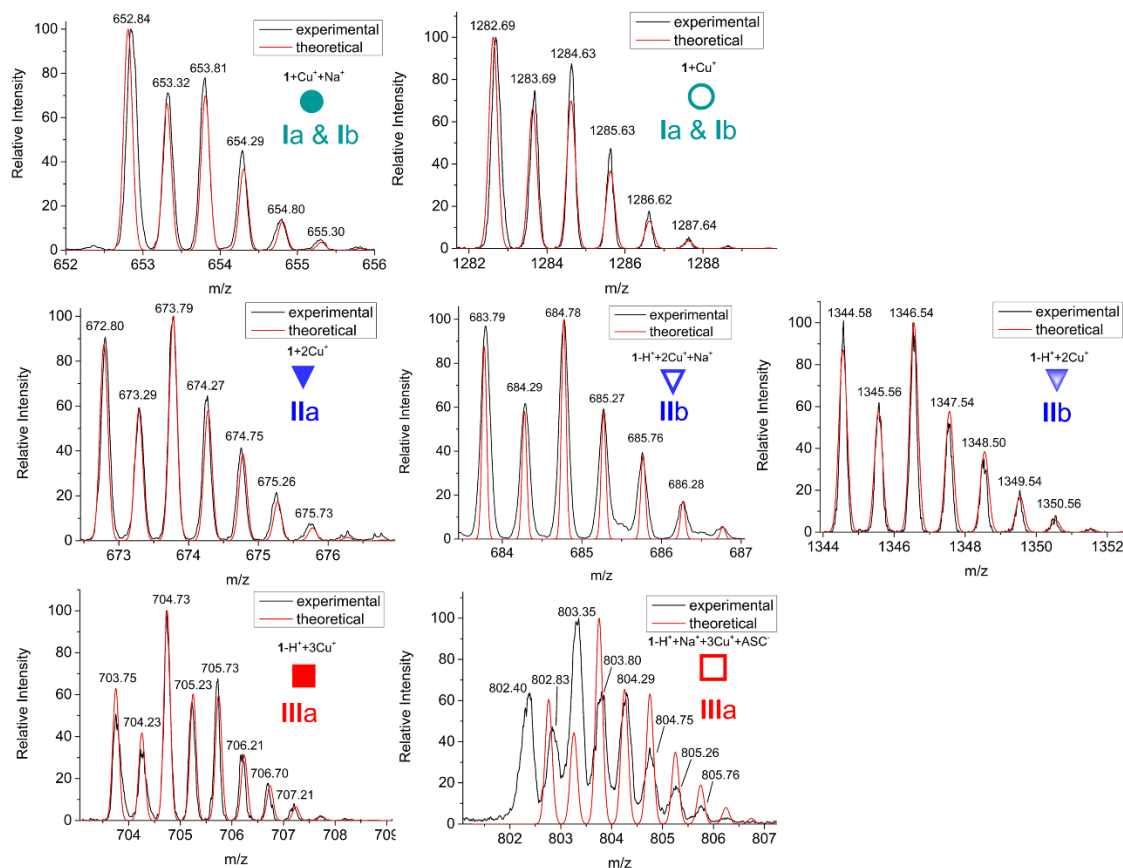


Figure 3-4 Isotopic pattern for 1-Cu_n species in Figure 3-3. Experimental isotopic patterns were obtained by zoom scans centered on selected m/z . Theoretical isotopic patterns (red) of the proposed ions were calculated using IsoPro 3.0, and overlaid on the experimental isotope pattern (black). Each zoom scan spectrum represents an average of 50–100 individual scans during direct infusion of an aqueous solution of the copper(I)/ligand mixture. The assignment of each adduct is based on comparison of experimental and theoretical isotopic pattern.

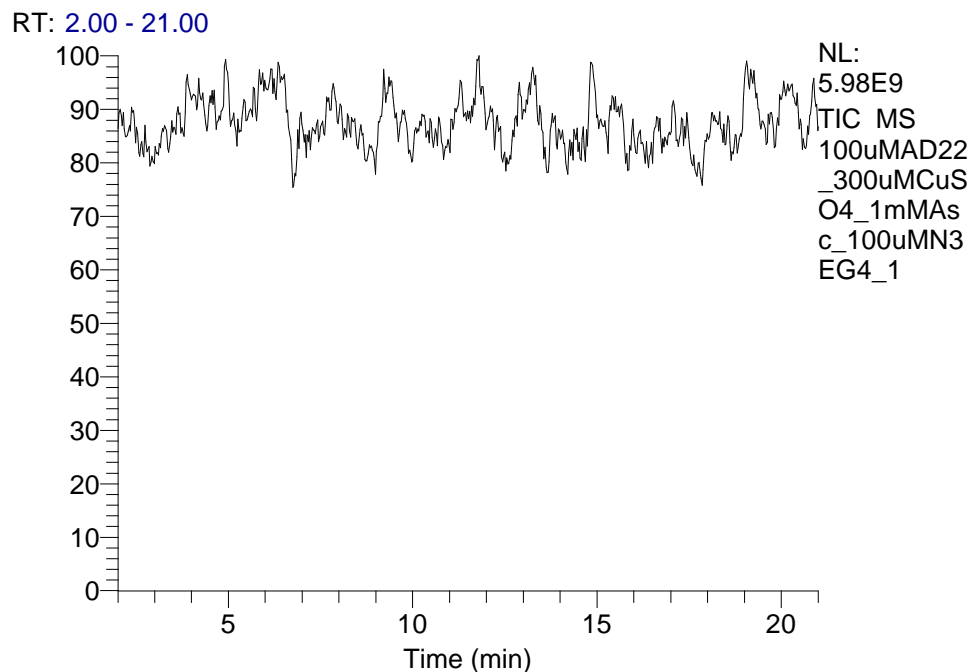


Figure 3-5 Total ion-intensity variation during the CuAAC reaction. The solutions of **1** (100 μ M) and 3 equiv. of copper(I) generated from CuSO_4 and Na-Ascorbate (1 mM) in deoxygenated water were mixed with 1 equiv. of N_3EG_4 and infused into ESI-MS. The consistence of total ion intensity could be attributed to the similar response factors of triazolide/triazole product vs. the acetylide/alkyne reagent.

In the Cu/**1** 1:1 solution, the predominately charged species were the mono-copper alkyne sodium adduct ($[\text{1}+\text{Cu}+\text{Na}]^{2+}$, Figure 3-3A) together with a trace amount of $[\text{1}+\text{Cu}]^+$, which were assigned to the copper complexes **Ia** or **Ib** (Scheme 3-2). The presence of the π -complex **Ib** was indicated by the large downfield shift (0.19 ppm) of the propargylic proton signal upon addition of 1 equiv. Cu(I) to the solution of **1** in D_2O (Figure 3-6, *vide infra*).

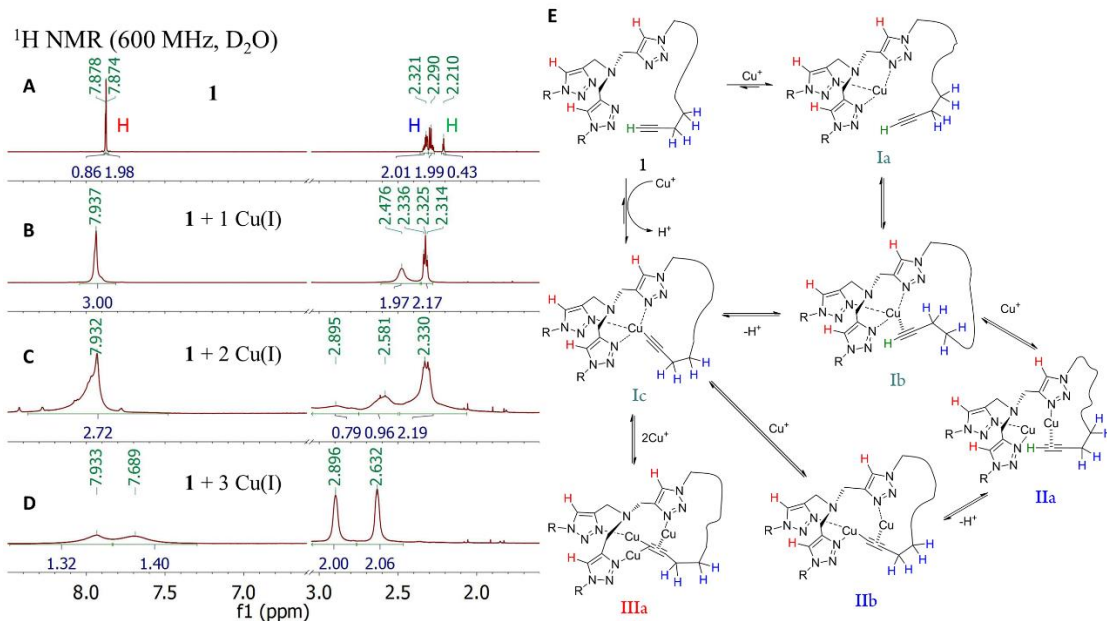


Figure 3-6 ^1H NMR spectra of **1** (20 mM) and Na-ascorbate (100 mM) in deoxygenated D_2O after addition of 0 (A), 1.0 (B), 2.0 (C) and 3.0 (D) equiv. of CuSO_4 . The NMR spectra for two selected regions: the triazole proton (red) and the adjacent methylene protons of the alkyne (blue, A_2B_2 spin system before addition of copper). Due to the high melting point of the solvent (D_2O) and the low thermo stability of the copper complexes, attempt to perform variable temperature ^1H NMR of the above samples was not successful. (E) The proposed structures of the copper acetylene/acetylide complexes that are in fast equilibria in the solutions. The curved lines in the structures represent the linker $-(\text{CH}_2\text{CH}_2\text{O})_{11}\text{CH}_2\text{CH}_2-$.

The large downfield shift of the propargylic protons (blue) upon addition of copper(I) clearly indicated the interaction between copper(I) and the alkyne. Since the ESI-MS data indicated that in the presence of 1 equiv. of copper, the alkyne was not deprotonated (Figures 3-3), the downfield shift of the propargylic protons in Figure 3-6A is likely due to the presence of the π / η^2 -complex **Ib** in fast exchange with the free ligand **Ia**. The absence of the acetylenic proton signal could be attributed to the π -coordination of copper(I) to the alkyne that is known to greatly decrease the $\text{p}K_a$ of the acetylenic proton,⁹³ promoting H/D exchange via a trace amount of the di-Cu acetylide **IIb** present at pH 6.0. The propargylic proton signal was broadened and the splitting

by the adjacent CH₂ (A₂X₂ spin system) was lost, probably due to ligand exchange at a rate comparable to the NMR time scale and the presence of ⁶³copper(I)/⁶⁵copper(I) nuclei (I = 3/2) with a relatively large quadrupole. Note that the **Ia** / **Ib** ratio cannot be derived from the current data.

In the ESI-MS spectra of the Cu/**1** 1:1 solution, the expected sodium adduct of **Ic** was not observed (Figure 3-3A and Figure 3-7A), while a trace amount of the di-copper acetylide **IIb** (blue triangles, [**1**-H+2Cu]⁺) and tri-copper acetylide (**IIIa**, Figure 3-7A) were present. This result suggested that the mono-copper acetylide **Ic** was highly labile to hydrolysis, but could be stabilized by coordination with additional copper atom(s). Indeed, in the Cu/**1** 3:1 solutions, all alkynes were deprotonated (*vide infra*).

To our surprise, increasing the Cu/**1** ratio to 2:1 did not bring the di-copper alkyne/acetylide **IIa/IIb** to majority (Figure 3-3A). Instead, the mixture consisted of a significant portion of the mono-copper (**Ia/Ib**) and tri-copper species (red squares, **IIIa**). Only ~5% of the Cu₂-acetylide **IIb** was present. This result revealed the tendency of the alkyne-**TL** conjugate to form tri-copper rather than di-copper acetylides, the proposed active intermediates in the catalytic cycle. The coordination modes in **IIb** and **IIIa** (Scheme 3-2) were tentatively assigned based on the structures of few reported non-aggregated multinuclear copper acetylide complexes.^{52, 55, 65, 77-78}

In the NMR spectra, increasing the Cu/**1** ratio to 2:1 (Figure 3-6B) resulted in further down field shift of both ethylene signals. The broad and unsymmetrical signals in the Cu/**1** 2:1 mixture was in consistent with the presence of fast equilibria among multiple mono-, di- and tri-copper acetylide complexes as detected by ESI-MS (Figure 3-3A, see Figure 3-6E for the proposed structures).

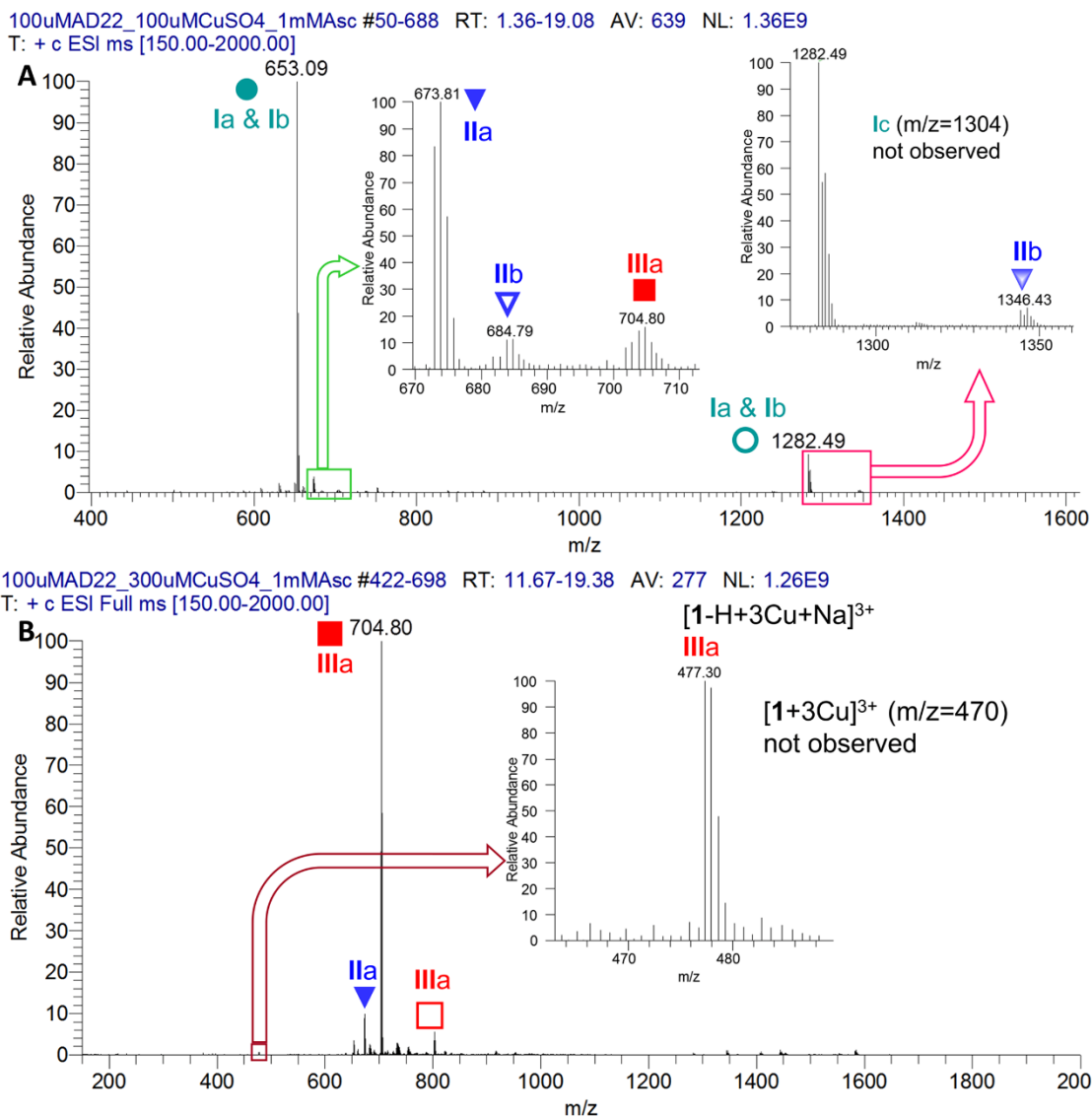


Figure 3-7 (A) Amplified total ion spectra of Cu/**1** = 1:1 solution. The di-copper and tri-copper acetylide **IIb** and **IIIa** were both detected with a noise to signal ratio of over 5:1. The sodium adduct of mono-copper acetylide **Ic** was not observed. (B) Amplified total ion spectra of Cu/**1** = 3:1 solution. The tri-copper alkyne adduct was not observed.

As the ratio of Cu/**1** was increased to 3:1, the ESI-MS spectrum became remarkably simple, showing dominantly the tri-copper acetylide **IIIa** (Figure 3-3A). Significantly, no protonated tri-copper alkyne complexes were detected (Figure 3-7B). The result attests to the superior stability

of the tri-copper ligand–acetylide complex against protonation, even under low concentration in aqueous conditions. It is worth noting that Cu(I) acetylides are well known to aggregate.⁵⁷ Few mono-acetylide copper complexes have been reported, especially those consisting of two or three copper atoms.^{52, 55, 65, 77-78} Strong ligands (CAAC and organophosphines) were employed in those cases to isolate the monomers. We now show that the **TL** ligand in **IIIa** successfully stabilizes the tri-copper acetylide against aggregation. Indeed, most of the copper complexes detected in the Cu/**1** 1:1 and 3:1 mixtures were the mono- and tri-copper complexes bearing only one acetylide and one **TL** ligand, rather than multi-acetylide-copper aggregates found in low intensity in the Cu/**1** 2:1 mixture (peaks labeled with stars, Figure 3-3A & Figure 3-4).

In the NMR spectra of the Cu/**1** 3:1 mixture (Figure 3-6C), the large downfield shift of the relatively sharp and symmetrical methylene signals were attributed to formation of exclusively the tri-copper acetylide **IIIa**, and the large broadening of the triazolyl proton signals to the exchange of binding between the triazolyl ligands to the three non-equivalent copper atoms at an intermediate rate.

Overall, the stability of the acetylides against hydrolysis increased with increasing number of coordinating copper(I) (**IIIa** > **IIb** > **Ic**). The unprecedented tri-copper acetylide **IIIa** was more stable against hydrolysis, dissociation and aggregation than the di-copper acetylide **IIb**. Addition of NaOH led to increasing amount of **IIb** (Figures 3-3A, and Figure 3-8).

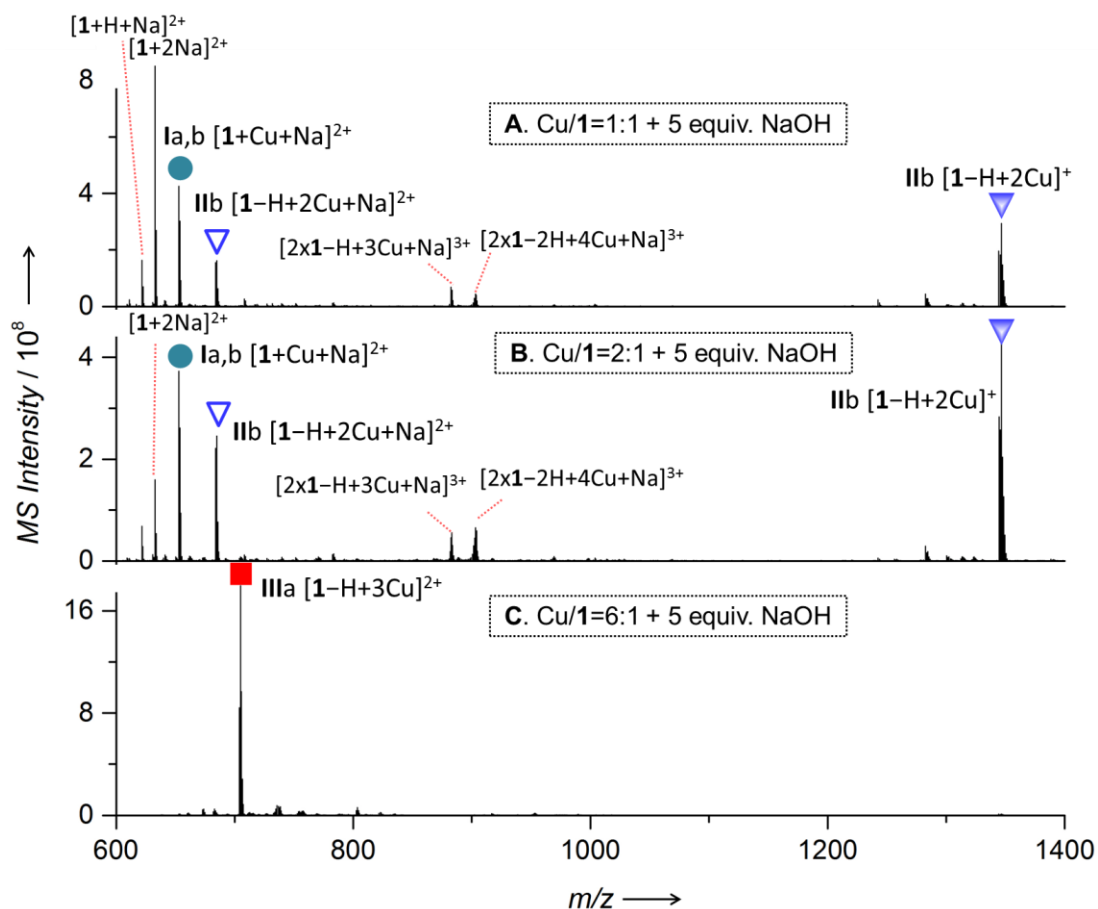


Figure 3-8 (A) ESI-MS spectra of 100 μM **1**, 100 μM copper(I), 500 μM NaOH in deoxygenated water; (B) ESI-MS spectra of 100 μM **1**, 200 μM copper(I), 500 μM NaOH in deoxygenated water; (C) ESI-MS spectra of 100 μM **1**, 600 μM copper(I), 500 μM NaOH in deoxygenated water. Each spectrum represents an average of 100 individual scans during direct infusion. Due to the weak coordination of OH^- group, copper(I) was partially dissociated from the multi-Cu acetylide species, but increasing the Cu/**1** ratio to 6:1 was able to inhibit the dissociation and shift all the equilibria back to **IIIa**.

3.2.2.3 Monitoring the Reaction Between the Ligand **1**-copper(I) Complexes and Azide

Due to the increased positive charges and coordination sites, the tri-copper complex **IIIa** is expected to enhance the weak coordination with azides which has been shown to greatly accelerate the CuAAC reactivity (by using copper-chelating azides).^{30, 44, 96, 101}

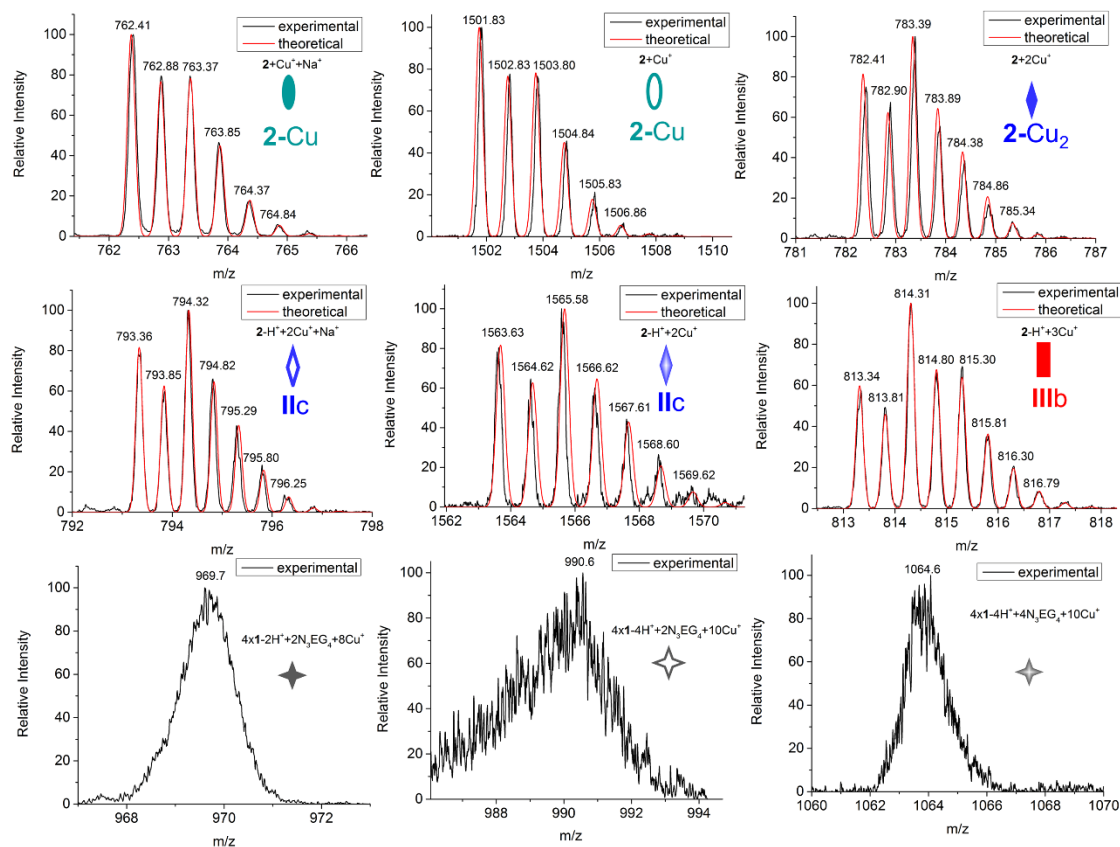


Figure 3-9 Isotopic pattern for CuAAC reaction ($1-Cu_n$ with N_3EG_4) intermediate peaks in Figure 3-3B. Starred peaks in Figure 3-3 are probably high-nuclear aggregates. We were unable to obtain the isotopic patterns of these species due to the limited resolution of the MS spectrometer. Several detected peaks showed lower m/z compared to theoretical mass of the corresponding species, which is likely due to the inelastic collisions in the quadrupole ion trap that lead to dissociation and early ejection of those weakly-bound polyatomic species.¹⁸¹⁻¹⁸²

To study the intermediates of the CuAAC reaction with TL-copper-acetylide complexes, we added 1 equiv. of an azide (N_3EG_4) to the above mixtures with a $Cu/1$ ratio of 1:1 – 3:1, and infused the solution to ESI-MS (Scheme 3-1B). Figure 3-3B shows the averaged total ion MS obtained during the early stage of the reaction (4 – 6 min). In addition to the above copper acetylide/alkyne complexes, several new peaks appeared in the spectra, which are assigned to the di-copper triazolide ($[2-H+2Cu+Na]^2+$ & $[2-H+2Cu]^+$, **IIc**), the tri-copper triazolide ($[2-$

H+3Cu)²⁺, **IIIb**), the di-copper triazole ([2+2Cu)²⁺, 2-Cu₂) and the mono-copper triazole complex ([2+Cu)⁺ & [2+Cu+Na)²⁺, 2-Cu) (see Figure 3-9 for the isotopic patterns). The assignment was further supported by the fragmentation patterns in the tandem mass spectra (MS/MS) (Figures 3-10, 3-11, 3-12), which indicated that the assigned triazolide signals were not contributed by their isobaric precursors (Scheme 3-3).

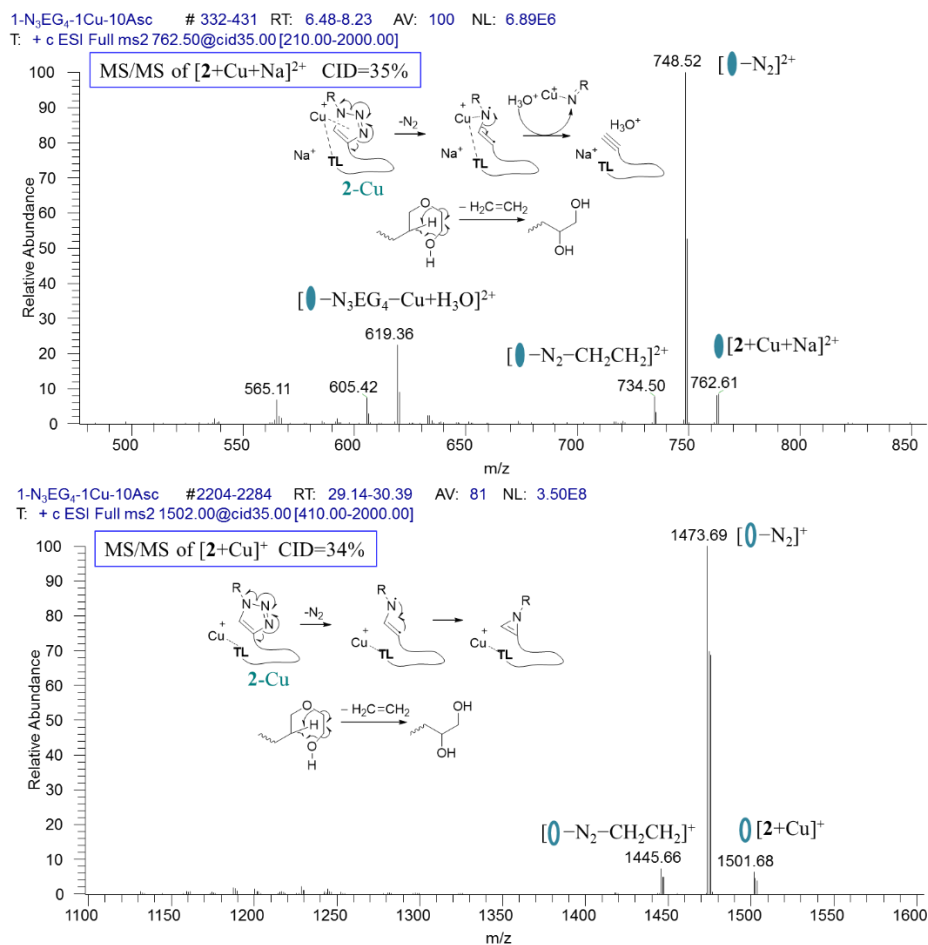
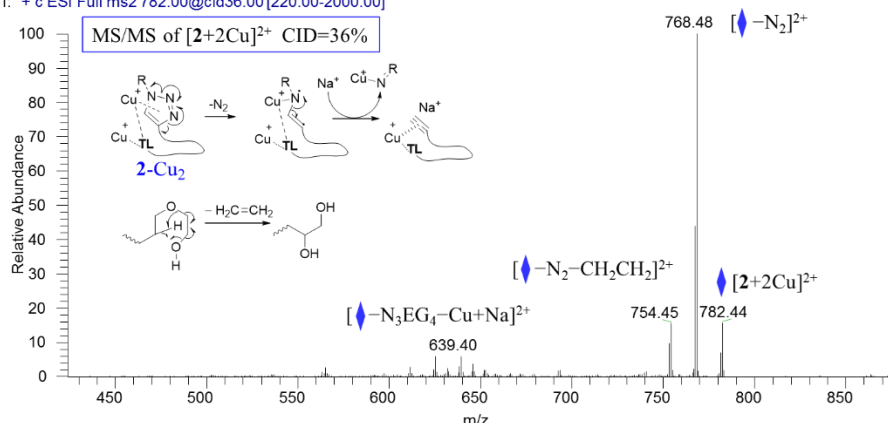
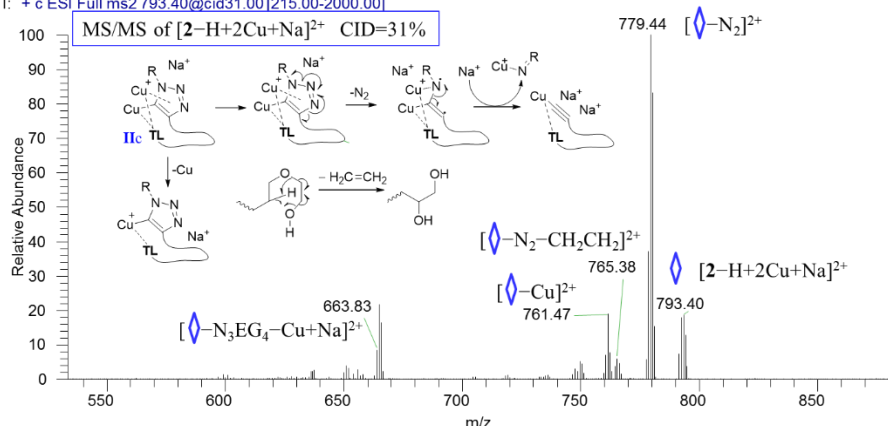


Figure 3-10 MS/MS spectra of mono-copper adduct including mass unit of “1+N₃EG₄” or “2”, and proposed fragmentation mechanism. Infused solution concentrations: 100 μM **1**, 100 μM CuSO₄ and 1 mM Na ascorbate.

1-N₃EG₃-2Cu-10Asc #2589-2708 RT: 45.09-47.25 AV: 120 NL: 5.36E6
 T: + c ESI Full ms2 782.00@cid36.00[220.00-2000.00]



1-N₃EG₃-2Cu-10Asc #155-326 RT: 2.91-5.83 AV: 172 NL: 2.00E7
 T: + c ESI Full ms2 793.40@cid31.00[215.00-2000.00]



1-N₃EG₃-2Cu-10Asc #341-445 RT: 6.09-8.24 AV: 105 NL: 6.49E5
 T: + c ESI Full ms2 1565.50@cid31.00[430.00-2000.00]

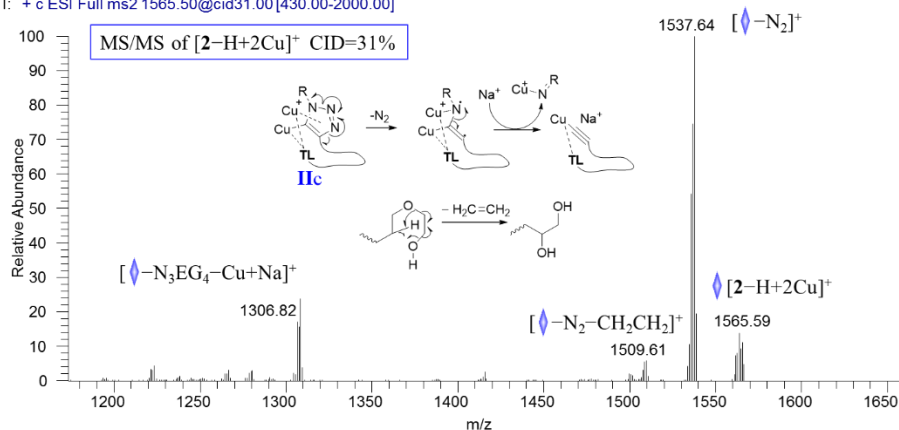


Figure 3-11 MS/MS spectra of di-copper adduct including mass unit of “1+N₃EG₄” or “2”, and proposed fragmentation mechanism. Infused solution concentrations: 100 μM **1**, 200 μM CuSO₄ and 1 mM Na ascorbate.

1-N₃EG₃-3Cu-10Asc #1145-1268 RT: 21.49-23.57 AV: 124 NL: 1.36E8
 T: + c ESI Full ms2 814.00@cid30.00[220.00-2000.00]

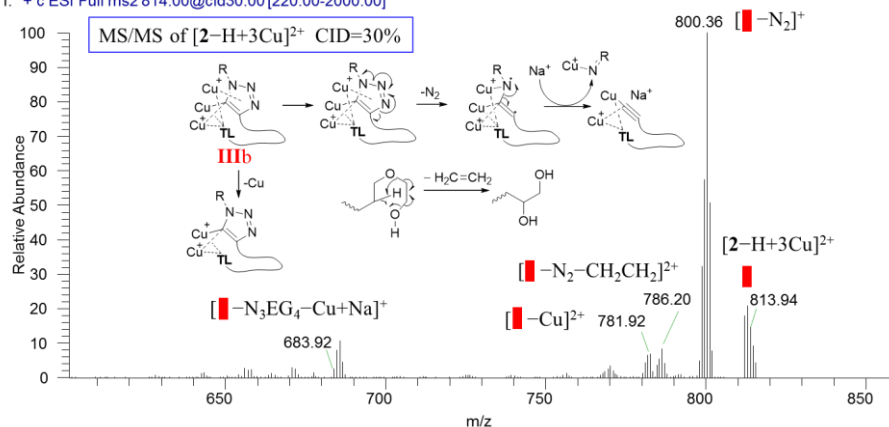
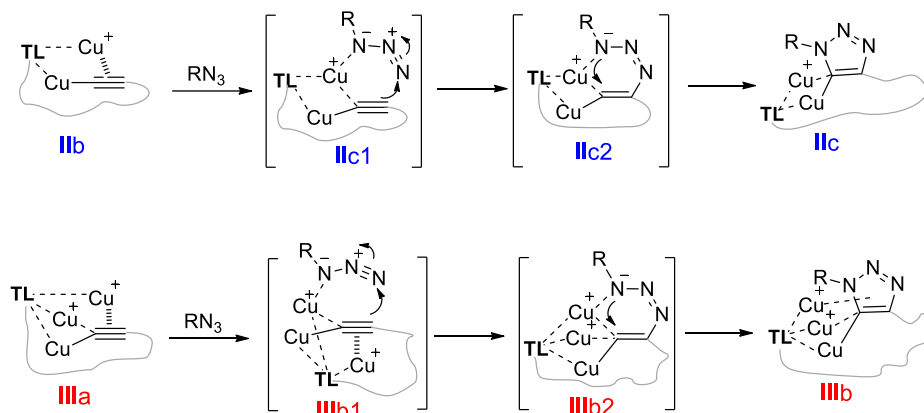


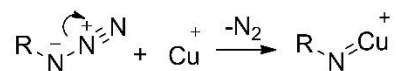
Figure 3-12 MS/MS spectra of di-copper adduct including mass unit of “1+N₃EG₄” or “2”, and proposed fragmentation mechanism. Infused solution concentrations: 100 μM **1**, 300 μM CuSO₄ and 1 mM Na ascorbate. Each MS/MS spectrum was obtained using collision-induced dissociation (CID) method, and represents an average of about 100 individual scans during the direct infusion of the CuAAC reaction mixture.



Scheme 3-3 Proposed Triazolide-formation Mechanism involving the Isobaric Intermediates

The MS/MS of the ions assigned to the mono- (**2**-Cu), di- (**IIc** and **2**-Cu₂) and tri-copper (**IIIb** and **2**-Cu₃) triazolide/triazole complexes (Figure 3-10, 3-11, 3-12) gave a prominent product ion with neutral loss of N₂, consistent with the breaking of N–N bond in triazole ring.¹⁸³ Most of these intermediate ions also showed a minor loss of N₃EG₄ accompanied by the loss of Cu⁺, even in the

case of mono-copper-triazole complex **2**-Cu ($[\mathbf{2}+\text{Cu}]^+$, Figure 3-10). Since the fragmentation energy required was relatively high (CID = 30-31%), these product ions were likely formed by cleavage of a copper-nitrene moiety generated from the triazolide/triazole after release of N_2 , as proposed in Figure 3-10–3-12.



Scheme 3-4 Fragmentation of Copper(I)-azide Complex

Although the ions assigned to **IIc** and **IIIb** have the same m/z values as the azide-copper-acetylide adducts (**IIc1** & **IIIb1**, Scheme 3-3), the secondary fragmentation patterns in their tandem mass spectra (MS/MS) indicates that they may not corresponding to these species. Specifically, the azide-copper-acetylide adducts are expected to lose the weakly coordinated N_3EG_4 before the dissociation of any covalent bonds. However, dissociation of the weak non-covalent $\text{Cu}-\text{N}_3\text{EG}_4$ interaction, even at the lowest collision energy for obtaining any fragment, was not observed. One should also consider the possibility that the azide may form nitrene by losing N_2 from N_3EG_4 . If this process preceded the dissociation of N_3EG_4 from the copper complex, N_3EG_4 and Cu^+ could be lost as $\text{N}_2 + \text{Cu}^+$ -nitrene complex (Scheme 3-4). This process may be promoted by coordination of the azide with Cu^+/Na^+ . Indeed, major secondary ion of N_3EG_4 corresponding to the loss of N_2 dominated upon addition 0.5 equiv. of copper(I) and Na-ascrobate (Figure 3-13). However, the required collision energy was substantially lower than that for the fragmentation of the ions from the reaction mixture (CID = 26%, vs 30% – 36%). Also, we only found the sodium adduct of N_3EG_4 without any copper adducts, indicating that the coordination of N_3EG_4 with copper(I) was weak. Therefore, the new ions detected in Figure 3-3B are unlikely to be the azido-copper adducts, although we cannot completely exclude this possibility. The harder detection of azide-acetylide-copper(I) precursor complexes (**IIc1** & **IIIb1**, Scheme 3-2 & Scheme 3-3) in our

system indicated that their formation from **IIb** and **IIIa** is endothermic, in agreement with results from computational studies.^{42, 48-49, 53}

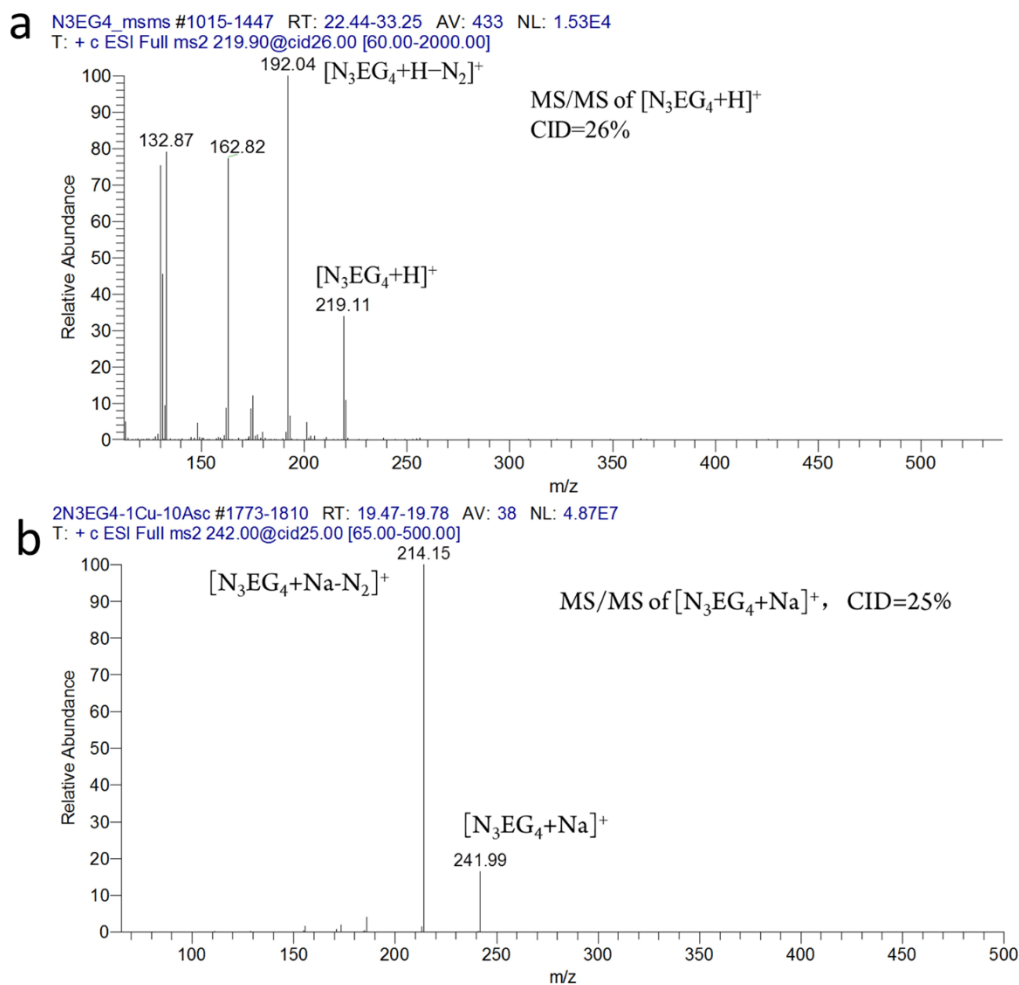


Figure 3-13 MS/MS spectra of azido-tetraethylene glycol (N_3EG_4). Infused solution concentrations: (a) 100 μM N_3EG_4 . (b) 100 μM N_3EG_4 , 50 μM CuSO_4 and 500 μM Na ascorbate. Each MS/MS spectra was obtained by collision-induced dissociation (CID), and represents an average of about 100 individual scans during the direct infusion of N_3EG_4 solution (100 μM) or N_3EG_4 -copper(I) solution (100 μM N_3EG_4 , 50 μM CuSO_4 and 500 μM Na ascorbate).

On the other hand, the signals assigned to **IIc** and **IIIb** were unlikely contributed by the proposed isobaric copper metallacycle intermediates (**IIc2** & **IIIb2**, Scheme 3-3) due to their high

instability. Indeed, the previously proposed copper metallacycle intermediates have not been detected. DFT calculations have shown that these intermediates reside at a much-higher energy state compared to the azido-copper acetylide adducts, and have a small barrier to irreversibly form the triazole product.⁴⁸⁻⁴⁹

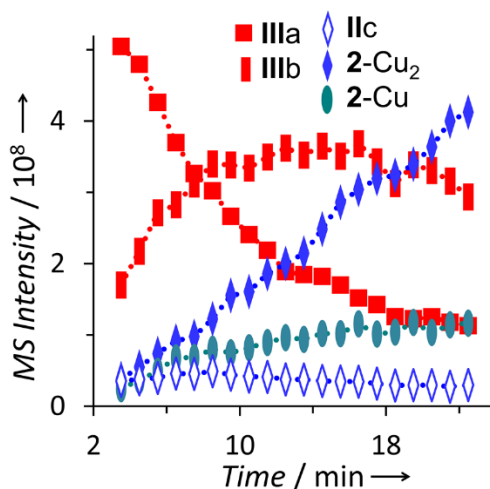
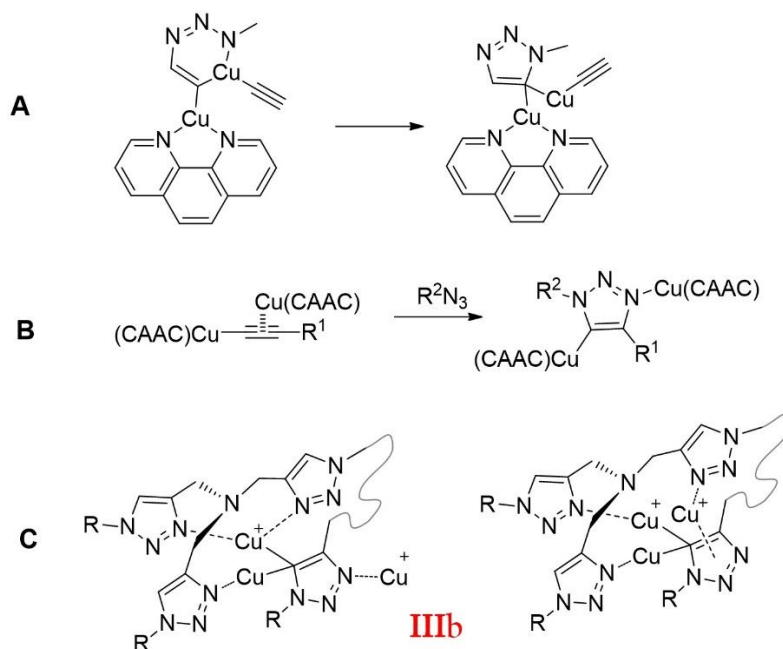


Figure 3-14 Time course of ESI-MS intensities of the assigned intermediates during the reaction of **1** with N_3EG_4 . Conditions: 100 μM **1**, 300 μM $CuSO_4$, 100 μM N_3EG_4 and 1 mM Na-Ascorbate in deoxygenated water at room temperature. For the labels, see Scheme 3-2.

To probe the reactivity of the unprecedented tri-copper acetylide **IIIa**, we first investigated its reactivity by monitoring the reaction of the Cu/**1** 3:1 mixture (containing ~86% **IIIa**, Table 3-1) with 1 equiv. of N_3EG_4 . As shown in Figure 3-14, the MS intensity of **IIIa** dropped drastically over the first 10 min, accompanied by a rapid increase of the Cu^I_3 -triazolide **IIIb** whose signal intensity exceeded that of **IIIa** after 10 min, and then decreased after ~15 min. Consumption of **IIIa** and accumulation of **IIIb** as the most abundant intermediate were faster than formation of the copper(I)-triazole complexes **2-Cu₂** and **2-Cu** possibly via hydrolysis of **IIIb** to the transient **2-Cu₃** and dissociation of copper(I) from **2-Cu₃** to **2-Cu₂**, or from **IIIb** to **IIc** followed by hydrolysis (Scheme 3-2).



Scheme 3-5 (A) Proposed structures of stable di-copper triazolide intermediate with both copper(I) bound to the C(5) via a 3-center 2-electron bond.⁴⁸ (B) A di-(CAAC-copper) triazolide isolated following the reaction of a di-(CAAC-copper) acetylide with an azide, in which the two copper atoms bound to C(5) and N(3) of the triazolide, respectively.⁵² In this case, it is not clear whether the CAAC-copper(I) on N(3) was originally dissociated from the metallacycle or later from the 3-center 2-electron bond to C(5) of the triazolide. (C) The proposed coordination mode of the tri-copper triazolide **IIIb** analogous to the di-copper triazolide. The two Cu atoms may bind to C(5) via a 3-center-2-electron bond, while the third copper atom may coordinate to the N(3) or the triazolide ring. The formation of 3-center 2-electron bond might be disfavored due to the large steric hindrance of the two CAAC ligands in B, but in our case the coordination could be established with little steric hindrance by the ligand.

Although mono-copper triazolide intermediates from CuAAC reaction have been isolated,⁷⁹⁻⁸⁰ unless protected by a hydrophobic environment such as an interlocked rotaxane, these species are highly labile to hydrolysis.⁸⁰ In fact, they were not observed here and in a reported system using ESI-MS,⁸⁵ but the di-copper triazolides were detected in both cases. In several theoretical studies, triazolides were proposed to form from an azide-Cu₂-acetylide adduct through stepwise formation

of two C-N bonds with the second step involving a six-membered copper metallacycle (**IIc2**, Scheme 3-3).^{46, 48-49} In the previously proposed di-copper pathway, accompanying the formation of the second C–N bond, the two copper atoms either remain bonding to C(5) of the resultant triazolide via a 3-center 2-electron bond (Scheme 3-5A),⁴⁸⁻⁴⁹ or one of them dissociates (Scheme 3-5B).^{40, 43, 52, 85} For the latter, the dissociated Cu(I) may then coordinate to N(3), as found in the isolated di-(CAAC-Cu) triazolide,⁵² in which the two copper atoms coordinated to C(5) and N(3) of the triazolide, respectively. For the former, computational studies have indicated that such intermediates are thermodynamically stable.⁴⁸⁻⁴⁹ Nevertheless, they have never been isolated, presumably due to their liability to hydrolysis and/or copper-dissociation in water. It is worth noting that 3-center 2-electron bonds are common in organocopper compounds, such as mesitylcopper¹⁸⁴ and bridged copper(I) hydrides.¹⁵⁰⁻¹⁵¹

In contrast to the above di- and mono-copper triazolides, tri-copper triazolides have not been mentioned in the literature. The structure of **IIIb** could be analogous to the proposed di-copper triazolide,⁴⁸⁻⁴⁹ in which two Cu atoms bind to C(5) via a 3-center 2 electron bond, while the third Cu atom may coordinate to the triazolide ring or to N(3). The coordination mode of Cu₃-triazolide **IIIb** is tentatively proposed in Scheme 3-5C. The susceptibility of triazolides towards protonation is expected to decrease with increasing number of coordinating copper(I) ions that reduce the electron density of the triazolide. Hence, the rapid accumulation of tri-copper triazolide **IIIb** in the first 15 min was attributable to its relatively slow hydrolysis (generating **2-Cu₃**) and/or copper dissociation (generating **IIc**). Hydrolysis of **IIIb** would be simultaneously accompanied by the dissociation of Cu(I) to give **2-Cu₂**, since the elusive tri-copper complex **2-Cu₃** was not found in the reaction mixture. The di-copper triazolide **IIc** was detectable but exhibited a low intensity throughout the reaction (Figure 3-15), and the copper(I)-triazolide **Ic** was not detectable.

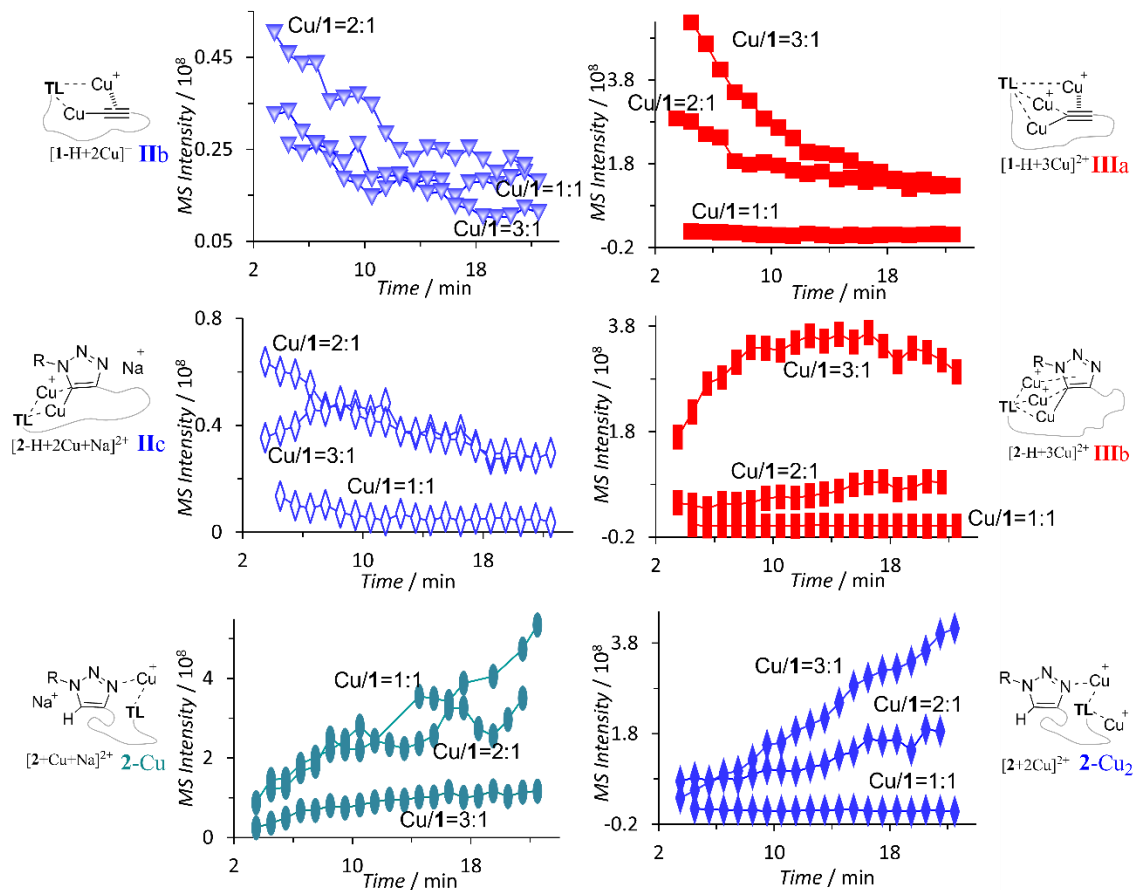


Figure 3-15 MS signal intensities of selected copper(I)-containing intermediates in reaction of **1** (100 μM) and 1, 2 or 3 equiv. of copper(I) (generated from CuSO_4 and Na ascorbate) with 1 equiv. of N_3EG_4 .

3.2.3 Quantitative Analysis of CuAAC Reactivity of Di-copper(I) and Tri-copper(I)

Acetylide

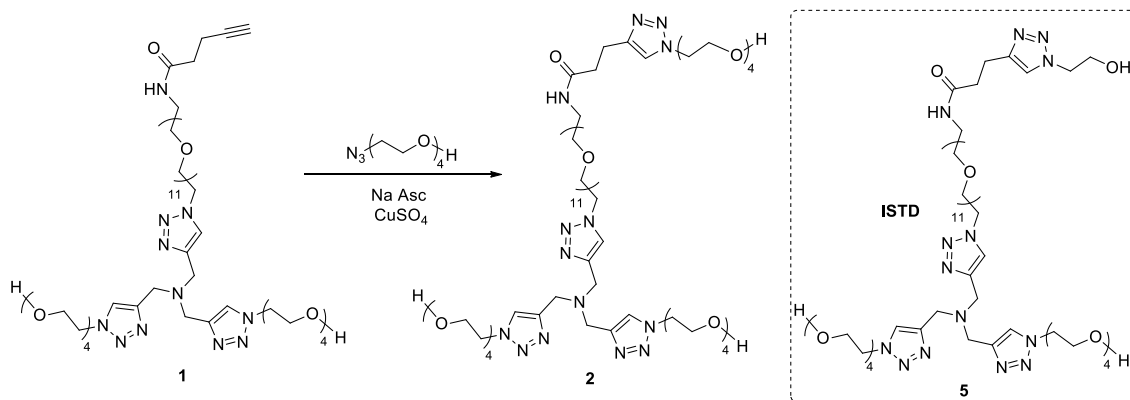
We next compared the the reactivity of Cu_3^1 -acetylide **IIIa** with the di-nuclear Cu_2^1 -acetylide **Ib**, which is proposed in the di-copper pathway in literature (Scheme 3-3).^{30, 40, 42, 46, 48-49, 100, 185} To facilitate comparison, we performed optimization to enrich **Ib** in the mixture (Figure 3-8). Addition of 5 equiv. NaOH to the **1**/copper(I) 1:2 solution gave the highest percentage of **Ib**

(67%, Table 1) in the mixture; further addition of NaOH promoted the formation of dimers and CuOH.

Table 3-1 MS Intensities of the copper(I)-acetylides in Ligand **1** System and Observed Rate Constants vs. Calculated Rate Constants Based on Fittings of the Respective Rate Constants of k'_{II} and k'_{III} .

Cu/1	MS intensity / 10 ⁷				Calculated Values				Fitted $k_{cat} / M^{-1} \cdot s^{-1}$	Measured $k_{obs} / M^{-1} \cdot s^{-1}$	IIIa % contribution to overall k
	Ia/Ib	IIb	IIIa	IIa	x_{IIb}	k'_{II}	x_{IIIa}	k'_{III}			
1:1	149	1.5	0.8	5.3	0.0096	783	0.0051	27	7.6	8.5	2
2:1	45.1	5.4	43.7	31.6	0.0429	783	0.3474	27	43.0	41	22
3:1	4.3	4.7	132	12.3	0.0307	783	0.8611	27	47.3	47	49
1:1+NaOH	47.2	45.9	0	0	0.4930	783	0.0000	27	386.0	386	0
2:1+NaOH	40.2	67.2	0.8	0.7	0.6171	783	0.0073	27	483.4	471	0
6:1+NaOH	1.2	6.3	185	5	0.0319	783	0.9367	27	50.3	38	50

The stoichiometric reactions of **1** with N₃EG₄ in the presence of 1–6 equiv. of copper(I) (and 5 equiv. of NaOH) in deoxygenated water (Figures 3-16, and Table 3-1) were conducted in an anaerobic chamber at room temperature, and the reaction yields were quantitatively measured by LC-MS using compound **5** (structure similar to **2**) as internal standard (Scheme 3-6).



Scheme 3-6 Quantitative Analysis of CuAAC Reactivity of Tri-copper(I) Acetylide **IIIa** and Di-copper(I) Acetylide **IIb**.

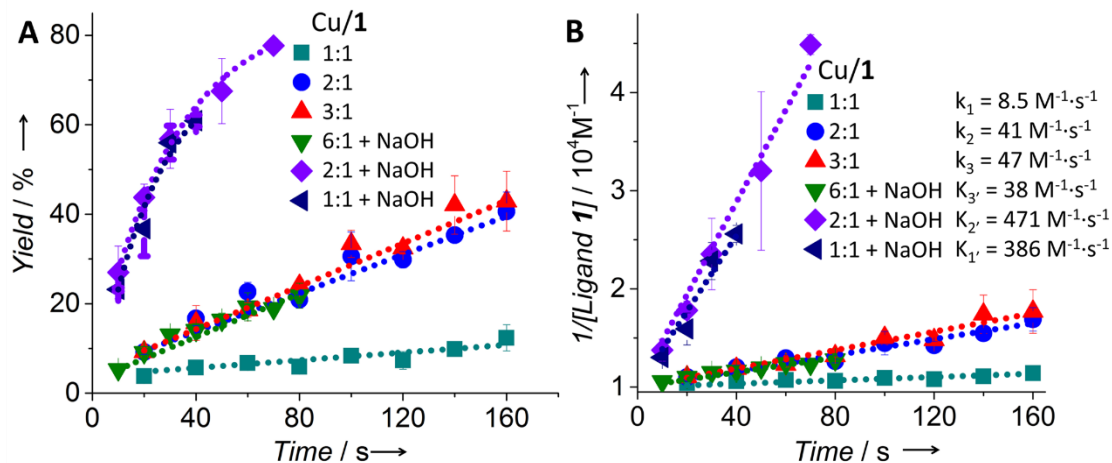


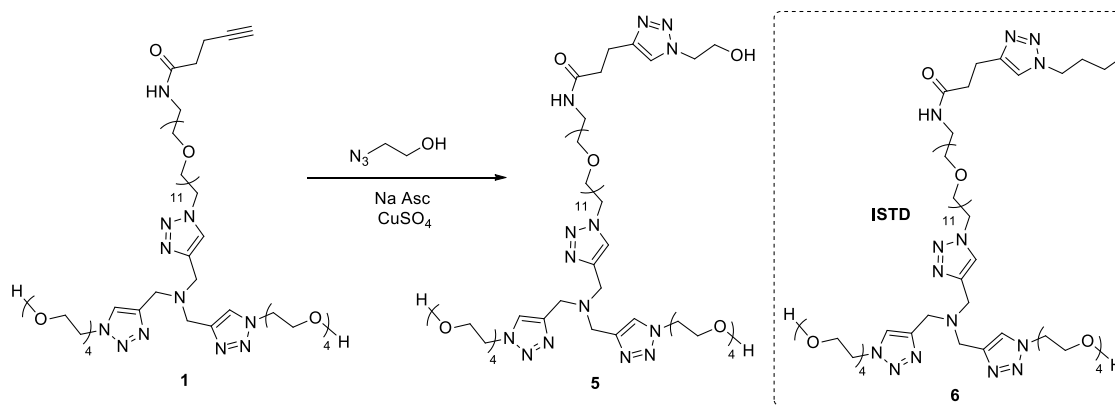
Figure 3-16 Apparent second-order rate constants for reaction of **1** with N_3EG_4 quantitatively measured by LC-MS. Conditions: $100 \mu\text{M}$ **1**, $100 \mu\text{M}$ N_3EG_4 and 1 mM Na-ascorbate in deoxygenated water at room temperature, with: $100 \mu\text{M}$ CuSO_4 (cyan); $200 \mu\text{M}$ CuSO_4 (blue); $300 \mu\text{M}$ CuSO_4 (red); $600 \mu\text{M}$ CuSO_4 & $500 \mu\text{M}$ NaOH (green); $200 \mu\text{M}$ CuSO_4 & $500 \mu\text{M}$ NaOH (purple); and $100 \mu\text{M}$ CuSO_4 & $500 \mu\text{M}$ NaOH (navy).

The apparent second-order rate constants (k_{obs}) were then determined from the rate curve of each reaction (Figure 3-16). According to most theoretical calculations, the highest barrier for CuAAC reaction is the first C-N bond formation from the acetylide-Cu₂-azide adduct.^{42, 48-49, 53} Assuming the rate-limiting step is the first C-N bond formation from the Cu-acetylide-azide adduct, derived from a generalized pre-equilibrium approximation method,¹⁸⁶ Eq. (1) can be used to extract the apparent rate constants for the transformation of **IIb** to **IIc** (k'_{II}) and **IIIa** to **IIIb** (k'_{III}) from the data in Table 3-1:

$$k_{obs} = x_{IIb}k'_{II} + x_{IIIa}k'_{III} \quad \text{Eq. (1)}$$

in which x_{IIb} and x_{IIIa} are the molar fraction of **IIb** and **IIIa** in each solution derived from the ESI-MS intensities of the intermediates; $k'_{II} = K_2k_{II}$ and $k'_{III} = K_3k_{III}$, where K_2 and K_3 are the equilibrium constants of **IIb** to **IIc1** and **IIIa** to **IIIb1** (Scheme 3-2), and k_{II} and k_{III} are the rate constants for **IIc1** to **IIc** and **IIIb1** to **IIIb**. Fitting the data using Eq (1) gives $k'_{II} = K_2k_{II} = 783 \text{ M}^{-1}\cdot\text{s}^{-1}$

$^1\text{s}^{-1}$ and $k'_{\text{III}} = K_3 k_{\text{III}} = 27 \text{ M}^{-1}\text{s}^{-1}$, and a good agreement of the calculated rate constants k_{cal} with the measured k_{obs} (Table 3-1).



Scheme 3-7 Kinetic Studies for Reaction between **1** and 2-Azidoethanol w/ Various Amount of Copper(I).

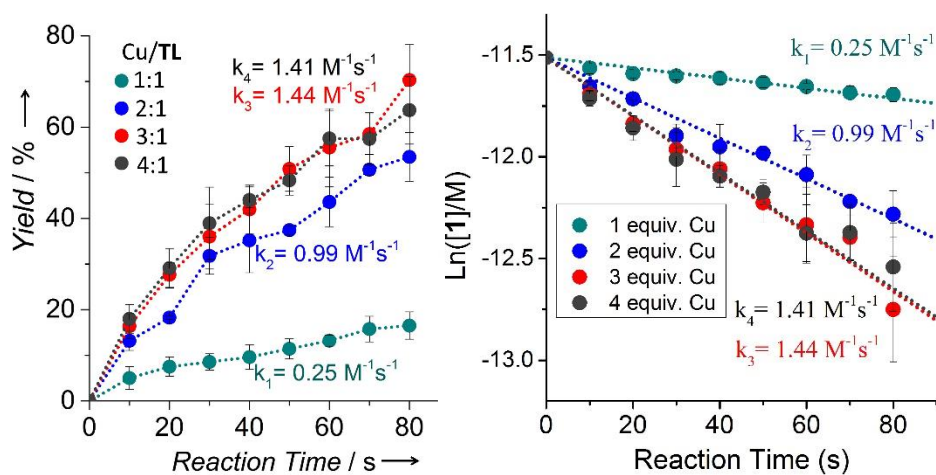


Figure 3-17 (A) Reaction yield vs. time plot of reaction between **1** ($10 \mu\text{M}$) and 1–4 equivalent copper(I) (generated from CuSO_4 and Na ascorbate) with excess amount of 2-azidoethanol (1 mM). (B) Natural logarithm of concentration of **1** vs time at different copper(I) stoichiometry. Second-order rate constants are calculated based on pseudo-first order reaction condition.

Kinetic studies for reaction of **1** ($10 \mu\text{M}$) and 1–4 equivalent copper(I) (generated from CuSO_4 and Na ascorbate) with excess amount of 2-azidoethanol (1 mM) (pseudo-first order reaction)

was also performed at 0 °C (Scheme 3-7). We observed a substantial increase of the rate for the formation of product (Figure 3-17), which further confirmed the tri-copper acetylide **IIIa** to be an active intermediate in the tri-copper(I) pathway involving three copper atoms for the formation of **IIIb**.

3.3 Mechanistic Studies in Aqueous Solutions under Catalytic Condition

The above measurement of the rate constants k'_{II} and k'_{III} was realized by using the alkyne-TL conjugate **1** with a long flexible EG₁₁ linker that entropically stabilized the TL-Cu_n^I-acetylides (**IIIa** & **IIb**) and yet did not affect the activation energy for the C-N bond formation. This model system exhibited a much higher k_{obs} (41–471 M⁻¹•s⁻¹) compared to the previously reported value ($k_{obs} = 0.002–3.5$ M⁻¹•s⁻¹) for TL ligands under catalytic conditions, in which excess alkyne can inhibit the formation of multi-nuclear copper(I) species and decrease their molar fraction.⁴³

3.3.1 Ligand Design

The TL ligand (Scheme 3-1) was employed as an independent ligand for studying its accelerating mechanism under catalytic condition. A water-soluble alkyne **3** (Figure 3-18) bearing a tetra-ethylene glycol substitution group was used as the reagent.

3.3.2 Intermediate Detection and Characterization

3.3.2.1 Copper(I)-acetylide Complexes Solution Equilibria

As shown in the ESI-MS (Figures 3-18A), addition of the free alkyne **3** even in slight excess (**3**/Cu 10:6) to the copper(I)/TL 3:1 solution generated a significant amount of mono-Cu-alkyne (**3**-copper(I)), TL-copper(I) complexes, and the Cu-acetylide aggregates, which were low in reactivity and led to a large decrease of the overall k_{obs} (*vide infra*).⁷⁸ The active acetylides TL-

Cu¹-acetylide (**ii**a, [3-H+TL+2Cu]²⁺, Scheme 3-8) and TL-Cu¹-acetylide (**iii**a, [3-H+TL+3Cu]²⁺) were present in the range of 2%–27% among all copper(I) complexes in the system (Table 3-2). Kinetic studies for reaction between **3** (100 μM) and N₃EG₄ (100 μM) catalyzed by various amount of copper(I) (30, 60, 90, 120, 180, 240, 300 μM), Cu/TL (1:1, 2:1, 3:1) were performed and the observed fractional rate orders in [Cu] in reaction of **3** with N₃EG₄ (Figure 3-18B) is in agreement with the low concentration of active copper(I) acetylides.

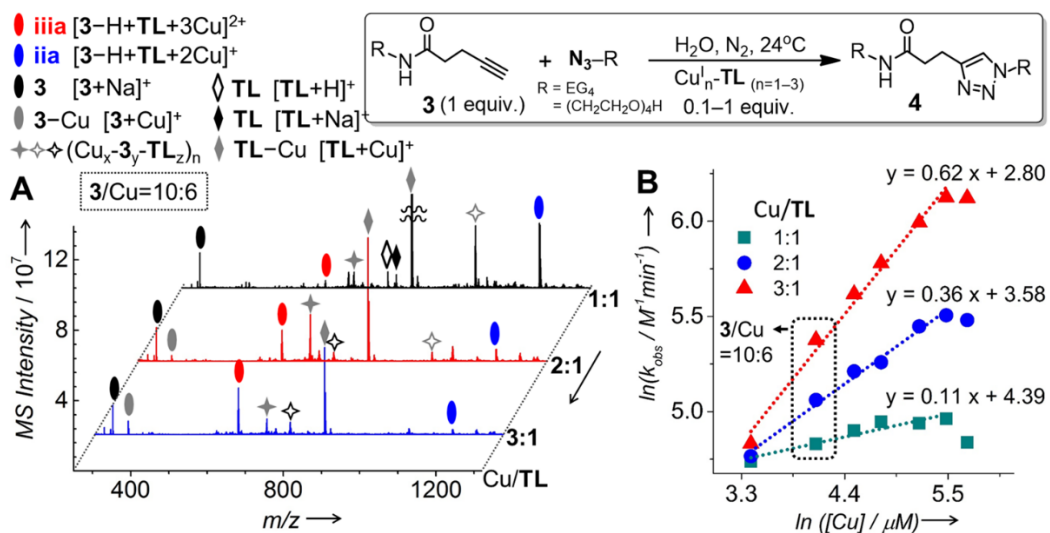
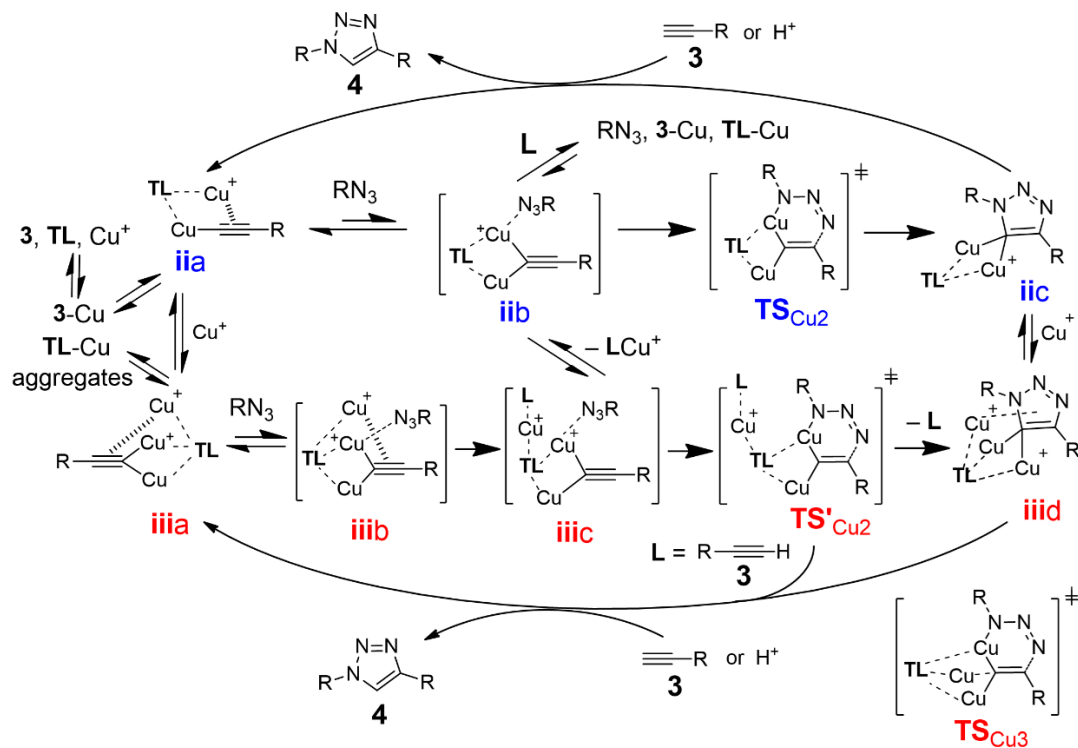


Figure 3-18 (A) ESI-MS spectra for the solutions of **3** (100 μM), TL (20, 30, 60 μM), and copper(I) (60 μM) (generated from CuSO₄ and Na-ascorbate (0.5 mM)) in deoxygenated water. For assignment of the labeled ions, see Figure 3-25. (B) Effect of copper(I)/TL ratio on CuAAC reaction rate under catalytic conditions, a rate order plot: **3** (100 μM), N₃EG₄ (100 μM), copper(I) (30, 60, 90, 120, 180, 240, 300 μM), Cu/TL (1:1, 2:1, 3:1).

Table 3-2 The MS Intensity of copper(I)-acetylides in solution containing 100 μM **3**, 60 μM copper(I), and 20/30/60 μM TL.

Cu/TL	MS intensity / 10 ⁷					
	[3-H+TL+3Cu] ²⁺	[3-H+TL+2Cu] ²⁺	[TL+Cu] ⁺	[2x3-2H+4TL+6Cu] ⁴⁺	[4x3-2H+2TL+6Cu] ⁴⁺	[2x3-2H+4TL+8Cu] ⁶⁺
1:1	0.29	2.85	15.2	2.4	0	0.74
2:1	1.78	0.69	7	0.51	0.52	2.68
3:1	2.61	0.27	5	0.11	0.67	1.1



Scheme 3-8 Proposed mechanism for the CuAAC reaction of **3** and RN_3 ($\text{R} = \text{EG}_4$) in the presence of catalytic amount of $\text{Cu}^{\text{I}}/\text{TL}$. Intermediates in a bracket were not detectable. L = ligands **3** and TL , etc.

3.3.2.2 Intermediate Detection in the Reaction Between the 3-copper(I) Complexes and Azide

To study the intermediates of the CuAAC reaction under catalytic condition, we added 1 equiv. of N_3EG_4 into the solutions of **3** (100 μM), TL (20, 30, 60 μM), and copper(I) (60 μM), and infused the mixtures to ESI-MS. Figure 3-19 shows the averaged total ion MS spectra obtained during the reaction (5–10 min). The ESI-MS spectra showed a detectable amount of both $\text{TL}-\text{Cu}^{\text{I}}_3$ -triazolide **iiid** [$\text{4-H}+\text{TL}+3\text{Cu}$] $^{2+}$ and $\text{TL}-\text{Cu}^{\text{I}}_2$ -triazolide **iic** [$\text{4-H}+\text{TL}+2\text{Cu}$] $^+$. In addition to the ligand stabilized copper(I)-triazolides, we also observed a Cu^{I}_2 -acetylide-triazole complex generated after the product formation ($[\text{3-H}+\text{4}+2\text{Cu}]^+$). The assignment was supported by the isotopic

distributions (Figure 3-27) and fragmentation patterns in the tandem mass spectra (MS/MS) (Figure 3-29).

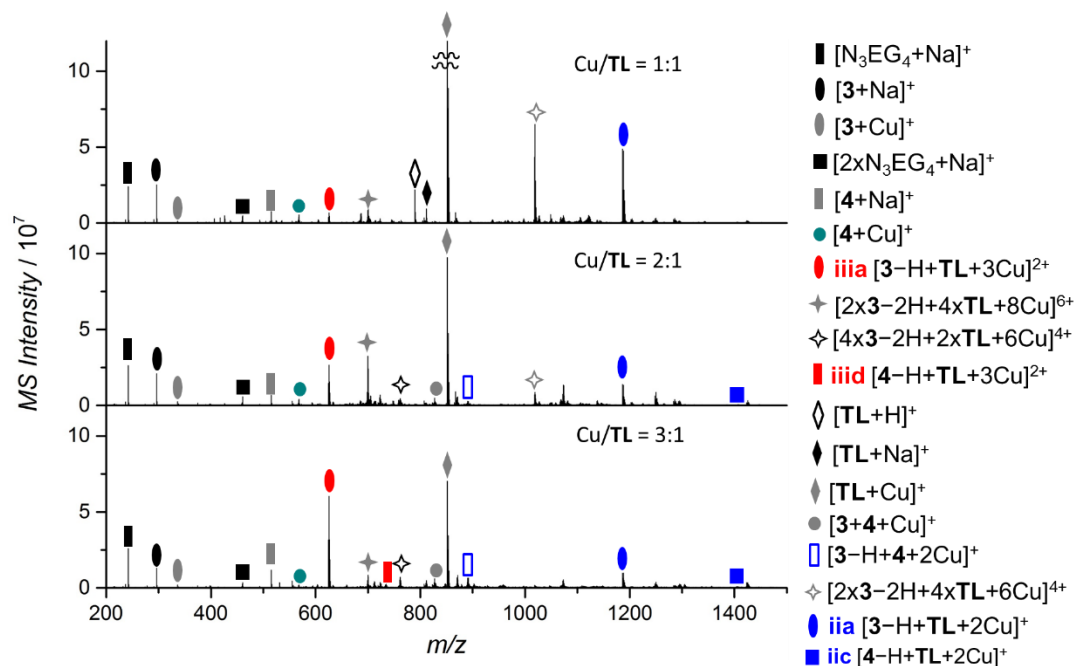


Figure 3-19 ESI-MS Spectra of Intermediates in Reaction between **3** and N_3EG_4 at **3**/Cu 10:6. Concentrations: **3** (100 μ M), copper(I) (30, 60, 90, 120, 180, 240, 300 μ M), Cu/TL (1:1, 2:1, 3:1).

3.3.3 Quantitative Analysis of CuAAC Reactivity of Di-copper(I) and Tri-copper(I) Acetylide Under Catalytic Condition

Kinetic studies for reaction between **3** (100 μ M) and N_3EG_4 (100 μ M) catalyzed by various amount of copper(I) (30, 60, 90, 120, 180, 240, 300 μ M), Cu/TL (1:1, 2:1, 3:1) were performed and the apparent second-order rate constants (k_{obs}) were determined from the rate curve of reactions (Figure 3-20A).

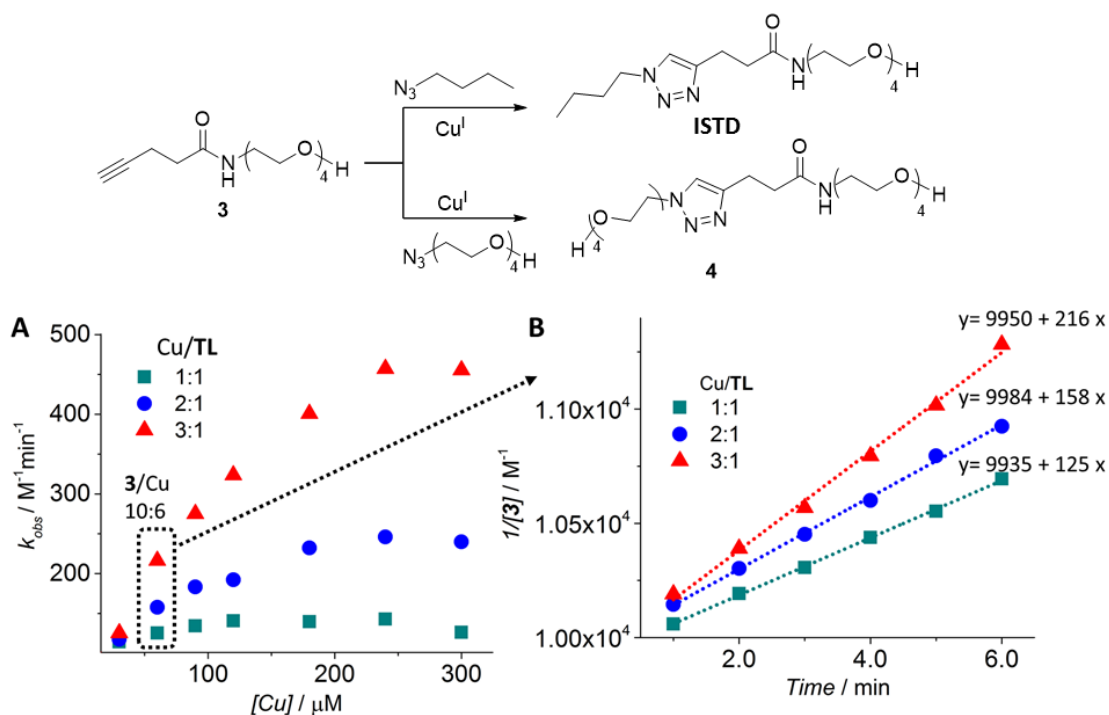


Figure 3-20 Kinetic Studies for Reaction between **3** and N_3EG_4 with Various Amount of copper(I). (A) Reaction rate dependence of **3** with N_3EG_4 on concentration of Cu (k_{obs} data of Figure 3-18B). Concentrations: **3** (100 μM), N_3EG_4 (100 μM), copper(I) (30, 60, 90, 120, 180, 240, 300 μM), Cu/**TL** (1:1, 2:1, 3:1). (B) Second-order rate constants k_{obs} fitting at condition: **3** (100 μM), N_3EG_4 (100 μM), copper(I) (60 μM), Cu/**TL** (1:1, 2:1, 3:1).

We assumed that all the **TL**-containing ions have a similar MS intensity-concentration response factor (f).

$$I = C \times f \quad \text{Eq. (2)}$$

Where C and I are the concentration and MS intensity of detected **TL**-containing ions, f is the MS intensity-concentration response factor of $[TL-Cu]^+$ ion. The high stability of $[TL-Cu]^+$ ion allows us to determine its response factor in aqueous solution ($(1.0 \pm 0.1) \times 10^7 \mu M^{-1}$). Thus, the concentrations of **ia** ($[3-H+TL+2Cu]^+$) and **iii** ($[3-H+TL+3Cu]^{2+}$) were calculated using

Equation 2. The molar fraction of **ii**a ($x_{\text{ii}a}$) and **iii**a ($x_{\text{iii}a}$) in total alkyne species were calculated based on Equation 3.

$$x_{\text{ii}a} = C_{\text{ii}a}/C_{\text{alkyne}} ; x_{\text{iii}a} = C_{\text{iii}a}/C_{\text{alkyne}} \quad \text{Eq. (3)}$$

The respective rate constants of **ii**a (k'_{II}) and **iii**a (k'_{III}) were fitted based on Equation (1)

$$k_{\text{obs}} = x_{\text{ii}a}k'_{\text{II}} + x_{\text{iii}a}k'_{\text{III}} \quad \text{Eq. (1)}$$

Remarkably, the apparent rate constants $k'_{\text{II}}/k'_{\text{III}}$ ratio drastically dropped from 29 in the model system to 0.38 in the catalytic system (Tables 3-3), showing a greatly enhanced contribution to k_{obs} by the tri-Cu acetylide **iii**b. Compared to the di-Cu acetylide **ii**b, the tri-Cu acetylide **iii**b is expected to have stronger interaction with the negatively charged internal nitrogen of azide.^{30, 96, 100-101, 185, 187} As illustrated in Scheme 3-8, ligand coordination to the tri-Cu-azide adduct **iii**b will facilitate the dissociation of a Cu^{I} (internally) from the acetylide **iii**c to generate a di-Cu transition state TS_{Cu_2} via **ii**b or TS'_{Cu_2} (through the internal dissociation) for C-N bond formation. Furthermore, the triazolides **ii**c and **iii**d (detected by ESI-MS, Figure 3-19) may serve as a base to deprotonate the alkyne **3**, especially those formed from TS'_{Cu_2} in which the coordinated alkyne is proximal to the triazolide, to generate the product **4** and regenerate the copper acetylides **ii**a and **iii**a (Scheme 3-8).

Table 3-3 Observed Rate Constants vs. Calculated Rate Constants Based on Fittings of the Respective Rate Constants of k'_{II} and k'_{III} in Reaction between **3** and N_3EG_4 at **3**/Cu 10:6.

Cu/TL	Calculated Values						Fitted k_{cal} / $\text{M}^{-1}\cdot\text{s}^{-1}$	Measured k_{obs} / $\text{M}^{-1}\cdot\text{s}^{-1}$
	$C_{\text{iii}a}$ μM^{-1}	$x_{\text{iii}a}$	k'_{III} $\text{M}^{-1}\cdot\text{s}^{-1}$	$C_{\text{ii}a}$ μM^{-1}	$x_{\text{ii}a}$	k'_{II} $\text{M}^{-1}\cdot\text{s}^{-1}$		
1:1	0.26	0.0026	146	2.59	0.026	55	2.09	2.1
2:1	1.62	0.016	146	0.62	0.0062	55	2.45	2.6
3:1	2.37	0.024	146	0.24	0.0024	55	3.74	3.6

Increasing the **3**/copper(I) ratio to 100:6 (Figure 3-21 and Figure 3-22) further decreased the contribution of di-copper(I) acetylide, with a ratio of k'_{II}/k'_{III} dropped to 0.20 (Table 3-4). It suggested increasing competition from **L** coordination to **iiib** and **iib**, in which **iib** was more influenced.

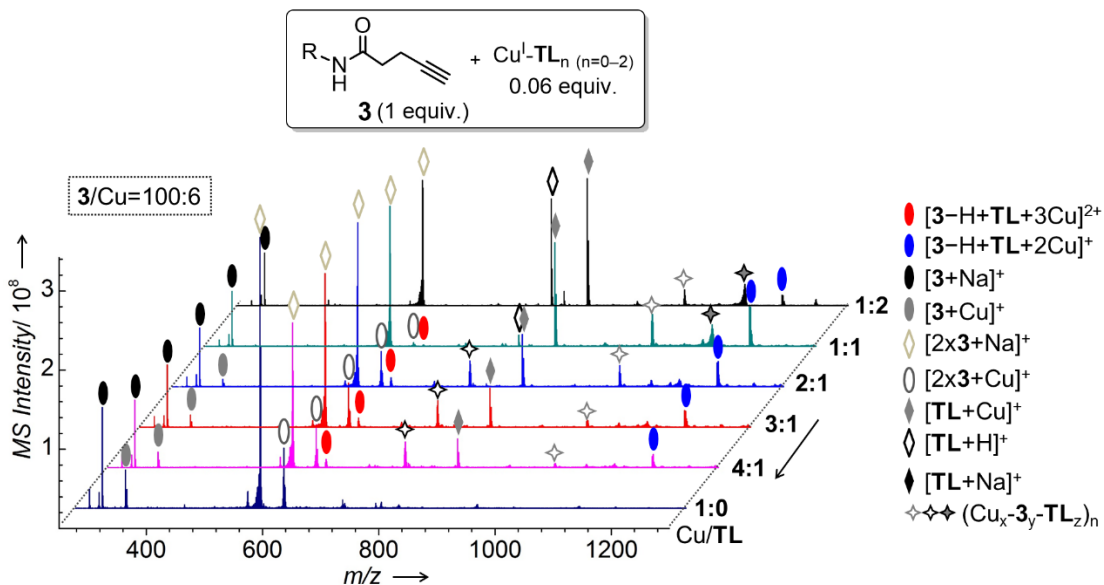


Figure 3-21 ESI-MS spectra for the solutions of **3** (1 mM), **TL** (0, 15, 20, 30, 60, 120 μ M), and copper(I) (60 μ M) (generated from CuSO_4 and Na-ascorbate (0.5 mM)) in deoxygenated water. For assignment of the labeled ions, see Figure 3-25 and 3-26.

Table 3-4 The MS Intensity of copper(I)-acetylides in solution containing 1 mM **3**, 60 μ M copper(I), and 15/20/30/60 μ M **TL** (Figure 3-21); the molar fraction of **iiia** (x_{iiia}) ($[\mathbf{3-H+TL+2Cu}]^+$) and **iiiia** (x_{iiiia}) ($[\mathbf{3-H+TL+3Cu}]^{2+}$) calculated from the MS intensities; and the fitted respective rate constants of k'_{II} and k'_{III} based on Equation (1) and the apparent rate constant k_{obs} in reaction with 100 μ M N_3EG_4 (Figure 3-22).

Cu/TL	MS intensity / 10^7						Fitted $k_{\text{cal}} / \text{M}^{-1}\cdot\text{s}^{-1}$	Measured $k_{\text{obs}} / \text{M}^{-1}\cdot\text{s}^{-1}$
	$[\mathbf{3-H+TL+3Cu}]^{2+}$	$[\mathbf{3-H+TL+2Cu}]^+$	$[\mathbf{TL+Cu}]^+$	$[\mathbf{2x3-2H+4TL+6Cu}]^{++}$	$[\mathbf{4x3-2H+2TL+6Cu}]^{++}$	$[\mathbf{2x3-2H+4TL+6Cu+2NaAsc}]^{++}$		
1:1	0.16	5.03	13.1	4.09	0.32	2.68		
2:1	1.14	3.15	6.61	2.69	3.26	0.96		
3:1	1.15	2.08	4.9	0.87	4.38	0		
4:1	1.03	1.64	3.7	0.67	3.84	0		
Cu/TL	Calculated Values						Fitted $k_{\text{cal}} / \text{M}^{-1}\cdot\text{s}^{-1}$	Measured $k_{\text{obs}} / \text{M}^{-1}\cdot\text{s}^{-1}$
	$C_{\text{iiiia}} \mu\text{M}^{-1}$	x_{iiiia}	$k'_{\text{III}} \text{M}^{-1}\cdot\text{s}^{-1}$	$C_{\text{iiia}} \mu\text{M}^{-1}$	x_{iiia}	$k'_{\text{II}} \text{M}^{-1}\cdot\text{s}^{-1}$		
1:1	0.14	0.00014	260	4.57	0.00457	53	0.28	0.29
2:1	1.04	0.00104	260	2.86	0.00286	53	0.42	0.40
3:1	1.04	0.00104	260	1.89	0.00189	53	0.37	0.38
4:1	0.94	0.00094	260	1.49	0.00149	53	0.32	0.39

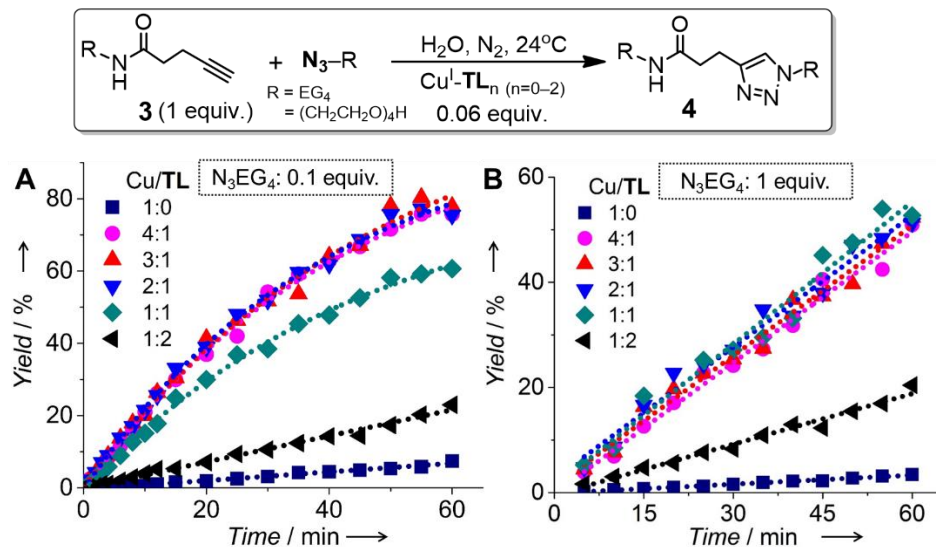


Figure 3-22 Effect of $\text{Cu}^{\text{I}}/\text{TL}$ ratio on reaction rate under catalytic conditions: **3** (1 mM), N_3EG_4 (0.1 mM in A and 1 mM in B), copper(I) (60 μ M), **TL** (0, 15 μ M, 20 μ M, 30 μ M, 60 μ M, 120 μ M).

Even though the concentrations of **TL**-Cu^I_n-acetylides (n = 2,3) were low, the kinetic profiles of the reaction between **3** and N₃EG₄ showed a vast rate enhancement by **TL** (Figure 3-22), consistent with the role of **TL** to stabilize the di- and tri-copper acetylides that were not detected in the absence of **TL** (Figure 3-21).

3.4 Comparison of Copper(I)-Chelating Ability of Tris-, Bis-, and Mono-(triazolymethyl)amine Ligands in Aqueous Solutions

Compared to the tris(triazolymethyl)amine ligands, mono- and bi-dentate triazoles prefer to coordinate only one mole equivalent rather than two or more metals ions.¹⁰⁸ To study the synergistic interaction of these ligands with alkyne on copper(I) chelation, we synthesized two additional alkyne-ligated ligands bearing mono(triazolymethyl)amine and bis(triazolymethyl)amine moiety (ligand (**Tr**)₁ and (**Tr**)₂, respectively, Chart 3-1).

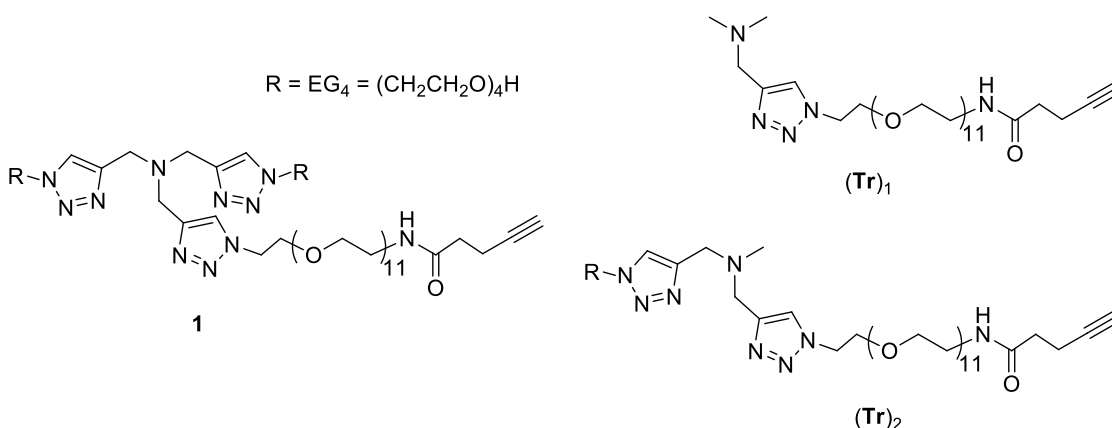


Chart 3-1 Structure of mono- and bis-(triazolymethyl)amine-alkyne compounds

The mono- or bis-triazole ligands (1 equiv.) were mixed with copper(I) salt (Cu(MeCN)₄PF₆) in MeCN, the solution of which were lyophilized to completely remove MeCN, and then the residues were re-dissolved in water in an anaerobic chamber to make 500 μM stock solutions,

which were further diluted to 100 μM with addition of excess sodium ascorbate to keep the copper(I) oxidation state, and directly infused into the ESI-MS source for detection of copper(I)-acetylide complexes.

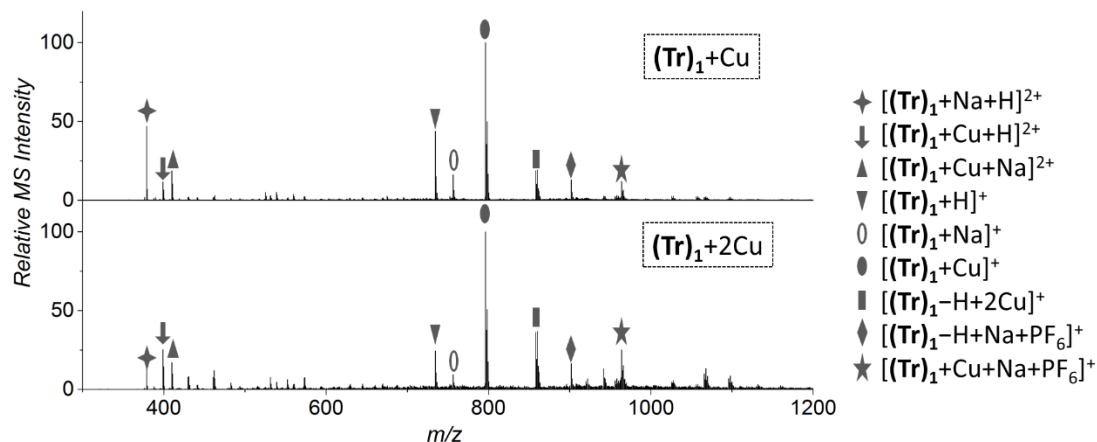


Figure 3-23 ESI-MS spectra for the solutions of $(\text{Tr})_1$ (100 μM), $\text{Cu}(\text{MeCN})_4\text{PF}_6$ (100 or 200 μM), and Na ascorbate (0.5 mM) in deoxygenated water.

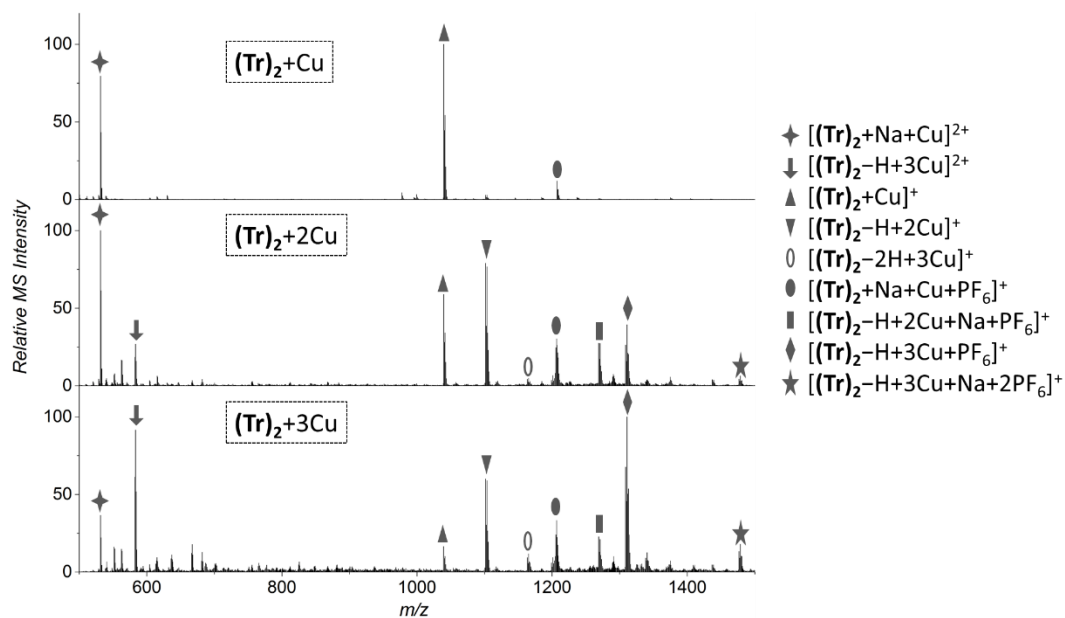


Figure 3-24 ESI-MS spectra for the solutions of $(\text{Tr})_2$ (100 μM), $\text{Cu}(\text{MeCN})_4\text{PF}_6$ (100, 200, or 300 μM), and Na ascorbate (0.5 mM) in deoxygenated water.

As shown in Figure 3-23, the mono-triazole ligand (**Tr**)₁ predominantly stabilizes one mole equivalent of copper(I). Only a small amount of di-copper(I) complex (rectangular, Figure 3-23) was observed. In contrast, the bis-triazole ligand (**Tr**)₂ is able to stabilize up to three equivalent of copper(I) at a copper(I)/ligand ratio ≥ 2 (Figure 3-24). Similar to the tris-triazole ligand **1**, the tri-copper(I) acetylide complex of (**Tr**)₂ also appears in the solution with two equivalent of copper(I), and becomes the major species at a copper(I)/ligand ratio = 3. However, the stability of the tri-copper(I)-acetylide (**Tr**)₂ complex is evidently lower than that of ligand **1**, indicating the importance of the third triazole arm of ligand **1** in multi-copper(I) stabilization.

3.5 Conclusions

In summary, we reported the first example of tri-Cu-acetylide as an active intermediate in CuAAC reaction, the reactivity of which has been proposed by Meldal and Tornøe.¹³ Compared to the di-Cu-acetylides, the tri-Cu-acetylide showed superior stability against protonation under neutral conditions. The **TL** ligand is important in stabilizing the di- and tri-Cu-acetylide active intermediates, but the limited strength of multi-Cu-**TL** coordination greatly reduced the efficiency of the catalyst at a low catalyst loading, where they were destabilized by the large excess of alkyne. This limitation is more pronounced when using CuAAC for bioconjugation in complex environment, such as live cells where strong copper(I) ligands are present.¹⁹ The next generation CuAAC ligands are expected to enhance the stability of the di-Cu-acetylide-azide complex to reduce the total catalyst loading.

3.6 Experimental Section

3.6.1 General Methods

Reagents and solvents were purchased from Sigma-Aldrich or VWR and used without further purification. The ultrapure water for all experiments was obtained by Milli-Q Water Purification Systems. Deoxygenated water was obtained by stirring the Milli-Q water in anaerobic chamber for two days. Positive ion ESI-MS data were acquired using a Thermo Finnigan LCQ Deca XP ion trap mass spectrometer equipped with a Surveyor HPLC system. NMR spectra were recorded on the JEOL ECX-400, ECA-500 or ECA-600 spectrometer using CDCl₃ or D₂O as solvent. Positive ion MALDI-TOF mass was recorded on an AB SCIEX 4800 MALDI TOF/TOF analyzer using α -cyano-4-hydroxycinnamic acid as a matrix. Lyophilization was carried out with a SCANVAC CoolSafe 110 freeze-dryer. UV-Vis spectra were recorded on a Varian CARY 50 UV-Vis spectrophotometer using water as solvent.

3.6.2 Supplementary Figures

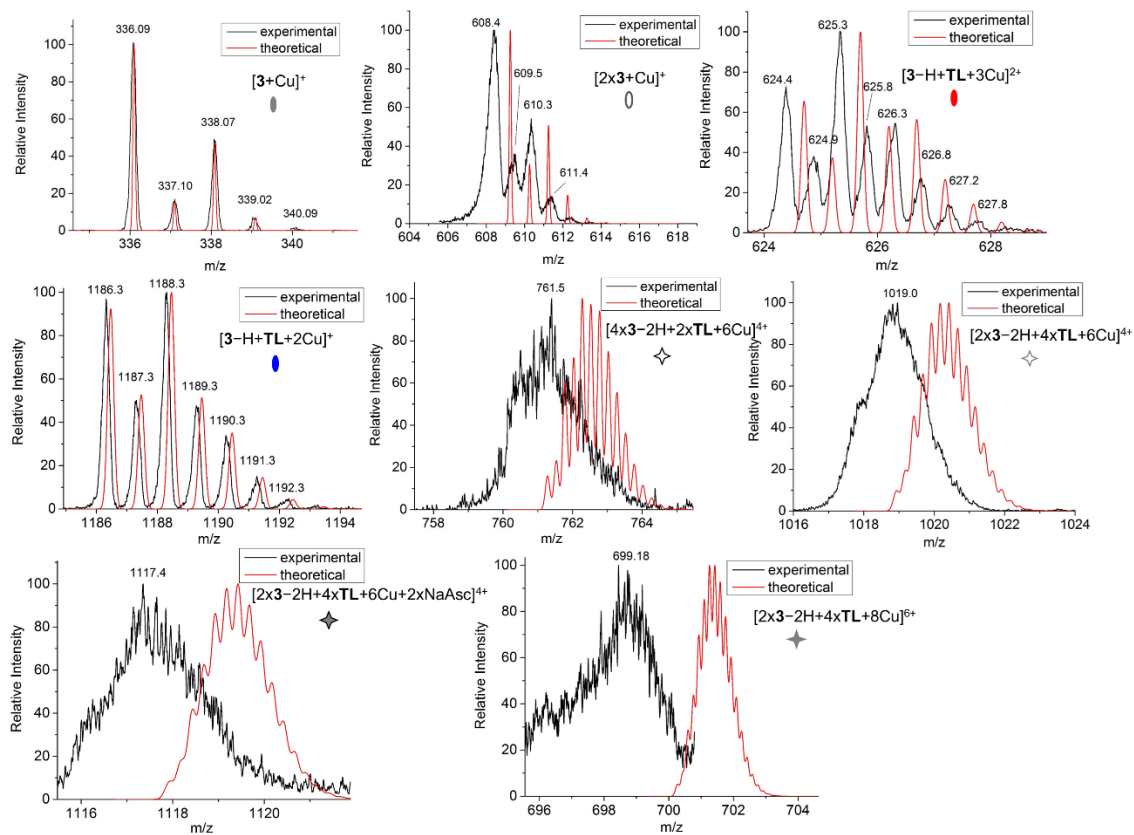
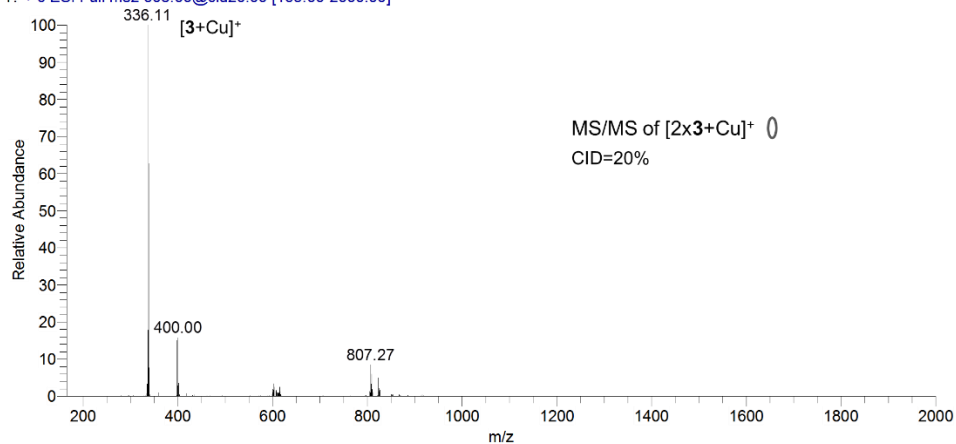
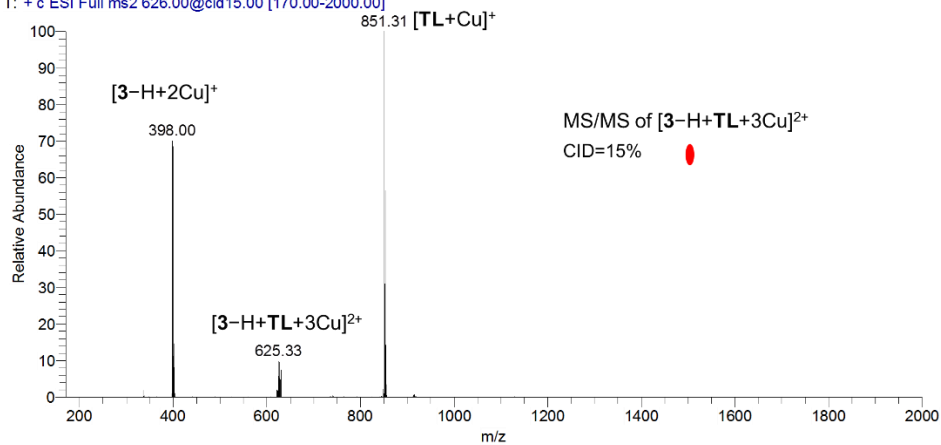


Figure 3-25 Isotopic patterns for detected copper(I) containing species in Figure 3-18A and 3-21.

100uAD28_60uCu_30uTL-500uAsc #2066-2078 RT: 39.15-39.36 AV: 13 NL: 8.12E6
T: + c ESI Full ms2 608.00@cid20.00 [165.00-2000.00]



100uAD28_60uCu_30uTL-500uAsc #1493-1500 RT: 30.72-30.85 AV: 8 NL: 6.31E6
T: + c ESI Full ms2 626.00@cid15.00 [170.00-2000.00]



100uAD28_60uCu_30uTL-500uAsc #1422-1429 RT: 29.72-29.86 AV: 8 NL: 2.01E6
T: + c ESI Full ms2 1188.00@cid25.00 [325.00-2000.00]

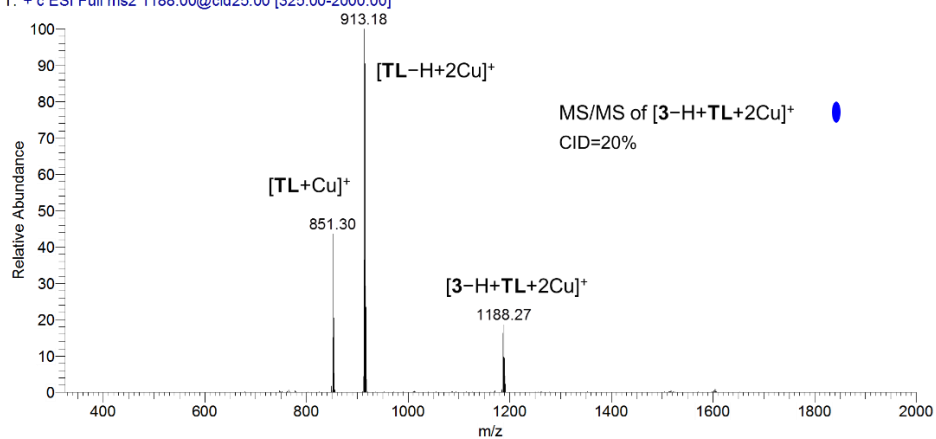


Figure 3-26 MS/MS Spectra for Selected copper(I)-containing Species in Figure 3-18A and 3-21.

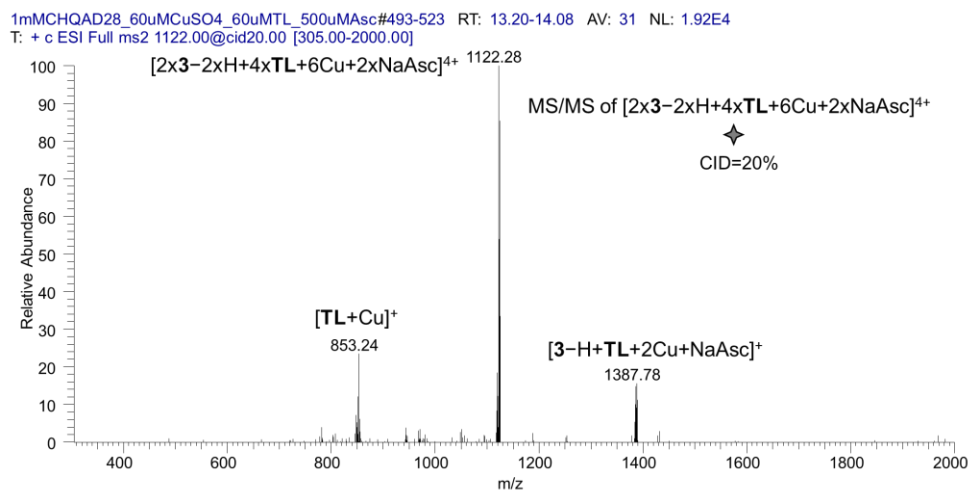
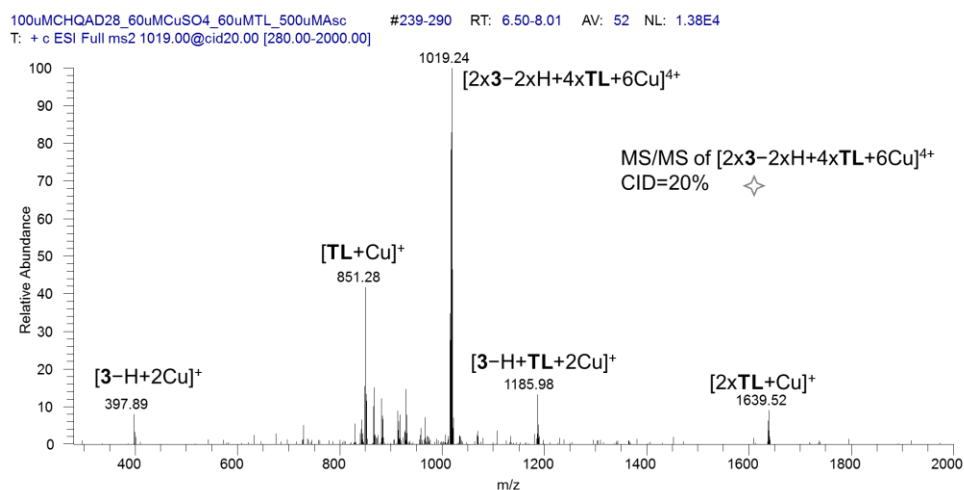
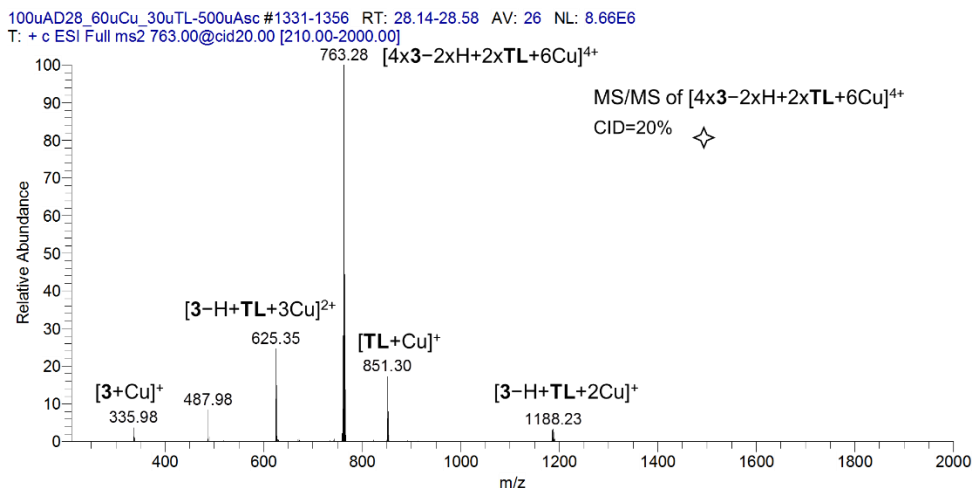


Figure 3-26 (continued) MS/MS Spectra for Selected copper(I)-containing Species in Figure 3-18A and 3-21.

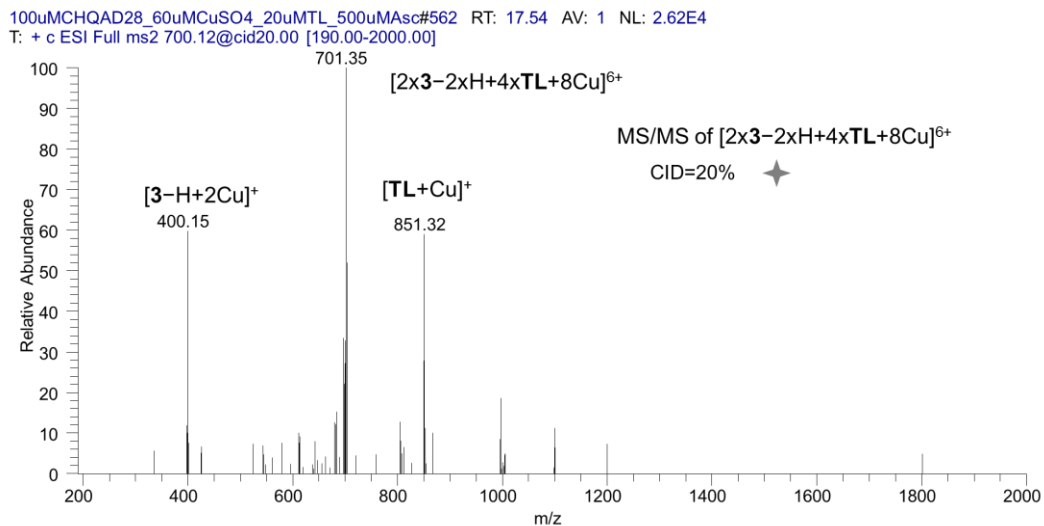
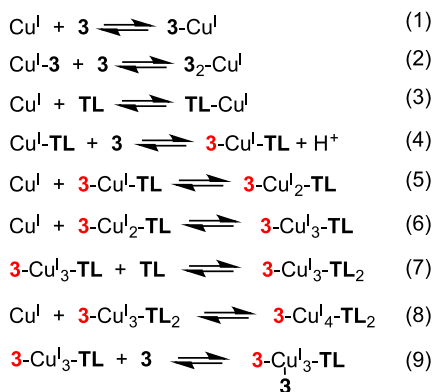
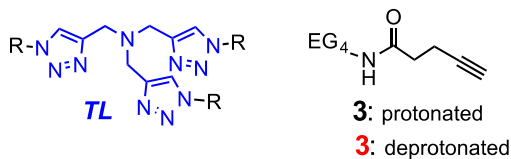


Figure 3-26 (continued) MS/MS Spectra for Selected copper(I)-containing Species in Figure 3-18A and 3-21.

Proposed equilibria

3 (100 μ M), Cu^I (15–300 μ M) in deoxygenated water



Scheme 3-9 The solution equilibria in **3**-Cu-TL system. Proposed based on the ESI-MS data (Figure 3-18A, 3-21).

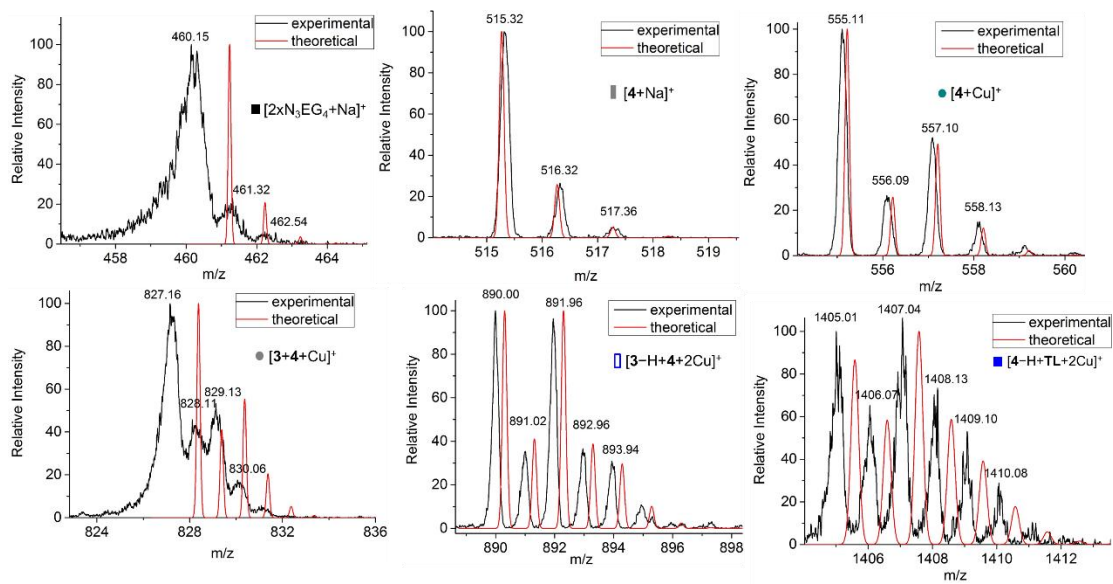


Figure 3-27 Isotopic patterns for detected copper(I) containing species in Figure 3-19

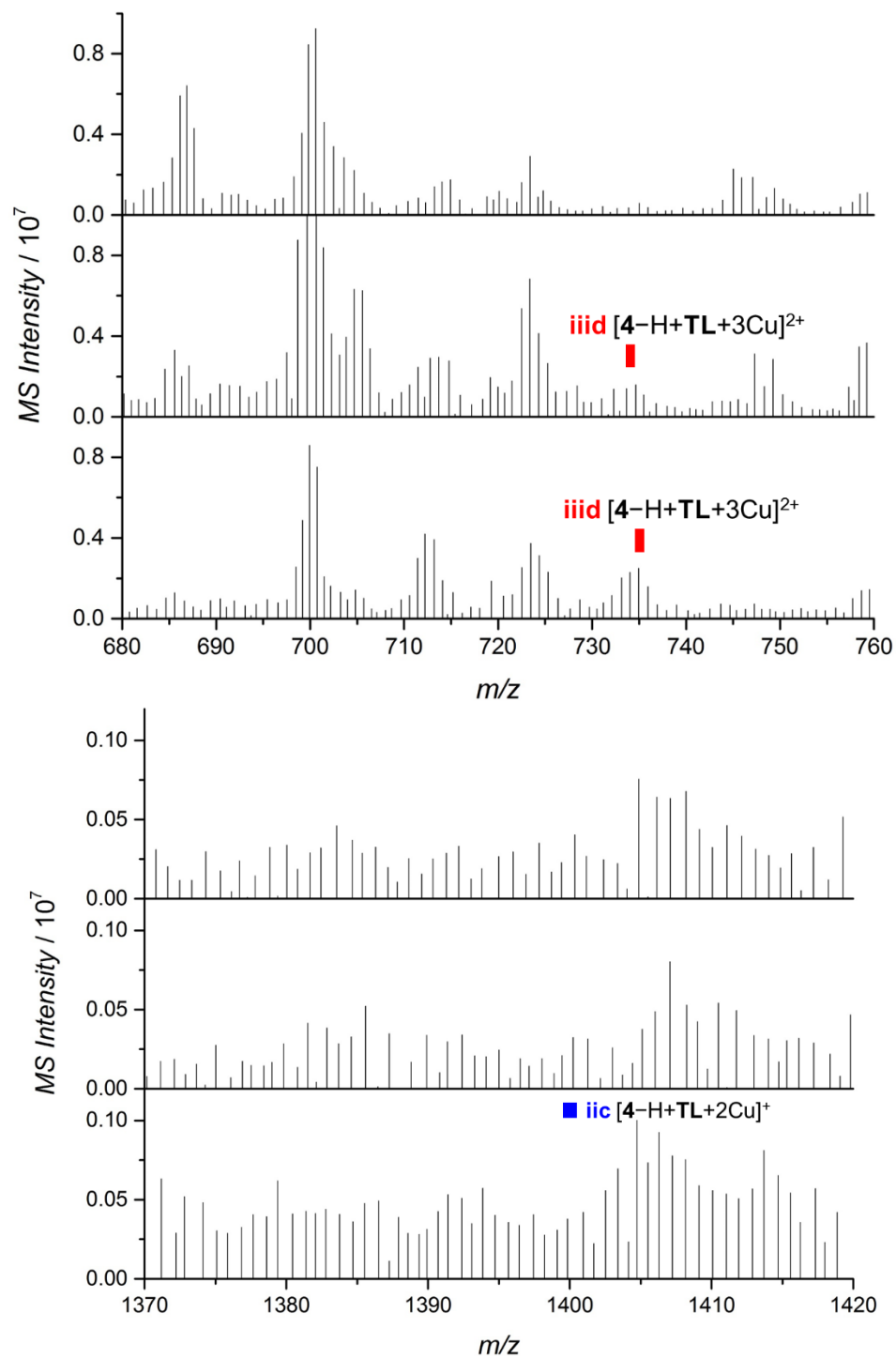


Figure 3-28 The expanded region in ESI-MS spectra of CuAAC reaction between **3** and N₃EG₄ at **3**/Cu 10:6 in Figure 3-19. The ESI-MS spectra showed a detectable amount of both TL-Cu^I₃-triazolide [4-H+TL+3Cu]²⁺ and TL-Cu^I₂-triazolide [4-H+TL+2Cu]⁺ just above the baseline.

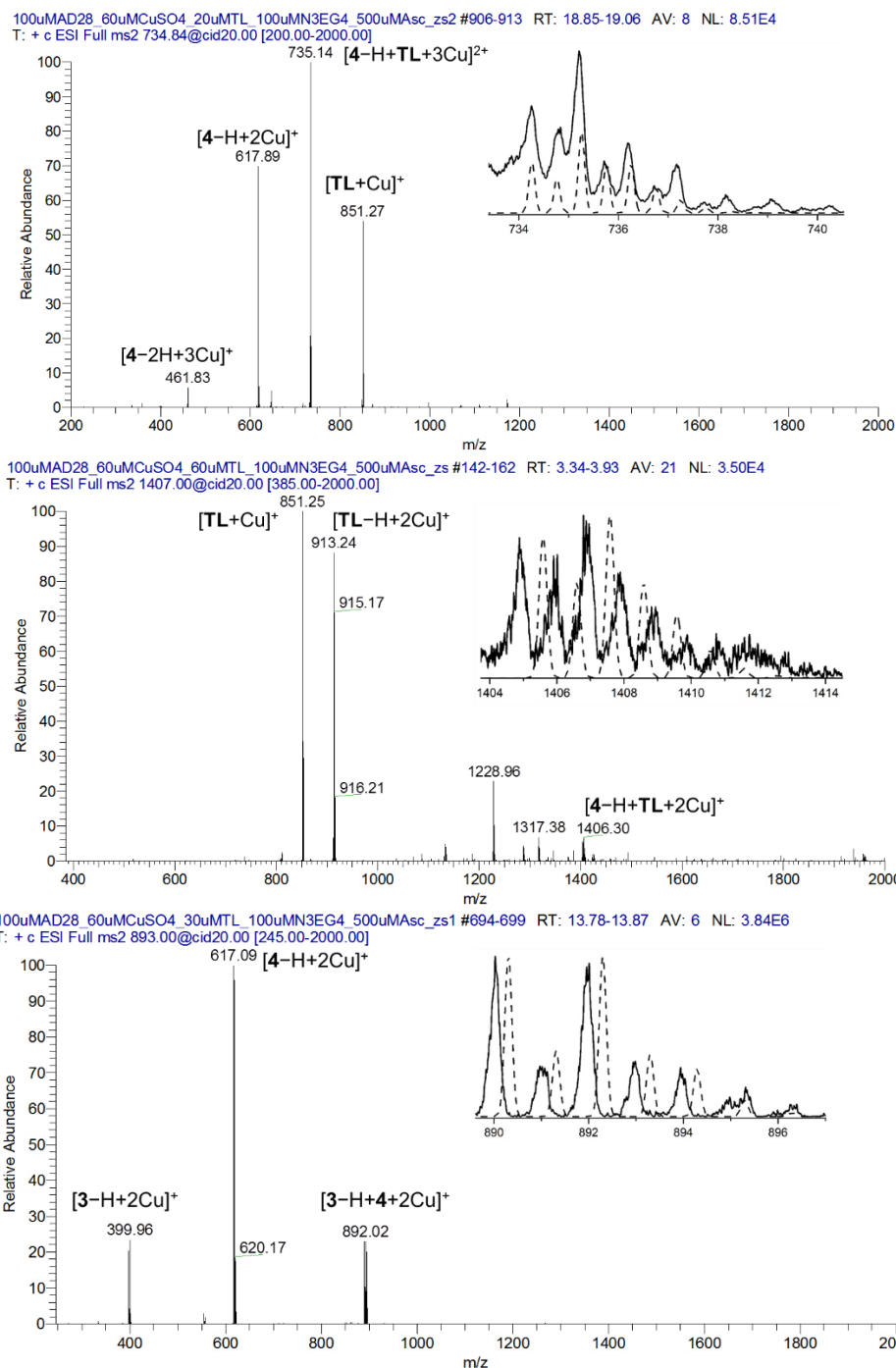


Figure 3-29 MS/MS spectra of the intermediates **iiid** $[4\text{-H+TL+3Cu}]^{2+}$ and **iiic** $[4\text{-H+TL+2Cu}]^+$ confirmed their identity. The zoom scan of $[4\text{-H+TL+3Cu}]^{2+}$ overlapped with the peak of $[3\text{-N}_3\text{EG}_4\text{+Na}]^+$ ($m/z = 734$). During the reaction, increased amount of $[3\text{-H+4+2Cu}]^+$ was detected, indicating the easy dissociation of **TL**-copper(I)-acetylide-azide complex competed by the triazole product **4**.

3.6.3 UV-Vis Spectra of 1-copper(I) Complexes at Various Cu/1 Ratio

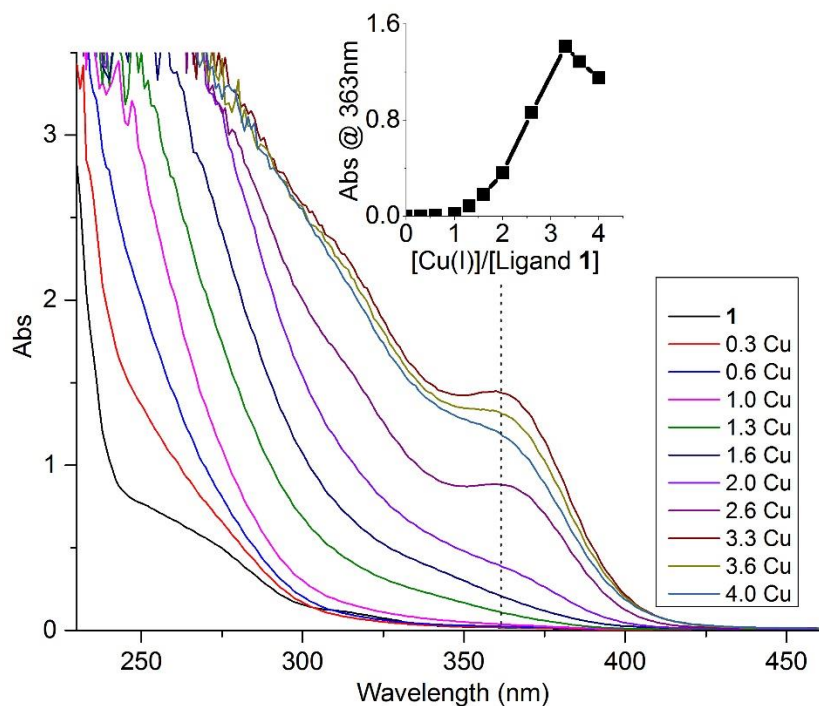


Figure 3-30 UV-Vis spectra of **1**-Cu complexes at 500 μ M concentration in deoxygenated water.

The copper(I)-acetylide interaction was further characterized by UV-Vis absorption spectrum of $[\text{Cu}_n(\mathbf{1})]$ in water. Acetonitrile solutions containing 1 equivalent ligand **1** and 0–4 equivalent $\text{Cu}(\text{MeCN})_4\text{BF}_4$ were frozen under -80°C , lyophilized, and dissolved in water in anaerobic chamber to generate a series of **1**-copper(I) solutions containing 500 μ M ligand **1**. The solutions were transferred to UV cuvettes, sealed with rubber septa, move out of anaerobic chamber, and characterized by UV-Vis spectroscopy. The spectra exhibit an absorption shoulder at 363 nm, which is likely to involve an acetylide to Cu ligand to metal charge transfer transition. Addition of copper(I) between 0 and 1 mole-equivalent has no effect on the 363 nm absorption, but the intensity of which starts to increase with further addition of copper(I), and reaches a maximum at 3 mole-equivalents of Cu(I) (Figure 3-30 insert).

3.6.4 Experimental Details

3.6.4.1 *Visible Comparison of copper(I) Chelating Ability of Ligand 1 and TL (Figure 3-1)*

Vials A₁–A₃ were charged with ligand **TL** (7.88 mg, 0.01 mmol) and vials B₁–B₄ were charged with ligand **1** (12.2 mg, 0.01 mmol). To the vials were added various amount of Cu(MeCN)₄PF₆ (A₁ & B₁: 3.73 mg, 0.01 mmol, 1 equiv.; A₂ & B₂: 7.46 mg, 0.02 mmol, 2 equiv.; A₃ & B₃: 11.19 mg, 0.03 mmol, 3 equiv.; B₄: 14.92 mg, 0.04 mmol, 4 equiv.). The vials were put into an anaerobic chamber and each vial was charged with deoxygenated MeCN (5 mL) and then deoxygenated water (1 mL). The vials were sealed, removed from anaerobic chamber and lyophilized for two days until pale yellow residues left. Subsequently, the vials were quickly moved into the anaerobic chamber and charged with deoxygenated water (20 mL) to generate the 0.5 mM ligand-copper(I) complex solutions.

3.6.4.2 *ESI-MS Spectra of TL–Cu_n Complexes in Deoxygenated Water (Figure 3-2)*

For studying solution equilibria of **TL**–Cu_n complexes, 100 μL 1 mM **TL**, 100/200/300 μL 1 mM CuSO₄, 100 μL 10 mM Na ascorbate, and 700/600/500 μL deoxygenated water were mixed in separate Eppendorf tubes in an anaerobic chamber, vortexed, and then directly infused into ESI source by a syringe pump at a flow rate of 10 μL/min. Each full MS spectrum was an average of 100 individual scans.

3.6.4.3 *ESI-MS analysis for intermediate solution equilibria in Cu^I_n1 solutions w/ or w/o N₃EG₄ (Figure 3-3 & Figure 3-14)*

ESI-MS spectra of Cu^I_n**1** solutions and the CuAAC reaction mixtures (with N₃EG₄) were acquired using a Thermo Finnigan LCQ Deca XP Plus ion trap mass spectrometer at capillary temperature

of 40°C, spray voltage 4 kV, capillary voltage 28 V, multipole 1 offset -3 V, multipole 2 offset -12 V, entrance lens voltage -61 V. In anaerobic chamber, all stock solutions were prepared in deoxygenated Milli-Q water.

For studying solution equilibria of Cu^I**1** complexes (Figure 3-1A), 100 µL 1 mM ligand **1**, 100/200/300 µL 1 mM CuSO₄, 100 µL 10 mM Na ascorbate, and 700/600/500 µL deoxygenated water were mixed in 3 separate Eppendorf tubes in an anaerobic chamber, vortexed, and then directly infused into the ESI source by a syringe pump at a flow rate of 10 µL/min. Each full MS spectrum was an average of 100 individual scans.

For studying solution equilibria of CuAAC reaction (Figure 3-1B), 100 µL 1 mM ligand **1**, 100/200/300 µL 1 mM CuSO₄, 100 µL 1 mM azido-tetraethylene glycol (N₃EG₄), 100 µL 10 mM Na ascorbate, and 600/500/400 µL deoxygenated water, were mixed in Eppendorf tubes in anaerobic chamber, vortexed, and then immediately infused into ESI source by a syringe pump at a flow rate of 10 µL/min. Reaction time was recorded on a timer. Each full MS spectrum in Figure 3-1B was an average of scans during the reaction time of 4–6 min. The reaction mixture was continuously infused into the ESI source during a period of 20 min. At Cu/**1** = 3:1, the variation of ESI-MS intensities of selected intermediates during the reaction time was plotted on Figure 3-2A.

3.6.4.4 NMR Spectra of Cu/1** 1:1 – 3:1 Mixtures in Deoxygenated D₂O (Figure 3-6)**

In anaerobic chamber, the mixture of ligand **1** (23.4 mg, 20 mM) and Na ascorbate (19.0 mg, 100 mM) in deoxygenated D₂O (959 µL) was added into a screw-capped NMR tube (Wilmad-Labglass), and treated with 38.3 µL of 500 mM CuSO₄ (1 equiv.) stock solution in deoxygenated D₂O. The tube was sealed and moved out of the anaerobic chamber for NMR measurement (Figure 3-6B). After the NMR experiment, the same sample tube was put back into the anaerobic

chamber, and a second equivalent of CuSO₄ (38.3 μL of 500 mM stock solution) was added. The solution was resealed with the scree cap and thoroughly mixed for NMR measurement (Figure 3-6C). After the NMR experiment, the third equivalent of copper was added in the same way (Figure 3-6D).

3.6.4.5 *Kinetic studies for reaction between 1 and N₃EG₄ (Figure 3-16)*

The reactions were conducted in an anaerobic chamber at room temperature. Solutions in 900 μL deoxygenated Milli-Q water was added into separate Eppendorf tubes, containing 100 nmol **1**, 1 μmol sodium ascorbate, and: A: 100 nmol CuSO₄, B: 200 nmol CuSO₄, C: 300 nmol CuSO₄, D: 100 nmol CuSO₄ and 500 nmol NaOH, E: 200 nmol CuSO₄ and 500 nmol NaOH, F: 600 nmol CuSO₄ and 500 nmol NaOH. 100 μL 1 mM azido tetraethylene glycol (N₃EG₄) aqueous solution were added into each tube to initiate the reaction. At 20 s (for A, B, C) or 10 s (for D, E, F) intervals, 20 μL aliquots of the reaction mixture were added into a 96-well plate, each well containing 180 μL air-saturated aqueous solution of 20 nmol diethylene triamine pentaacetic acid (DTPA) (pH adjusted to 7 by NaOH) and 1 nmol **5** as internal standard. After 8 aliquots were collected, the 96-well plate was moved out of anaerobic chamber. The samples were injected to a Thermo Finnigan LCQ Deca XP Plus ion trap mass spectrometer by a Thermo Finnigan Surveyor HPLC system. Reagents and product were separated by first static elution in 3% (MeCN, 0.1% formic acid): 97% (H₂O, 0.1% formic acid) for 5 min and then a linear gradient elution to 95% (MeCN, 0.1% formic acid):5% (H₂O, 0.1% formic acid) for 5 min. A set of calibration standards of product **2**, ranging from 100 nM to 10 μM, using **5** as internal standard, was injected before the unknowns. The concentration of product **2** in each sample was calculated based on the calibration curve. Each reaction under same condition was repeated three times.

3.6.4.6 *Kinetic studies for reaction between 1 and 2-azidoethanol (Figure 3-17)*

LC-MS was performed for quantification of the yield of product **5** from the CuAAC reaction of **1** (10 μM) and 1–4 equivalent copper(I) (generated from CuSO_4 and Na ascorbate) with excess amount of 2-azidoethanol (1 mM) (pseudo-first order reaction). In anaerobic chamber, 1 mL Titertube® micro test tubes (Bio-Rad) were placed in 96-well Titertube holder filled with ice and water. All stock solutions were prepared in deoxygenated Milli-Q water (pH=7.0) and balanced for 30 min in ice bath. 300/250/200/150 μL of deoxygenated water, 50 μL of 100 μM ligand **1**, 50/100/150/200 μL of 100 μM CuSO_4 and 50 μL of 100 mM 2-azidoethanol was mixed in four separate cluster tubes. 50 μL of 1 mM Na ascorbate was added to each tube to initiate the reaction. At 10 s intervals, 20 μL aliquots of the reaction mixture were added into a 96-well plate, each well containing 180 μL air-saturated diethylene triamine pentaacetic acid (DTPA) aqueous solution (pH adjusted to 7 by NaOH). After eight aliquots were collected, the 96-well plate was moved out of anaerobic chamber. The quenched aliquots were desalted by C18 tips (100 μL bed, Pierce™, Thermo Scientific). The desalting procedure is as follows: the tips were washed 3 times with 100 μL 60% MeCN/water, balanced 3 times with 100 μL 0.1% formic acid in water, and pipetted 10 times with each sample solution, washed twice with 100 μL of 50 μM DTPA solution (to remove Cu^{2+}) and 3 times with 0.1% formic acid in water (to remove Na^+). In a new 96-well plate, 160 μL 60% MeCN/water as eluent was added into each well. Every sample-loaded tip were pipetted through each eluent for 10 cycles. 40 μL 0.5 μM compound **6** water solution was added into each well as internal standard. The samples were injected to the Thermo Finnigan LCQ Deca XP Plus ion trap mass spectrometer by a Thermo Finnigan Surveyor HPLC system. Reagents and product were separated by linear gradient elution with a mobile phase composition starting from 3% (MeCN, 0.1% formic acid): 97% (H_2O , 0.1% formic acid) to 90% (MeCN, 0.1% formic acid): 10% (H_2O , 0.1% formic acid). A set of calibration standards of reagent **1** and

product **5**, ranging from 10 nM to 1.28 μ M, was injected before and after each set of samples. The concentration of reagents and product in each sample was calculated based on the calibration curve, and product yield was averaged by three repeated experiments.

3.6.4.7 *ESI-MS analysis for intermediate solution equilibria in $\text{Cu}^I_n\mathbf{3}$ solutions (Figure 3-18A, Figure 3-21)*

ESI-MS spectra of $\text{Cu}^I_n\mathbf{3}$ solutions were acquired using a Thermo Finnigan LCQ Deca XP Plus ion trap mass spectrometer at capillary temperature of 40°C, spray voltage 4.5 kV, capillary voltage 32 V, multipole 1 offset -5V, multipole 2 offset -12V, entrance lens voltage -51 V. In anaerobic chamber, all stock solutions were prepared in deoxygenated Milli-Q water.

For studying solution of $\mathbf{3}/\text{Cu} = 10:6$, 50 μ L of 10 mM sodium ascorbate was added into 950 μ L of aqueous solution containing 100 nmol **3**, 60 nmol CuSO_4 , and 60/30/20 nmol **TL**.

For studying solution of $\mathbf{3}/\text{Cu} = 100:6$, 50 μ L of 10 mM sodium ascorbate was added into 950 μ L of aqueous solution containing 1 μ mol **3**, 60 nmol CuSO_4 , and 120/60/30/20/15/0 nmol **TL**.

The mixtures were directly infused into ESI source by a syringe pump at flow rate of 10 μ L/min. Each full MS spectrum was an average of about 100 individual scans. Zoom scan analysis were carried out to determine the charge state and isotopic pattern for selected copper(I) adducts. Each zoom scan spectra represents an average of 50–100 individual scans. MS/MS analysis were carried out to determine the fragmentation pattern of selected copper(I) adducts.

3.6.4.8 *Kinetic studies for reaction between **3** and N_3EG_4 with various amount of copper(I) (Figure 3-18B)*

In an anaerobic chamber, eight 1 mL Titertube® micro test tubes (Bio-Rad) were placed in a 96-well Titertube rack. Solutions in 900 μ L deoxygenated Milli-Q water (pH=7.0) was added into

these tubes, each containing 100 nmol **3**, 100 nmol azido tetraethylene glycol and 10, 20, 30, 40, 60, 80, 100 nmol [(CuSO₄)₃(**TL**)] or [(CuSO₄)₂(**TL**)] or [(CuSO₄)(**TL**)]. 100 μL of 5 mM sodium ascorbate aqueous solution were added into the eight tubes by a multichannel pipette to start the reaction. At 1 min intervals, 100 μL aliquots of the reaction mixture were added into a 96-well plate, each well containing 90 μL air-saturated DTPA aqueous solution (pH adjusted to 7.0 by NaOH). After 6 sets of aliquots were collected, the 96-well plate was moved out of anaerobic chamber. 10 μL 100 μM **S10** water solution was added into each aliquots as internal standard. The samples were injected to a Thermo Finnigan LCQ Deca XP Plus ion trap mass spectrometer by a Thermo Finnigan Surveyor HPLC system. Reagents and product were separated by first static elution in 3% (MeCN, 0.1% formic acid): 97% (H₂O, 0.1% formic acid) for 2 min and then a linear gradient elution to 90% (MeCN, 0.1% formic acid):10% (H₂O, 0.1% formic acid) for 5 min. A set of calibration standards of reagent **3** and product **4**, ranging from 500 nM to 50 μM, using **S10** as internal standard, was injected before and after each set of samples. The concentration of reagents and product in each sample was calculated based on the calibration curve.

3.6.4.9 Kinetic studies for reaction between 3 and N₃EG₄ with catalytic amount of copper(I)
(Figure 3-22)

In an anaerobic chamber, six 1 mL Titertube® micro test tubes (Bio-Rad) were placed in a 96-well Titertube rack. Solutions in 900 μL deoxygenated Milli-Q water was added into these tubes, each containing 1 μmol **3**, 100 nmol (Figure 3-22A) or 1 μmol (Figure 3-22B) azido tetraethylene glycol (N₃EG₄), 60 nmol CuSO₄ and 120/60/30/20/15/0 nmol **TL**. 100 μL of 5 mM sodium ascorbate aqueous solution were added into each tube by a multichannel pipette to initiate the reaction. At 1 min (first 10min) and 5 min (10-60min) intervals, 20 μL aliquots of the reaction mixture were added into a 96-well plate, each well containing 180 μL air-saturated aqueous solution of 20 nmol DTPA (pH adjusted to 7 by NaOH) and 1 nmol **S10** (Scheme S1) as internal

standard. After 60 min of aliquots were collected, the 96-well plate was moved out of anaerobic chamber. The samples were injected to a Thermo Finnigan LCQ Deca XP Plus ion trap mass spectrometer by a Thermo Finnigan Surveyor HPLC system. Reagents and product were separated by first static elution in 3% (MeCN, 0.1% formic acid): 97% (H₂O, 0.1% formic acid) for 5 min and then a linear gradient elution to 95% (MeCN, 0.1% formic acid):5% (H₂O, 0.1% formic acid) for 5 min. A set of calibration standards of product **4**, ranging from 100 nM to 10 μM, using **S10** as internal standard, was injected before the unknowns. The concentration of product **4** in each sample was calculated based on the calibration curve.

3.6.4.10 Intermediate detection for reaction between 3 and N₃EG₄ at 3/Cu 10:6 (Figure 3-19)

ESI-MS spectra of intermediates in reaction between **3** and N₃EG₄ at 3/Cu 10:6 were acquired using a Thermo Finnigan LCQ Deca XP Plus ion trap mass spectrometer at capillary temperature of 40°C, spray voltage 4.5 kV, capillary voltage 32 V, multipole 1 offset -5V, multipole 2 offset -12V, entrance lens voltage -51 V. In anaerobic chamber, all stock solutions were prepared in deoxygenated Milli-Q water. 100 μL 1mM N₃EG₄ stock solution was added into 900 μL solution containing 100 nmol **3**, 60 nmol CuSO₄, 60/30/20 nmol **TL**, and 500 nmol sodium ascorbate. The reaction mixture was vortexed and directly infused into the ESI source by a syringe pump at flow rate of 10 μL/min. Each full MS spectra was an average of the scans during 5–10 min of the reaction. Zoom scan analysis were carried out to determine the charge state and isotopic pattern for selected copper(I) adducts. MS/MS analysis were carried out to determine the fragmentation pattern of selected copper(I) adducts.

3.6.5 Calculations

3.6.5.1 Second-order rate constants k_{obs} (Figure 3-16B)

Second-order rate constants k_{obs} in Figure 3-16B were calculated based on the following equations:

$$Rate = k_{obs} [1][azide] = k_{obs}[1]^2$$

$$1/[1] = k_{obs}t + 1/[1_0]$$

3.6.5.2 Second-order rate constants k_{obs} (Figure 3-17)

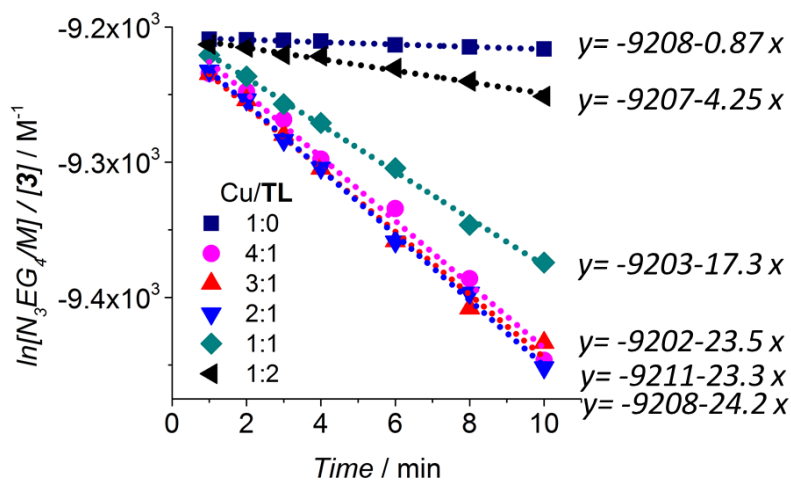
Second-order rate constants k_{obs} in Figure 3-17 were calculated based on pseudo-first-order reaction condition. For reaction between alkyne and excess azide:

$$Rate = k [alkyne][azide] = k'[alkyne]$$

According to integrated first-order rate law:

$$\ln[alkyne] = -k't + \ln[alkyne_0]$$

3.6.5.3 Calculation of k_{obs} of reaction between 3 and N_3EG_4

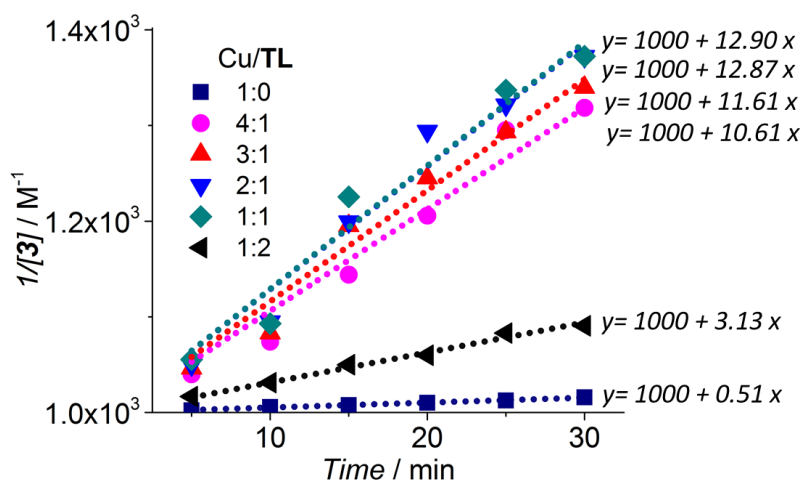


The second-order rate constants in Figure 3-22A was calculated based on the data points of initial 10 mins and pseudo-first order kinetics. Concentrations: $[3] = 1 \text{ mM}$, $[\text{Azide}_0] = 100 \text{ }\mu\text{M}$, $[\text{Cu}] = 60 \text{ }\mu\text{M}$, $\text{Cu}/\text{TL} = 1:0, 4:1, 3:1, 2:1, 1:1, 1:2$.

$$\text{Rate} = k_{obs} [3][\text{Azide}] \approx k'[\text{Azide}]$$

$$\ln[\text{Azide}] = -k't + \ln[\text{Azide}_0]$$

$$\ln[\text{Azide}]/[3] = -k_{obs}t + \ln[\text{Azide}_0]/[3]$$



The second-order rate constants in Figure 3-22B was calculated based on the data points of initial 30 mins. Concentrations: $[3] = 1 \text{ mM}$, $[\text{Azide}_0] = 1 \text{ mM}$, $[\text{Cu}] = 60 \text{ }\mu\text{M}$, $\text{Cu}/\text{TL} = 1:0, 4:1, 3:1, 2:1, 1:1, 1:2$.

$$\text{Rate} = k_{obs} [3][\text{azide}] = k_{obs}[3]^2$$

$$1/[3] = k_{obs}t + 1/[3_0]$$

Second-order rate constants k_{obs} in reaction between **3** and N_3EG_4 with various amount of copper(I) (Figure 3-20) was calculated based on the following equations:

$$\text{Rate} = k_{obs} [3][\text{azide}] = k_{obs}[3]^2$$

$$1/[3] = k_{obs}t + 1/[3_0]$$

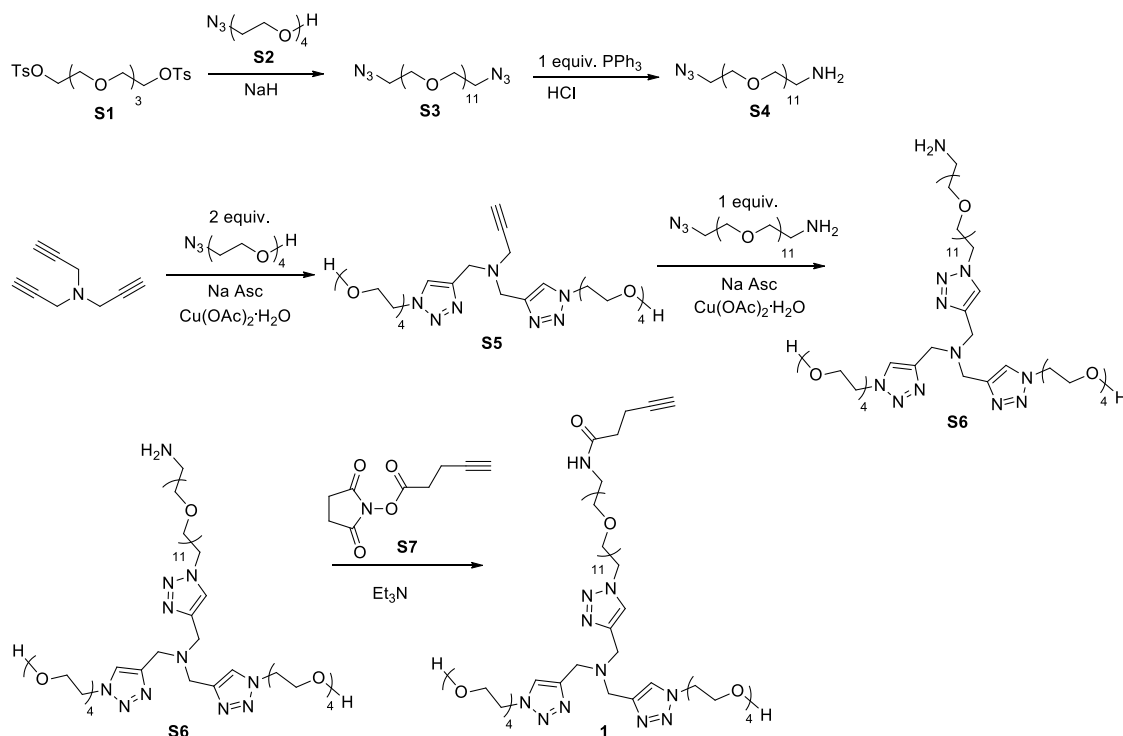
3.6.6 Synthetic Procedure and Compound Characterizations

Warning! Low-molecular-weight organic azides are potentially explosive, especially upon heating, shocking or in the presence of transition metals. These compounds should be handled as explosives.

Ligand **TL** was prepared using the literature procedure¹¹⁷.

Synthesis scheme of tris[(1-oligoethylene glycol-1H-1,2,3-triazol-4-yl)methyl]amine-4-pentynamide (**1**).

Compound **S1**, **S2**, **S7** were prepared using the literature procedures.¹⁸⁸⁻¹⁹⁰



Dodecaethylene glycol bisazide **S3**

To a 500 mL round-bottom flask was added sodium hydride (powder, 840 mg, 35.0 mmol) and DMF (200 mL). The suspension was stirred at 0 °C for 5 min, then a solution of tetraethylene glycol bistosylate **S1** (5.72 g, 11.4 mmol) and tetra(ethylene glycol) monoazide **S2** (5.10 g, 23.3 mmol) in DMF (20 mL) was added at 0 °C. The mixture was vigorously stirred at room temperature for 16 h and quenched with water (10 mL). The solvent was removed under vacuum, and the oily residue was dissolved in water (100 mL), extracted with dichloromethane (4 × 30 mL). The combined organic layer was dried over Na₂SO₄, filtered, and concentrated under vacuum. The crude product was purified by column chromatography (using 1-5% MeOH in CH₂Cl₂) to yield **S3** (4.50 g, 7.54 mmol, 66%) as a colorless oil. ¹H NMR (400 MHz, CDCl₃) δ 3.65–3.34 (m, 44H), 3.36 (t, *J* = 5.1 Hz, 4H). ¹³C NMR (101 MHz, CDCl₃) δ 70.7, 70.7, 70.6, 70.6, 70.1, 50.7. HRMS (MALDI-TOF): calculated for C₂₄H₄₉N₄O₁₁ [M+H-N₂]⁺ *m/z* 569.3398, found 569.3367.

***α*-Amino-*ω*-azido-*α,ω*-dideoxydodeca(ethylene glycol) (S4)**

To a 100 mL Schlenk tube was added bisazide **S3** (1.66 g, 2.78 mmol) and aqueous HCl (1 M, 60 mL). The solution was vigorously stirred at 0 °C for 30 min, then a solution of triphenylphosphine (729 mg, 2.78 mmol) in Et₂O (60 mL) was added via a dropping funnel during 30 min. The mixture was first stirred for 2 h at 0 °C, then stirred at room temperature for 48 h. The ether layer was removed, and the white precipitate was filtered. The aqueous filtrate was washed with ether (3 × 10 mL), and then its pH was adjusted to 12 with 1N NaOH solution. The solution was extracted with CH₂Cl₂ (6 × 30 mL), and the combined organic layer was dried over Na₂SO₄, filtered, and concentrated under vacuum. The crude product was purified by column chromatography (using 5% MeOH in CH₂Cl₂ and then 10% MeOH in CH₂Cl₂ + 1% Et₃N) to yield **S4** (1.23g, 2.16 mmol, 78%) as a pale yellow oil. ¹H NMR (400 MHz, CDCl₃) δ 3.87(s,

2H), 3.50–3.42 (m, 44H), 3.20 (t, $J = 5.0$ Hz, 2H), 2.77(s, 2H). ^{13}C NMR (101 MHz, CDCl_3) δ 71.2, 70.5, 70.5, 70.5, 70.5, 70.5, 70.5, 70.4, 70.4, 70.4, 70.4, 70.4, 70.4, 70.3, 70.3, 70.1, 70.0, 50.6, 41.1. HRMS (MALDI-TOF): calculated for $\text{C}_{24}\text{H}_{51}\text{N}_4\text{O}_{11}$ $[\text{M}+\text{H}]^+$ m/z 571.3554, found 571.3503.

N,N-bis((1-(tetraethylene glycol)-1H-1,2,3-triazol-4-yl)methyl)prop-2-yn-1-amine S5

To a 50 mL Schlenk tube was added tripropargylamine (516 mg, 3.94 mmol), tetra(ethylene glycol) monoazide **S2** (1.68 g, 7.67 mmol), and $\text{Cu}(\text{OAc})_2\cdot\text{H}_2\text{O}$ (158 mg, 0.79 mmol) under N_2 . MeOH (5 mL) and H_2O (5 mL) was added and the mixture was stirred for 10 min. A solution of sodium ascorbate (313 mg, 1.58 mmol) in H_2O (2 mL) was dropped into the above solution under N_2 . The mixture was sealed and stirred at room temperature overnight. The reaction was quenched by addition of an aqueous solution of diethylenetriaminepentaacetic acid pentasodium salt (Na_5DTPA , 500 mM, 5 mL). The aqueous solution was extracted with CH_2Cl_2 (3×10 mL). The combined organic layer was dried over Na_2SO_4 , filtered, and concentrated under vacuum. The crude product was purified by column chromatography (using 20% MeOH in EtOAc) to yield **S5** (931 mg, 1.63 mmol, 41%) as a colorless oil. ^1H NMR (400 MHz, CDCl_3) δ 7.77 (s, 1H), 4.48 (t, $J = 4.9$ Hz, 2H), 3.81 (t, $J = 4.6$ Hz, 4H), 3.66 (t, $J = 4.3$ Hz, 2H), 3.60–3.52 (m, 10H), 3.30 (s, 2H), 2.28 (s, 1H). ^{13}C NMR (101 MHz, CDCl_3) δ 144.0, 124.6, 72.6, 70.6, 70.6, 70.5, 70.3, 69.5, 61.6, 50.3, 47.9, 41.8. HRMS (MALDI-TOF): calculated for $\text{C}_{25}\text{H}_{44}\text{N}_7\text{O}_8$ $[\text{M}+\text{H}]^+$ m/z 570.3252, found 570.3237.

Compound S6

To a 25 mL Schlenk tube was added bistriazole propargyl amine **S5** (520 mg, 0.91 mmol), amino PEG azide **S4** (564 mg, 0.99 mmol) and $\text{Cu}(\text{OAc})_2\cdot\text{H}_2\text{O}$ (19 mg, 0.097 mmol) under N_2 . H_2O (6 mL) was added and the mixture was stirred for 10 min. A solution of sodium ascorbate (54 mg,

0.27 mmol) was dissolved in H₂O (2 mL) and dropped into the above solution under N₂. The mixture was sealed and stirred at room temperature overnight. The reaction was quenched by addition of an aqueous solution of Na₅DTPA (500 mM, 1 mL). The aqueous solution was extracted with CH₂Cl₂ (3 × 10 mL). The combined organic layer was dried over Na₂SO₄, filtered, and concentrated under vacuum. The crude product was purified by column chromatography (using 5-10% MeOH in CH₂Cl₂ + 0.5% Et₃N) to yield **S6** (1.002 g, 0.88 mmol, 96%) as a pale yellow oil. ¹H NMR (400 MHz, CDCl₃) δ 7.93 (s, 2H), 7.88 (s, 1H), 4.52 (q, *J* = 5.0 Hz, 6H), 3.85 (t, *J* = 5.1 Hz, 6H), 3.72 (s, 6H), 3.68 (t, *J* = 4.3 Hz, 4H), 3.61–3.54 (m, 60H), 3.41 (s, 2H), 3.06 (s, 4H), 2.89 (t, *J* = 5.1 Hz, 2H). ¹³C NMR (101 MHz, CDCl₃) δ 143.8, 125.1, 72.7, 71.9, 70.6, 70.6, 70.5, 70.4, 70.3, 70.3, 69.6, 61.6, 50.6, 50.3, 47.3, 47.1, 41.5. HRMS (MALDI-TOF): calculated for C₄₉H₉₄N₁₁O₁₉ [M+H]⁺ *m/z* 1140.6727, found 1140.6709.

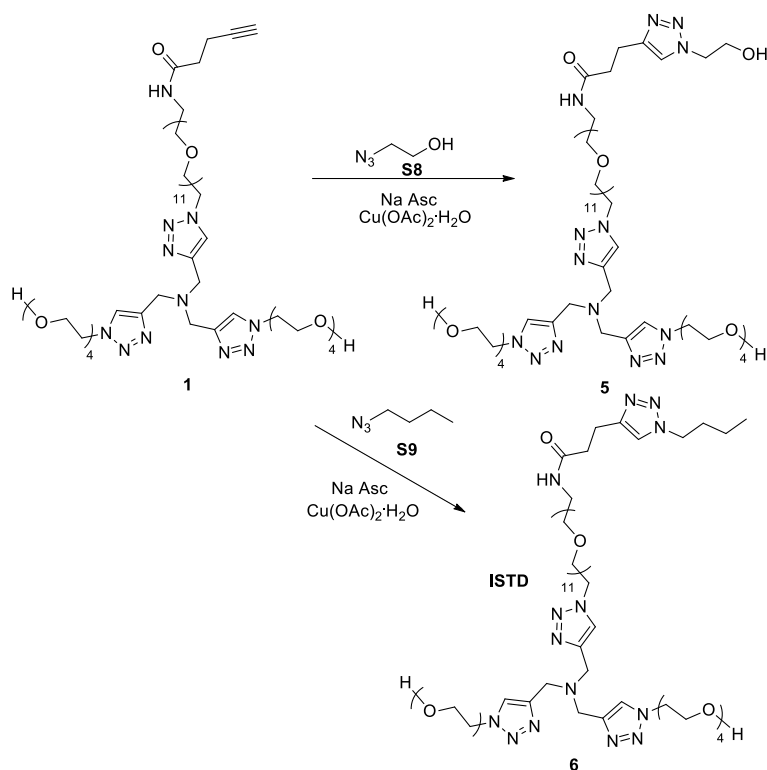
Tris[(1-oligoethylene glycol-1H-1,2,3-triazol-4-yl)methyl]amine-4-pentynamide 1

To a 50 mL Schlenk tube was added **S6** (1.002 g, 0.88 mmol) and triethylamine (178 mg, 1.76 mmol) and DMF (10 mL). The solution was stirred at 0 °C for 30 min, then a solution of 4-pentynoic acid succinimidyl ester **S7** (177 mg, 0.91 mmol) in DMF (3 mL) was dropped into the above ice-cooled solution. The mixture was stirred at room temperature overnight. The solvent was removed under vacuum, and the residue was purified by column chromatography (using 15% MeOH in CH₂Cl₂) to yield **1** (849 mg, 0.70 mmol, 80%) as a pale yellow oil. ¹H NMR (600 MHz, D₂O) δ 7.88 (s, 1H), 7.88 (s, 2H), 4.47 (t, *J* = 4.9 Hz, 6H), 3.81 (t, *J* = 4.9 Hz, 6H), 3.64 (s, 6H), 3.53–3.40 (m, 68H), 3.24 (t, *J* = 5.3 Hz, 2H), 3.18 (s, 1H), 2.33–2.27 (m, 4H), 2.21 (t, *J* = 2.3 Hz, 1H). ¹³C NMR (151 MHz, D₂O) δ 174.6, 143.2, 125.7, 83.3, 71.7, 69.6, 69.5, 69.4, 68.9, 68.8, 60.3, 50.0, 47.1, 39.0, 34.4, 14.6. HRMS (MALDI-TOF): calculated for C₅₄H₉₈N₁₁O₂₀ [M+H]⁺ *m/z* 1220.6990, found 1220.7003.

Triazole product 2

To a 10 mL Schlenk tube was added **1** (30 mg, 0.025 mmol), tetra(ethylene glycol) monoazide **S2** (24 mg, 0.11 mmol) and Cu(OAc)₂·H₂O (2 mg, 0.01 mmol) under N₂. H₂O (2 mL) was added and the mixture was stirred for 10 min. A solution sodium ascorbate (5 mg, 0.025 mmol) in H₂O (1 mL) was dropped into the above solution under N₂. The mixture was sealed and stirred at room temperature overnight. The reaction was quenched by addition of an aqueous solution of Na₅DTPA (500 mM, 0.5 mL). The aqueous solution was extracted with CH₂Cl₂ (6 × 10 mL). The combined organic layer was dried over Na₂SO₄, filtered, and concentrated under vacuum. The crude product was purified by column chromatography (using 10% MeOH in CH₂Cl₂) to yield **2** (30mg, 0.020mmol, 83%) as a yellow oil. ¹H NMR (500 MHz, D₂O) δ 7.89 (s, 3H), 7.69 (s, 1H), 4.49 (t, *J* = 4.9 Hz, 6H), 4.46 – 4.38 (m, 2H), 3.83 (t, *J* = 5.0 Hz, 6H), 3.82 – 3.77 (m, 2H), 3.66 (s, 6H), 3.60 – 3.34 (m, 78H), 3.19 (t, *J* = 5.3 Hz, 2H), 2.86 (t, *J* = 7.3 Hz, 2H), 2.47 (t, *J* = 7.3 Hz, 2H). ¹³C NMR (126 MHz, D₂O) δ 175.0, 146.4, 143.2, 125.8, 123.7, 71.7, 69.7, 69.6, 69.5, 69.4, 68.8, 68.8, 60.4, 50.0, 49.9, 47.2, 38.9, 35.1, 21.1. HRMS (MALDI-TOF): calculated for C₆₂H₁₁₄N₁₄O₂₄ [M+H]⁺ m/z 1438.8130, found 1438.8151.

Synthesis of calibration standards (**5** & **6**).



Compound **S8** and **S9** were prepared by literature procedures.¹⁹¹⁻¹⁹²

Compound **5**

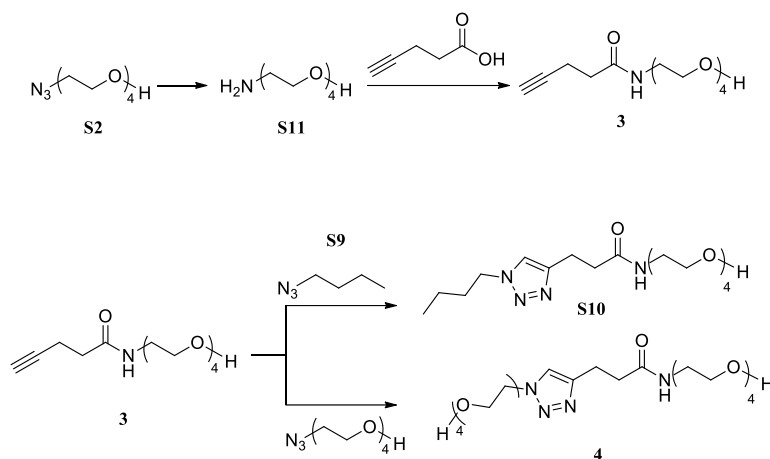
To a 10 mL Schlenk tube was added **1** (30 mg, 0.025 mmol), azido ethanol **S8** (10 mg, 0.11 mmol) and Cu(OAc)₂·H₂O (2 mg, 0.01 mmol) under N₂. H₂O (2 mL) was added and the mixture was stirred for 10 min. A solution sodium ascorbate (5 mg, 0.025 mmol) in H₂O (1 mL) was dropped into the above solution under N₂. The mixture was sealed and stirred at room temperature overnight. The reaction was quenched by addition of an aqueous solution of Na₃DTPA (500 mM, 0.5 mL). The aqueous solution was extracted with CH₂Cl₂ (6 × 5 mL). The combined organic layer was dried over Na₂SO₄, filtered, and concentrated under vacuum. The crude product was purified by column chromatography (using 10% MeOH in CH₂Cl₂) to yield **5** (27 mg, 0.021 mmol, 83%) as a colorless oil. ¹H NMR (500 MHz, CDCl₃) δ 7.92 (s, 2H), 7.88 (s, 1H), 7.51 (s, 1H), 6.48 (s, 1H), 4.52 (dd, *J* = 10.7, 5.4 Hz, 6H), 4.40 (t, *J* = 4.9 Hz, 2H), 3.96 (br, 2H), 3.86 (t, *J* =

5.1 Hz, 6H), 3.73 (s, 6H), 3.69 (t, $J = 4.6$ Hz, 4H), 3.60–3.55 (m, 60H), 3.48 (t, $J = 5.1$ Hz, 2H), 3.36 (dd, $J = 10.5, 5.3$ Hz, 2H), 3.00 (t, $J = 7.2$ Hz, 2H), 2.55 (t, $J = 7.2$ Hz, 2H). ^{13}C NMR (126 MHz, CDCl_3) δ 172.2, 146.4, 143.8, 125.1, 122.7, 72.6, 70.7, 70.6, 70.4, 70.1, 69.8, 69.6, 61.6, 61.1, 52.6, 50.3, 47.3, 47.1, 39.2, 35.8, 21.7. HRMS (MALDI-TOF): calculated for $\text{C}_{56}\text{H}_{103}\text{N}_{14}\text{O}_{21}$ $[\text{M}+\text{H}]^+$ m/z 1307.7422, found 1307.7434.

Compound 6

To a 10 mL Schlenk tube was added **1** (30 mg, 0.025 mmol), azido butane **S9** (10 mg, 0.10 mmol) and $\text{Cu}(\text{OAc})_2\cdot\text{H}_2\text{O}$ (2 mg, 0.01 mmol) under N_2 . H_2O (2 mL) was added and the mixture was stirred for 10 min. A solution sodium ascorbate (5 mg, 0.025 mmol) in H_2O (1 mL) was dropped into the above solution under N_2 . The mixture was sealed and stirred at room temperature overnight. The reaction was quenched by addition of an aqueous solution of Na_5DTPA (500 mM, 0.5 mL). The aqueous solution was extracted with CH_2Cl_2 (3×5 mL). The combined organic layer was dried over Na_2SO_4 , filtered, and concentrated under vacuum. The crude product was purified by column chromatography (using 10% MeOH in CH_2Cl_2) to yield **6** (30 mg, 0.023 mmol, 91%) as a colorless oil. ^1H NMR (500 MHz, CDCl_3) δ 7.92 (s, 2H), 7.87 (s, 1H), 7.32 (s, 1H), 6.28 (s, 1H), 4.51 (dd, $J = 10.9, 5.5$ Hz, 6H), 4.26 (t, $J = 7.3$ Hz, 2H), 3.85 (t, $J = 5.1$ Hz, 6H), 3.73 (s, 6H), 3.69 (t, $J = 4.3$ Hz, 4H), 3.60–3.55 (m, 62H), 3.48 (t, $J = 5.1$ Hz, 2H), 3.37 (dd, $J = 10.5, 5.3$ Hz, 2H), 3.28 (s, 2H), 3.00 (t, $J = 7.2$ Hz, 2H), 2.56 (t, $J = 7.2$ Hz, 2H), 1.84–1.78 (m, 2H), 1.29 (dq, $J = 14.8, 7.4$ Hz, 2H), 0.90 (t, $J = 7.4$ Hz, 3H). ^{13}C NMR (126 MHz, CDCl_3) δ 172.0, 146.6, 143.8, 125.1, 121.4, 72.6, 70.7, 70.7, 70.6, 70.5, 70.4, 70.3, 69.8, 69.6, 61.6, 50.3, 50.0, 47.2, 47.1, 39.3, 35.8, 32.3, 21.5, 19.8, 13.6. HRMS (MALDI-TOF): calculated for $\text{C}_{58}\text{H}_{107}\text{N}_{14}\text{O}_{20}$ $[\text{M}+\text{H}]^+$ m/z 1319.7786, found 1319.7798.

Synthesis of calibration standards (**3**, **4** & **S10**).



Synthesis of N-(tetraethylene glycol)pent-4-ynamide (3)

To a 100 mL Schlenk tube was added 4-pentynoic acid (360 mg, 3.7 mmol), EDC·HCl (1.1 g, 5.5 mmol), HOBt (249 mg, 5.5 mmol) and Et₃N (1.1 g, 11 mmol) in CH₂Cl₂ (10 ml). The mixture was stirred for 10 min, then amino tetra-ethylene glycol (1.3 g, 5.5 mmol) was added under nitrogen. The solution was stirred at room temperature for 24 h, and then the solvent was removed under vacuum. The residue was dissolved in 100 mL saturated NaHCO₃ aqueous solution and extracted with CH₂Cl₂ × 4. The organic layer was combined, dried over anhydrous MgSO₄, filtered and concentrated under vacuum. The crude product was further purified by column chromatography (5% MeOH in EtOAc) to yield 470 mg (47%) pure product **3** as pale yellow oil. ¹H NMR (500 MHz, CDCl₃) δ 7.22 (s, 1H), 3.70 (s, 1H), 3.66 – 3.62 (m, 4H), 3.59 – 3.54 (m, 6H), 3.54 – 3.51 (m, 2H), 3.45 (t, *J* = 5.0 Hz, 2H), 3.37 – 3.34 (m, 2H), 2.43 (td, *J* = 7.1, 2.5 Hz, 2H), 2.33 (t, *J* = 7.1 Hz, 2H), 1.93 (t, *J* = 2.5 Hz, 1H). ¹³C NMR (126 MHz, CDCl₃) δ 171.3, 83.3, 72.6, 70.7, 70.4, 70.1, 70.0, 70.0, 69.1, 61.5, 39.2, 35.1, 14.9.

Synthesis of 4

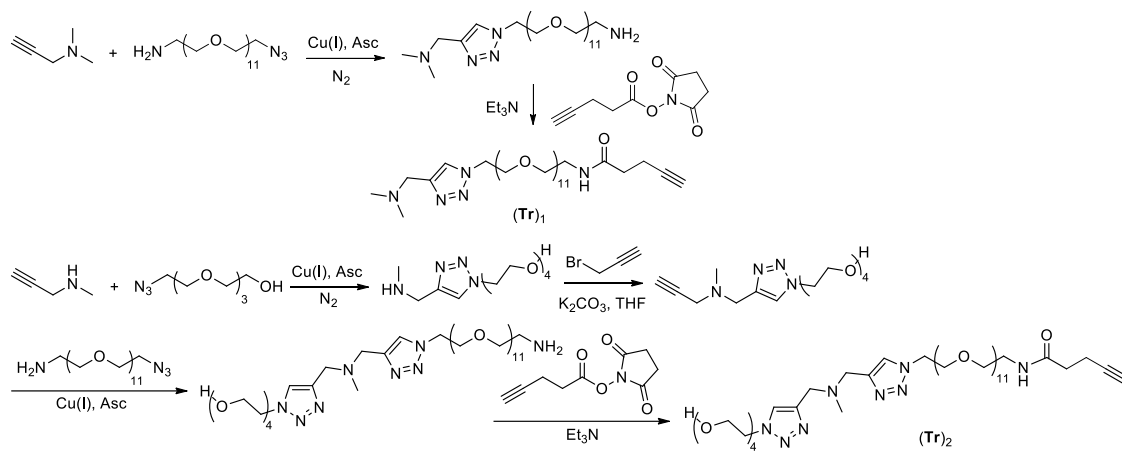
To a 10 mL Schlenk tube was added N-(tetraethylene glycol)pent-4-ynamide (60 mg, 0.22 mmol), azido tetraethylene glycol (100 mg, 0.45 mmol) and CuSO₄·5H₂O (6 mg, 0.024 mmol) under N₂.

H₂O (2 mL) was added and the mixture was stirred for 5 min. A solution of sodium ascorbate (40 mg, 0.20 mmol) in H₂O (0.5 mL) was dropped into the above solution under N₂. The mixture was sealed and stirred at room temperature overnight. After the reaction was completed, 150 mg Chelex® 100 Resin was added to the mixture and stirred in air for 1 h. The resin was filtered through a small plug of cotton in Pasteur pipette, and the filtrate was concentrated under vacuum. The crude product was purified by column chromatography (20% MeOH in EtOAc) to yield **4** (88 mg, 0.18 mmol, 82%) as a colorless oil. ¹H NMR (500 MHz, CDCl₃) δ 7.56 (s, 1H), 7.29 (t, *J* = 5.1 Hz, 1H), 4.42 (t, *J* = 4.9 Hz, 2H), 4.11 (s, 2H), 3.76 (t, *J* = 5.0 Hz, 2H), 3.67 – 3.62 (m, 4H), 3.52 (s, 22H), 3.43 (t, *J* = 4.7 Hz, 2H), 3.34 – 3.31 (m, 2H), 2.96 (t, *J* = 7.6 Hz, 2H), 2.52 (t, *J* = 7.6 Hz, 2H). ¹³C NMR (126 MHz, CDCl₃) δ 172.3, 146.5, 122.9, 72.6, 70.6, 70.6, 70.5, 70.4, 70.3, 70.0, 69.5, 61.5, 61.3, 50.2, 39.2, 35.6, 21.5.

Synthesis of S10

To a 10 mL Schlenk tube was added N-(tetraethylene glycol)pent-4-ynamide (62 mg, 0.22 mmol), 1-azidobutane (50 mg, 0.50 mmol) and CuSO₄·5H₂O (6 mg, 0.024 mmol) under N₂. H₂O (2 mL) was added and the mixture was stirred for 5 min. A solution of sodium ascorbate (40 mg, 0.20 mmol) in H₂O (0.5 mL) was dropped into the above solution under N₂. The mixture was sealed and stirred at room temperature overnight. After the reaction was completed, 150 mg Chelex® 100 Resin was added to the mixture and stirred in air for 1 h. The resin was filtered through a small plug of cotton in Pasteur pipette, and the filtrate was concentrated under vacuum. The crude product was purified by column chromatography (5% MeOH in CH₂Cl₂) to yield **S10** (76 mg, 0.20 mmol, 93%) as a colorless oil. ¹H NMR (500 MHz, CDCl₃) δ 7.32 (br, 2H), 4.23 (t, *J* = 7.2 Hz, 2H), 4.13 (s, 1H), 3.70 – 3.65 (m, 2H), 3.64 – 3.62 (m, 2H), 3.58 – 3.56 (m, 6H), 3.54 – 3.52 (m, 2H), 3.45 (t, *J* = 5.0 Hz, 2H), 3.36 – 3.33 (m, 2H), 2.97 (br, 2H), 2.54 (br, 2H), 1.79 (tt, *J* = 7.4 Hz, 2H), 1.26 (tq, *J* = 7.4 Hz, 2H), 0.87 (t, *J* = 7.4 Hz, 3H). ¹³C NMR (126 MHz, CDCl₃) δ

172.2, 146.7, 121.9, 77.5, 77.2, 77.0, 72.6, 70.7, 70.4, 70.0, 70.0, 61.4, 50.1, 39.2, 35.6, 32.2, 21.6, 19.7, 13.5.



The mono- and bis-triazolylmethylamine ligands **(Tr)₁** and **(Tr)₂** were prepared according to the procedure for synthesizing ligand **1** (*vide supra*).

Ligand **(Tr)₁**: ¹H-NMR (400 MHz, CDCl₃) δ 7.71 (s, 1H, triazole), 6.52 (s, 1H, NHCO), 4.47 (t, *J* = 5.0 Hz, 2H, triazole-NCH₂), 3.80 (t, *J* = 5.0 Hz, 2H, Triazole-NCH₂CH₂), 3.70 – 3.43 (m, 44H, OEG), 3.39 (t, *J* = 5.1 Hz, 2H, CH₂triazole), 2.50 – 2.39 (m, 2H, CH₂CH₂CCH), 2.35 (t, *J* = 7.3 Hz, 2H, CH₂CH₂CCH), 2.28 (s, 6H, CH₃), 1.96 (t, *J* = 2.0 Hz, 1H, CCH). ¹³C-NMR (101 MHz, CDCl₃) δ 171.1, 143.6, 124.3, 83.2, 70.6, 70.6, 70.6, 70.6, 70.6, 70.5, 70.5, 70.3, 69.9, 69.5, 69.3, 53.9, 50.3, 44.7, 39.3, 35.2, 14.9.

Ligand **(Tr)₂**: ¹H NMR (400 MHz, CDCl₃) δ 7.79 (s, 1H, triazole), 7.72 (s, 1H, triazole), 6.42 (s, 1H, NHCO), 4.48 (q, *J* = 4.8 Hz, 6H, triazole-NCH₂), 3.89 – 3.27 (m, 64H, OEG), 2.54 – 2.38 (m, 2H, CH₂CH₂CCH), 2.38 – 2.29 (m, 2H, CH₂CH₂CCH), 2.23 (s, 3H, CH₃), 1.96 (t, *J* = 2.6 Hz, 1H, CCH). ¹³C NMR (101 MHz, CDCl₃) δ 171.1, 143.8, 143.5, 124.6, 124.4, 83.2, 72.6, 70.6, 70.3, 70.3, 69.8, 69.6, 69.5, 69.4, 61.6, 51.1, 50.9, 50.3, 41.8, 39.3, 35.2, 14.9.

Chapter 4 Mechanistic Investigations on

Tris(triazolylmethyl)amine Ligand-accelerated CuAAC

Reaction in Organic Solvents

4.1 Introduction

In Chapter 3, we have discussed the finding of an alternative pathway of the tris(triazolylmethyl)amine ligand-accelerated CuAAC reaction in aqueous solutions, which involves a tri-copper-acetylide complex stabilized by one tris(triazolylmethyl)amine ligand (acetylide-Cu₃-**TL**). This intermediate is highly active especially under catalytic conditions. The finding was made using a water-soluble tris(triazolylmethyl)amine ligand conjugated with an alkyne via a long linker, which entropically stabilizes the copper acetylide intermediates and facilitated the interception of these intermediates and evaluation of their reactivity using electrospray ionization mass spectrometry (ESI-MS). However, the detail structural information of these intermediates could not be obtained since the flexible linker does not crystallize.

In 2007, the Williams group isolated the copper(I) and copper(II) complexes bearing tris(benzyltriazolylmethyl)amine (**TBTA**) ligands with good CuAAC activity (note: the copper(II) complex was applied in CuAAC reaction with reducing agent sodium ascorbate).¹⁹³ In the monomeric copper(II) complex, both the central nitrogen atom and the three triazole arms coordinate with copper(II), which is also stabilized by chloride ion (Figure 4-1A). The copper(I) complex [(**TBTA**)₂Cu₂] is a dimer bridged by one of the triazole arms, the N³ and N² of which coordinate with two copper(I) ions (Figure 4-1B). The other triazoles only adopt η¹ coordination mode. Unlike the copper(II) complex, the central nitrogen of [(**TBTA**)₂Cu₂] does not interact with the metal, since the saturated amines are poor π-acceptors for stabilizing the highly occupied d¹⁰

orbital of copper(I). In comparison, the copper(I) complex bearing NHC-trimethylamine ligands exhibited a much shorter Cu–N distance of 2.365 Å, indicative of higher positive charges on copper(I).¹⁹⁴

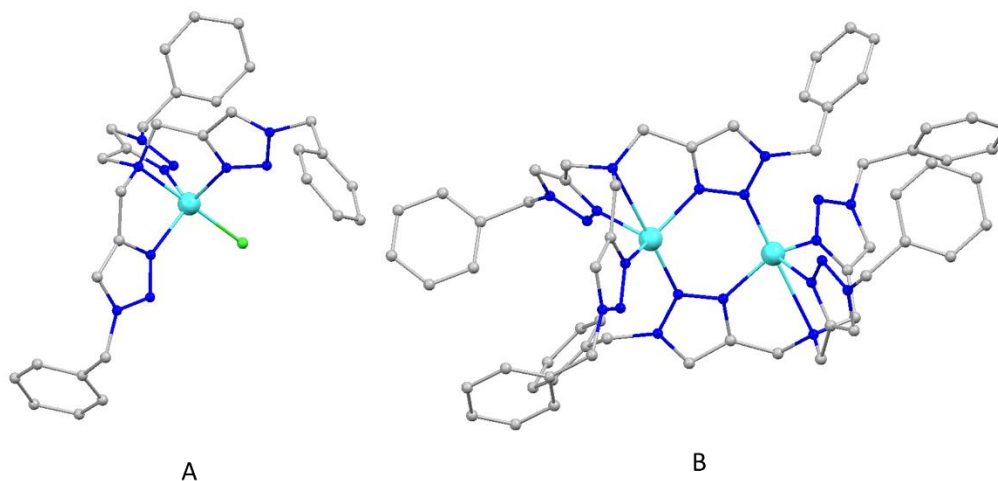


Figure 4-1 Molecular structure of isolated (A) copper(II) and (B) copper(I) complexes bearing tris(benzyltriazolylmethyl)amine ligands. Hydrogen atoms were omitted for clarity.

In this Chapter, we will discuss the structure and CuAAC activity of the first isolated tri-copper(I)-acetylide complex bearing tris(triazolylmethyl)amine ligand.

4.2 Isolation of Tri-copper(I) Acetylide Complex Bearing Tris(triazolylmethyl)amine Ligand

4.2.1 Ligand Design and Single Crystal Growth

In order to shed light on the origin of the high reactivity of the tri-copper(I)-acetylide complex, we first attempted to obtain its single crystal structure. We screened a range of substituents on the tris(triazolylmethyl)amine ligands and the alkynes, as well as the crystallization conditions (Chart 4-1). A series of ligands with different substitution groups on tris(triazolylmethyl)amine skeleton,

and various types of alkynes and copper(I) sources were tested for single crystal growth of ligand-copper(I)-acetylide. The ratio of Cu/ligand/alkyne varied from 1:1:1, 2:1:1, 3:1:1, 4:2:1 to 4:1:2 were tested, among which only the Cu₃-ligand-acetylide single crystal structure was obtained. The ligands bearing phenyl group, t-butyl group, benzyl group and cyclohexyl group could also generate pale yellow Cu₃-ligand-acetylide complexes (ball-shaped solid), but no single crystal was isolated from these ligands probably due to the π - π interactions between the aromatic rings and the higher flexibility of other substitution groups. Among the tris(triazolylmethyl)amine ligands tested, only the tris[(1-adamantyl-1*H*-1,2,3-triazol-4-yl)methyl] amine (**TATA**, Scheme 4-1) gave the pure single crystals, which is attributable to the bulky and relatively rigid adamantyl groups that facilitate crystallization and also prevent aggregation of the Cu-acetylides.⁵⁷

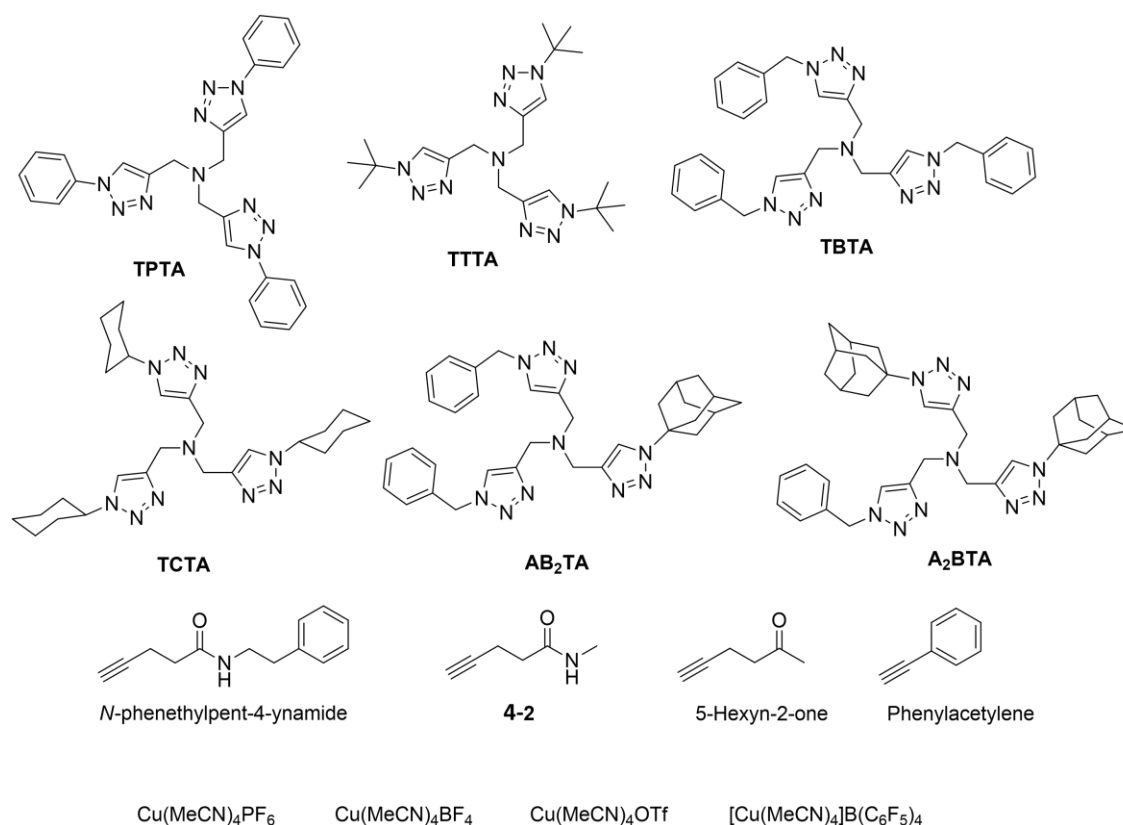
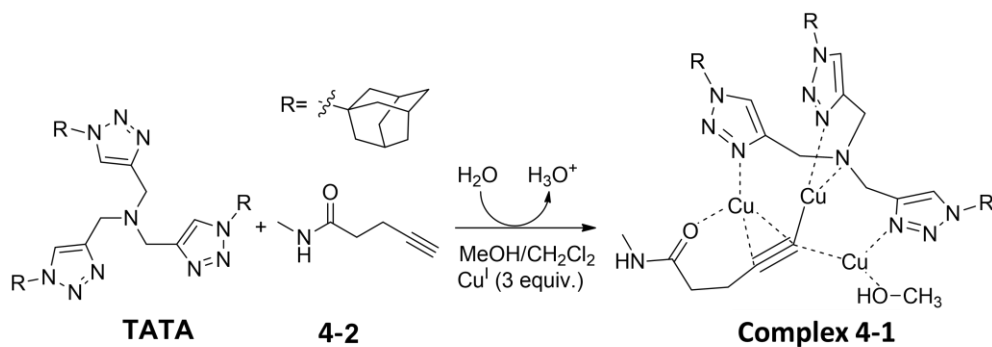


Chart 4-1 Tested Ligands, Alkynes, and Copper(I) Sources in Single Crystal Growth

Methanol, dichloromethane, ethanol, acetone, ethyl acetate, acetonitrile and DMSO were examined as solvent. Toluene and hexanes could not dissolve the ligand due to their low polarity. Acetonitrile, DMSO, ethyl acetate and acetone acted as strong competing solvent that coordinated with copper(I) and dissociated the copper(I)-acetylides. On the other hand, pure dichloromethane could not stabilize the tri-copper(I) complex and led to copper(I) aggregates, while addition of alcoholic solvents was able to maintain a high concentration of tri-copper(I)-acetylide at room temperature, indicating coordination from the hydroxyl group in the copper(I)-acetylide complex. Since the pure methanol and ethanol cannot fully dissolve the complexes, we chose a 1:1 mixture of dichloromethane and methanol as the solvent for single crystal growth.

The copper(I)-acetylide complex (**4-1**) was obtained by mixing the **TATA** ligand, *N*-methyl-4-pentynamide (**4-2**) and Cu(MeCN)₄PF₆ in 1:1:3 ratio in MeOH/CH₂Cl₂ containing about 3% H₂O as a base (Scheme 4-1). Single crystals suitable for X-ray analysis were obtained by ether diffusion into the solution of complex **4-1** in methanol and dichloromethane.



Scheme 4-1 Preparation of the Tri-copper(I) Acetylide Complex **4-1**.

Apart from the complex **4-1**, we also obtained single crystals from a combination of **TATA** (1 equiv.), Cu(MeCN)₄BF₄ (3 equiv.), *N*-phenethylpent-4-ynamide (Chart 4-1, 1 equiv.) in methanol-dichloromethane mixture using H₂O as a base for deprotonation. We failed to solve the

structure of this complex due to its high degree of disorder and the difficulty in identification of BF_4^- counterion, but the core structure of this complex is very similar to complex **4-1**. The combination of **TATA** (1 equiv.), $\text{Cu}(\text{MeCN})_4\text{PF}_6$ (4 equiv.), **4-2** (2 equiv.) in methanol-dichloromethane mixture also yielded the complex **4-1**, together with bright yellow aggregates formed from the excess copper(I) and **4-2**.

4.2.2 Characterization of Single Crystal of Tri-copper(I) Acetylide Complex **4-1**: X-ray Structure, ESI-MS, NMR and FT-IR Spectra

The X-ray structure of the single crystal of complex **1** features a centrosymmetric dimer connected by two Cu^{I} ions (Figure 4-2). The relatively weak cuprophilic interaction⁵⁵ between $\text{Cu}(1)$ and $\text{Cu}(1')$ is indicated by their distance of 2.510(2) Å, which is slightly shorter than that in metallic copper (2.56 Å)¹⁴² and much shorter than the sum of van der Waals radii of two copper atoms (2.8 Å).¹⁴³ In solution, this $\text{Cu}^{\text{I}}\text{-Cu}^{\text{I}}$ interaction was not strong enough for stabilizing the dimer, as observed in the ESI-MS spectra where only the monomers were present (Figure 4-3).

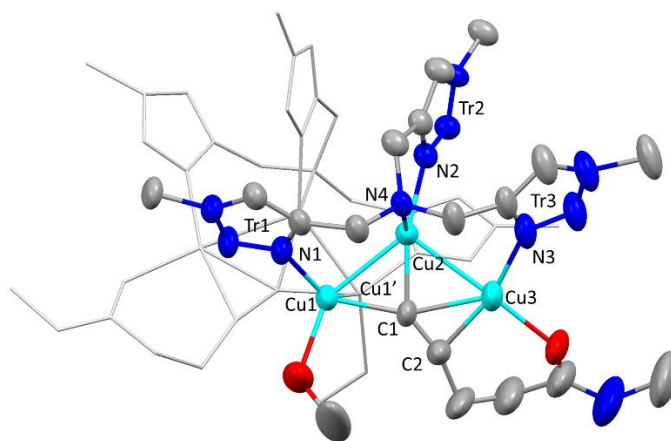


Figure 4-2 X-ray structure of the cation of the dimeric **TATA**-tri-copper(I)-acetylide **4-1**. The hydrogen atoms, adamantyl groups and hexafluorophosphate counter-ions are omitted for clarity. Thermal ellipsoids are at 50% probability.

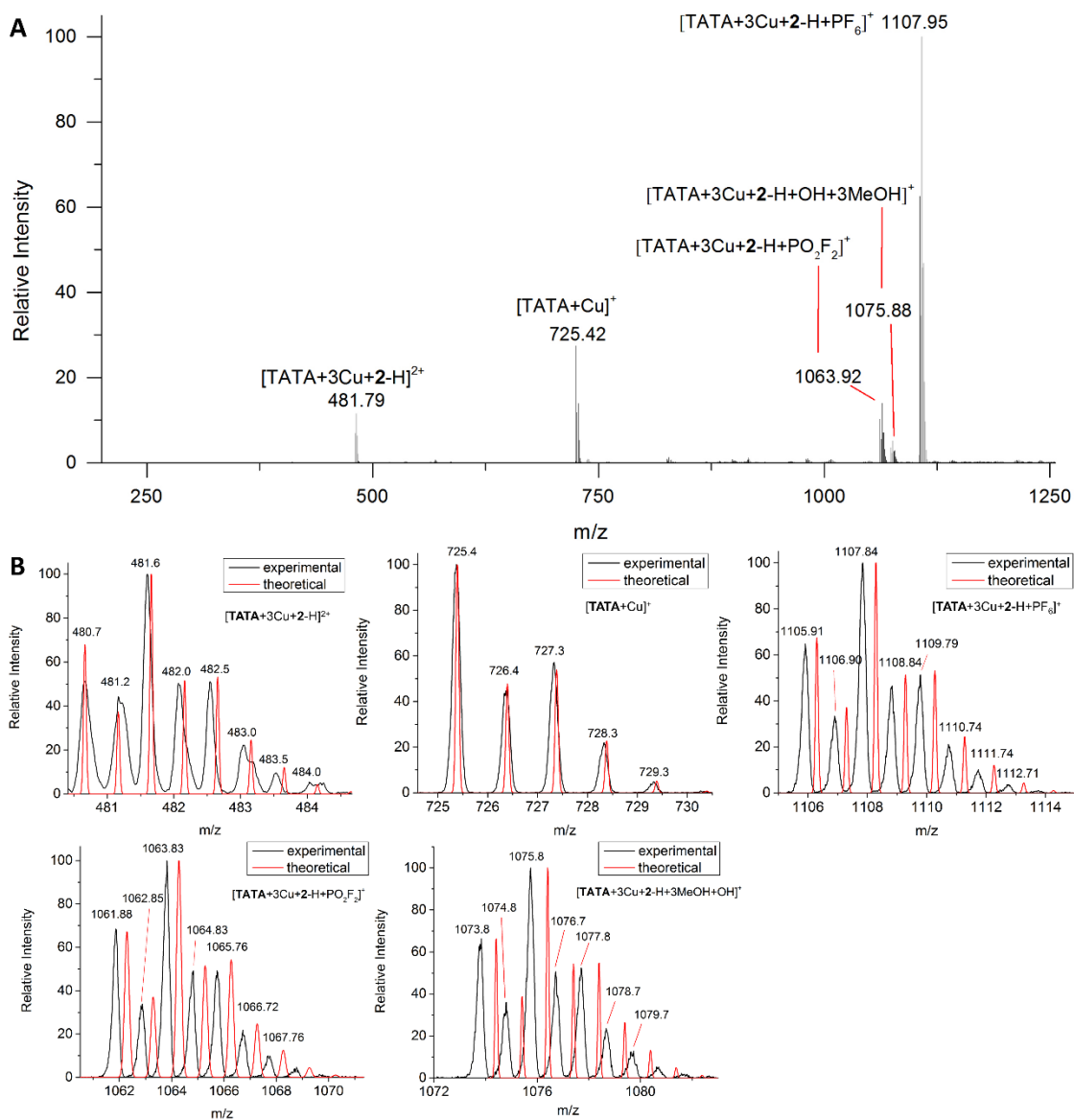


Figure 4-3 A. ESI-MS spectrum of complex **4-1** (100 μ M in MeOH). B. Experimental isotopic patterns obtained by zoom scans centered on selected m/z. Theoretical isotopic patterns (red) of the proposed ions were calculated using IsoPro 3.0, and overlaid on the experimental isotope pattern (black).

Each monomer $[Cu_3(\mu_3-\eta^{1,1,2}-C\equiv CC_2H_4CONHCH_3)(\mu_3-\kappa^{1,1,2}-TATA)]^{2+}$ contains three copper(I) ions bridged by the acetylide and located in approximately the same plane. Each Cu is stabilized by coordinating to N(3) of a triazole ring of **TATA**. The **TATA** ligand occupies one side of the

“Cu^I plane”, which blocks the access of another copper-acetylide and prevents the formation of aggregates that were known to inhibit the CuAAC reaction.¹⁹⁵ In solution, the weak Cu(1)-Cu(1') connection is broken, thus the other side of the “Cu^I plane” is free for coordination with an azide during the reaction. The crystal structure of **1** is quite similar to the structure of a **TL**-Cu^I₃-acetylide complex optimized by the ONIOM method¹⁹⁶ (see Chapter 5, Figure 5-1).

The Cu-Cu distances in each monomer (2.482(1) Å for Cu(1)-Cu(2) and 2.555(1) Å for Cu(2)-Cu(3)) are shorter than those in most Cu catalysts employed in CuAAC,^{35, 45, 127, 131-132, 140} but not uncommon in multi-nuclear copper-acetylide complexes.^{56-58, 80} These short distances were forced by the bridging of acetylide and indicative of intramolecular cuprophilic interactions that are possibly strengthened by the electron-deficiency of the tri-copper(I) acetylide.⁵⁵

The C(1)≡C(2) triple bond is activated in this complex, indicated by the significantly lengthened acetylide C(1)≡C(2) bond from typically 1.178 Å¹⁹⁷ to 1.235(8) Å and bending (168(1)° or 157(1)° for two positions of C(3), see experimental section) of C(1)≡C(2)-C(3), which is similar to those in a reported di-copper(I) acetylide complex bearing cyclic alkyl amino carbene (**CAAC**) ligands (C≡C: 1.232 Å; C(1)≡C(2)-C(3): 171.4°).⁵² The distances and angles reveal a partial sp² hybridization of the acetylide carbons in the tri-copper-acetylide, which can be attributed to the stronger alkyne to Cu σ-donation and Cu to alkyne π-backbonding.¹⁵⁶

Compared to the reported Cu/**TL** 1:1 complex without an acetylide, such as [(**TBTA**)₂Cu₂] (**TBTA**: tris[(1-benzyl-1*H*-1,2,3-triazol-4-yl)methyl]amine),¹⁹³ the Cu-triazole interactions in complex **1** are strengthened (Cu-N bond lengths 1.948(4)-1.990(5) Å vs. 2.028-2.049 Å in [(**TBTA**)₂Cu₂]). In particular, Cu(2) has the strongest interaction with the triazole ligand (Cu(2)-N(2) 1.948(4) Å). Copper(I) was considered a poor π back-bonding ion,¹⁵⁴ but the longer bond distances in triazole **2** (Table 4-2) may indicate the Cu(2) d → triazole 2 π* back-bonding. The enhanced Cu-triazole interaction¹² further stabilizes the complex. The back-bonding can relieve

excess electron density of Cu(2) and increase its positive charge compared to Cu(1), which is confirmed by the charge calculation results (Figure 5-1). The $^1\text{H-NMR}$ of complex **4-1** (Figure 4-4 and Figure 4-5) displayed a pair of more deshielded methylene proton ($\text{NCH}_2\text{Triazole}$) compared to other four methylene proton, which is possibly caused by the higher electron deficiency on Cu(2).

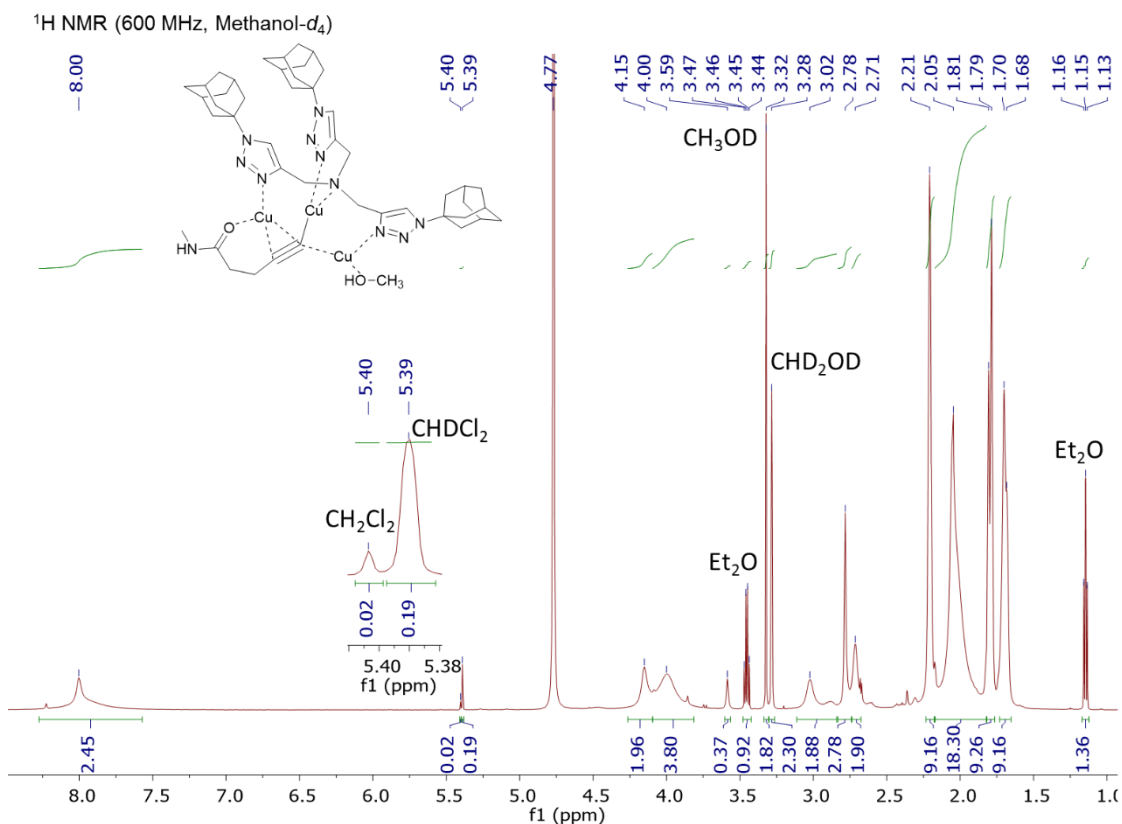


Figure 4-4 $^1\text{H NMR}$ of the newly grown single crystal of complex **4-1** dissolved in 70% CD_3OD and 30% CD_2Cl_2 at room temperature. $^1\text{H NMR}$ (600 MHz, locked on Methanol- d_4) δ 8.00 (s, 3H, triazole-H), 5.40 (s, 0.02H, CH_2Cl_2), 5.39 (s, 0.19H, CHDCl_2 , solvent residual peak in CD_2Cl_2), 4.77 (s, HOD), 4.15 (s, 2H, $\text{NCH}_2\text{-triazole}$, more deshielded, likely coordinate to Cu(2) that is of higher electron deficiency), 4.00 (s, 4H, $\text{NCH}_2\text{-triazole}$), 3.45 (q, $J = 7.0$ Hz, 0.92H, $(\text{CH}_3\text{CH}_2)_2\text{O}$), 3.32 (s, 2H, CH_3OD , the methanol that originally coordinated with copper, the lower integral value was attributed to evaporation), 3.28 (s, 2H, CHD_2OD , solvent residual peak in CD_3OD), 3.02 (br, 2H, $\text{C}\equiv\text{CCH}_2$), 2.78 (s, 3H, CONHCH_3), 2.71 (br, 2H, $\text{C}\equiv\text{CCH}_2\text{CH}_2$), 2.21 (br, 9H,

adamantyl), 2.05 (br, 18H, adamantyl), 1.80 (br, 9H, adamantyl), 1.69 (br, 9H, adamantyl), 1.15 (t, $J = 7.0$ Hz, 1.36H, $(\text{CH}_3\text{CH}_2)_2\text{O}$). The assignment was based on the chemical shifts, integrals and COSY.

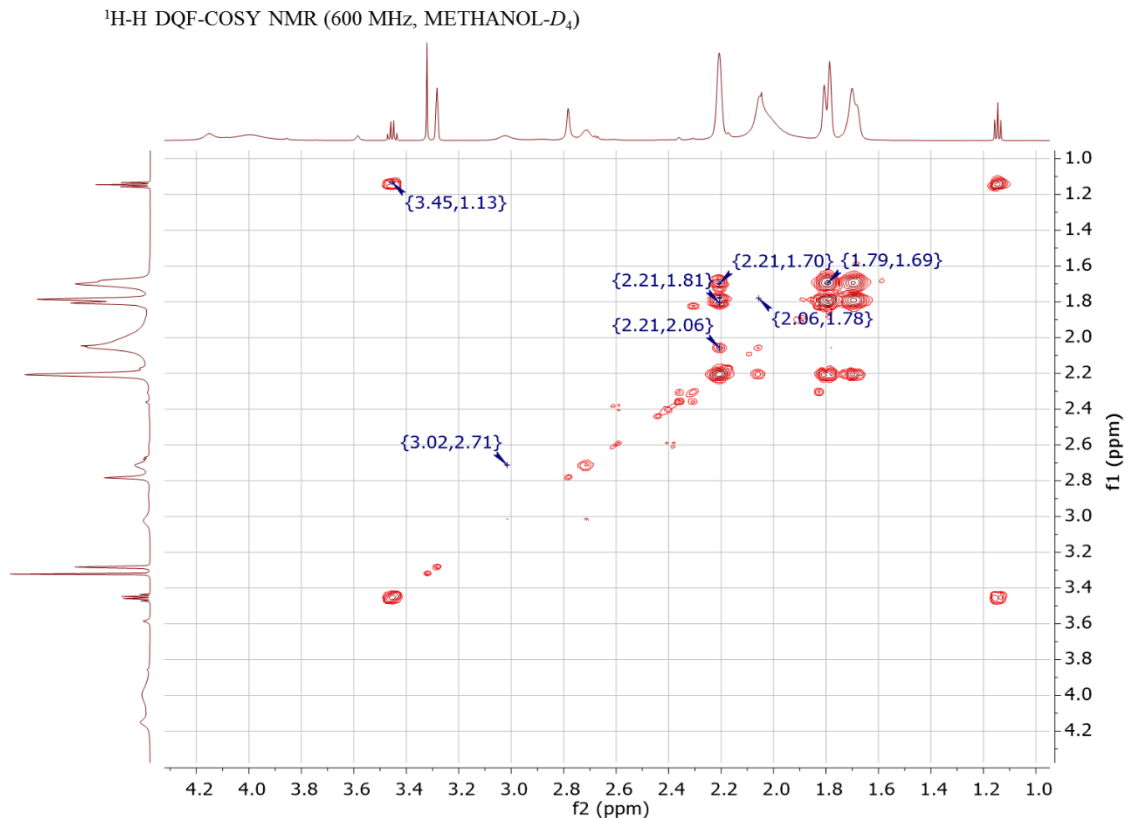


Figure 4-5 H-H COSY NMR of the newly grown single crystal of complex **4-1** dissolved in 70% CD_3OD and 30% CD_2Cl_2 at room temperature.

Due to the higher charge on copper(I), the tri-copper(I)-acetylide **1** is expected to coordinate with azide better than a di-copper(I)-acetylide. In most copper(I) complexes, the ligand-copper(I) interactions are contributed mainly by the electrostatic attraction, together with a small portion of orbital interactions.^{53, 164} Hence, compared to di-copper(I) acetylides, the higher positive charge on copper(I) of the tri-copper(I) acetylide should enhance the electrophilic interaction with the alkylated nitrogen of azide,^{32, 47} forming a more stable azide-copper(I)-acetylide ternary complex.

It has been showed that CuAAC reaction can be greatly accelerated by using chelating azides^{28-30, 100-101} and electron deficient alkynes which stabilize the azide-copper(I)-acetylide ternary complex.^{35, 103-105}

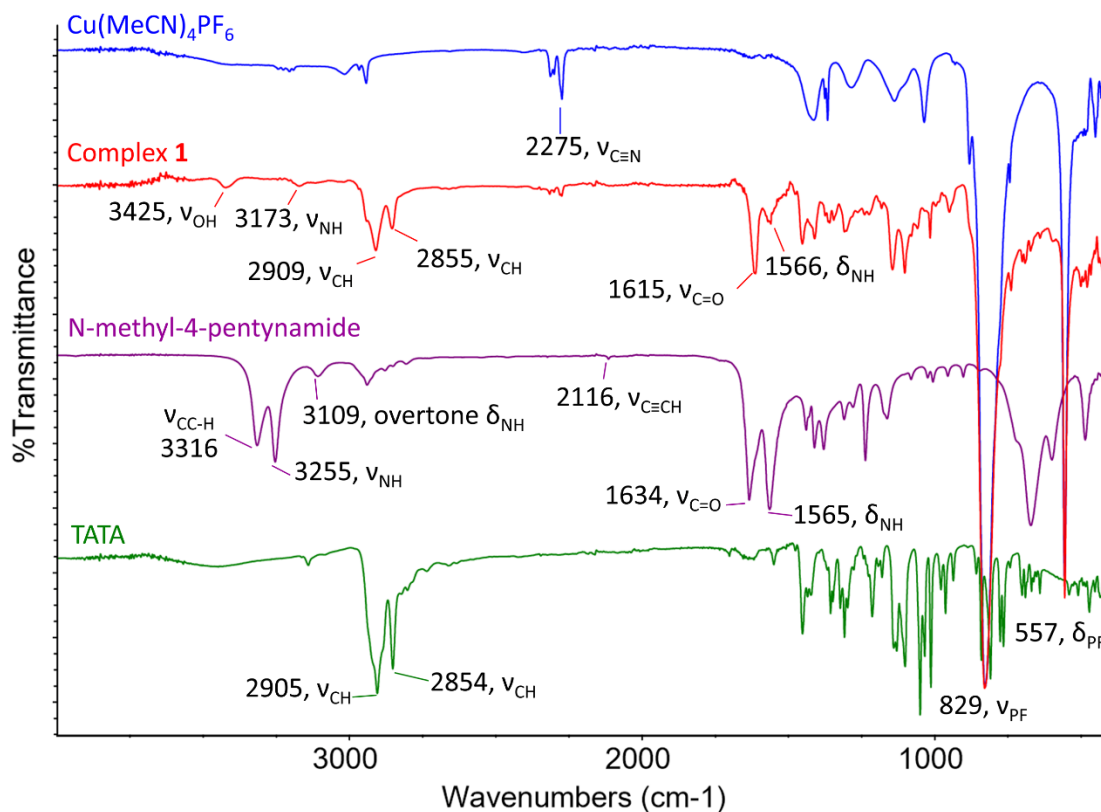


Figure 4-6 FT-IR of complex **4-1** compared with **TATA**, N-methyl-4-pentynamide (**2**) and $\text{Cu}(\text{MeCN})_4\text{PF}_6$

Weak interactions of copper(I) with methanol as the solvent, the amide oxygen of **2**, and the tertiary amine nitrogen N(4) in **TATA** also help to stabilize the structure. The back-bonding of Cu(3) to the C=O group is indicated by a slight red-shift of the C=O peak in the FT-IR spectra of complex **1** (Figure 4-6). The Cu(2)–N(4) distance (2.330(5) Å) is shorter than that in the copper(I) complex $[(\text{TBTA})_2\text{Cu}_2]^{2+}$ (Cu–N(4): 2.742 Å) but longer than that in the copper(II) complex $[(\text{TBTA})\text{CuCl}_2]$ (Cu–N(4): 2.119 Å).¹⁹³ The enhanced interaction between Cu(2) and N(4) in

complex **4-1** is possibly due to the increased electron deficiency of Cu(2). The largely elongated thermal ellipsoids of the triazole 3 indicated the thermal motion along the Cu(3)–N(3) bond. Hence, the coordination of Cu(3) to N(3) is weak and the Cu(3) could dissociate by excess alkyne under catalytic CuAAC condition to reduce steric hindrance of azide coordination and first N–C bond formation. Overall, the above structural analysis of the tri-copper(I)-acetylide complex **1** reveals the origin of its stability and the features promoting its coordination with an azide.

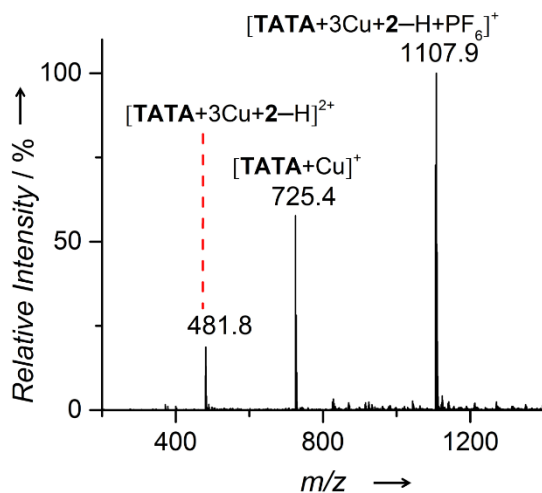


Figure 4-7 ESI-MS spectrum of 100 μ M **TATA**/(**4-2**)/Cu(MeCN)₄PF₆ 1:1:3 solution (0.1 mM in MeOH containing 1% H₂O). The assignment of each signal was based on analysis of the isotopic pattern (Figure 4-3).

The above results revealed the origin of the stability of the tri-copper(I)-acetylide complex **4-1** and stronger copper(I)-azide interaction. The ESI-MS spectrum of **TATA**/(**4-2**)/Cu(MeCN)₄PF₆ 1:1:3 solution (0.1 mM in MeOH containing 1% H₂O) (Figure 4-7) is similar to the ESI-MS spectrum of complex **4-1** (0.1 mM in MeOH) (Figure 4-3), both containing a majority of the complex **4-1** monomer and a small portion of the **TATA**-copper(I) complex due to protonation of the acetylide. The absence of mono- and di-copper(I) acetylide complexes indicates their instability against protonation in methanol.

4.3 Activity Studies

4.3.1 CuAAC Reaction in Nitrogen Atmosphere

In CuAAC reaction, the complex **4-1** showed a much higher catalytic activity than the “free” copper(I) under N₂. The CuAAC reaction of the alkyne **4-2** and benzyl azide in the presence of 2% of the complex **4-1** (calculated based on monomer structure) reached 70% yield in an hour at room temperature (Figure 4-8). Under the same conditions using the same amount (6%) of copper(I) (Cu(MeCN)₄PF₆) but without the TATA ligand, only 4% yield was obtained. Replacing 2% complex **4-1** with 6% TATA and 6% copper(I) result in similar rate, but further addition of TATA largely decreased the rate.

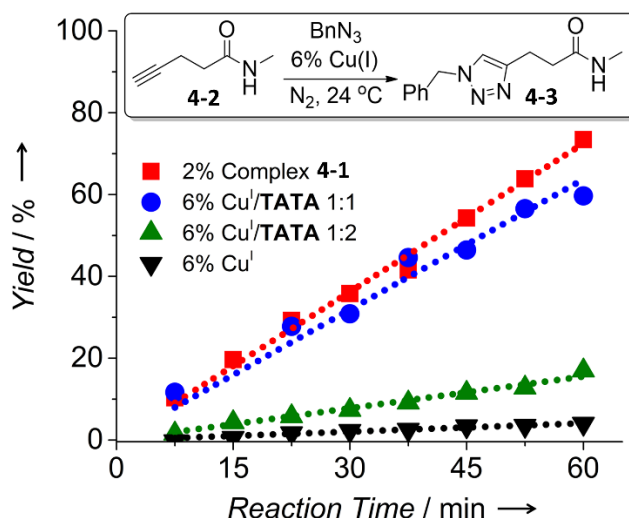


Figure 4-8 Comparison of the catalytic efficiency of **4-1** vs Cu(MeCN)₄PF₆/TATA at various ratios during the CuAAC reaction of **4-2** (10 mM) with benzyl azide (BnN₃, 10 mM) in methanol at 24°C under N₂. Reaction yield was measured by LC-MS/MS.

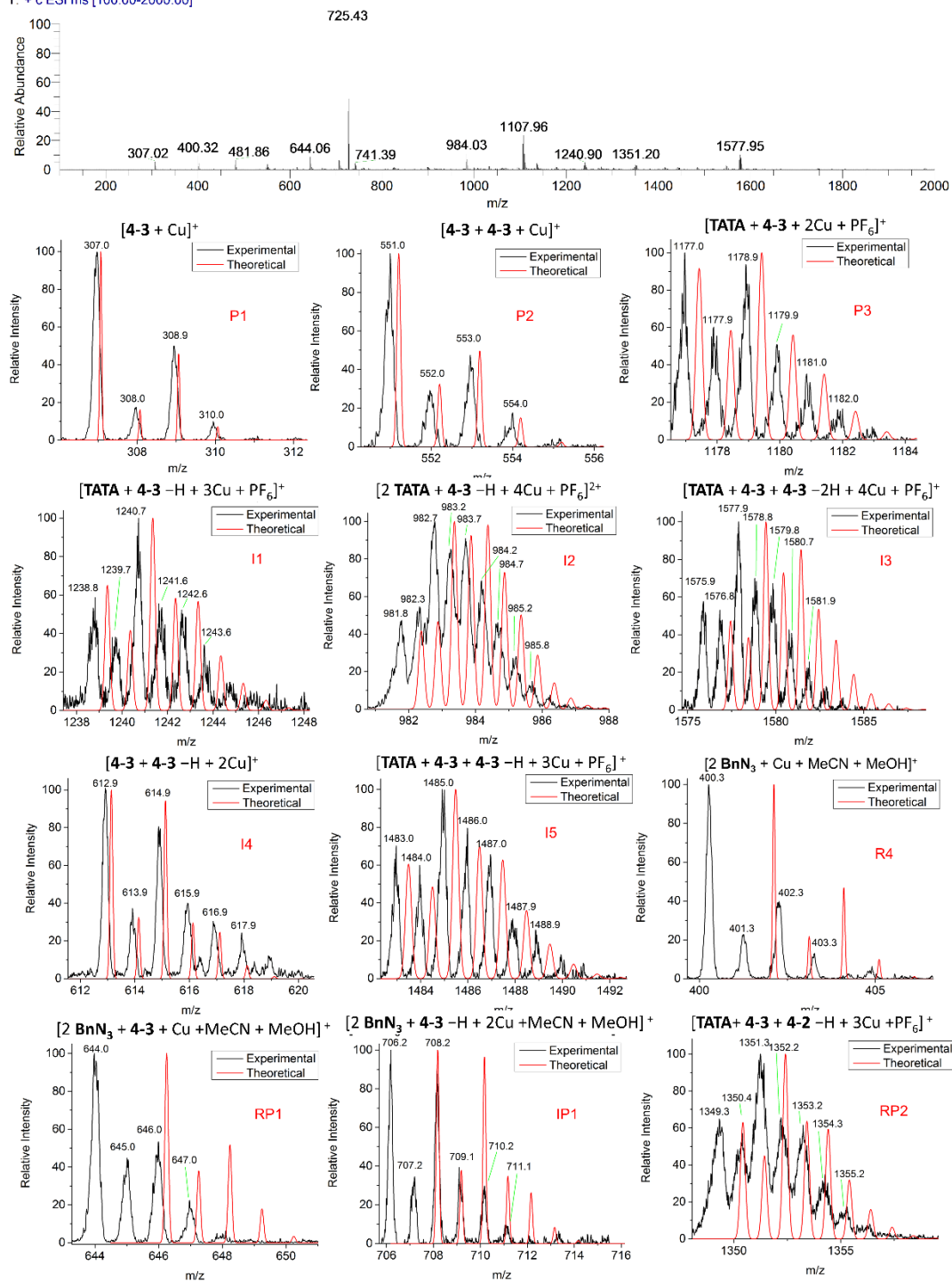


Figure 4-9 ESI-MS Spectrum of Tri-copper(I)-TATA-acetylide Reacting with BnN₃, and Isotopic Patterns of Selected Peaks.

The ESI-MS of the reaction mixtures (Figure 4-9) showed both the presence of the tri-copper(I) and di-copper(I) intermediates, as well as other high nuclear aggregates.

4.3.2 Reaction in Air

Complex **4-1** was air-stable in solid state but can be slowly oxidized overnight in MeOH. The oxidation of copper(I) resulted a decrease in the rate of the reaction in air (Figure 4-10A). Increasing the ratio of **TATA**/Cu to 1:1 could protect copper(I) from oxidation during the reaction, indicated by the same rates for the reaction run in air and in N₂. Higher yields were obtained for the reaction run in air catalyzed by **TATA**-copper(I) or (**TATA**)₂-copper(I) than by the commonly used ligand **TBTA**¹¹⁰ (Figure 4-10B). This result indicates that the bulky adamantyl groups at the triazole arms of **TATA** might reduce the air oxidation of copper(I).

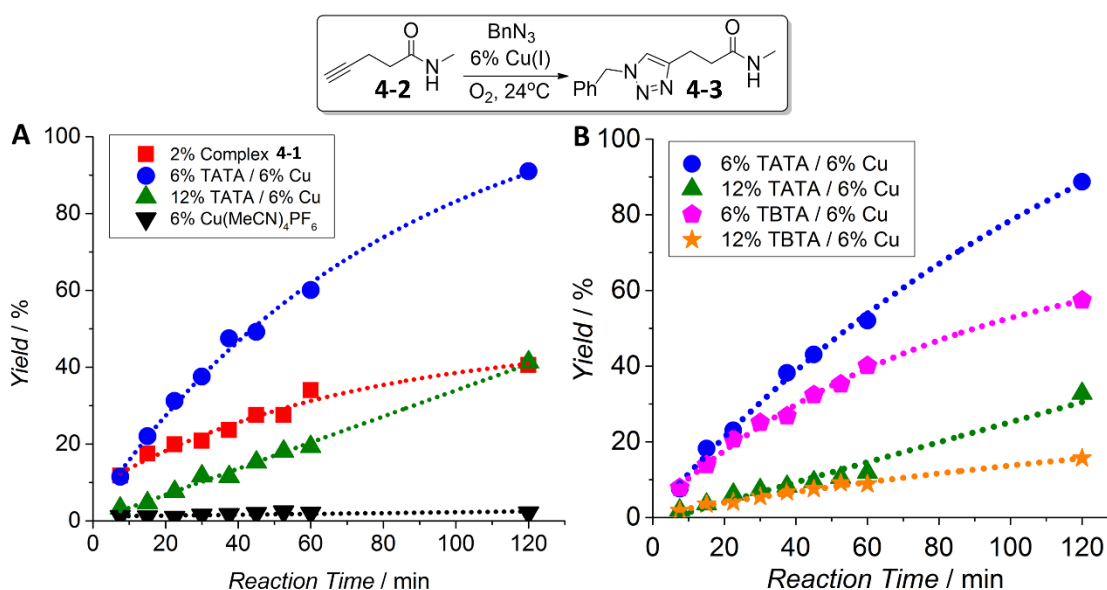
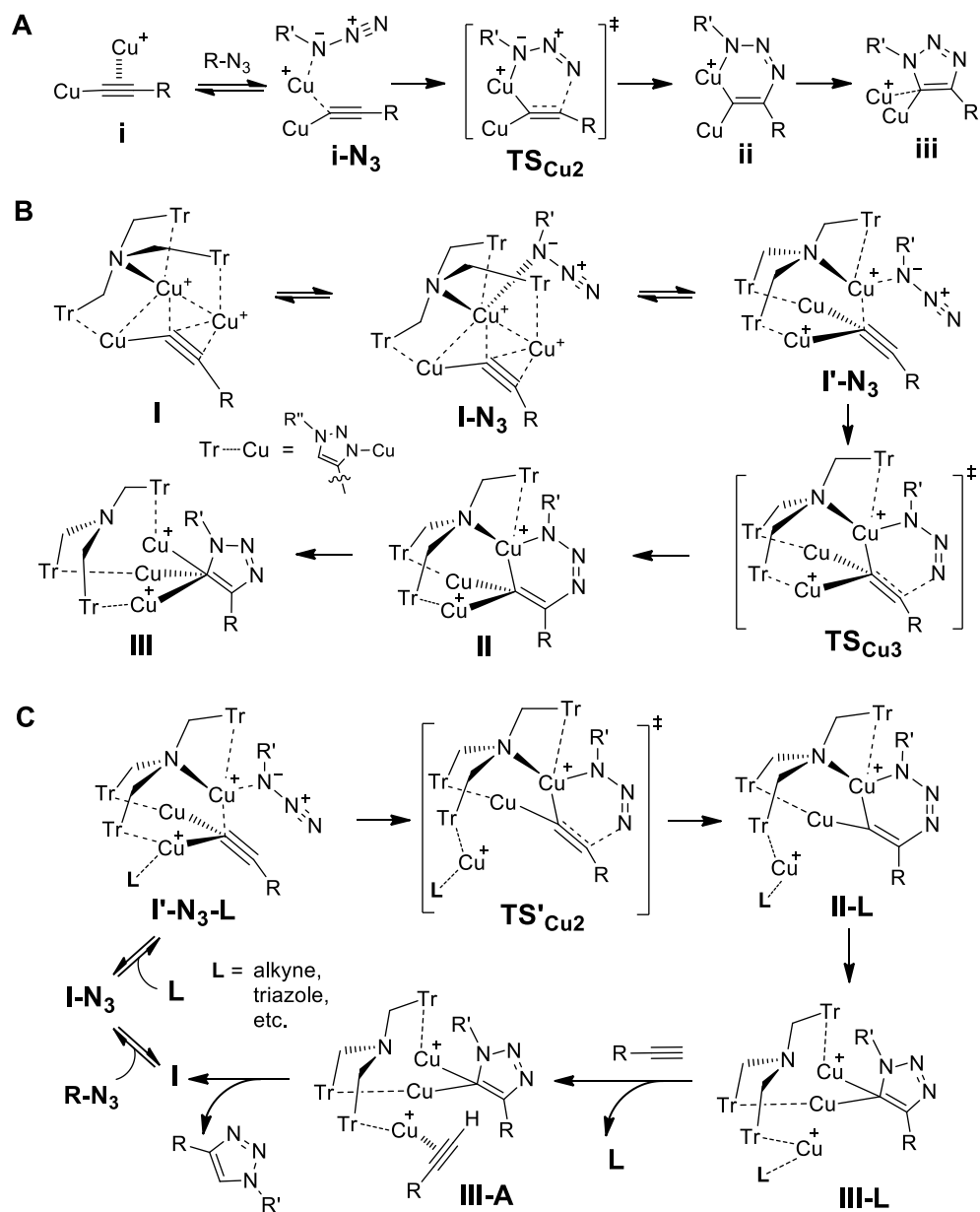


Figure 4-10 Kinetic profiles for the CuAAC reaction of **4-2** (10 mM) with benzyl azide (10 mM) in methanol at 24°C. A. Comparison of the anti-oxidation ability of **4-1** vs Cu(MeCN)₄PF₆/**TATA** at various ratios in air. B. Comparison of the anti-oxidation ability of **TATA** vs **TBTA** during the reaction in air. Reaction yield was measured by LC-MS/MS as described in experimental method.

4.4 Mechanism Proposal

On the basis of the unique structure of complex **4-1** and the previously proposed mechanism involving a di-copper-acetylide (Scheme 4-2A),^{40, 46, 48-49, 52, 85, 89} we proposed the mechanism for C-N bond formation from the tri-copper acetylide **I** (Scheme 4-2B). To form the azide-copper-acetylide precursor complex (**I-N₃**), the alkylated nitrogen of the azide is expected to preferentially interact with the electron-deficient Cu(2). Calculations suggested that the Cu-acetylide bond is weakened by this coordination, resulting in a more symmetric $\mu_2, \eta^{1,1}$ coordination mode.^{47, 53} Thus, the weakly coordinated Cu(3) can then σ -coordinate with the acetylide to form the complex **I'-N₃**, which reduces the steric hindrance for N-C bond formation. Through the transition state **TS_{Cu3}** involving three Cu atoms, the acetylide and the distal nitrogen of the azide form the first C-N bond, resulting in the metallacycle intermediate **II** that readily eliminates one Cu^I to yield the tri-copper triazolide **III** (Scheme 4-2B). Under catalytic conditions (Scheme 4-2C), the excess ligands (**L** = alkyne, triazole product, etc.) readily coordinate to copper of the azide adduct **I-N₃**, forming **I'-N₃-L**. This process promotes the dissociation of the copper from the acetylide in the complex **I'-N₃-L**, forming a more favorable transition state **TS'_{Cu2}** with two copper atoms rather than three copper atoms in **TS_{Cu3}** for the first C-N bond formation as the rate-limiting step, leading to the metallacycle **II-L** and then the triazolide **III-L**. During this process, other ligand **L** may exchange with the alkyne to form the triazolide-alkyne adduct **III-A** that rapidly undergo protonation of the triazolide by the proximal alkyne to generate the triazole product and regenerate the catalyst **I**.



Scheme 4-2 A. Previously proposed mechanism of C-N bond formation during CuAAC reaction, involving two Cu^I atoms in the rate-determining transition state $\text{TS}_{\text{Cu}2}$. Ligands are omitted. B. Analogous mechanism involving three Cu^I atoms in the transition state $\text{TS}_{\text{Cu}3}$. C. Proposed mechanism of CuAAC under catalytic conditions where excess ligands L may promote a more favorable transition state ($\text{TS}'_{\text{Cu}2}$) with two copper atoms for the C-N bond formation

4.5 Conclusions

In this work, we isolated and characterized the tri-copper acetylide complex bearing **TATA** ligand. The multi-dentate coordination of **TATA**, electron-deficiency of the tri-copper-acetylide, and π back-bonding from copper to the ligands stabilize the complex and facilitate the coordination with the azide. The tri-copper-acetylide complex **1** showed good catalytic activity in CuAAC reaction.

4.6 Experimental Section

4.6.1 General Methods

Reagents and solvents were purchased from Sigma-Aldrich, VWR or TCI America and used without further purification. LC-MS grade solvent was purchased from VWR. Single-crystal X-ray structure was obtained using a Bruker DUO platform diffractometer equipped with a 4K CCD APEX II detector. Positive ion ESI-MS data were acquired using a Thermo Finnigan LCQ Deca XP ion trap mass spectrometer. Positive ion MALDI-TOF mass was recorded on an AB SCIEX 4800 MALDI TOF/TOF analyzer using α -cyano-4-hydroxycinnamic acid as a matrix. FT-IR was characterized using a Nicolet iS10 FT-IR Spectrometer. NMR spectra were recorded on JEOL ECX-400 or ECA-500 spectrometer.

4.6.2 Experimental Details

4.6.2.1 *Synthesis of Complex 4-1*

The experiment was performed in a nitrogen glove box and all solvents were degassed. To a stirred solution of **TATA** (20 mM in CH_2Cl_2 , 1 mL) was added **2** (100 mM in MeOH, 200 μL), $\text{Cu}(\text{MeCN})_4\text{PF}_6$ (30 mM in MeOH, 2 mL), and H_2O (100 μL) under N_2 . The solution was stirred for 6 hours, transferred to a small beaker, and blow-dried with a flow of N_2 . The pale yellow

residue was re-dissolved in a mixed solvent of MeOH (1 mL) and CH₂Cl₂ (1 mL) (1:1 ratio), filtered into a 5 mL glass vial. The open vial was placed inside a tightly capped 20 mL glass vial containing ether (5 mL) to allow slow diffusion of ether vapor into the complex solution. To reduce vibration, stabilize the temperature and protect from light, the 20 mL vial was wrapped with cotton and placed inside a beaker covered with aluminum foil. After a week of incubation at room temperature inside the N₂ glove box, complex **1** was obtained as pale yellow needling single crystals. The single crystals were taken out from the mother liquor and immediately frozen to -150°C for X-ray analysis.

For melting point measurement, newly grown single crystal of complex **1** was washed with methanol × 1, ether × 1, dried in glove box. The pale yellow small needle crystals were moved out of the glove box and the melting point was measured in air. The complex did not melt below 210°C. The pale yellow small needle crystals started to turn brown at 165°C (decompose) and turned black at 180°C.

4.6.2.2 *NMR Spectroscopy of Complex 4-1*

In a nitrogen glove box, newly grown single crystal of complex **1** was washed briefly with methanol × 1, ether × 1 (the solvents were removed by pipettes) and dried for several minutes. The drying procedure resulted in breaking down of the needle-shaped crystals into tiny pale yellow solids. The complex were dissolved in 70% (99.8% D) CD₃OD and 30% (99.9% D) CD₂Cl₂ (measured by micropipette). The solution was sealed in a screw-capped NMR tube and the ¹H NMR (Figure 4-4), ¹H-¹H DQF-COSY NMR (Figure 4-5), ¹⁹F NMR (Figure 4-11) were recorded at room temperature.

^{19}F NMR (565 MHz, Methanol- d_4) (crystals of complex **1** synthesized using water as base)

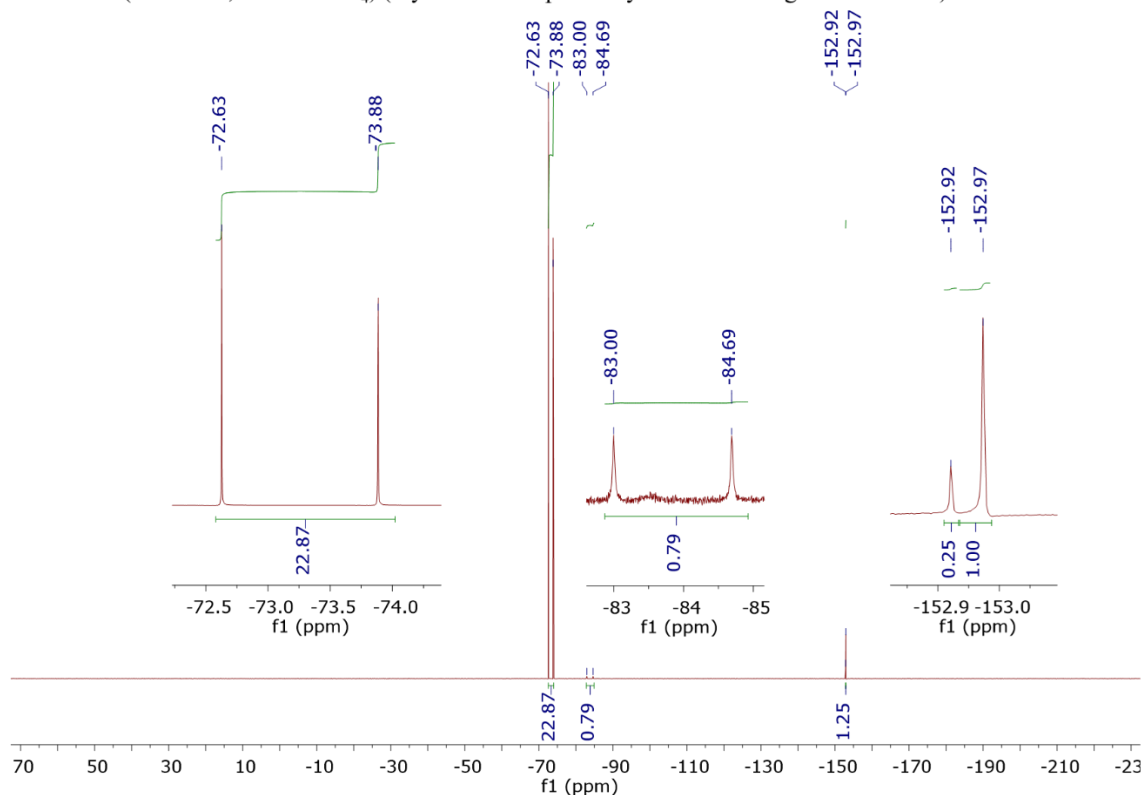


Figure 4-11 ^{19}F -NMR of complex **4-1** synthesized using water as base.

^{19}F NMR (565 MHz, locked on Methanol- d_4) δ -73.26 (d, $J = 710.0$ Hz, 22.87 F, PF_6^-), -83.84 (d, $J = 955.4$ Hz, 0.79 F, PO_2F_2^-), -152.92 (s, 0.25 F, $^{10}\text{BF}_4^-$), -152.97 (s, 1 F, $^{11}\text{BF}_4^-$). The ^{19}F NMR of the complex **1** crystal dissolved in 70% CD_3OD and 30% CD_2Cl_2 indicates the presence of approximately 1.68 PF_6^- , 0.18 PO_2F_2^- , 0.14 BF_4^- as anions in each tri-copper(I) acetylide. The doublet at $\delta = -83.84$ is assigned as PO_2F_2^- according to literature reported value, which is generated by the hydrolysis of PF_6^- .¹⁹⁸⁻²⁰² The peaks at $\delta = -152.92$ and $\delta = -152.97$ are assigned to the anion BF_4^- , with an integral ratio of 1:4, in agreement with the natural abundance of the two boron isotopes ^{10}B and ^{11}B .²⁰³ The ^{19}F NMR of $\text{Cu}(\text{MeCN})_4\text{BF}_4$ in a 70% CD_3OD 30% CD_2Cl_2 mixture was recorded as control (see the spectrum below), in which $^{10}\text{BF}_4^-/^{11}\text{BF}_4^-$ appeared at $\delta = -154.22$ and $\delta = -154.27$ with integral ratio of 1:4. The spin quantum numbers of ^{10}B and ^{11}B are 3 and 3/2, respectively. The expected ^{11}B -F coupling in $^{11}\text{BF}_4^-$ was

also absent in this system, probably due to the adjacent spin $3/2$ $^{65}\text{Cu}^{\text{I}}/^{63}\text{Cu}^{\text{I}}$. The BF_4^- anion should be generated by reaction of HF with borosilicate glass.²⁰⁴ HF was originated from hydrolysis of PF_6^- catalyzed by the Cu^{I} complex¹⁹⁸⁻²⁰² during the crystallization process. In the control group, we attempted to grow the single crystal of complex **1** using one equivalent of sodium hydroxide or potassium hydroxide as a base to deprotonate one equivalent of alkyne, instead of using water as a base that can generate significant amount of protons that facilitate the hydrolysis of PF_6^- .¹⁹⁸ The resulted crystals contain a much-lower amount of BF_4^- anions (see the corresponding ^{19}F NMR), but the crystals obtained using this method were very thin and not suitable for X-ray diffraction analysis.

^{19}F NMR (565 MHz, METHANOL- D_4) $\text{Cu}(\text{MeCN})_4\text{BF}_4$ in 70% CD_3OD and 30% CD_2Cl_2

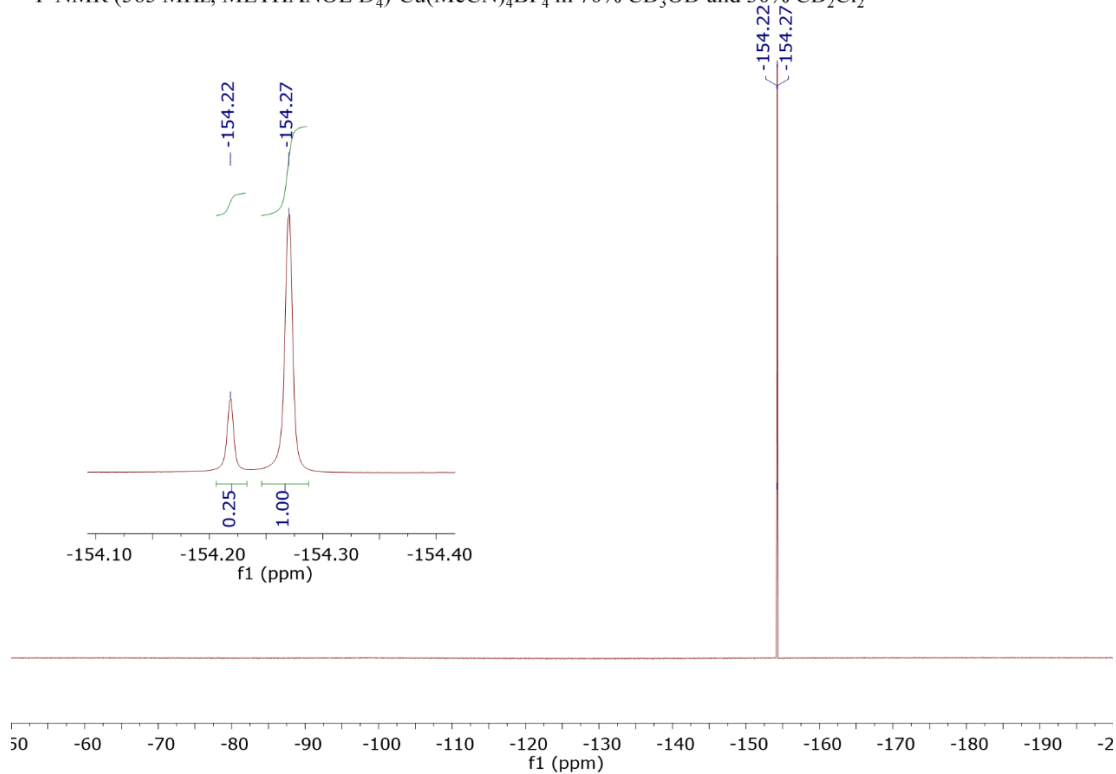


Figure 4-12 ^{19}F -NMR of $\text{Cu}(\text{MeCN})_4\text{BF}_4$.

^{19}F NMR (565 MHz, METHANOL- D_4) Complex **1** in 70% CD_3OD and 30% CD_2Cl_2
 Crystals of complex **1** synthesized using NaOH as base

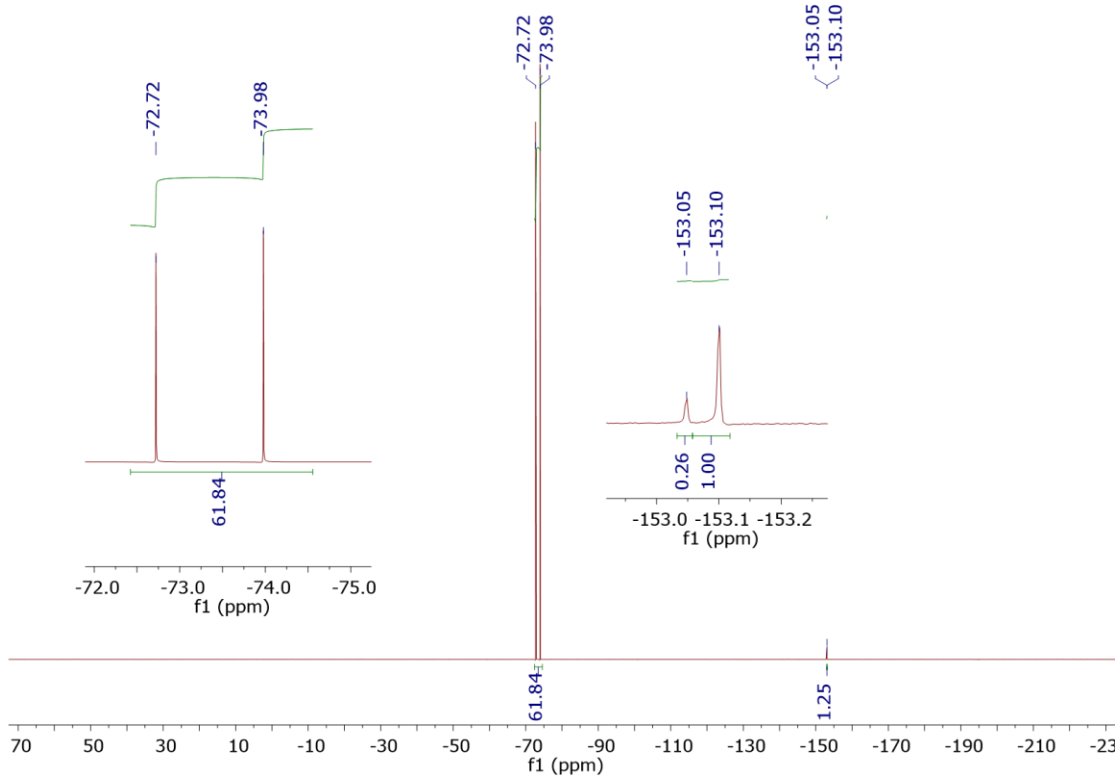
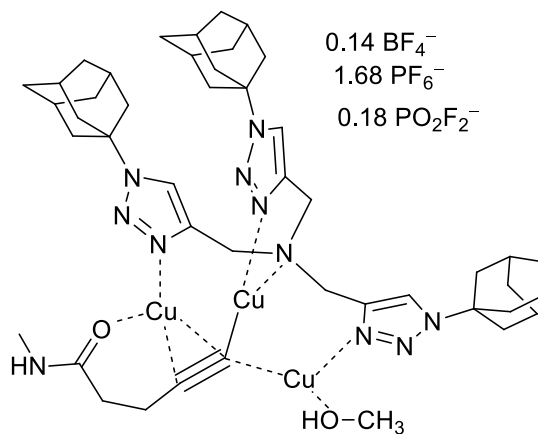


Figure 4-13 The ^{19}F -NMR of the single crystal obtained by addition of one equivalent NaOH into the solution for making complex **4-1** (TATA, **4-2**, $\text{Cu}(\text{MeCN})_4\text{PF}_6$ mixture), which inhibited the hydrolysis of PF_6^- .

4.6.2.3 Elemental Analysis of Complex 4-1



Newly grown single crystal of complex **1** was washed with methanol \times 1, ether \times 1, dried in glove box, stored in dry ice and shipped overnight to Midwest Micro lab, LLC for elemental analysis. Found: C, 43.40 \pm 0.3%; H, 5.18 \pm 0.3%; N, 11.73 \pm 0.3%; P, 4.41 \pm 0.4%. According to the ^{19}F NMR of complex **1**, each tri-copper(I) acetylide unit contains approximately 1.68 PF_6^- , 0.18 PO_2F_2^- , 0.14 BF_4^- as anions (see discussion above). Calculated elemental composition based on the above structure (Chemical Formula: $\text{C}_{47.2}\text{H}_{69.4}\text{B}_{0.14}\text{Cl}_{0.2}\text{Cu}_3\text{F}_{11}\text{N}_{11}\text{O}_{2.86}\text{P}_{1.86}$): C, 43.52%; H, 5.24%; N, 12.14%; P, 4.54%.

4.6.2.4 UV-Vis Spectrum of Complex 4-1

One piece of single crystal was taken out from the mother liquor and dissolved in 1 mL MeOH (LC-MS grade) to make a colorless stock solution, and the solution was diluted 10 times with MeOH, and added into a plastic UV cuvette, capped with rubber septa, and test the UV-vis absorption (Figure 4-11). The spectra exhibit an absorption shoulder at 310 nm, which is likely to involve an acetylide to Cu ligand to metal charge transfer transition.

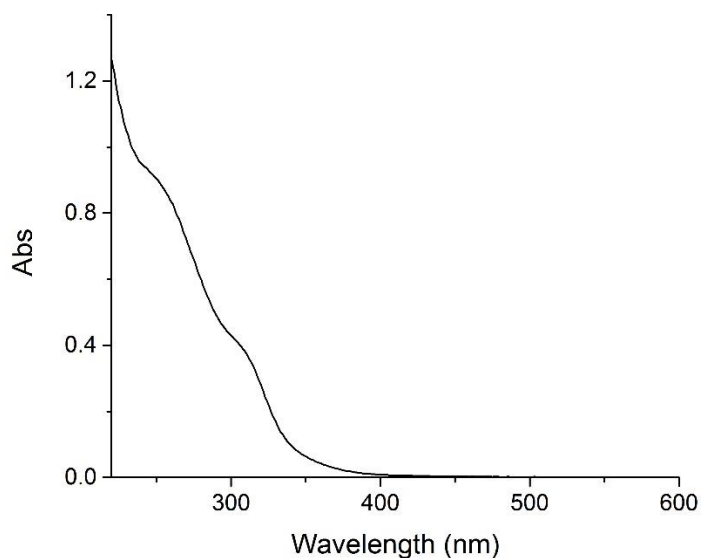


Figure 4-14 UV-Vis Spectra of Complex **4-1** in Methanol under Room Temperature.

4.6.2.5 *Single Crystal X-ray Diffraction Analysis of Complex 4-1*

All measurements were made with a Bruker DUO platform diffractometer equipped with a 4K CCD APEX II detector and an Incoatec 30 Watt Cu microsource with compact multilayer optics. A hemisphere of data (2713 frames at 4 cm detector distance) was collected using a narrow-frame algorithm with scan widths of 0.50° in omega and an exposure time of 40 s/frame at 123K. The data were integrated using the Bruker SAINT program, with the intensities corrected for Lorentz factor, polarization, air absorption, and absorption due to variation in the path length through the detector faceplate. The data were scaled, and an absorption correction was applied using SADABS. The structure was solved with SHELXT 2014, and refined with SHELXL 2014 using full-matrix least-squares refinement. The non-H atoms were refined with anisotropic thermal parameters, and all of the H atoms were calculated in idealized positions and refined riding on their parent atoms. Part of highly disordered solvent molecules and charge-balancing anions could not be determined and their contributions to the electron density were treated using the PLATON/SQUEEZE program. Each unit cell contains two molecules of $\{[\text{Cu}_6(\text{TATA})_2(\mu_3\text{-}\eta^1, \eta^1, \eta^2\text{-C}\equiv\text{CR})_2][\text{PF}_6]_2\}^{2+}$ with other anions and solvents. There are two voids in the unit cell with similar sizes (550 and 539 \AA^3) and electron densities (201 and 196 electrons, respectively). There voids can be filled with highly disordered anions and solvent molecules including 1.36 PF_6^- , 0.36 PO_2F_2^- , 0.28 BF_4^- (ratio based on ^{19}F NMR data, 125 electrons), and possibly 1.81 or 1.69 CH_2Cl_2 and/or Et_2O (76 or 71 electrons, respectively).

4.6.2.6 *ESI-MS Spectra of CuAAC Intermediates between Complex 4-1 and Benzyl Azide*

In an anaerobic chamber, 1 mL TATA (10 mM in MeOH) was mixed with 1 mL $\text{Cu}(\text{MeCN})_4\text{PF}_6$ (30 mM in MeOH), 200 μL 2 (50 mM in MeOH) and 100 μL Na ascorbate (100 mM in H_2O). The mixture was added into 7.7 mL MeOH to generate a TATA- Cu^{I}_3 -acetylide 1 mM stock solution, then further dilute to 100 μM by MeOH. 100 μL of the above solution was added into

800 μL MeOH. 100 μL of benzyl azide (1 mM in MeOH) was added to start the reaction. The spectrum was an averaged scans during 20 – 30 min (Figure 4-9).

4.6.2.7 Comparison of Reaction Yield in Anaerobic Chamber

In an anaerobic chamber, four 1 mL micro test tubes (Titertube®, Bio Rad) were placed in a 96-well Titertube rack. To each tube was added 800 μL solution (1% H_2O in methanol), containing 10 mM **4-2**, 0.1 mM Na ascorbate, and tube A also containing 0.2 mM complex **4-1**, tube B containing 0.6 mM **TATA** and 0.6 mM $\text{Cu}(\text{MeCN})_4\text{PF}_6$, tube C containing 1.2 mM **TATA** and 0.6 mM $\text{Cu}(\text{MeCN})_4\text{PF}_6$, and tube D containing 0.6 mM $\text{Cu}(\text{MeCN})_4\text{PF}_6$. The reaction was started by adding 200 μL benzyl azide (50 mM in MeOH). At 7.5 min intervals, 20 μL aliquots of the reaction mixture were added into four micro test tubes, each containing 980 μL air-saturated solution (40% MeOH, 60% H_2O) of 100 μM DTPA (pH adjusted to 7.0 by NaOH) and 20 μM internal standard (**4-S2**). After 8 sets of aliquots were collected, the 96-well rack was moved out of anaerobic chamber. The samples were injected to a Thermo Finnigan LCQ Deca XP Plus ion trap mass spectrometer by a Thermo Finnigan Surveyor HPLC system. Reagents and product were separated by first static elution in 5% (MeCN, 0.1% formic acid): 95% (H_2O , 0.1% formic acid) for 5 min and then a linear gradient elution to 97% (MeCN, 0.1% formic acid):3% (H_2O , 0.1% formic acid) for 5 min. A set of calibration standards of product **4-3**, ranging from 2 μM to 200 μM , using **4-S2** as internal standard, was injected before the set of samples. The concentration of product in each sample was calculated based on the calibration curve using LC-MS/MS method.

4.6.2.8 Comparison of Reaction Yield in Air

For comparison of **TATA**/complex **4-1**: In an anaerobic chamber, four 1 mL micro test tubes (Titertube®, Bio Rad) were placed in a 96-well Titertube rack. To each tube was added 800 μL

solution (1% H₂O in methanol), containing 10 mM **4-2**, 0.1 mM Na ascorbate. Tube A also containing 0.2 mM complex **4-1**, tube B containing 0.6 mM **TATA** and 0.6 mM Cu(MeCN)₄PF₆, tube C containing 1.2 mM **TATA** and 0.6 mM Cu(MeCN)₄PF₆, and tube D containing 0.6 mM Cu(MeCN)₄PF₆.

For comparison of **TATA/TBTA**: In an anaerobic chamber, four 1 mL micro test tubes (Titertube®, Bio Rad) were placed in a 96-well Titertube rack. To each tube was added 800 µL solution (1% H₂O in methanol), containing 10 mM **4-2**, 0.1 mM Na ascorbate, and tube A also containing 0.6 mM **TATA** and 0.6 mM Cu(MeCN)₄PF₆, tube B containing 1.2 mM **TATA** and 0.6 mM Cu(MeCN)₄PF₆, tube C containing 0.6 mM **TBTA** and 0.6 mM Cu(MeCN)₄PF₆, and tube D containing 1.2 mM **TBTA** and 0.6 mM Cu(MeCN)₄PF₆.

Then the mixtures were moved out of anaerobic chamber. The reaction was started by adding 200 µL benzyl azide (50 mM in air-saturated MeOH). The tubes were exposed in air without cap. During the first hour, at 7.5 min intervals, 20 µL aliquots of the reaction mixture were added into four micro test tubes, each containing 980 µL air-saturated solution (40% MeOH, 60% H₂O) of 100 µM DTPA (pH adjusted to 7.0 by NaOH) and 20 µM internal standard (**4-S2**). After 8 sets of aliquots were collected, the last aliquot was taken at 120 min. The samples were injected to a Thermo Finnigan LCQ Deca XP Plus ion trap mass spectrometer by a Thermo Finnigan Surveyor HPLC system using the same quantitation method as discussed above.

4.6.3 Crystal Data for Complex $[\text{Cu}_6(\text{TATA})_2(\mu_3\text{-}\eta^1, \eta^1, \eta^2\text{-C}\equiv\text{CR})_2]^{4+}$

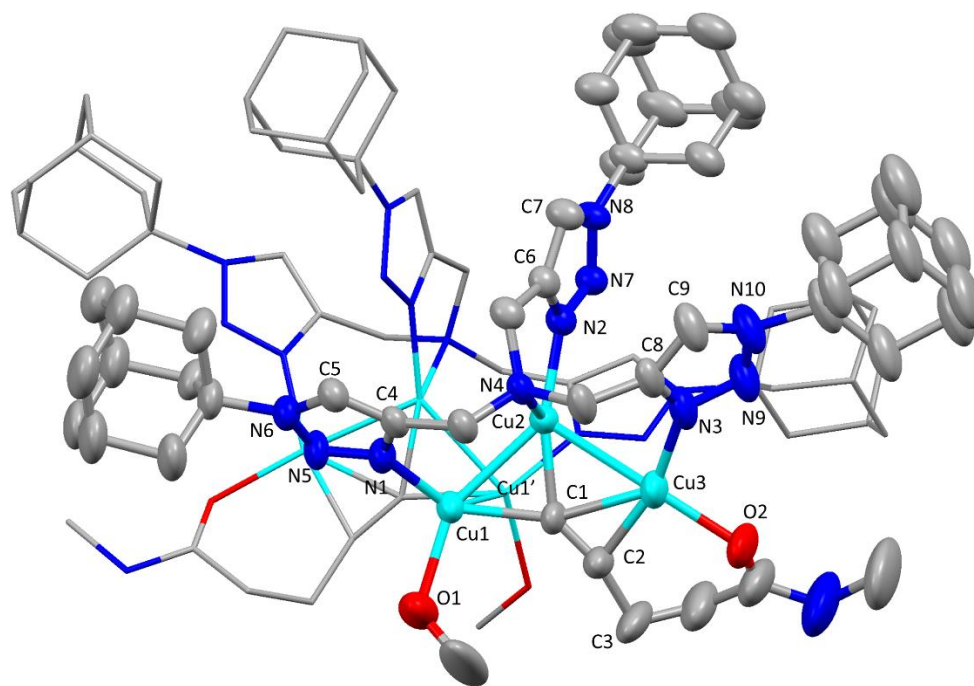


Table 4-1 Crystal Data and Structure Refinement for Complex $[\text{Cu}_6(\text{TATA})_2(\mu_3\text{-}\eta^1, \eta^1, \eta^2\text{-C}\equiv\text{CR})_2]^{4+}$.

Empirical formula	$\text{C}_{92}\text{H}_{132}\text{Cu}_6\text{F}_{12}\text{N}_{22}\text{O}_4\text{P}_2$	
Formula weight	2281.37	
Temperature	123(2) K	
Wavelength	1.54178 Å	
Crystal system	Monoclinic	
Space group	$P 2/c$	
Unit cell dimensions	$a = 20.7182(14)$ Å	$\alpha = 90^\circ$.
	$b = 14.8867(9)$ Å	$\beta = 116.741(4)^\circ$.
	$c = 21.1658(13)$ Å	$\gamma = 90^\circ$.
Volume	$5829.9(7)$ Å ³	
Z	2	
Density (calculated)	1.300 Mg/m ³	
Absorption coefficient	2.056 mm ⁻¹	
F(000)	2364	
Crystal size	$0.50 \times 0.15 \times 0.08$ mm ³	
Theta range for data collection	2.968 to 66.756° .	
Index ranges	$-20 \leq h \leq 23$, $-17 \leq k \leq 16$, $-25 \leq l \leq 24$	
Reflections collected	36647	
Independent reflections	9908 [R(int) = 0.0380]	
Completeness to theta = 66.756°	95.6 %	
Absorption correction	Empirical	
Max. and min. transmission	0.7528 and 0.4969	
Refinement method	Full-matrix least-squares on F ²	
Data / restraints / parameters	9908 / 1622 / 835	
Goodness-of-fit on F ²	1.027	
Final R indices [I > 2σ(I)]	R1 = 0.0808, wR2 = 0.2057	
R indices (all data)	R1 = 0.0987, wR2 = 0.2262	
Largest diff. peak and hole	1.744 and -0.511 e Å ⁻³	

Table 4-2 Selected Bond Lengths for Complex $[\text{Cu}_6(\text{TATA})_2(\mu_3\text{-}\eta^1, \eta^1, \eta^2\text{-C}\equiv\text{CR})_2]^{4+}$.

Atom	Atom	Length/Å	Atom	Atom	Length/Å
Cu1	Cu2	2.4818(10)	C1	C2	1.235(8)
Cu2	Cu3	2.5548(11)	N1	N5	1.312(6)
Cu1	Cu1'	2.5097(19)	N2	N7	1.329(6)
Cu1	C1	2.015(5)	N3	N9	1.331(7)
Cu2	C1	1.933(5)	N1	C4	1.363(7)
Cu3	C1	2.151(5)	N2	C6	1.365(7)
Cu3	C2	1.994(6)	N3	C8	1.349(8)
Cu1	O1	2.159(7)	N5	N6	1.343(6)
Cu3	O2	1.964(11)*	N7	N8	1.341(6)
Cu3	O2A	2.042(11)*	N9	N10	1.330(8)
Cu1	N1	1.990(5)	C4	C5	1.357(8)
Cu2	N2	1.948(4)	C6	C7	1.384(7)
Cu3	N3	1.977(6)	C8	C9	1.348(9)
Cu2	N4	2.330(5)			

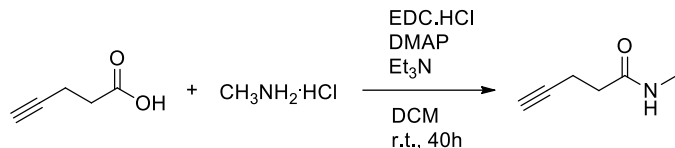
Table 4-3 Selected Bond Angles for Complex $[\text{Cu}_6(\text{TATA})_2(\mu_3\text{-}\eta^1, \eta^1, \eta^2\text{-C}\equiv\text{CR})_2]^{4+}$.

Atom	Atom	Atom	Angle/°	Atom	Atom	Atom	Angle/°
C1	C2	C3	167.6(11)*	Cu1	Cu2	C1	52.6(2)
C1	C2	C3A	156.9(13)*	Cu3	Cu2	C1	55.2(2)
Cu1	C1	Cu2	77.8(2)	Cu3	Cu2	N2	113.0(1)
Cu1	C1	C2	141.3(5)	Cu1	Cu2	N2	142.2(1)
Cu2	C1	C2	140.8(5)	N4	Cu2	Cu1	94.5(1)
Cu2	C1	Cu3	77.2(2)	N4	Cu2	N2	81.2(2)
Cu3	C1	C2	65.9(4)	N4	Cu2	Cu3	97.9(1)
Cu3	C2	C1	79.8(4)	N4	Cu2	C1	115.1(2)
Cu2	Cu1	C1	49.6(2)	Cu2	Cu3	C1	47.6(2)
Cu2	Cu1	N1	96.5(1)	C1	Cu3	C2	34.4(3)
C1	Cu1	O1	102.3(3)	O2	Cu3	C2	90.3(6)
N1	Cu1	O1	97.3(2)	O2	Cu3	N3	105.5(6)
Cu2	Cu1	Cu1'	70.09(4)	Cu2	Cu3	N3	84.6(2)
Cu1	Cu2	Cu3	104.76(4)				

* The acetylide molecule is disordered from C3 to the amide group. From C3 to the amide it has two different positions in the crystal with 50% occupancy for each possibility. The distance of Cu(3)–O(2), and the angle of C(1)–C(2)–C(3) corresponds to the two different O(2) and C(3) positions.

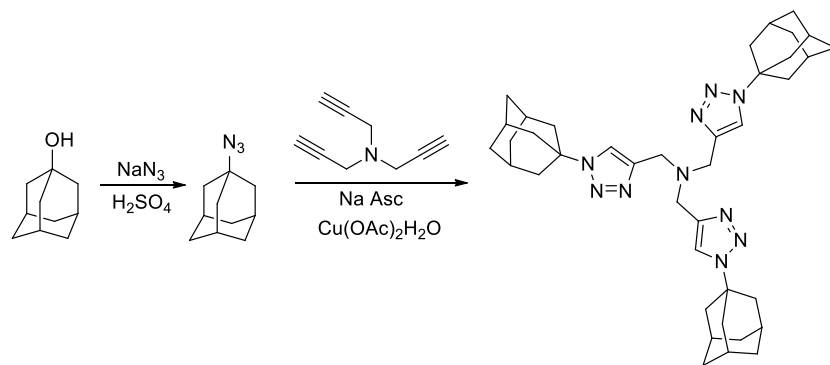
4.6.4 Compound Synthesis Procedure

N-methyl-4-pentynamide (4-2)



To a stirred solution of 4-pentynoic acid (294 mg, 3 mmol), methylamine hydrochloride (405 mg, 6 mmol), DMAP (37 mg, 0.3 mmol) and Et_3N (1.68 mL, 12 mmol) in CH_2Cl_2 (3 mL) was added EDC·HCl (766 mg, 4 mmol) in CH_2Cl_2 (3 mL). The mixture was stirred for 40 h at room temperature, then washed with $\text{H}_2\text{O} \times 2$, saturated $\text{NaCl} \times 1$, and dried over Na_2SO_4 . The crude product was purified by column chromatography (EtOAc) to yield 160.9 mg (48%) pure product as white crystal. ^1H NMR (500 MHz, CDCl_3) δ 6.09 (br, 1H), 2.78 (d, $J = 4.7$ Hz, 3H), 2.49 (td, $J = 7.1, 2.1$ Hz, 2H), 2.37 (t, $J = 7.1$ Hz, 2H), 1.96 (t, $J = 2.1$ Hz, 1H). ^{13}C NMR (126 MHz, CDCl_3) δ 171.8, 83.1, 69.3, 35.2, 26.4, 15.0.

Tris((1-adamantanyl-1*H*-1,2,3-triazol-4-yl)methyl)amine (TATA)

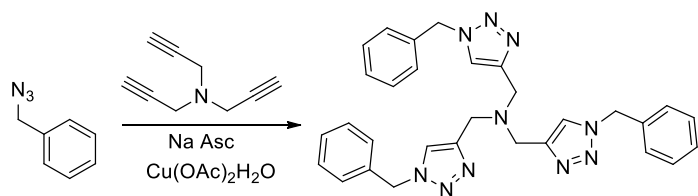


1-azidoadamantane was prepared according to literature procedure.²⁰⁵

To a 100 mL Schlenk tube was added tripropargylamine (262 mg, 2 mmol), 1-azidoadamantane (1.24 g, 7 mmol) and $\text{Cu}(\text{OAc})_2\cdot\text{H}_2\text{O}$ (100 mg, 0.5 mmol) under N_2 . Methanol (10 mL) and

CH₂Cl₂ (10 mL) were added and the mixture was stirred for 10 min. A solution of sodium ascorbate (198 mg, 1 mmol) in H₂O (2 mL) was added into the above solution under N₂. The mixture was sealed and stirred at 50 °C for 48 h. After cooling, the reaction was quenched by addition of an aqueous solution of Na₅DTPA (500 mM, 3 mL). The solvent was removed, and the residue was dissolved in 60 mL CH₂Cl₂/H₂O mixture, extracted with CH₂Cl₂ (3 × 30 mL). The combined organic layer was dried over Na₂SO₄, filtered, and concentrated under vacuum. The crude product was purified by recrystallization using acetone to yield **TATA** (1.13 g, 1.7 mmol, 85%) as a white crystal. ¹H NMR (400 MHz, CDCl₃) δ 7.94 (s, 3H), 3.75 (s, 6H), 2.24 (s, 27H), 1.77 (s, 18H). ¹³C NMR (101 MHz, CDCl₃) δ 142.2, 121.0, 59.6, 46.9, 43.1, 36.0, 29.5. HRMS (MALDI-TOF): m/z 663.4589 ([M+H]⁺, calcd 663.4611). Melting point: 184–185°C.

Tris[(1-benzyl-1*H*-1,2,3-triazol-4-yl)methyl]amine (TBTA)

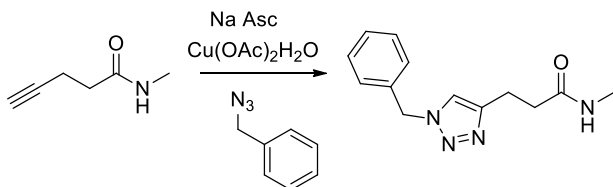


To a 100 mL Schlenk tube was added tripropargylamine (262 mg, 2 mmol), benzyl azide (932.5 mg, 7 mmol) and Cu(OAc)₂·H₂O (100 mg, 0.5 mmol) under N₂. Methanol (5 mL) and CH₂Cl₂ (5 mL) were added and the mixture was stirred for 10 min. A solution of sodium ascorbate (198 mg, 1 mmol) in H₂O (2 mL) was added into the above solution under N₂. The mixture was sealed and stirred at 50 °C for 24 h. After cooling, the reaction was quenched by addition of an aqueous solution of Na₅DTPA (500 mM, 3 mL). The solvent was removed, and the residue was dissolved in 60 mL CH₂Cl₂/H₂O mixture, extracted with CH₂Cl₂ (3 × 30 mL). The combined organic layer was dried over Na₂SO₄, filtered, and concentrated under vacuum. The crude product was purified by column chromatography (5% MeOH in DCM) to yield 658 mg (62%) pure **TBTA** as white

solid. ^1H NMR (400 MHz, CDCl_3) δ 7.67 (s, 3H), 7.39 – 7.17 (m, 15H), 5.49 (s, 6H), 3.71 (s, 6H).

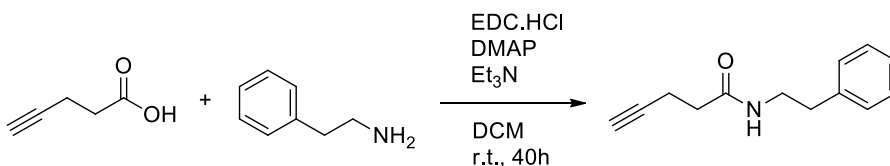
^{13}C NMR (101 MHz, CDCl_3) δ 144.1, 134.8, 129.2, 128.8, 128.1, 54.2, 47.1.

3-(1-benzyl-1H-1,2,3-triazol-4-yl)-N-methylpropanamide (4-3)



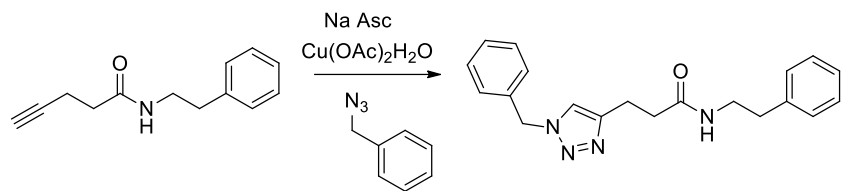
To a 25 mL Schlenk tube was added **4-2** (22 mg, 0.2 mmol), benzyl azide (40 mg, 0.3 mmol) and $\text{Cu}(\text{OAc})_2\cdot\text{H}_2\text{O}$ (4 mg, 0.02 mmol) under N_2 . Methanol (1 mL) and CH_2Cl_2 (1 mL) were added and the mixture was stirred for 10 min. A solution of sodium ascorbate (20 mg, 0.1 mmol) in H_2O (1 mL) was added into the above solution under N_2 . The mixture was sealed and stirred at room temperature overnight, then quenched by addition of an aqueous solution of Na_5DTPA (100 mM, 3 mL). The mixture was extracted with CH_2Cl_2 (3×10 mL). The combined organic layer was dried over Na_2SO_4 , filtered, and concentrated under vacuum. The crude product was purified by column chromatography (2% MeOH in EtOAc and then 20% MeOH in DCM) to yield 24 mg (70%) pure product as white solid. ^1H NMR (500 MHz, CDCl_3) δ 7.36 – 7.17 (m, 6H), 6.25 (s, 1H), 5.44 (s, 2H), 2.97 (t, $J = 7.1$ Hz, 2H), 2.68 (d, $J = 4.8$ Hz, 3H), 2.55 (t, $J = 7.2$ Hz, 2H). ^{13}C NMR (126 MHz, CDCl_3) δ 172.7, 147.1, 134.8, 129.1, 128.8, 128.0, 121.6, 54.1, 35.7, 26.3, 21.6. ESI-MS: m/z 245.10 ($[\text{M}+\text{H}]^+$, calcd 245.13).

N-phenethylpent-4-ynamide (4-S1)



To a stirred solution of 4-pentynoic acid (196 mg, 2 mmol), phenethylamine (363 mg, 3 mmol), DMAP (25 mg, 0.2 mmol) and Et₃N (1.12 mL, 8 mmol) in CH₂Cl₂ (2 mL) was added EDC•HCl (575 mg, 3 mmol) in CH₂Cl₂ (2 mL). The mixture was stirred for overnight at room temperature, then washed with H₂O × 2, saturated NaCl × 1, and dried over Na₂SO₄. The crude product was purified by column chromatography (EtOAc : hexane = 1 : 2) to yield 306 mg (76%) pure product as white solid. ¹H NMR (400 MHz, CDCl₃) δ 7.38 – 7.09 (m, 5H), 5.75 (s, 1H), 3.53 (q, *J* = 6.5 Hz, 2H), 2.82 (t, *J* = 6.9 Hz, 2H), 2.49 (td, *J* = 7.3, 2.5 Hz, 2H), 2.34 (t, *J* = 7.1 Hz, 2H), 1.93 (t, *J* = 2.6 Hz, 1H). ¹³C NMR (101 MHz, CDCl₃) δ 171.0, 138.9, 128.9, 128.8, 126.6, 83.0, 69.5, 40.8, 35.7, 35.4, 15.0.

3-(1-benzyl-1*H*-1,2,3-triazol-4-yl)-*N*-phenethylpropanamide (4-S2)



To a 25 mL Schlenk tube was added **4-S1** (30 mg, 0.15 mmol), benzyl azide (40 mg, 0.3 mmol) and Cu(OAc)₂·H₂O (4 mg, 0.02 mmol) under N₂. Methanol (1 mL) and CH₂Cl₂ (1 mL) were added and the mixture was stirred for 10 min. A solution of sodium ascorbate (20 mg, 0.1 mmol) in H₂O (1 mL) was added into the above solution under N₂. The mixture was sealed and stirred at room temperature overnight, then quenched by addition of an aqueous solution of Na₅DTPA (100 mM, 3 mL). The mixture was extracted with CH₂Cl₂ (3 × 10 mL). The combined organic layer was dried over Na₂SO₄, filtered, and concentrated under vacuum. The crude product was purified by column chromatography (EtOAc and then 2% MeOH in EtOAc) to yield 40 mg (79%) pure product as white solid. ¹H NMR (500 MHz, CDCl₃) δ 7.37 – 7.05 (m, 11H), 6.03 (s, 1H), 5.43 (s, 2H), 3.41 (q, *J* = 6.9 Hz, 2H), 2.97 (t, *J* = 7.2 Hz, 2H), 2.69 (t, *J* = 7.1 Hz, 2H), 2.52 (t, *J* = 7.2 Hz,

2H). ^{13}C NMR (126 MHz, CDCl_3) δ 172.0, 147.0, 139.0, 134.8, 129.2, 128.8, 128.7, 128.1, 126.5, 121.6, 54.1, 40.7, 35.8, 35.7, 21.6. ESI-MS: m/z 335.40 ($[\text{M}+\text{H}]^+$, calcd 335.41).

Chapter 5 DFT Calculations on Tri-copper(I) and Di-copper(I) CuAAC Reaction Pathways

5.1 Introduction

Density functional theory (DFT) is a computational method describing the electronic density properties of atoms, molecules, and materials using functionals (functions of another function). It has relatively low computational costs compared to the Hartree–Fock theory, but the accuracy of which is sufficient for small systems. Therefore, this method has been widely applied for complex chemical systems, especially transition metals complexes.²⁰⁶

The energies and properties of proposed mono- and di-copper(I) intermediates and transition state structures in CuAAC reaction have been extensively studied by theoretical calculations (see Chapter 1). However, little attention was paid to the activity of tri-copper(I) acetylide complexes. In this Chapter, we will discuss our work on computational studies of the proposed tri-copper(I) pathway, including energy barriers calculations as well as the effect of tris(triazolylmethyl)amine ligand.

** The result in this Chapter was achieved in collaboration with Prof. Shereen Ghaoui and Prof. Thomas A. Albright. The calculation model was built together and the calculations were performed by Prof. Shereen Ghaoui.*

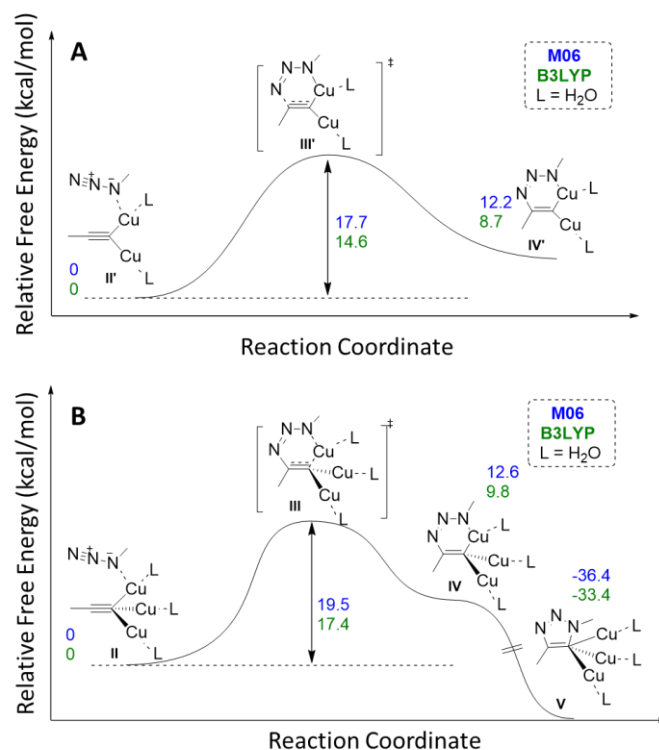
5.2 Results and Discussion

5.2.1 Geometric Optimization and Energy Calculations of Intermediates in Di-Copper(I) and Tri-Copper(I) Reaction Pathways

Based on previous proposed mechanisms and calculations,⁴⁶ herein we performed the DFT calculations to obtain the energies and structures of di-copper(I) and tri-copper(I) pathway. The calculation was performed with Gaussian 09 program²⁰⁷ using a simplified model to minimize the calculation cost. Propyne and methyl azide were selected as the reactants and water was chosen as ligands. Structures were optimized both in gas- and solution-phase (water, solvation model: IEFPCM) and free energies were calculated with the M06²⁰⁸ and B3LYP²⁰⁹ functional. LANL2DZ basis set with ECP was used on Cu atoms, and 6-311+G**²¹⁰ was used on the other elements (solvation model: IEFPCM). The energies in gas phase were corrected for the basis-set superposition error (BSSE) by the counterpoise correction method.²¹¹

As shown in Scheme 5-1, the relative free energy of di-copper(I)-azide-acetylide complex **II'** and the tri-copper(I)-azide-acetylide **II** are set as zero. The transition state energy barriers of the two pathways (**III**, **III'**) are similar, but the tri-copper(I) pathway is 2 kcal/mol higher than the di-copper(I) pathway. This result is also in agreement with the calculated ratio of $k'_{II}/k'_{III} = 29:1$ (see Chapter 3) in stoichiometric condition. After passing the transition state, the tri-copper(I) metallacycle (**IV**) intermediate is more stable than di-copper(I) counterparts (**IV'**).

It is worth noting that the calculation was done without tris(triazolylmethyl)amine ligand. With the stabilization of ligand, both the di-copper(I) acetylide and tri-copper(I) acetylide could be more stable and lower in energy, while the tri-copper(I) acetylide is more stable and lower in energy than the di-Cu acetylide, making the former easier to form the azide/copper(I)/acetylide ternary complex that facilitate the CuAAC reaction.¹⁰⁰



Scheme 5-1 Energy profile of di-copper(I) and tri-copper(I) pathway calculated using M06 (blue) and B3LYP (green) method.

5.2.2 Optimization of Crystal Structure for Orbital Explanation

The structure of ligand-stabilized tri-copper(I) acetylide complex was optimized by the ONIOM method.¹⁹⁶ All calculations were performed by the Gaussian 09 package.²⁰⁷ The complex was divided into two layers, known as high and low layers, **a** and **b**, respectively, as shown in Chart 5-1. The central structure with H atoms as substitution on triazole groups was treated at the M06²⁰⁸ level of theory with the 6-311+G(d,p)²¹⁰ basis set. The complete structure including the tris(triazolymethyl)amine ligand was treated with the molecular mechanics method, universal force field (UFF).²¹² Charge distribution behavior is analyzed by Hirshfeld charge calculations.

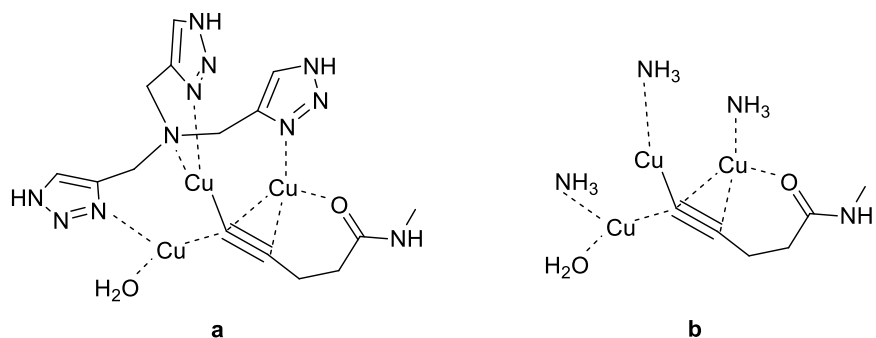


Chart 5-1 Optimization of Ligand-stabilized Tri-copper(I) Acetylide Complex by ONIOM Calculations. A. High layer calculated by molecular mechanics method. B. Low layer calculated by DFT method.

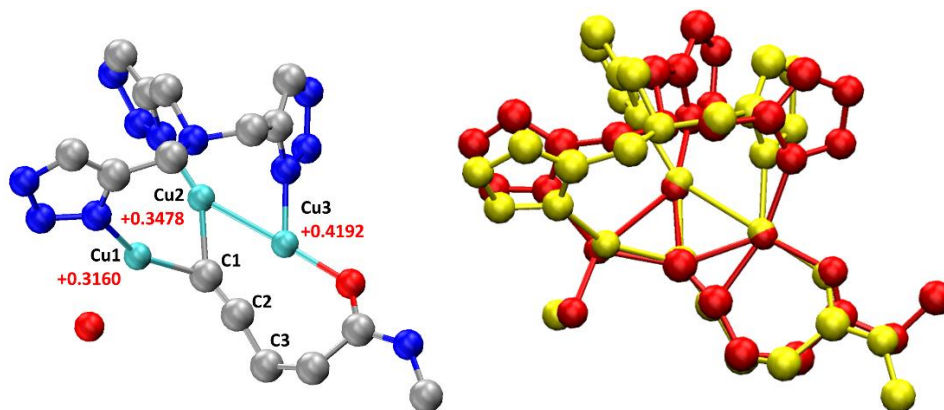


Figure 5-1 Optimized structure of ligand-stabilized tri-copper(I) acetylide complex and its alignment with the crystal structure.

As shown in Figure 5-1, the optimized structure of the complex (left) has a slightly decreased dihedral angle between the Cu(2)–C(1)–Cu(1) plane and the Cu(3)–Cu(2)–C(1) plane (140.5°) compared to the crystal structure (157.6°). A lengthening of the C(1)–C(2) bond was also observed in the calculated structure (1.246 \AA). Hirshfeld charge analysis (red) showed higher positive charges on Cu(2) compared to Cu(1), in consistent with the stronger backbonding from Cu(2). The overall structural superposition of the optimized structure (yellow) with the crystal

structure (red) as shown in the right figure suggested no significant conformational difference between the two structures.

5.3 Conclusions

In order to get a thorough understanding of the mechanism of ligand-accelerated CuAAC reaction, we performed the experimental studies in aqueous solutions (Chapter 3) and in organic solvent (Chapter 4), from which an unprecedented tri-copper(I) pathway was discovered. The activation energy of this new pathway was calculated 2 kcal/mol higher than the previously proposed di-copper(I) pathway, which makes the reaction via a tri-copper(I) acetylide slower than di-copper(I) acetylide. However, the stability of tri-copper(I) acetylide-azide adduct is higher, indicated by experimental and theoretical studies. Thus, under catalytic condition, the reaction still prefers to proceed through the tri-copper(I) acetylide.

5.4 Experimental Section

5.4.1 The Gas- and Solution-phase Energetics for the Reaction of Di-Cu / Tri-Cu Propynide with Methyl Azide

Table 5-1 Energies (kcal/mol) for the Reaction Pathway from Di-Cu Acetylide

Structure	Absolute Energies (hartrees)				Relative Energies to Reactants (kcal/mol)			
	B3LYP (gas)	B3LYP (water)	M06 (gas)	M06 (water)	B3LYP (gas)	B3LYP (water)	M06 (gas)	M06 (water)
II'	-865.3684	-865.4531	-865.1389	-865.2220	0	0	0	0
III'	-865.3408	-865.4298	-865.1064	-865.1939	17.3	14.6	20.4	17.7
IV'	-865.3430	-865.4392	-865.1074	-865.2026	15.9	8.7	19.8	12.2

Table 5-2 Energies (kcal/mol) for the Reaction Pathway from Tri-Cu Acetylide

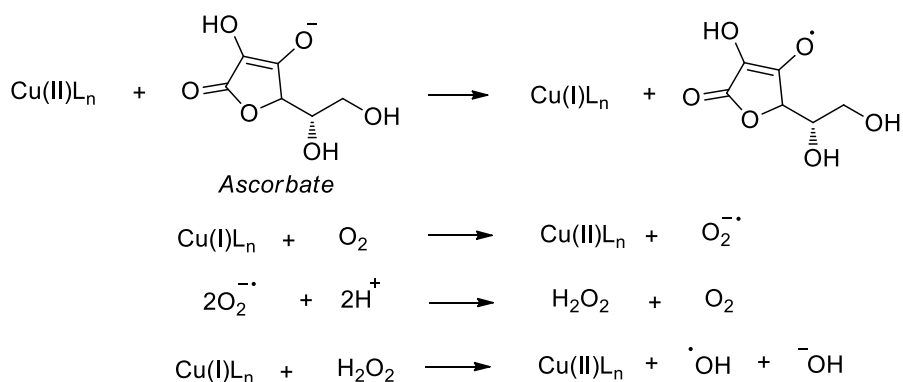
Structure	Absolute Energies (hartrees)				Relative Energies to Reactants (kcal/mol)			
	B3LYP (gas)	B3LYP (water)	M06 (gas)	M06 (water)	B3LYP (gas)	B3LYP (water)	M06 (gas)	M06 (water)
II	-1137.7207	-1137.9715	-1137.4864	-1137.7405	0	0	0	0
III	-1137.6811	-1137.9439	-1137.4484	-1137.7095	24.8	17.4	23.8	19.5
IV	-1137.6842	-1137.9559	-1137.4496	-1137.7204	22.9	9.8	23.0	12.6
V	-1137.7395	-1138.0247	-1137.5146	-1137.7985	-11.8	-33.4	-17.7	-36.4

Chapter 6 Study of the Ligand Effects on CuAAC

Reactivity and Antioxidation Ability

6.1 Introduction

The oxidation of copper(I) species by dioxygen in air greatly hampered the application of CuAAC reaction in bioconjugation. The copper(I) species generated *in situ* from reduction of copper(II) by ascorbate readily undergoes a “Fenton” reaction²¹³ catalyzing the generation of cytotoxic reactive oxygen species (ROS) (Scheme 6-1),²¹⁴⁻²¹⁶ which is one of the major drawbacks of CuAAC reaction compared to the copper(I)-free bioconjugation methods.²¹⁷



Scheme 6-1 Oxidative damage from reactive oxygen species (ROS).

To suppress the copper(I)-catalyzed oxidative damage to biomolecules, specific ligands have been developed to prevent or reduce the oxidation of copper(I) during the reaction. In general, larger chelating ring size, more chelating arms, electron-withdrawing and steric hindered substitution groups on ligands can offer better protection on copper(I) ion against oxidation.¹⁷⁶

6.2 Results and Discussion

6.2.1 Ligand Design

Inspired by the high reactivity of tris(triazolylmethyl)amine ligands, we designed a family of ancillary ligands based on the (triazolylalkyl)amine skeleton (Chart 6-1, ligand **6-1** to **6-9**).

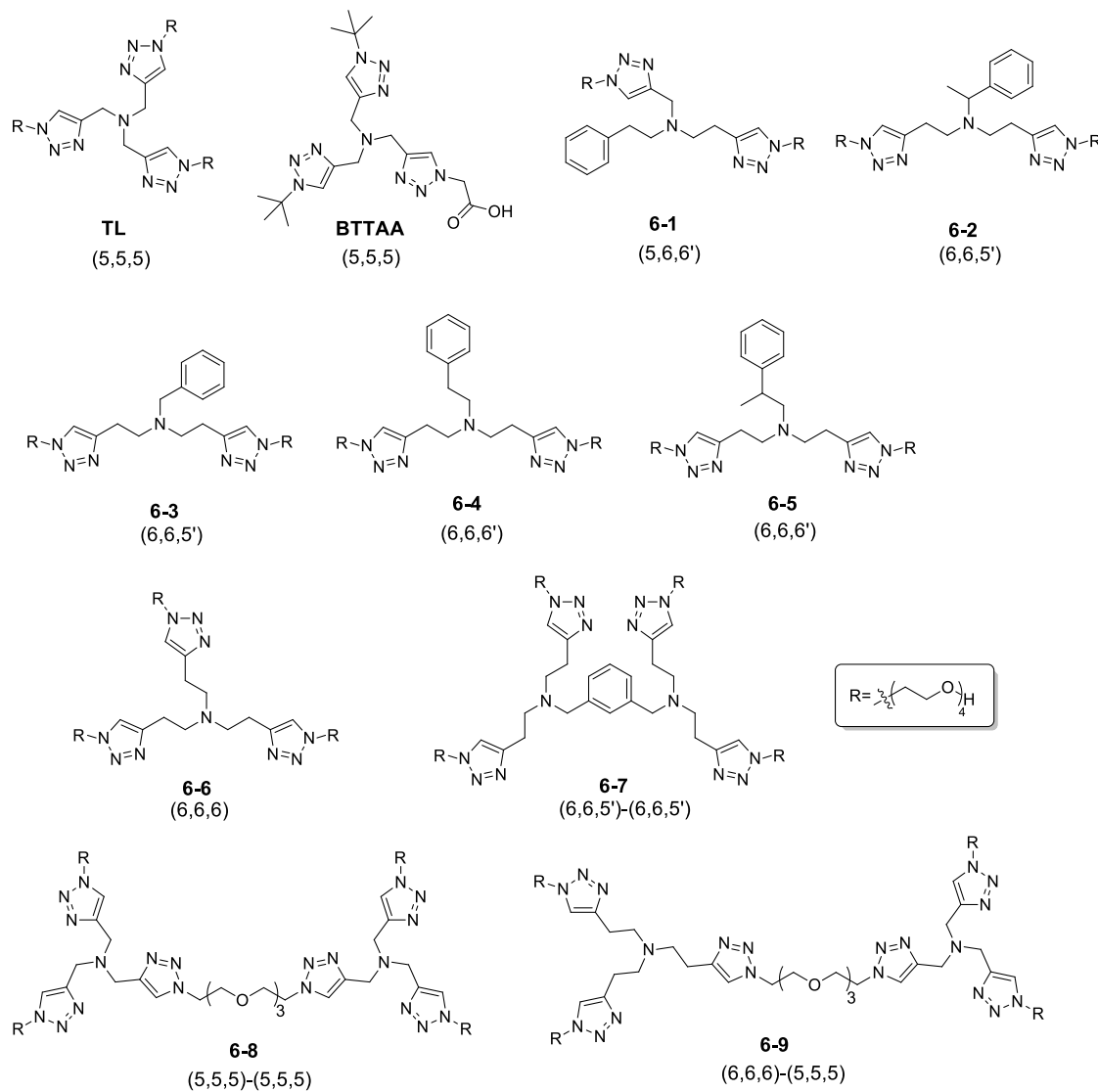


Chart 6-1 Ancillary ligands for accelerating CuAAC reaction and preventing copper(I) oxidation.

In the isolated mono-copper(II) complex bearing the tris(triazolylmethyl)amine ligands, the coordination of the central amine and the triazole nitrogen to the copper(I) atom generates three five-membered copper-chelating arm length (5,5,5).¹⁹³ Mechanistic studies revealed that the enlarged chelating ring size can reduce the air-sensitivity of copper(I).¹⁷⁴ Therefore, in this work, most of the ligands were designed on the basis of tripodal tetradentate structure, in which one or two methylene groups were inserted between the central amine and the aromatic chelating arm to expand the copper chelating arm length to six-atoms [(5,6,6) or (6,6,6)].

In addition, the interaction between the π system of phenyl group and copper(I) can offer weak but sufficient protection on copper(I) against oxidation.¹⁷⁷ Therefore, apart from the two triazole arms that were incorporated to provide N-donor coordination and catalytic activity, the third arm was designed as a triazole (**6-6**) or a phenyl ring (**6-1-6-5**). In selected ligands (**6-2** & **6-5**), a methyl group at the benzylic CH₂ was incorporated to reduce the free rotation of phenyl ring and enhance the copper(I)-phenyl π interaction.¹⁷⁷

On the other hand, considering the high activity of di-copper(I) complexes in CuAAC reaction, we also synthesized three dimeric ligands **6-7**, **6-8** and **6-9**, in which the two monomers were linked by a phenyl group (**6-7**) or by a flexible oligo(ethyleneglycol) chain (**6-8** and **6-9**) to bring two copper(I) atoms at a high local concentration.

6.2.2 Kinetic Studies on CuAAC Reaction

The activity of these newly synthesized ligands were compared by a fluorescent assay (Figure 6-1). In a model reaction, 7-hydroxycoumarin azide (2 equiv.) was reacted with propargyl alcohol (1 equiv.) in presence of ligand-copper(I) 1:1 complex (2 equiv.) *in situ* generated from reducing CuSO₄ by ascorbate. The product hydroxymethyl triazolyl-coumarin exhibits strong fluorescent emission at $\lambda = 465$ nm, which can be quantitatively measured by a fluorescence microplate

reader. The reaction yield was continuously monitored during a reaction period of 60 min (Figure 6-1A) and the apparent second-order rate constants were calculated accordingly (Figure 6-1B).

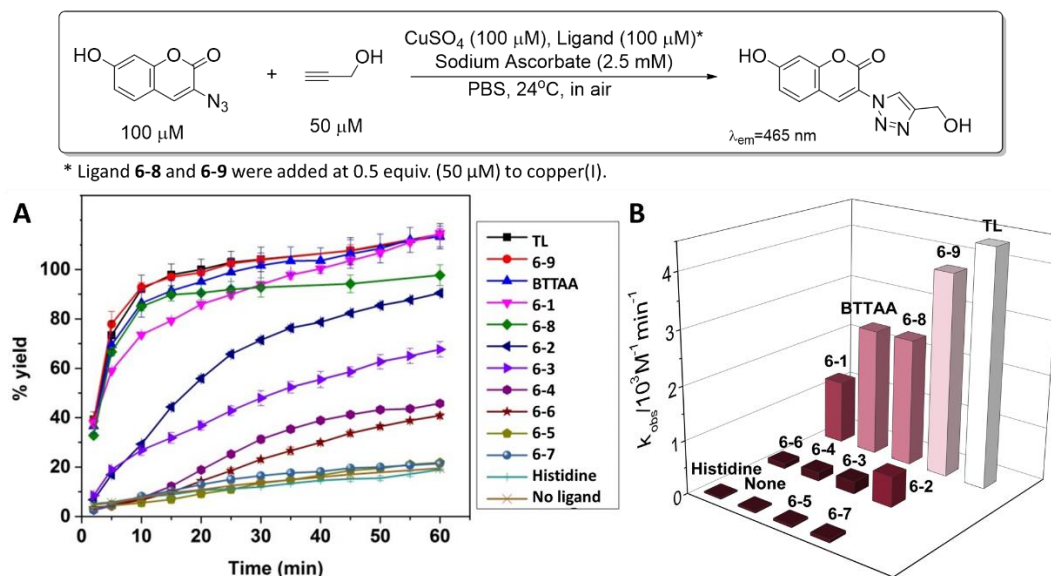


Figure 6-1 Fluorescent Assay for CuAAC Rates in the Presence of Ligands

Ligand efficiency in CuAAC reaction largely depends on chelating arm length. Similar to the reported copper(I)-dioxygen reactivity,¹⁷⁶ increasing the chelating arm length from five to six-atoms significantly reduced the CuAAC reaction rate as well. Among the monomeric ligands, tris(triazolylmethyl)amine ligands **TL** and **BTAA** still showed the highest rate, followed by ligand **6-1** bearing [NCH₂Triazole] and [NCH₂CH₂Triazole] arms. Ligand carrying two or more [NCH₂CH₂Triazole] arms displayed much lower efficacy.

Dimeric ligands **6-9** at ligand/copper(I) 1:2 ratio displayed similar activity compared to the **TL** ligand at ligand/copper(I) 1:1 ratio. The ligand **6-9** carries a [N(CH₂Triazole)₃] unit ligated with a [N(CH₂CH₂Triazole)₃] unit, which can form (5,5,5) and (6,6,6) chelating structure with copper(I). From the mechanistic study in Chapter 3, we have discovered that at ligand/ copper(I) 1:1 ratio, the active intermediates are the di-copper(I)-[N(CH₂Triazole)₃]-acetylides. Excess ligands in the

solution generate copper(I)-[N(CH₂Triazole)₃] complexes, which are in fast equilibrium with the copper(I) acetylides. Thus, for the ligand **6-9**, the [N(CH₂Triazole)₃] unit plays the key role in maintaining the high activity during the reaction, while the [N(CH₂CH₂Triazole)₃] unit can stabilize the second copper(I) with acetylide at a close position. In comparison, the dimeric ligand **6-8** bearing two tris(triazolylmethyl)amine units exhibited lower reaction rate and yield, possibly because of the facile oxidation of copper(I) through the formation of a di-copper(I) complex, which was found more sensitive to dioxygen compared to the mono-copper(I) complexes.¹⁷² At ligand/copper(I) 1:1 ratio, the dimeric ligands **6-8** and **6-9** displayed lower reaction rate during the initial period of 20 min, then rapidly reacted and reached completion at 60 min.

6.2.3 Inhibiting Effect of Excess Ligands

Interestingly, for the monomeric ligands (**6-2-6-6**) and ligand **6-7** bearing two or more [N(CH₂CH₂Triazole)₃] units, the CuAAC reaction was completely inhibited at ligand/copper(I) 2:1 ratio. This phenomena was also observed and reported in other ligand systems where the ligand-copper(I) interactions are stronger than triazoles.⁴³

We proposed that the copper(I) ion was chelated by four nitrogen donor triazoles from two ligands, forming a tetrahedral coordination geometry that is stable against dissociation. To confirm the interaction between copper(I) and ligands, we synthesized a tris(triazolyethyl)amine ligands bearing three six-membered chelating rings [N(CH₂CH₂Triazole)₃] (**6-10**, Figure 6-2). The ¹H-NMR of ligand **6-10** in D₂O exhibits a sharp peak of the triazole protons at δ = 7.69 ppm (Figure 6-2A), while the [(**6-10**)₂Cu(I)] complex displays a split of this signal at a ratio of 4H:2H, indicating four out of six triazoles are coordinated with copper(I), showing more deshielded signal due to the transfer of electron density from the triazoles to copper(I) (Figure 6-2B). In addition, the α-methylene protons next to the triazoles (NCH₂CH₂Triazole) also show two

different chemical environments: four CH₂ of which are shielded compared to the free ligands, in agreement with the higher electron-density introduced by copper(I)-coordination.

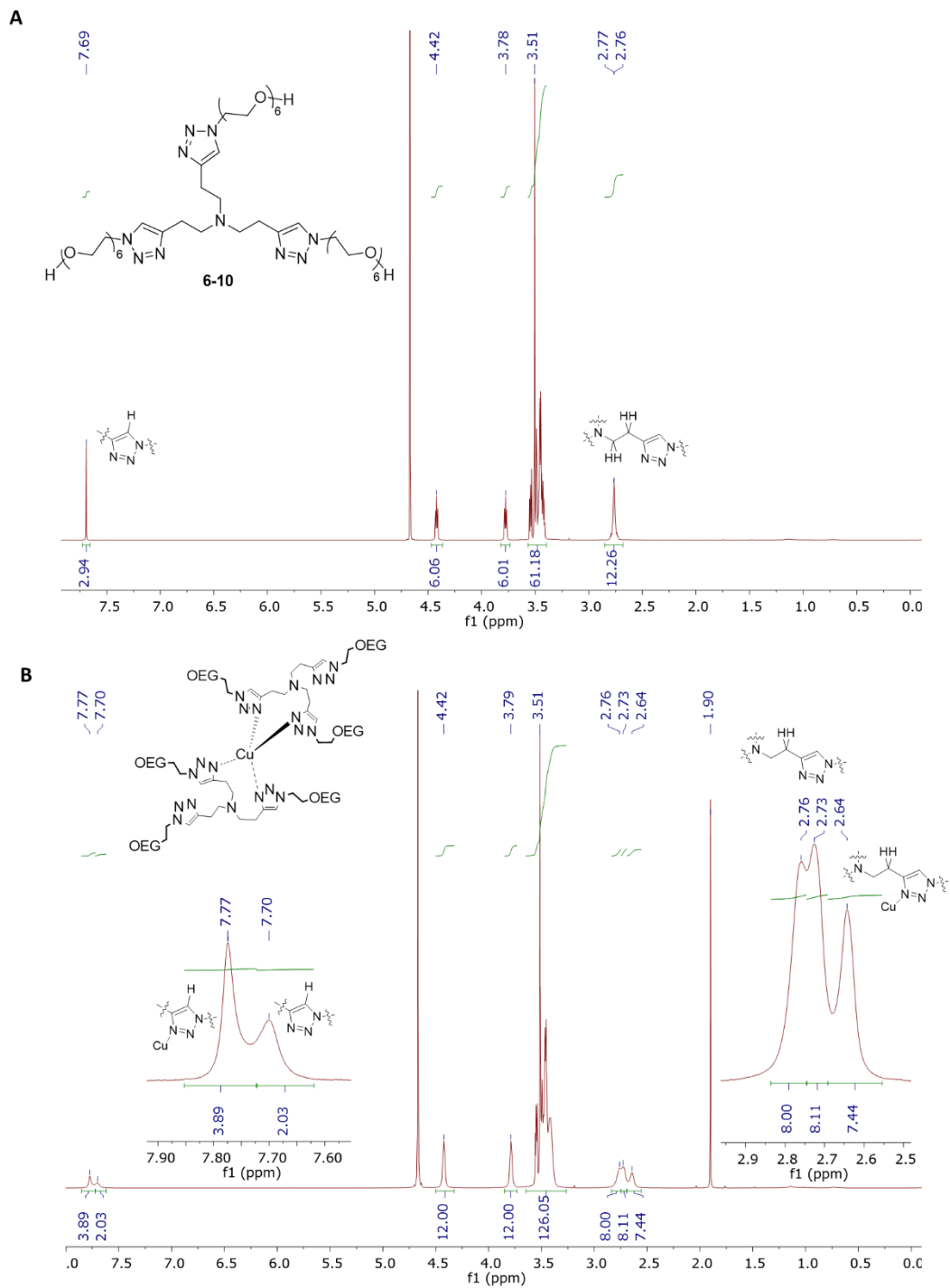


Figure 6-2 $^1\text{H-NMR}$ in D_2O : A. ligand **6-10**. B. $[(\mathbf{6-10})_2\text{Cu(I)}]$ complex generated with $\text{Cu}(\text{MeCN})_4\text{PF}_6$.

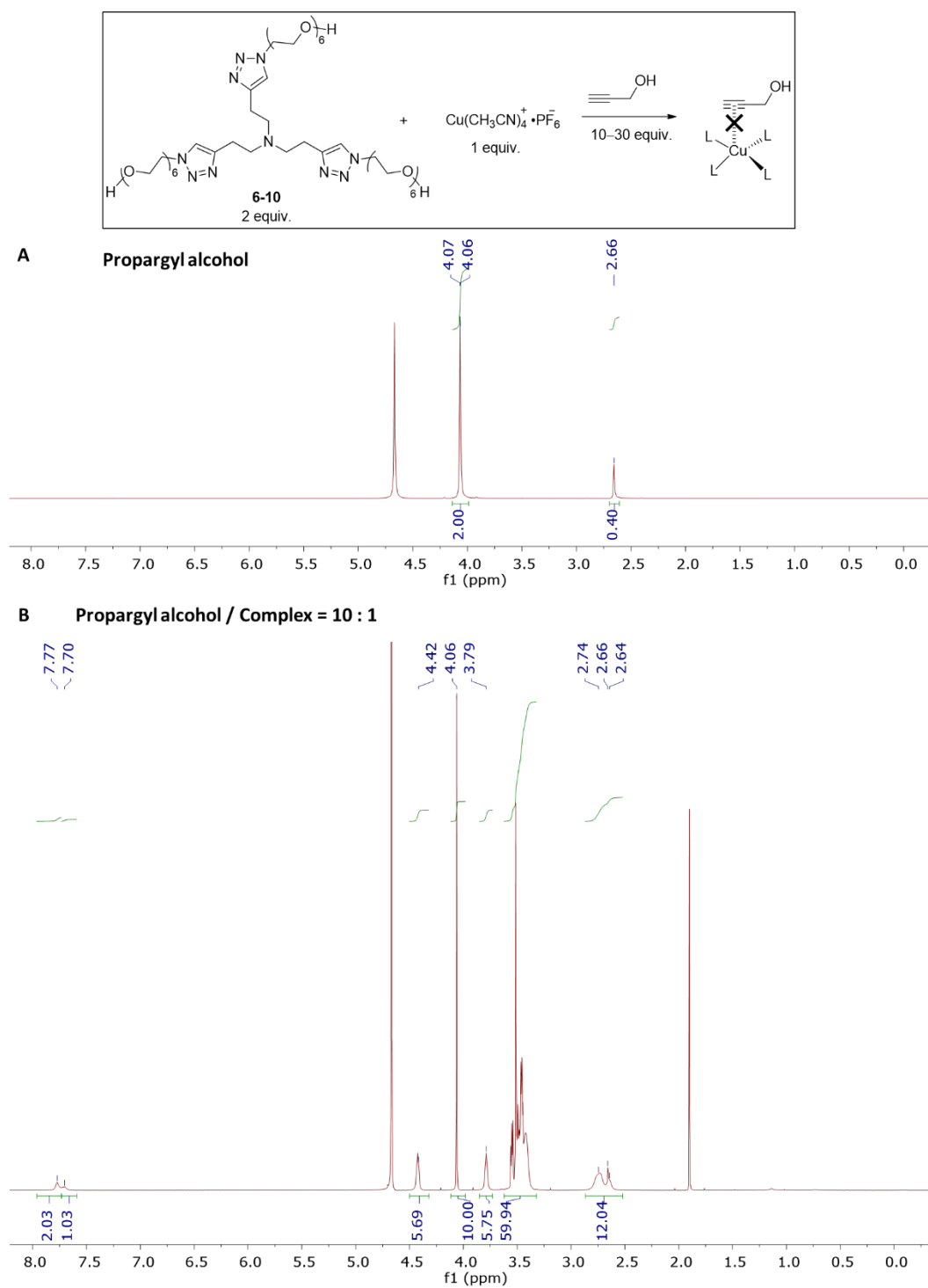


Figure 6-3 $^1\text{H-NMR}$ in D_2O : A. Propargyl alcohol. B. [(**6-10**) $_2\text{Cu(I)}$] complex with propargyl alcohol.

We next investigated the interaction between copper(I) and the alkyne (propargyl alcohol) in the [(**6-10**) $_2\text{Cu}$] complex. Addition of 10–30 equivalent of propargyl alcohol into the [(**6-10**) $_2\text{Cu}$] solution generated NMR signals corresponding to the CH_2OH of propargyl alcohol at exactly the same chemical shift ($\delta = 4.06$ ppm) compared to the free alkyne, suggesting no interaction between the alkyne and the ligand-chelated copper(I) ions. Therefore, the difficulty in forming copper(I)-acetylide complexes greatly hampered the CuAAC reaction rate, result in the observed inhibiting effect by these ligands.

6.2.4 Oxidation Rate of Copper(I) Complexes bearing Anti-oxidation Ligands

The efficiency of these ligands for preventing copper(I) against oxidation in air was quantitatively measured by the consumption rate of ascorbate, which was used as a sacrificing agent to reduce the oxidized copper(II) back to copper(I). The maximum absorbance of sodium ascorbate aqueous solution at 265 nm was monitored during a period of 20 min, in presence or absence of copper(I). Pure ascorbate solution is stable in air during the recorded period (Figure 6-4A), while the addition of one equivalent of CuSO_4 immediately created the re-dox cycle (Scheme 6-1) that led to the rapid loss of sodium ascorbate absorption at 265 nm (Figure 6-4B). In comparison, the copper(II) complex bearing two **6-10** ligands is completely inert towards sodium ascorbate (Figure 6-4C), and the copper(I) complex bearing two **6-10** ligands is also unreactive towards sodium ascorbate in air, as reflected by the unchanged absorbance during 20 min (Figure 6-4D). The results revealed the high stability of copper(I) and copper(II) complexes chelated by two $[\text{N}(\text{CH}_2\text{CH}_2\text{Triazole})_3]$ units, the coordination mode of which has been studied by NMR spectra (*vide supra*). The copper(I) complex bearing dimeric ligand containing one equivalent of $[\text{N}(\text{CH}_2\text{CH}_2\text{Triazole})_3]$ ligand (*e.g.*, one equivalent of ligand **6-9**, Figure 6-4E) is also stable in air,

but lower amount of ligand (e.g., 0.5 equiv. **6-9**, Figure 6-4F) is insufficient for protecting copper(I) from oxidation, although the oxidation rate is much slower than free copper(I).

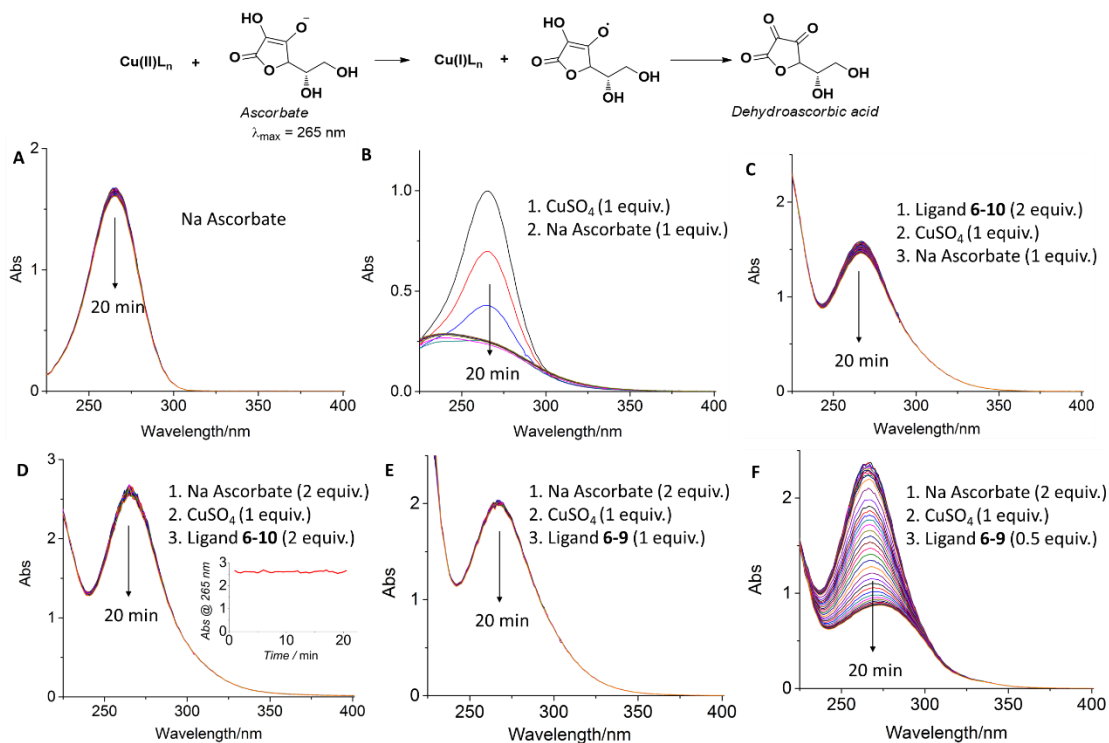


Figure 6-4 UV-Vis spectra of ascorbate solutions exposed in air during 20 min. Solutions containing: A. 0.125 mM ascorbate. B. 0.125 mM CuSO_4 and 0.125 mM ascorbate. C. 0.25 mM ligand **6-10**, 0.125 mM CuSO_4 , and 0.125 mM ascorbate. D. 0.25 mM ascorbate, 0.125 mM CuSO_4 , and 0.25 mM ligand **6-10**.

6.3 Conclusions

Enlarged chelating arm length of the ancillary ligands reduced the reactivity of copper(I) complexes both towards dioxygen in air and in CuAAC reaction. Although the generation of cytotoxic ROS can be minimized by these ligands, their corresponding CuAAC rates are lower than the ligands forming five-membered chelating ring with copper(I). To achieve the goal of applying an efficient CuAAC reaction in biological systems at low toxicity, we need to expand

the ligand library with different chelating arm numbers and employ other donors including N, P, C, S.

6.4 Experimental Section

6.4.1 Experimental Details

6.4.1.1 General Procedure for Kinetic Studies for CuAAC Activity of Selected Ligands

In a 96-well plate (black), to each well was added 80 μL phosphate-buffered saline (PBS) solution, containing 0.01 μmol ligand (0.005 μmol **6-8** and **6-9**), 0.01 μmol CuSO_4 , 0.01 μmol coumarin azide, and 0.005 μmol propargyl alcohol. 20 μL sodium ascorbate stock solution (25 mM in PBS) was added into each well by a multichannel pipette to initiate the reaction. The plate was placed in a fluorescence microplate reader and the fluorescence intensity (excitation 405 nm / emission 465 nm) was recorded during reaction time from 2 min to 60 min. Each experiment was repeated three times (Figure 6-1).

The yield of product was calculated based on the calibration curve at different concentrations of the hydroxymethyl triazolyl-coumarin (21 stock solution from 0.5 mM to 0 mM). The calibration solutions also contained 0.1 mM coumarin azide and 0.05 mM propargyl alcohol to control the fluorescent interference caused by reagents. Each concentration was repeated three times. (Figure 6-5)

Calculation of apparent second-order rate constants k :

$$r = \frac{dP}{dt} = k[\text{Azide}][\text{Alkyne}]$$
$$\frac{1}{[\text{Azide}]_{ini} - [\text{Alkyne}]_{ini}} \ln \frac{[\text{Azide}][\text{Alkyne}]_{ini}}{[\text{Azide}]_{ini}[\text{Alkyne}]} = kt$$

6.4.1.2 Oxidation Rate of Copper(I) Complexes bearing Anti-oxidation Ligands

The oxygen gas in sodium ascorbate, CuSO₄ and PBS buffer solution was removed by a freeze-vacuumize-defreeze (4 times) procedure. UV cuvette was capped and filled with nitrogen gas. Stock solutions were subsequently added into the UV cuvettes by syringe. To cuvette 1 was added 0.125 mM sodium ascorbate. To cuvette 2 were added 0.125 mM CuSO₄ and 0.125 mM sodium ascorbate, subsequently. To cuvette 3 were added 0.25 mM ligand **6-10**, 0.125 mM CuSO₄, and 0.125 mM sodium ascorbate, subsequently. To cuvette 4 were added 0.25 mM sodium ascorbate, 0.125 mM CuSO₄, and 0.25 mM ligand **6-10**, subsequently. Then the cap of each cuvette was removed and the cuvette was put into a Varian Cary 50 Bio UV-Visible Spectrophotometer to record the absorbance of each cuvette during 20min. Scan rate: fast. Scan range: 200 nm~800 nm. Cycle time: 30s. Cycle count: 40. Baseline correction: PBS solution.

6.4.2 Supplementary Figures

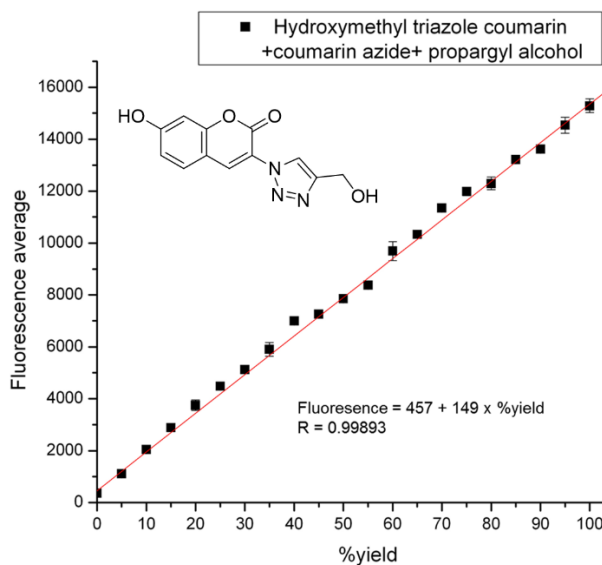
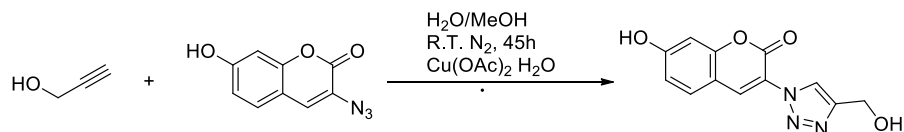


Figure 6-5 Calibration curve for fluorescence vs. concentration of hydroxymethyl triazolyl-coumarin product.

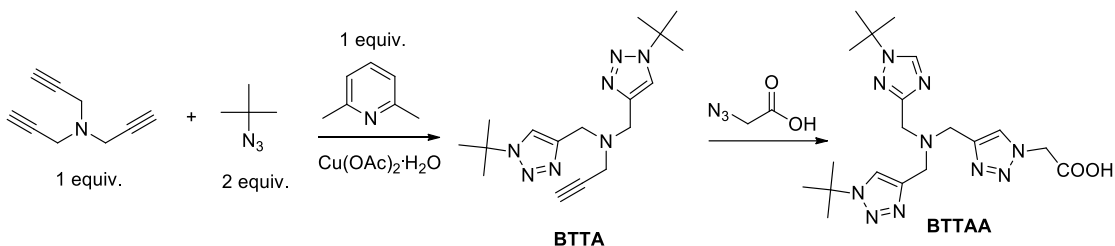
6.4.3 Compound Synthesis Procedure



Hydroxymethyl Triazolyl-Coumarin

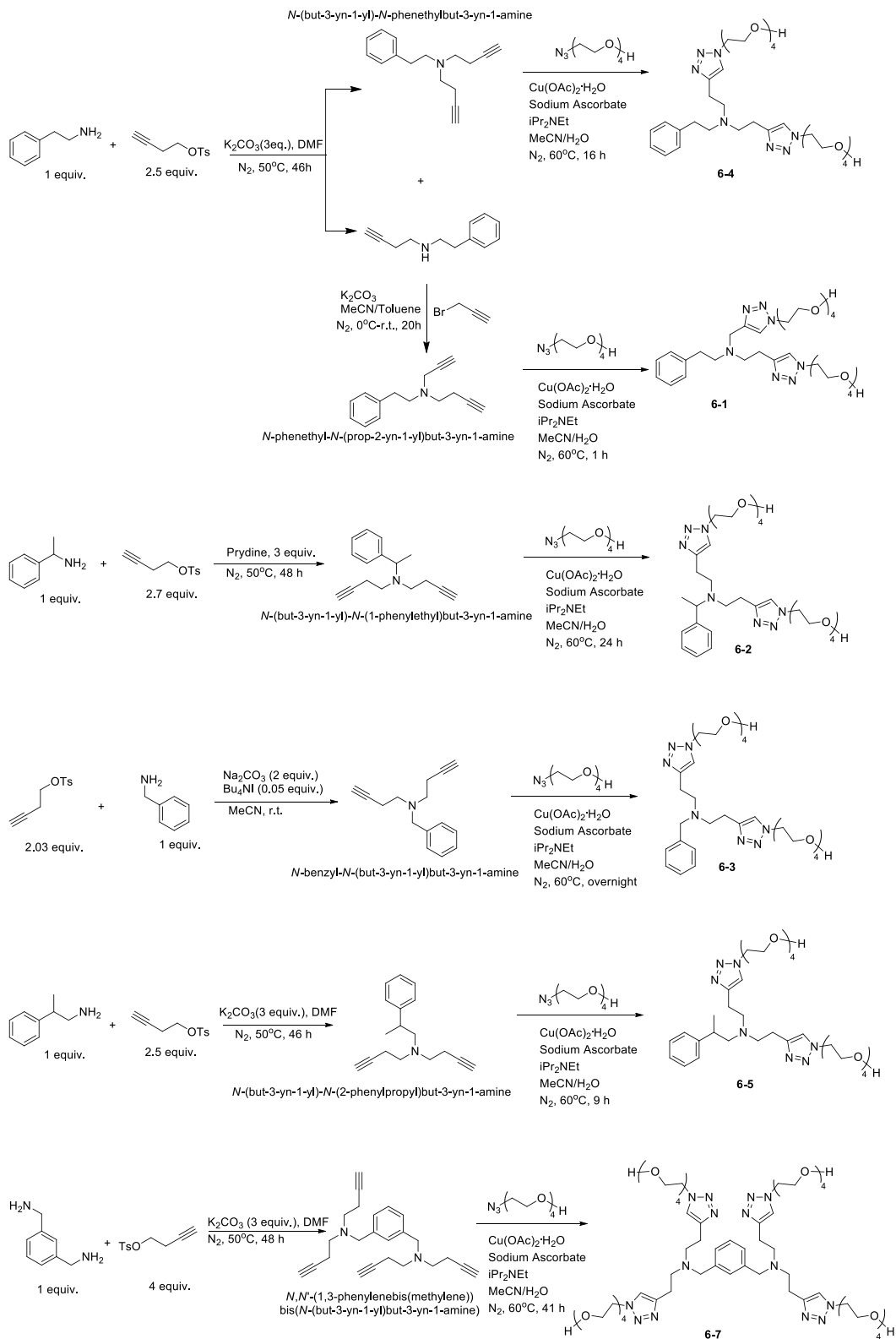
To a 10 mL Schlenk tube was added coumarin azide (20 mg, 0.1 mmol), propargyl alcohol (32.4 mg, 0.6 mmol), Cu(OAc)₂·H₂O (2 mg, 0.01 mmol) and MeOH (1 mL) under N₂. A solution of sodium ascorbate (20 mg, 0.1 mmol) in H₂O (1 mL) was added into the above solution under N₂. The mixture was sealed and stirred at room temperature for 45 h. The reaction was quenched by addition of an aqueous solution of Na₅DTPA (100 mM, 0.5 mL). The solvent was removed and the crude product was purified by column chromatography (5% MeOH in EtOAc) to yield **Hydroxymethyl Triazolyl-Coumarin** (25 mg, 0.96 mmol, 96 %) as a yellow solid. The product can hardly dissolve in CH₂Cl₂, MeCN, ethyl acetate, water, but can dissolve in MeOH and DMSO. ¹H-NMR (500 MHz, DMSO-D₆) δ 8.54 (1H, triazole), 8.37 (1H, CH, next to triazole), 7.71 (1H, d, CHCH), 6.86 (1H, d, CHCH), 6.80 (1H, CH next to OH), 5.30 (1H, coumarin OH), 4.57 (2H, CH₂OH), 3.98 (ethyl acetate), 3.32(MeOH), 3.13(MeOH), 2.46 (DMSO), 1.95 (ethyl acetate), 1.57, 1.14 (ethyl acetate).

TL was synthesized by literature reported procedure.¹¹⁷



BTAA

To a 50 mL Schlenk tube was added tert-butyl azide (200 mg, 2.02 mmol), tripropargylamine (131 mg, 1 mmol), Cu(OAc)₂·H₂O (40 mg, 0.2 mmol), 2,6-dimethylpyridine (107 mg, 1 mmol) and MeCN (10 mL) under N₂. A solution of sodium ascorbate (198 mg, 1 mmol) in H₂O (2 mL) was added into the above solution under N₂. The mixture was sealed and stirred at room temperature for 48 h. The reaction was quenched by addition of an aqueous solution of Na₅DTPA (500 mM, 3 mL). The solvent was removed, and the residue was dissolved in 60 mL CH₂Cl₂/H₂O mixture, extracted with CH₂Cl₂ (3 × 30 mL). The combined organic layer was dried over Na₂SO₄, filtered, and concentrated under vacuum. The crude product was purified by column chromatography (5% MeOH in CH₂Cl₂) to yield **BTTA** (190 mg, 0.58 mmol, 58 %) as a white solid. ¹H NMR (500 MHz, CDCl₃) δ 7.67 (s, 2H, CH), 3.86 (s, 4H, CH₂), 3.39 (d, 2H, CH₂), 2.28 (t, 1H, CH), 1.66 (s, 18H, CH₃). The **BTTA** was reacted with 2-azidoacetic acid (1 equiv.) using the same CuAAC procedure to yield **BTAA** (purified by column chromatography 10% MeOH in CH₂Cl₂) as a white solid (233 mg, 0.52 mmol, 90 %). ¹H NMR (400 MHz, D₂O) δ 8.16 (s, 2H, CH), 8.09 (s, 1H, CH), 5.03 (s, 2H, CH₂), 4.35 (s, 6H, CH₂), 1.59 (s, 18H, CH₃).

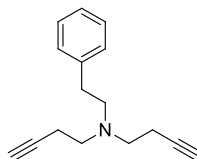


General procedure for synthesis of alkynes

2-phenylethanamine (121 mg, 1 mmol) in DMF (1 ml) was added into a Schlenk tube containing K_2CO_3 (414 mg, 3 mmol). The mixture was stirred for 0.5 h, followed by addition of but-3-yn-1-yl 4-methylbenzenesulfonate (560 mg, 2.5 mmol). The reaction mixture was heated at 50 °C, stirred for 46 h. Saturated NH_4Cl was added to quench reaction. Organic layer was separated and aqueous layer was extracted with EtOAc x 3. Organic solution was combined and dried over Na_2SO_4 . The crude product was further purified via flash chromatography (EtOAc/Hexane=1/15) to get 81.4 mg **N-(but-3-yn-1-yl)-N-phenethylbut-3-yn-1-amine** (36 %) and 79.5 mg N-phenethylbut-3-yn-1-amine (46 %) as light yellow oils.

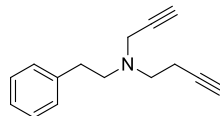
N-phenethylbut-3-yn-1-amine (48.8 mg, 0.282 mmol) in MeCN (1 ml) was added into a Schlenk tube containing K_2CO_3 (47 mg, 0.341 mmol). The mixture was stirred for 0.5 h, followed by addition of propargyl bromide (36.7 μ L, 0.338 mmol, 80% in Toluene) in an ice bath. The reaction mixture was then warmed up to room temperature and stirred for 20 h. Saturated NH_4Cl was added to quench reaction. Organic layer was separated and aqueous layer was extracted with EtOAc x 3. Organic solution was combined and dried over Na_2SO_4 . The crude product was further purified via flash chromatography (EtOAc/Hexane=1/15) to get 48.1 mg **N-phenethyl-N-(prop-2-yn-1-yl)but-3-yn-1-amine** as light yellow oil (yield 81%).

N-(but-3-yn-1-yl)-N-phenethylbut-3-yn-1-amine



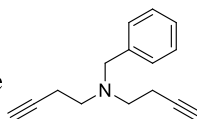
1H -NMR (500 MHz, $CDCl_3$) δ 7.33 – 7.11 (m, 5H, aryl), 2.78 (t, 4H, CH_2CH_2CCH), 2.75 (s, 4H, CH_2CH_2 aryl), 2.32 (td, 4H, CH_2CH_2CCH), 1.97 (t, 2H, CH_2CH_2CCH). ^{13}C NMR (126 MHz, $CDCl_3$) δ 140.3, 128.9, 128.5, 126.2, 83.0, 69.3, 55.9, 52.7, 34.2, 17.5.

***N*-phenethyl-*N*-(prop-2-yn-1-yl)but-3-yn-1-amine**



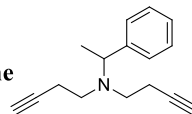
$^1\text{H-NMR}$ (500 MHz, CDCl_3) δ 7.34 – 7.18 (m, 5H, aryl), 3.51(d, 2H, NCH_2CCH), 2.79 (t, 6H, CH_2CH_2 aryl & $\text{CH}_2\text{CH}_2\text{CCH}$), 2.37 (td, 2H, $\text{CH}_2\text{CH}_2\text{CCH}$), 2.22 (t, 1H, CH_2CCH), 2.00 (t, 1H, $\text{CH}_2\text{CH}_2\text{CCH}$). $^{13}\text{C-NMR}$ (126 MHz, CDCl_3) δ 140.2, 128.8, 128.5, 126.2, 82.7, 78.5, 73.3, 69.3, 55.5, 52.4, 42.2, 34.3, 17.8.

***N*-benzyl-*N*-(but-3-yn-1-yl)but-3-yn-1-amine**



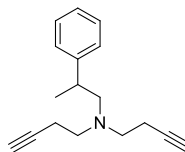
$^1\text{H NMR}$ (400 MHz, CDCl_3) δ 7.56 – 6.96 (m, 5H, aryl CH), 3.66 (s, 2H, PhCH_2), 2.75 (t, 4H, $\text{CH}_2\text{CH}_2\text{CH}$), 2.34 (td, 4H, $\text{CH}_2\text{CH}_2\text{CH}$), 1.95 (t, 2H, $\text{CH}_2\text{CH}_2\text{CH}$). $^{13}\text{C-NMR}$ (101 MHz, CDCl_3) δ 139.3, 128.7, 128.4, 127.2, 83.0, 69.2, 58.3, 52.5, 17.4.

***N*-(but-3-yn-1-yl)-*N*-(1-phenylethyl)but-3-yn-1-amine**



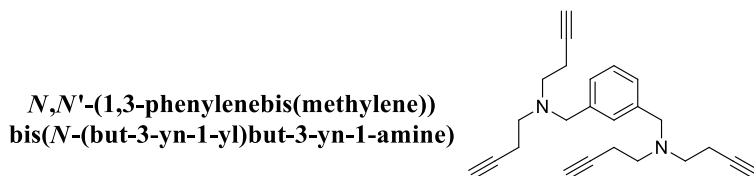
$^1\text{H-NMR}$ (400 MHz, CDCl_3) δ 7.42 – 7.16 (m, 5H, aryl), 3.84 (q, 1H, CHCH_3), 2.82 – 2.63 (m, 4H, $\text{CH}_2\text{CH}_2\text{CCH}$), 2.28 (td, 4H, $\text{CH}_2\text{CH}_2\text{CCH}$), 1.94 (t, 2H, $\text{CH}_2\text{CH}_2\text{CCH}$), 1.35 (d, 3H, CHCH_3). $^{13}\text{C-NMR}$ (101 MHz, CDCl_3) δ 144.2, 128.3, 127.6, 126.9, 83.1, 69.1, 59.7, 49.5, 18.5, 17.2.

***N*-(but-3-yn-1-yl)-*N*-(2-phenylpropyl)but-3-yn-1-amine**



$^1\text{H-NMR}$ (500 MHz, CDCl_3) δ 7.33 – 7.13 (m, 5H, aryl), 2.85 (q, 1H, CHCH_3), 2.70 (tt, 4H, $\text{CH}_2\text{CH}_2\text{CCH}$), 2.57 (dq, 2H, CHCH_2N), 2.24 (td, 4H, $\text{CH}_2\text{CH}_2\text{CCH}$), 1.94 (t, 2H, $\text{CH}_2\text{CH}_2\text{CCH}$),

1.27 (d, 3H, CHCH₃). ¹³C-NMR (126 MHz, CDCl₃) δ 146.0, 128.4, 127.4, 126.3, 83.1, 69.1, 62.1, 53.2, 38.8, 19.6, 17.4.



¹H-NMR (500 MHz, CDCl₃) δ 7.40 – 7.12 (m, 4H, aryl), 3.65 (s, 4H, CCH₂N), 2.75 (t, 8H, CH₂CH₂CCH), 2.34 (td, 8H, CH₂CH₂CCH), 1.96 (t, 4H, CH₂CH₂CCH). ¹³C-NMR (126 MHz, CDCl₃) δ 139.3, 129.0, 128.3, 127.5, 83.0, 69.2, 69.2, 58.3, 52.5, 17.4.

General procedure for synthesis of ligands using CuAAC reaction

To a 50 mL Schlenk tube was added the alkyne (0.2 mmol), tetra(ethylene glycol) monoazide (87 mg, 0.4 mmol), and Cu(OAc)₂·H₂O (12 mg, 0.06 mmol) under N₂. *N,N*-Diisopropylethylamine (26 mg, 0.2 mmol) in MeCN (1 mL) was added and the mixture was stirred for 10 min. A solution of sodium ascorbate (40 mg, 0.2 mmol) in H₂O (1 mL) was dropped into the above solution under N₂. The mixture was sealed and stirred at 60°C for 1 h – 41 h. The reaction was quenched by addition of an aqueous solution of diethylenetriaminepentaacetic acid pentasodium salt (Na₅DTPA, 100 mM, 1 mL). The aqueous solution was extracted with CH₂Cl₂ (3 × 10 mL). The combined organic layer was dried over Na₂SO₄, filtered, and concentrated under vacuum. The crude product was purified by column chromatography (10% MeOH in CH₂Cl₂) to yield the products as colorless oil.

6-1: ¹H-NMR (400 MHz, CDCl₃) δ 7.47(s, 1H, triazole), 7.41(s, 1H, triazole), 7.18–7.09 (m, 5H, aryl), 4.42 (m, 4H, OCH₂CH₂triazole), 3.84 (s, 2H, NCH₂triazole), 3.77 (m, 4H, OCH₂CH₂triazole), 3.55 (m, 24H, OCH₂CH₂O), 2.81–2.71(m, 8H, NCH₂CH₂). ¹³C-NMR (101

MHz, CDCl₃) δ 145.8, 144.3, 140.4, 128.9, 128.3, 125.9, 124.0, 122.7, 72.6, 72.6, 70.5, 70.5, 70.5, 70.4, 70.4, 70.4, 70.2, 70.2, 69.5, 69.5, 61.5, 55.2, 53.1, 50.1, 50.0, 48.4, 33.4, 23.6.

6-2: ¹H-NMR (500 MHz, CDCl₃) δ 7.37 (s, 2H, triazole), 7.30 – 7.13 (m, 5H, aryl), 4.45 (t, 4H, NCH₂CH₂O), 3.92 (q, 1H, CHCH₃), 3.81 (t, 4H, NCH₂CH₂O), 3.69 (t, 4H, OCH₂CH₂OH), 3.64 – 3.51 (m, 20H, OCH₂CH₂O), 3.14 (br, 2H, OH), 2.80 (m, 8H, NCH₂CH₂C), 1.33 (d, 3H, CHCH₃). ¹³C NMR (101 MHz, CDCl₃) δ 146.1, 143.9, 128.1, 127.8, 126.8, 122.5, 72.6, 70.6, 70.5, 70.4, 70.3, 69.6, 61.6, 59.2, 50.1, 49.9, 24.6, 16.5.

6-3: ¹H-NMR (400 MHz, CDCl₃) δ 7.44 (s, 2H, triazole), 7.34 – 7.18 (m, 5H, aryl), 4.49 (t, 4H, NCH₂CH₂O), 3.84 (t, 4H, NCH₂CH₂O), 3.75 – 3.53 (m, 28 H, OEG-H & NCH₂-aryl), 2.95 – 2.81 (m, NCH₂CH₂C). ¹³C-NMR (101 MHz, CDCl₃) δ 146.1, 139.3, 128.9, 128.2, 126.9, 122.5, 72.6, 70.5, 70.5, 70.4, 70.2, 69.6, 61.5, 58.4, 53.3, 50.0, 23.7.

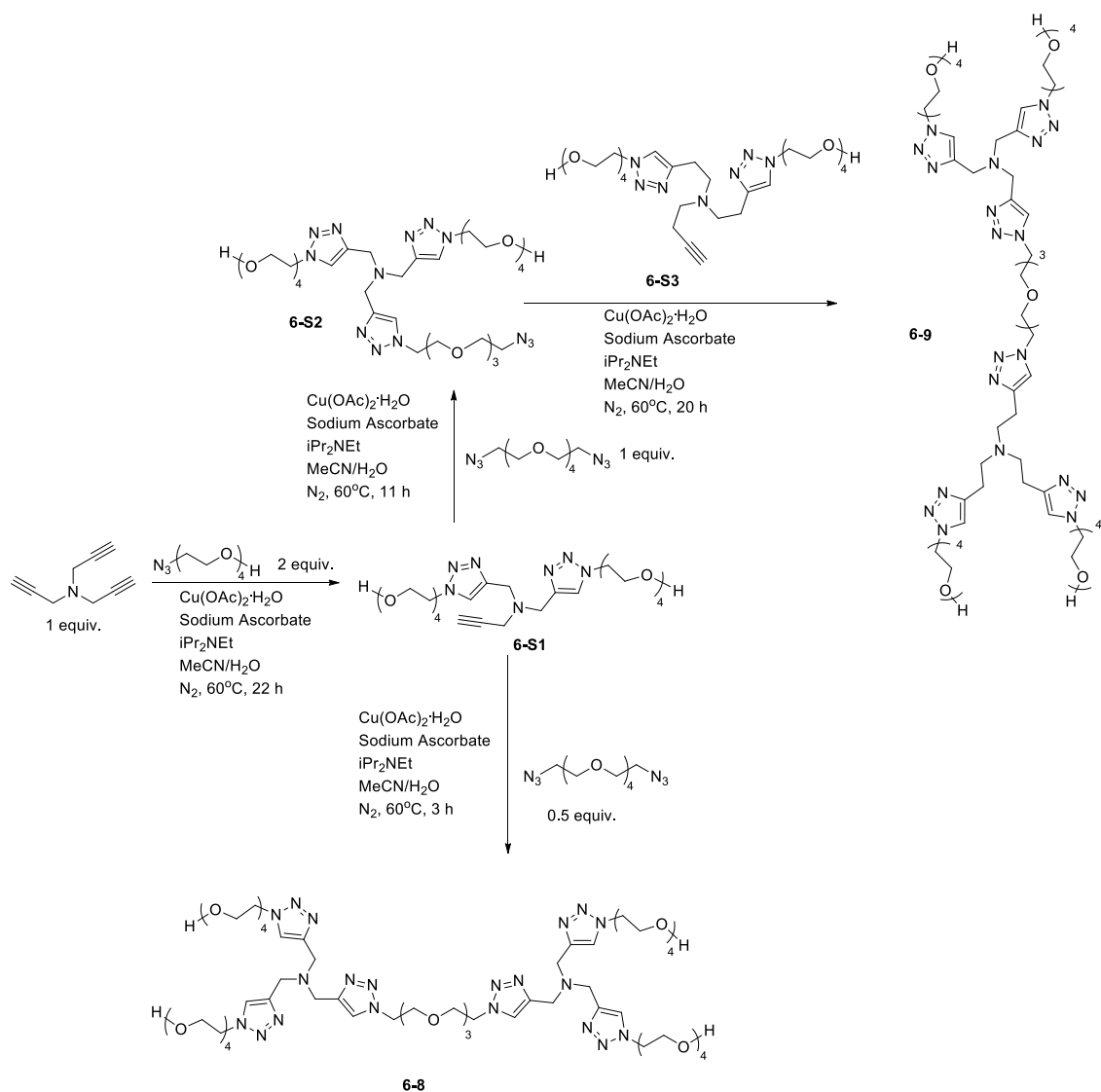
6-4: ¹H-NMR (500 MHz, CDCl₃) δ 7.46(s, 2H, triazole), 7.33 – 7.12 (m, 5H, aryl), 4.49 (t, 4H, NCH₂CH₂O), 3.84 (t, 4H, NCH₂CH₂O), 3.72 (t, 4H, OCH₂CH₂OH), 3.70 – 3.54 (m, 20H, OEG-H), 2.99 – 2.86 (m, 8H, NCH₂CH₂C), 2.86 – 2.73 (m, 4H, NCH₂CH₂-aryl). ¹³C-NMR (126 MHz, CDCl₃) δ 146.0, 140.5, 128.8, 128.4, 126.0, 122.7, 72.6, 70.6, 70.5, 70.4, 70.3, 69.6, 61.6, 55.6, 53.4, 50.1, 33.4, 23.7.

6-5: ¹H NMR (500 MHz, D₂O) 2.71 (h, *J* = 6.8 Hz, 1H), 2.55 (d, *J* = 10.5 Hz, 9H), 2.42 (dd, *J* = 13.1, 6.1 Hz, 1H), 0.93 (d, *J* = 6.9 Hz, 3H). ¹H-NMR (500 MHz, D₂O) δ 7.35 (s, 2H, triazole), 7.14 – 6.89 (m, 5H, aryl), 4.32 (t, 4H, NCH₂CH₂O), 3.71 (t, 4H, NCH₂CH₂O), 3.51 (t, 4H, OCH₂CH₂OH), 3.40 (m, 20H, OEG-H), 2.72 (h, 1H, CH₂CHCH₃), 2.59 – 2.40 (m, 10H, CH₂NCH₂CH₂C), 0.94 (s, 3H, CHCH₃). ¹³C-NMR (101 MHz, D₂O) δ 146.4, 146.1, 128.6, 127.2, 126.3, 123.7, 71.7, 69.6, 69.6, 69.4, 68.8, 60.3, 52.8, 49.8, 37.5, 21.7, 20.5.

filtered and rinsed with CH_2Cl_2 x 2. Filtrate was concentrated under vacuum, diluted with H_2O and extract with CH_2Cl_2 x 3. The organic layer was dried over Na_2SO_4 and concentrated under vacuum. Crude product was purified via flash chromatography (Hexane: EtOAc 12:1) to yield the tri(but-3-yn-1-yl)amine as yellow liquid (1.62 g, 47%).

To a 50 mL Schlenk tube was added tri(but-3-yn-1-yl)amine (35 mg, 0.2 mmol), tetra(ethylene glycol) monoazide (131 mg, 0.6 mmol), and $\text{Cu}(\text{OAc})_2 \cdot \text{H}_2\text{O}$ (12 mg, 0.06 mmol) under N_2 . N,N-Diisopropylethylamine (26 mg, 0.2 mmol) in MeCN (1 mL) was added and the mixture was stirred for 10 min. A solution of sodium ascorbate (40 mg, 0.2 mmol) in H_2O (1 mL) was dropped into the above solution under N_2 . The mixture was sealed and stirred at 60°C for 72 h. The reaction was quenched by addition of an aqueous solution of diethylenetriaminepentaacetic acid pentasodium salt (Na_5DTPA , 100 mM, 1 mL). The aqueous solution was extracted with CH_2Cl_2 (3×10 mL). The combined organic layer was dried over Na_2SO_4 , filtered, and concentrated under vacuum. The crude product was purified by column chromatography (40% MeOH in EtOAc) to yield **6-6** (81.2 mg, 0.1 mmol, 50 %) as a colorless oil. **6-6**: $^1\text{H-NMR}$ (500 MHz, CDCl_3) δ 7.46 (s, 3H, triazole), 4.40 (t, 6H, $\text{NCH}_2\text{CH}_2\text{O}$), 3.74 (t, 6H, $\text{NCH}_2\text{CH}_2\text{O}$), 3.61 (t, 6H, $\text{OCH}_2\text{CH}_2\text{OH}$), 3.56 – 3.46 (m, 30H, $\text{OCH}_2\text{CH}_2\text{O}$), 2.87 – 2.70 (m, 12H, $\text{NCH}_2\text{CH}_2\text{triazole}$). $^{13}\text{C-NMR}$ (126 MHz, CDCl_3) δ 145.8, 122.7, 72.6, 72.6, 72.6, 70.5, 70.5, 70.4, 70.3, 70.2, 70.2, 69.5, 61.4, 53.3, 50.0, 23.5.

6-10 was synthesized according to the procedure of **6-6**. hexa(ethylene glycol) monoazide was used instead of tetra(ethylene glycol) monoazide. $^1\text{H-NMR}$ (500 MHz, D_2O) δ 7.69 (s, 3H, Triazole-CH), 4.42 (t, 6H, $\text{NCH}_2\text{CH}_2\text{O}$), 3.78 (t, 6H, $\text{NCH}_2\text{CH}_2\text{O}$), 3.57 – 3.40 (m, 60H, OEG-H), 2.85 – 2.68 (m, 12H, $\text{NCH}_2\text{CH}_2\text{C}$). $^{13}\text{C NMR}$ (126 MHz, D_2O) δ 145.9, 123.8, 71.7, 69.6, 69.6, 69.5, 69.5, 69.5, 69.5, 69.4, 69.4, 68.8, 60.3, 52.2, 49.9, 21.8.



6-8 & 6-9

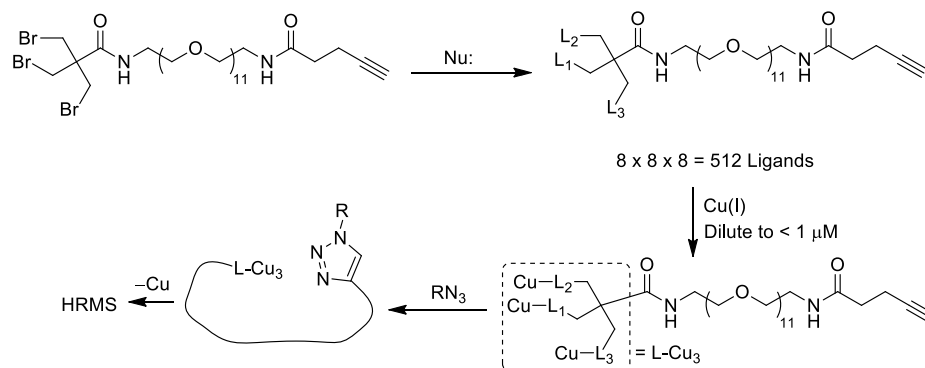
To a 50 mL Schlenk tube was added tripropargylamine (262 mg, 2 mmol), tetra(ethylene glycol) monoazide (880 mg, 4 mmol), Cu(OAc)₂·H₂O (120 mg, 0.6 mmol), N,N-Diisopropylethylamine (260 mg, 2 mmol) and MeCN (5 mL) under N₂. A solution of sodium ascorbate (198 mg, 1 mmol) in H₂O (5 mL) was added into the above solution under N₂. The mixture was sealed and stirred at room temperature for 22 h. The reaction was quenched by addition of an aqueous solution of Na₅DTPA (500 mM, 3 mL). The solvent was removed and the crude product was purified by

column chromatography (10% MeOH in CH₂Cl₂) to yield **6-S1** (475 mg, 42 %) as colorless oil. Using the same procedure, **6-S1** (1 equiv.) was reacted with 1-azido-2-(2-(2-(2-azidoethoxy)ethoxy)ethoxy)ethane (0.5 equiv.) to yield **6-8** as colorless oil (276 mg). ¹H-NMR (500 MHz, D₂O) δ 7.85 (s, 4H, triazole), 7.83 (s, 2H, triazole), 4.45 (t, 8H, NCH₂CH₂O), 4.42 (t, 4H, NCH₂CH₂O), 3.80 (t, 8H, NCH₂CH₂O), 3.74 (t, 4H, NCH₂CH₂O), 3.61 (s, 8H, NCH₂triazole), 3.60 (s, 4H, NCH₂triazole), 3.51 (t, 8H, CH₂CH₂OH), 3.48 (dd, 8H, CH₂CH₂OH), 3.45 – 3.37 (m, 36H, OEG), 3.32 (dd, 8H, OEG). ¹³C-NMR (101 MHz, D₂O) δ 143.1, 143.1, 125.6, 125.6, 71.7, 69.6, 69.5, 69.4, 68.7, 68.7, 60.3, 49.9, 47.1.

Using the same CuAAC procedure, **6-S1** (1 equiv.) was reacted with 1-azido-2-(2-(2-(2-azidoethoxy)ethoxy)ethoxy)ethane (1 equiv.) to yield **6-S2**, which was further reacted with **6-S3** (1 equiv.) to generate the final product **6-9** as colorless oil (32 mg). ¹H-NMR (500 MHz, D₂O) δ 7.86 (s, 2H, triazole-5), 7.83 (s, 1H, triazole-5), 7.68 (s, 2H, triazole-6), 7.64 (s, 1H, triazole-6), 4.43 (tq, 10H, NCH₂CH₂O), 4.37 (t, 2H, NCH₂CH₂O), 3.78 (tq, 10H, NCH₂CH₂O), 3.71 (t, 2H, NCH₂CH₂O), 3.61 (s, 4H, NCH₂triazole), 3.59 (s, 2H, NCH₂triazole), 3.54 – 3.29 (m, 56H, OEG), 2.74 (br, 12H, NCH₂CH₂triazole). ¹³C NMR (126 MHz, D₂O) δ 145.9, 145.8, 143.1, 143.1, 125.6, 125.6, 123.8, 123.7, 71.7, 71.6, 69.6, 69.6, 69.6, 69.4, 69.4, 69.4, 68.8, 68.7, 60.3, 60.3, 52.1, 49.9, 49.9, 49.8, 47.1, 21.8, 21.8.

Chapter 7 Feasibility Study on a Mass-Spectrometry-Based Method for High-Throughput Screening of Ligands for CuAAC Reaction

7.1 Introduction



Scheme 7-1 Screening of CuAAC ligands by high-resolution mass spectrometry (HRMS). Nu: nucleophiles. L_1 , L_2 , L_3 : mono-dentate ligands.

To develop an efficient ancillary ligand exhibiting both high CuAAC activity and anti-oxidation ability, a better choice is to screen a large library of ligands. In Chapter 3, we tethered the tris, bis, and mono(triazolylmethyl)amine ligands with an alkyne by a long flexible oligo(ethyleneglycol) chain to increase the local concentration of the ligands. The distance between the ancillary ligand and the terminal alkyne is approximately 5 nm, *i.e.*, a local concentration of ligand (to the alkyne) in millimolar range. If a mixture of alkynes ligated by different types of ligands was diluted to below micromolar concentration, according to the rate law, the CuAAC reaction accelerated by the ligated ligand can be over 1000 times faster than that accelerated by those unlinked ligands. Thus, the CuAAC reaction rate of each alkyne can be correlated to the ligated ligand since the interference from other unlinked ligands is neglectable. As shown in Scheme 7-1, to provide a

free movement of the ligated ligand, we continued using the highly flexible dodecaethylene glycol (EG₁₁) linker. Considering the CuAAC reaction mechanism involving three copper(I) ions, we designed a tri-bromide functional group to react with a mixture of nucleophiles for attaching three donor ligands, while the other end of the linker was conjugated by an alkyne as reagent. Combination of the three substituting arms will generate a library of > 512 ligands in one solution mixture, which can be complexed with copper(I) and diluted to sub-micromolar concentration. The efficient ligands can catalyze the CuAAC reaction between an azide and its ligated alkyne, generating a triazole product with a specific m/z to be identified by high-resolution mass spectrometry (HRMS).

7.2 Reaction Condition Optimization and Reactor Design

To screen the potential anti-oxidation ligands, the CuAAC reactions can be conducted in air because the copper(I) complexes are supposed to be air-stable. However, the ligands exhibiting high catalytic efficiency may not all well-protect the copper(I) against oxidation. It is necessary to compare the reactivity under inert atmosphere as well. We first optimized the reaction conditions for accurate measurement of reaction yield.

7.2.1 Contamination Control

Glass vials contain a high level of metal and other contaminations that could be introduced into the reaction solution.²¹⁸ In comparison, quartz and polytetrafluoroethylene (PTFE) are considered the cleanest container for trace metal reactions, but they are also the most expensive materials not suitable for this study. The plastic tubes are relatively “trace metal clean”, *e.g.*, the ultrapure water stored in pre-washed polyethylene (PE) tubes contains <1 ppt copper.²¹⁹ In trace metal analysis, the containers for sample preparation are usually soaked and washed in dilute acid, typically using HCl followed by 2% of trace-metal grade HNO₃.²²⁰ In this work, we chose the

polypropylene (PP) tubes as a substitution for the quartz or PTFE tubes. The metal contamination from this tubes was determined after washing the tubes with acids. 2% of trace-metal grade HNO₃ solution was put into this tubes and the copper(I) concentration detected by ICP-MS is below 0.05 ppb (Figure 7-1A, blank).

7.2.2 Purification and Concentration of Reaction Products

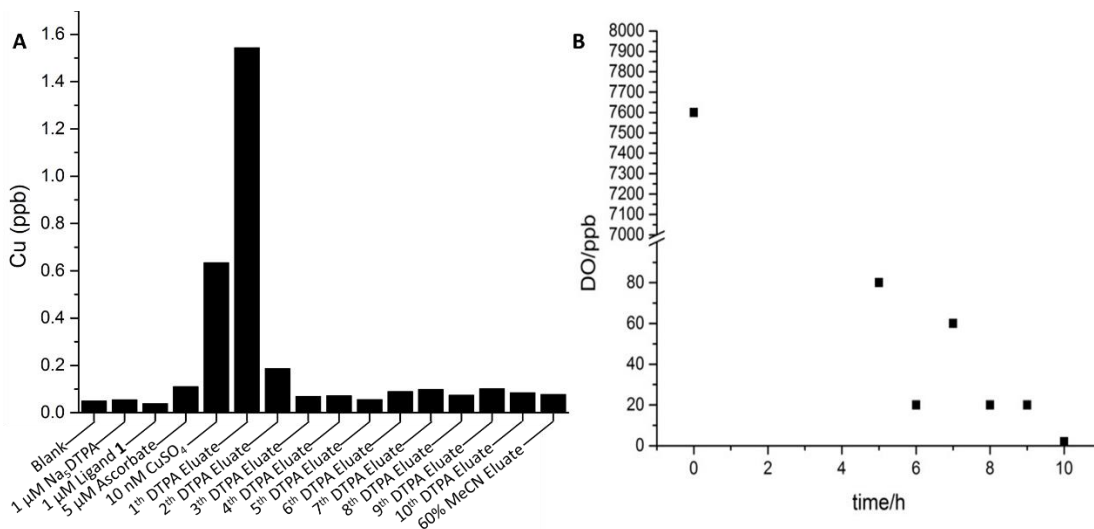


Figure 7-1 A. Copper concentration measured by ICP-MS (see experimental details). B. The drop of dissolved oxygen (DO) level in water stirred in an anaerobic chamber (measured by CHEM Met ampoule).

The triazole product yield at 0.1–1 nM (1–10 %) concentration is below the detection limit of our ion trap mass spectrometer. Therefore, we optimized the purification and concentration procedure of products to enhance the accuracy. The reaction solution was concentrated by lyophilization and C18 zip-tip (solid phase extraction). The excess copper(I) in the solution was removed before LC-MS analysis by flashing the zip-tip by a copper(II)-chelating ligand diethylenetriaminepentaacetic acid (DTPA, equilibrium constants $\log K_d = 21.5\text{--}23.4$).²²¹⁻²²² Using the optimized method we achieved over 96% recovery of the compounds (*e.g.*, ligand **1**), and the purification method was

validated by ICP-MS showing a low concentration of copper(I) after the second elution by DTPA (Figure 7-1A).

7.2.3 Oxygen Control

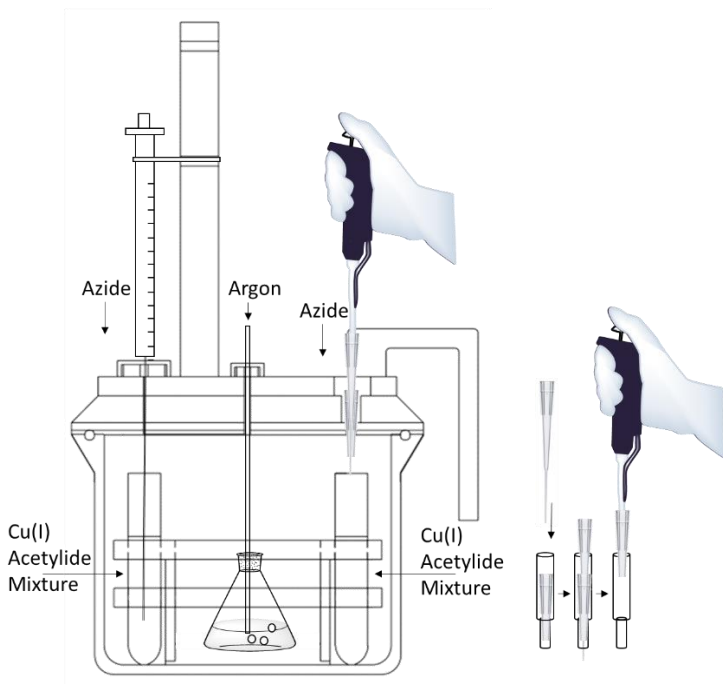


Figure 7-2 Schematic Diagram of the Ultra-low Oxygen Reactor for CuAAC Reaction Under Sub-micromolar Concentration.

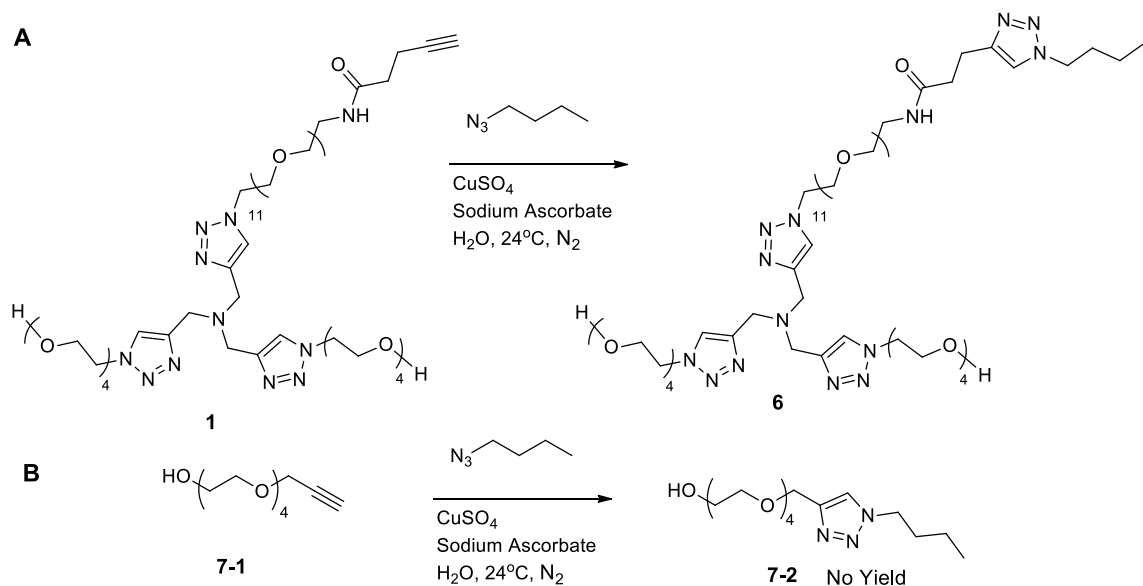
The Milli-Q water for reaction was stirred in a low-density polyethylene (LDPE) bottle in an anaerobic chamber for 24 h in order to reduce the dissolved oxygen to less than 2 ppb (Figure 7-1B). In order to reduce airborne particulates and get a faster gas exchange rate at the same time, a breathable sealing film was covered on top of the uncapped bottle. To further reduce the concentration of water-soluble oxygen in normal anaerobic chamber for sub-micromolar reaction to proceed, we designed and built an ultralow-oxygen reactor (Figure 7-2). A plastic holder for holding 15 mL polypropylene tubes was placed inside the reactor. The solution in each tube can

be stirred by magnetic stir bars. The reactor was sealed by an acrylic lid with a hole above one of the polypropylene tubes for dispensing the reagents, and a handle attached to the side of the lid for turning the hole to directly above a specific tube. In the middle of the lid was inserted a tubing for introducing argon gas continuously into the reactor to keep a positive inner pressure. The argon gas was filtered by a NANOCHEM® PuriFilter® to keep the oxygen level below 0.1 ppb. A stand was designed to hold a gas tight needle for introducing reagent solutions. Taking advantage of long needles and gas tight properties, the stock solutions can be added into each reaction tubes by various volume. However, using a glass syringe with a metal needle generates the risk of introducing metal contaminations. To solve this problem, micropipettes were used for charging the solutions. As shown in Figure 7-2, a wide orifice pipette tip was placed inside the hole to reduce contamination, in which a long pipette tip was inserted to dispense the reagent. The wide orifice tip can be taken out by a pipette. The reactor provided an ultralow-oxygen environment, in which the copper(I)-catalyzed ROS generation is largely inhibited and the oxidative damage to the EG₁₁ linker of the ligand is neglectable. A major drawback of this reactor is the reduced compound recovery caused by the strong compound absorption of PTFE stir bar.

7.3 Method Validation using CuAAC Reaction of Ligand 1

Kinetic studies were performed to validate the accuracy of this ligand-screening method under sub-micromolar concentration. We employed the extensively studied tris(triazolylmethyl)amine ligand system (compound **1**) as an example to quantitatively measure CuAAC reaction yield at 10 nM concentration (Scheme 7-2A), which reached 30% yield within an hour using 2 μM azide (1-azidobutane), 30 nM CuSO₄, and 5 μM ascorbate. The reaction is first order (0.95 ± 0.05) to azide (Figure 7-3A), second-order (2.29 ± 0.26) to copper(I) (Figure 7-3B), and a fractional positive order (0.7) to sodium ascorbate (Figure 7-3C). In the control experiment, the ligand-free alkyne (**7-1**) was mixed with **1** at 5 nM: 5 nM concentration to determine the interference of unlinked-

ligand on free alkyne (Scheme 7-2B). In the reaction with azide, no product yield was detected for the ligand-free alkyne **7-1** within 1 hour reaction time (Figure 7-3D).



Scheme 7-2 CuAAC Reaction of Ligand-ligated Alkyne and Ligand-free Alkyne under 10 nM Concentration.

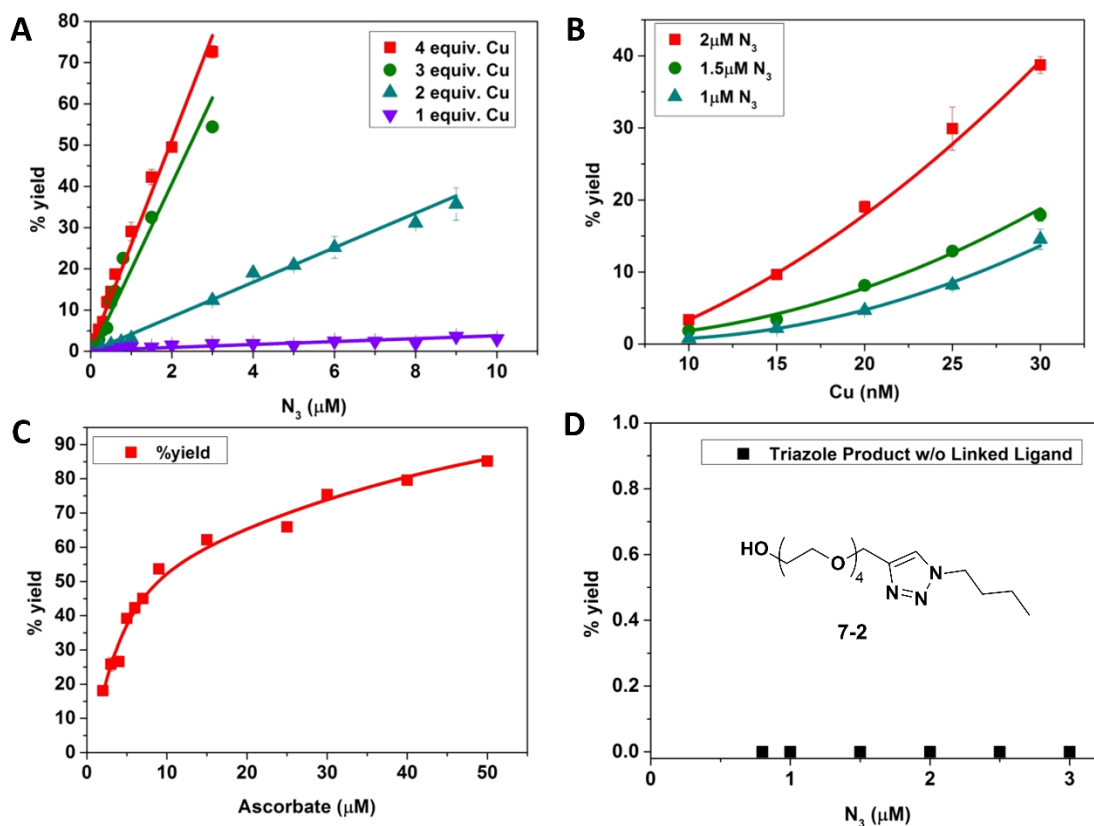


Figure 7-3 Reaction yield (1 hour) vs. concentration plots. A, B, C: yield of **6**. A. 10 nM **1**; 10, 20, 30, 40 nM CuSO_4 ; 100 nM–10 μM 1-azidobutane; 5 μM ascorbate. B. 10 nM **1**; 10–30 nM CuSO_4 ; 1, 1.5, 2 μM 1-azidobutane; 5 μM ascorbate. C. 10 nM **1**; 40 nM CuSO_4 ; 2 μM 1-azidobutane; 2–50 μM ascorbate. D. Yield of **7-2**. 5 nM **1**; 5 nM **7-1**; 40 nM CuSO_4 ; 2 μM 1-azidobutane; 5 μM ascorbate.

7.4 Conclusions

The method tethering ligand to alkyne for screening CuAAC ligands has been validated. No interference was observed between the unlinked ligands and the alkyne. CuAAC reaction under 10 nM concentration showed an over second-order dependence on copper(I), which is in agreement with our previous mechanistic study that a tri-copper(I) acetylide complex could be involved in the catalytic cycle. Oxidation control is hard to execute under such a low

concentration. Therefore, the method is best for air-stable copper(I) complexes such as NHC-copper(I) complexes. Our ligand screening of tri-podal NHC-copper(I) complexes using this method is underway.

7.5 Experimental Section

7.5.1 Preparation of Trace Metal Clean Reaction Containers

The BD Falcon round bottom PP tubes were submerged in 25% HCl (37% AR (ACS) grade HCl in Milli-Q water) for one day, and then washed with Milli-Q water three times, submerged in 2% HNO₃ (67% trace metal grade HNO₃ in Milli-Q water) for four days, then washed with Milli-Q water three times. The magnetic stir bars were also washed by the same procedure put into the reaction solutions.

7.5.2 Preparation of Deoxygenated Water

500 mL Milli-Q water was added into a pre-washed 1 L LDPE bottle containing a pre-washed PTFE stir bar, capped with LDPE cap with a hole in the middle, stirred for 24 h until the oxygen concentration dropped to 0 ppb.

7.5.3 ICP-MS Detection of Copper Concentration in Selected Solutions

ICP MS procedure (the numbers in [] are ppb values, 64 ppb=1 μ M Cu): 30 μ L 70% HNO₃ (Fluka, *traceSELECT*, for trace analysis) and 970 μ L H₂O (Milli-Q water) was added into a pre-washed PP tube **1** [**0.049**]. 10 μ L 100 μ M Na₅DTPA, 30 μ L 70% HNO₃ and 960 μ L H₂O was added into tube **2** [**0.054**]. 10 μ L 100 μ M ligand **1**, 30 μ L 70% HNO₃ and 960 μ L H₂O was added into tube **3** [**0.038**]. 10 μ L 500 μ M Sodium Ascorbate, 30 μ L 70% HNO₃ and 960 μ L H₂O was added into tube **4** [**0.110**]. 10 μ L MeCN, 10 μ L 1 μ M CuSO₄ and 30 μ L 70% HNO₃ and 950 μ L H₂O was added into tube **5** [**0.634**].

10 μL 5 mM Na_5DTPA , 10 μL 1 mM CuSO_4 , 10 μL 100 μM ligand **1**, 10 μL 5 mM Ascorbate and 60 μL H_2O was mixed and 10 μL of that solution was dispensed into a tube and stand in air for 10 min. A Zip-tip (Pierce™ C18 Tip, 10 μL bed) was used to aspirate and dispense the 10 μL solution 20 cycles. Zip-tip was washed with 10 μL 100 μM Na_5DTPA 10 times and the washing-solution was dispensed into a tube each time. 30 μL 70% HNO_3 and 960 μL H_2O was added into each tube for ICP-MS analysis. Eluate **1-10**: [**1.543, 0.187, 0.069, 0.071, 0.055, 0.089, 0.098, 0.074, 0.101, 0.084**]. Zip-tip was eluted with 10 μL MeCN into a tube containing 30 μL 70% HNO_3 and 960 μL H_2O [**0.077**].

7.5.4 Kinetic Studies for CuAAC Reaction of Ligand 1 at 10 nM Concentration

7.5.4.1 Rate Order in Copper(I)

Pre-leached Perkin Elmer PP ICP-MS auto-sampler tubes were filled with 8700 μL deoxygenized H_2O . All stock solutions were prepared with the deoxygenized water. 100 μL **1** solution (1 μM), 100 μL 1-azidobutane (100, 150, 200 μM for assay 1, assay 2, and assay 3), 100 μL Na Ascorbate (500 μM) were added into each reaction tube by aspirate and dispense 20 times. 1000 μL CuSO_4 (100–300 nM) was added into each reaction tube by aspirate and dispense 10 times to start the reaction. The tubes were capped and shaken for 1 h. The reaction was quenched by 1000 μL 10 μM air-saturated Na_5DTPA and moving out from the anaerobic chamber, frozen in -80°C freezer and placed into a CoolSafe freeze-drier to be freeze-dried for 36 h until all tubes were dried. 1 mL H_2O was added into the tubes and the inner walls were rinsed. The solutions were purified by a combined Zip-tip (1 ml pipette tip capped with 100 μL Zip-tip) by aspirating-dispensing 10 times. The Zip-tip was washed with 100 μL 100 μM Na_5DTPA x 2, 100 μL water x 5, and eluted with 100 μL 60%MeCN/ H_2O into an auto-sampler vial for LC-MS analysis. Each sample was injected 3 times, % yield was calculated based on calibration curve.

7.5.4.2 Rate Order in Azide

Kinetic studies for rate order in azide was conducted according to the above procedure. Concentrations: 100 μL **1** solution (1 μM), 100 μL 1-azidobutane (10 μM –3 mM), 100 μL Na Ascorbate (500 μM) were added into each reaction tube by aspirate and dispense 20 times. 1000 μL CuSO_4 (100, 200, 300, 400 nM for assay 1, 2, 3, 4) was added into reaction tube by aspirate and dispense 10 times to start the reaction.

7.5.4.3 Rate Order in Ascorbate

Kinetic studies for rate order in azide was conducted according to the above procedure. Concentrations: 100 μL **1** solution (1 μM), 100 μL 1-azidobutane (200 μM), 100 μL Na Ascorbate (200–5000 μM) were added into each reaction tube by aspirate and dispense 20 times. 1000 μL CuSO_4 (400 nM) was added into each reaction tube by aspirate and dispense 10 times to start the reaction.

7.5.4.4 CuAAC Reaction in Alkyne 1 & Alkyne 7-1 Mixture

Kinetic studies for the CuAAC reaction with alkyne **1** & alkyne **7-1** mixture was conducted according to the above procedure. Concentrations: 100 μL stock solution (0.5 μM **1** + 0.5 μM **7-1**), 100 μL 1-azidobutane (200 μM), 100 μL Na Ascorbate (500 μM) were added into each reaction tube by aspirate and dispense 20 times. 1000 μL CuSO_4 (400 nM) was added into each reaction tube by aspirate and dispense 10 times to start the reaction. % yield was calculated based on calibration curve of **7-1** & **7-2**.

7.5.5 Synthesis Procedure and NMR Spectra

Alkyne **7-1**:

To a 25 mL flask was added THF (5 mL), tetra(ethylene glycol) (776 mg, 4 mmol) and propargyl bromide (108 μ L, 1 mmol, 80% in Toluene) in an ice bath, and the mixture was stirred for 10 min. Sodium hydride (29 mg, 1.2 mmol) was added into the above solution. The mixture was sealed and stirred at room temperature for 4 h. The reaction was quenched by adding water, concentrated under vacuum, and the crude product was purified by column chromatography (EtOAc) to yield the products as colorless oil (203 mg, 87%). $^1\text{H-NMR}$ (400 MHz, CDCl_3) δ 4.20 (d, 2H, CH_2CCH), 3.74 – 3.63 (m, 14H, OEG), 3.60 (t, 2H, CH_2OH), 2.48 (s, 1H, OH), 2.42 (t, 1H, CCH). $^{13}\text{C NMR}$ (101 MHz, CDCl_3) δ 79.6, 74.6, 72.5, 70.7, 70.6, 70.6, 70.4, 70.4, 70.4, 69.1, 61.8, 58.5, 58.4.

Triazole **7-2**:

To a 25 mL Schlenk tube was added **7-1** (116 mg, 0.5 mmol), 1-azidobutane (198 mg, 2 mmol), $\text{Cu}(\text{OAc})_2\cdot\text{H}_2\text{O}$ (10 mg, 0.05 mmol), H_2O (2 mL) under N_2 . A solution of sodium ascorbate (99 mg, 0.5 mmol) in H_2O (1 mL) was added into the above solution under N_2 . The mixture was sealed and stirred at room temperature for 3 h. The reaction was quenched by addition of an aqueous solution of Na_5DTPA (100 mM, 1 mL). The solvent was removed and the crude product was purified by column chromatography (2% MeOH in CH_2Cl_2) to yield the product as colorless oil (140 mg, 0.42 mmol, 84%). $^1\text{H NMR}$ (400 MHz, CDCl_3) δ 7.57 (s, 1H), 4.65 (d, $J = 0.4$ Hz, 2H), 4.31 (t, $J = 7.2$ Hz, 2H), 3.72 – 3.53 (m, 16H), 3.07 (s, 1H), 1.93 – 1.77 (m, 2H), 1.32 (dq, $J = 14.8, 7.4$ Hz, 2H), 0.91 (t, $J = 7.4$ Hz, 3H). $^{13}\text{C NMR}$ (101 MHz, CDCl_3) δ 145.0, 122.6, 72.6, 70.6, 70.6, 70.5, 70.5, 70.3, 69.7, 64.7, 61.7, 50.1, 32.3, 19.7, 13.5.

Chapter 8 Summary

The highly efficient, orthogonal and versatile CuAAC reaction is a powerful tool in many fields, and a variety of protocols have been developed for CuAAC, including the use of ancillary ligands to accelerate reaction rate. The long-term goal of this project is to develop copper(I) complexes as high-efficient and air-stable CuAAC catalysts for bioorthogonal bioconjugation inside living cells.

Mechanism of the ligand-free CuAAC reaction has been studied, but the ligand-accelerated reaction has not been well clarified, especially for the tris(triazolylmethyl)amine ligands (**TL**), which are one of the most efficient and widely employed ligands. It is difficult to detect and isolate reactive intermediates due to the complicated solution equilibria generated by the weakly-coordinating triazole arms. In order to shed light on the future ligand design, the first objective in this project is to understand the detailed mechanism of **TL**-accelerated CuAAC.

We designed a ligand tethering the terminal alkyne to the **TL** ligand to increase the local concentration of copper(I) species and to facilitate the detection of reactive intermediates under stoichiometric conditions. Reactive intermediates were captured and monitored by direct-infusion ESI-MS and further characterized by tandem mass spectrometry (MS/MS) plus isotopic distribution analysis. The di-copper and tri-copper-**TL**-acetylides were successfully detected. ESI-MS revealed that tri-copper-acetylide was more stable against protonation than di-copper-acetylide in neutral aqueous solutions. An unprecedented tri-Cu-**TL**-triazolide was captured by ESI-MS in stoichiometric reaction with an azide and confirmed as a major intermediate produced from tri-copper-acetylide via a “tri-copper pathway”.

Conditions were optimized to enrich individual active copper acetylide complexes to facilitate measurement of their reaction kinetics by LC-MS/MS under stoichiometric or catalytic conditions. Kinetics studies indicated a higher activity of the di-copper-acetylide than tri-copper-acetylide

under stoichiometric condition. Deprotonation of di-copper alkyne was identified as the rate-limiting step in “di-copper pathway”. Kinetic studies demonstrated a preference of the “tri-copper pathway” under catalytic condition, attributed to the difficulty in forming di-copper azide-acetylide complex. Under catalytic condition, kinetic studies also suggested fractional rate order on copper concentration due to the presence of inactive copper(I) species generated by the extra alkyne.

Single crystal X-ray crystallography of the tri-copper-**TL**-acetylide revealed a planar tri-Cu-acetylide structure ($\mu^3\text{-}\eta^{1,1,2}$) with free coordination sites on copper(I) available for binding with an azide. Bond lengths and angles indicated that strong π back bonding from one of the σ -copper increased its positive charge for coordination with an azide. The copper complexes in the system were studied by NMR, FT-IR, UV-Vis.

Density functional theory (DFT) was performed in collaboration with Profs. Shereen Ghaoui and Thomas A. Albright to obtain the free energies and optimized structures of the proposed intermediates. DFT calculations confirmed a lower activation barrier of the “di-copper pathway”.

In bioconjugation, excessive **TL** ligand and sacrificing reducing agent (ascorbate) are commonly applied to prevent copper(I) from oxidation by air. However, additional **TL** ligand was found to slowdown the reaction, and the ascorbate/Cu(I)/O₂/Cu(II) redox cycle generates reactive oxygen species that can severely damage delicate biomolecules as a main reason for the cytotoxicity of excess copper. The second objective is to develop multi-dentate ligands with both high accelerating efficacy and anti-oxidation effect.

Potential accelerating ligands were designed and synthesized using **TL** as a template. In a mono-copper-**TL** complex, the tertiary amine and triazole nitrogen coordinate to copper(I) by forming three five-member metallacycle rings (5,5,5). Accordingly, we synthesized a series of tetra-

dentate and tri-dentate ligands with ring sizes adjusted from (5,5,5), (5,5,6), (5,6,6) to (6,6,6). The donor-acceptor strength was adjusted by changing triazoles to phenyls and steric effect was studied by employing α and β -substitution groups. The ligands' catalytic activities in CuAAC reaction were studied by *in vitro* fluorescent plate reader assays using coumarin azide as the fluorescent dye. The inhibitory effect of excess ligands was studied by changing the ligand/copper(I) ratio. The anti-oxidation properties of these ligands were characterized by ascorbate consumption in air monitored by UV-Vis spectra.

Chelating ring size was found as the most important factor impacting the catalytic efficiency and anti-oxidation properties of these ligands. Generally, enlarged ring size resulted in reduced activity but increased anti-oxidation ability, with ligands possessing an unsubstituted (5,5,5) structure showing the highest reactivity which was similar to **TL**. Phenyl substitution group offered partial protection of copper(I), but showed poorer activity and anti-oxidation efficiency compared to a triazole group which is a stronger ligand. The α -substitution dramatically decreased the reaction rate, probably due to the difficulty of forming multinuclear Cu-acetylide complexes. Ligands with a larger chelating ring offered more copper(I) protection than **TL** did, thus can be employed at a low ligand/copper(I) ratio. However, an excess amount of these ligands largely inhibited the reaction.

We also developed a high-throughput screening method for a large library of ligands. An alkyne was ligated with a mixture of ligands by a long, flexible oligo ethylene glycol chain. In this way, an active ligand can be identified under sub-micromolar concentration based on the specific m/z of the triazole product detected by high resolution mass spectrometry.

The insights into the structure and catalytic/anti-oxidation activity relationship of ligands will provide important guidance in future ligand design. We will continue this ligand screening project in the future to obtain the most efficient ligand. A successful ligand should gather multi-copper(I)

at alkyne reaction center without blocking azide access. The next generation of ligands could be developed by enhancing the stability and increasing the concentration of di-copper azide-acetylide species. The ligands with superior anti-oxidation capability can be employed in bioconjugation.

References

- (1) Huisgen, R.; Szeimies, G.; Möbius, L., *Chem. Ber.* **1967**, *100* (8), 2494-2507.
- (2) Huisgen, R., *Angew. Chem. Int. Ed. Engl.* **1963**, *2* (10), 565-598.
- (3) Huisgen, R., *Angew. Chem. Int. Ed. Engl.* **1963**, *2* (11), 633-645.
- (4) L'abbé, G., *Bull. Soc. Chim. Belg.* **1984**, *93* (7), 579-592.
- (5) Tornøe, C. W.; Christensen, C.; Meldal, M., *J. Org. Chem.* **2002**, *67* (9), 3057-3064.
- (6) Rostovtsev, V. V.; Green, L. G.; Fokin, V. V.; Sharpless, K. B., *Angew. Chem., Int. Ed.* **2002**, *41* (14), 2596-2599.
- (7) Kolb, H. C.; Finn, M. G.; Sharpless, K. B., *Angew. Chem., Int. Ed.* **2001**, *40* (11), 2004-2021.
- (8) Xi, W.; Scott, T. F.; Kloxin, C. J.; Bowman, C. N., *Adv. Funct. Mater.* **2014**, *24* (18), 2572-2590.
- (9) McKay, Craig S.; Finn, M. G., *Chem. Biol.* **2014**, *21* (9), 1075-1101.
- (10) Hein, C. D.; Liu, X.-M.; Wang, D., *Pharm. Res.* **2008**, *25* (10), 2216-2230.
- (11) Tron, G. C.; Pirali, T.; Billington, R. A.; Canonico, P. L.; Sorba, G.; Genazzani, A. A., *Med. Res. Rev.* **2008**, *28* (2), 278-308.
- (12) Schulze, B.; Schubert, U. S., *Chem. Soc. Rev.* **2014**, *43* (8), 2522-2571.
- (13) Meldal, M.; Tornøe, C. W., *Chem. Rev.* **2008**, *108* (8), 2952-3015.
- (14) Thirumurugan, P.; Matosiuk, D.; Jozwiak, K., *Chem. Rev.* **2013**, *113* (7), 4905-4979.
- (15) Ramil, C. P.; Lin, Q., *Chem. Commun.* **2013**, *49* (94), 11007-11022.
- (16) Lallana, E.; Riguera, R.; Fernandez-Megia, E., *Angew. Chem., Int. Ed.* **2011**, *50* (38), 8794-8804.
- (17) Ahmad Fuaad, A. A.; Azmi, F.; Skwarczynski, M.; Toth, I., *Molecules* **2013**, *18* (11), 13148-13174.
- (18) Tang, W.; Becker, M. L., *Chem. Soc. Rev.* **2014**, *43* (20), 7013-7039.
- (19) Yang, M.; Li, J.; Chen, P. R., *Chem. Soc. Rev.* **2014**, *43* (18), 6511-6526.
- (20) Hu, Q.-Y.; Allan, M.; Adamo, R.; Quinn, D.; Zhai, H.; Wu, G.; Clark, K.; Zhou, J.; Ortiz, S.; Wang, B., *Chem. Sci.* **2013**, *4* (10), 3827-3832.
- (21) Jiang, H.; Zheng, T.; Lopez-Aguilar, A.; Feng, L.; Kopp, F.; Marlow, F. L.; Wu, P., *Bioconjugate Chem.* **2014**, *25* (4), 698-706.
- (22) Lin, W.; Du, Y.; Zhu, Y.; Chen, X., *J. Am. Chem. Soc.* **2014**, *136* (2), 679-687.
- (23) El-Sagheer, A. H.; Brown, T., *Chem. Soc. Rev.* **2010**, *39* (4), 1388-1405.

- (24) Golas, P. L.; Matyjaszewski, K., *Chem. Soc. Rev.* **2010**, 39 (4), 1338-1354.
- (25) Himo, F.; Lovell, T.; Hilgraf, R.; Rostovtsev, V. V.; Noodleman, L.; Sharpless, K. B.; Fokin, V. V., *J. Am. Chem. Soc.* **2005**, 127 (1), 210-216.
- (26) Eglinton, G.; Galbraith, A., *J. Chem. Soc.* **1959**, 889-896.
- (27) Zhang, G.; Yi, H.; Zhang, G.; Deng, Y.; Bai, R.; Zhang, H.; Miller, J. T.; Kropf, A. J.; Bunel, E. E.; Lei, A., *J. Am. Chem. Soc.* **2014**, 136 (3), 924-926.
- (28) Kuang, G.-C.; Michaels, H. A.; Simmons, J. T.; Clark, R. J.; Zhu, L., *J. Org. Chem.* **2010**, 75 (19), 6540-6548.
- (29) Brotherton, W. S.; Guha, P. M.; Phan, H.; Clark, R. J.; Shatruk, M.; Zhu, L., *Dalton Trans.* **2011**, 40 (14), 3655-3665.
- (30) Kuang, G.-C.; Guha, P. M.; Brotherton, W. S.; Simmons, J. T.; Stanke, L. A.; Nguyen, B. T.; Clark, R. J.; Zhu, L., *J. Am. Chem. Soc.* **2011**, 133 (35), 13984-14001.
- (31) Nguyen, M. T.; Sengupta, D.; Ha, T.-K., *J. Phys. Chem.* **1996**, 100 (16), 6499-6503.
- (32) Dias, H. V. R.; Polach, S. A.; Goh, S.-K.; Archibong, E. F.; Marynick, D. S., *Inorg. Chem.* **2000**, 39 (17), 3894-3901.
- (33) Bräse, S.; Gil, C.; Knepper, K.; Zimmermann, V., *Angew. Chem., Int. Ed.* **2005**, 44 (33), 5188-5240.
- (34) Lin, F. L.; Hoyt, H. M.; van Halbeek, H.; Bergman, R. G.; Bertozzi, C. R., *J. Am. Chem. Soc.* **2005**, 127 (8), 2686-2695.
- (35) Berg, R.; Straub, J.; Schreiner, E.; Mader, S.; Rominger, F.; Straub, B. F., *Adv. Synth. Catal.* **2012**, 354 (18), 3445-3450.
- (36) Deraedt, C.; Pinaud, N. I.; Astruc, D., *J. Am. Chem. Soc.* **2014**, 136 (34), 12092-12098.
- (37) Fuchs, M.; Goessler, W.; Pilger, C.; Kappe, C. O., *Adv. Synth. Catal.* **2010**, 352 (2 - 3), 323-328.
- (38) Pachón, L. D.; Van Maarseveen, J. H.; Rothenberg, G., *Adv. Synth. Catal.* **2005**, 347 (6), 811-815.
- (39) Lewis, W. G.; Magallon, F. G.; Fokin, V. V.; Finn, M., *J. Am. Chem. Soc.* **2004**, 126 (30), 9152-9153.
- (40) Rodionov, V. O.; Fokin, V. V.; Finn, M. G., *Angew. Chem., Int. Ed.* **2005**, 44 (15), 2210-2215.
- (41) Rodionov, V. O.; Presolski, S. I.; Díaz Díaz, D.; Fokin, V. V.; Finn, M. G., *J. Am. Chem. Soc.* **2007**, 129 (42), 12705-12712.
- (42) Kalvet, I.; Tammiku-Taul, J.; Mäeorg, U.; Tamm, K.; Burk, P.; Sikk, L., *ChemCatChem* **2016**, 8 (10), 1804-1808.
- (43) Presolski, S. I.; Hong, V.; Cho, S.-H.; Finn, M. G., *J. Am. Chem. Soc.* **2010**, 132 (41), 14570-14576.

- (44) Bevilacqua, V.; King, M.; Chaumontet, M.; Nothisen, M.; Gabillet, S.; Buisson, D.; Puente, C.; Wagner, A.; Taran, F., *Angew. Chem., Int. Ed.* **2014**, *53* (23), 5872-5876.
- (45) Saha, S.; Kaur, M.; Bera, J. K., *Organometallics* **2015**, *34* (12), 3047-3054.
- (46) Ahlquist, M.; Fokin, V. V., *Organometallics* **2007**, *26* (18), 4389-4391.
- (47) Calvo-Losada, S.; Pino-González, M. S.; Quirante, J. J., *J. Phys. Chem. B* **2015**, *119* (4), 1243-1258.
- (48) Straub, B. F., *Chem. Commun.* **2007**, (37), 3868-3870.
- (49) Cantillo, D.; Avalos, M.; Babiano, R.; Cintas, P.; Jimenez, J. L.; Palacios, J. C., *Org. Biomol. Chem.* **2011**, *9* (8), 2952-2958.
- (50) Özen, C.; Tüzün, N. Ş., *J. Mol. Graphics Modell.* **2012**, *34*, 101-107.
- (51) Ikhlef, D.; Wang, C.; Kahlal, S.; Maouche, B.; Astruc, D.; Saillard, J.-Y., *Comp. Theor. Chem.* **2015**, *1073*, 131-138.
- (52) Jin, L.; Tolentino, D. R.; Melaimi, M.; Bertrand, G., *Sci. Adv.* **2015**, *1* (5).
- (53) Özkılıç, Y.; Tüzün, N. Ş., *Organometallics* **2016**, *35* (16), 2589-2599.
- (54) Yam, V. W.-W.; Lo, K. K.-W.; Wong, K. M.-C., *J. Organomet. Chem.* **1999**, *578* (1), 3-30.
- (55) Lang, H.; Jakob, A.; Milde, B., *Organometallics* **2012**, *31* (22), 7661-7693.
- (56) Yam, V. W.-W.; Lo, K. K.-W., *Chem. Soc. Rev.* **1999**, *28* (5), 323-334.
- (57) Chui, S. S.; Ng, M. F.; Che, C. M., *Chem. Eur. J.* **2005**, *11* (6), 1739-1749.
- (58) Higgs, T. C.; Parsons, S.; Bailey, P. J.; Jones, A. C.; McLachlan, F.; Parkin, A.; Dawson, A.; Tasker, P. A., *Organometallics* **2002**, *21* (26), 5692-5702.
- (59) Higgs, T. C.; Bailey, P. J.; Parsons, S.; Tasker, P. A., *Angew. Chem., Int. Ed.* **2002**, *41* (16), 3038-3041.
- (60) Baxter, C. W.; Higgs, T. C.; Bailey, P. J.; Parsons, S.; McLachlan, F.; McPartlin, M.; Tasker, P. A., *Chem. Eur. J.* **2006**, *12* (23), 6166-6174.
- (61) Noshchenko, G.; Mykhalichko, B.; Davydov, V., *Russ. J. Coord. Chem.* **2004**, *30* (5), 326-331.
- (62) Chang, X.-Y.; Low, K.-H.; Wang, J.-Y.; Huang, J.-S.; Che, C.-M., *Angew. Chem., Int. Ed.* **2016**, *55* (35), 10312-10316.
- (63) Lo, W.-Y.; Lam, C.-H.; Yam, V. W.-W.; Zhu, N.; Cheung, K.-K.; Fathallah, S.; Messaoudi, S.; Le Guennic, B.; Kahlal, S.; Halet, J.-F., *J. Am. Chem. Soc.* **2004**, *126* (23), 7300-7310.
- (64) Diez, J.; Gamasa, M. P.; Gimeno, J.; Aguirre, A.; Garcia-Granda, S., *Organometallics* **1991**, *10* (2), 380-382.

- (65) Yam, V. W.-W.; Lee, W.-K.; Cheung, K.-K.; Crystall, B.; Phillips, D., *J. Chem. Soc., Dalton Trans.* **1996**, (15), 3283-3287.
- (66) Yam, V.-W.; Fung, W.-M., *Chem. Commun.* **1997**, (10), 963-964.
- (67) Yam, V. W.-W.; Fung, W. K.-M.; Wong, M.-T., *Organometallics* **1997**, *16* (8), 1772-1778.
- (68) Yam, V. W.-W.; Fung, W. K.-M.; Cheung, K.-K., *Organometallics* **1998**, *17* (15), 3293-3298.
- (69) Yam, V. W.-W.; Lam, C.-H.; Cheung, K.-K., *Inorg. Chim. Acta* **2001**, *316* (1), 19-24.
- (70) Zhang, M.; Su, B.-C.; Li, C.-L.; Shen, Y.; Lam, C.-K.; Feng, X.-L.; Chao, H.-Y., *J. Organomet. Chem.* **2011**, *696* (13), 2654-2659.
- (71) Yam, V. W. W.; Fung, W. K. M.; Cheung, K. K., *Angew. Chem. Int. Ed. Engl.* **1996**, *35* (10), 1100-1102.
- (72) Gamasa, M. P.; Gimeno, J.; Lastra, E.; Solans, X., *J. Organomet. Chem.* **1988**, *346* (2), 277-286.
- (73) Wing-WaháYam, V.; Wing-KináChoi, S., *Chem. Commun.* **1996**, (17), 2067-2068.
- (74) Chan, C. L.; Cheung, K. L.; Lam, W. H.; Cheng, E. C. C.; Zhu, N.; Choi, S. W. K.; Yam, V. W. W., *Chem. Asian J.* **2006**, *1* (1 - 2), 273-286.
- (75) Knotter, D. M.; Spek, A. L.; Grove, D. M.; Van Koten, G., *Organometallics* **1992**, *11* (12), 4083-4090.
- (76) Drew, M. G.; Esho, F. S.; Nelson, S. M., *J. Chem. Soc., Chem. Commun.* **1982**, (23), 1347-1348.
- (77) Diez, J.; Gamasa, M. P.; Gimeno, J.; Lastra, E.; Aguirre, A.; Garcia-Granda, S., *Organometallics* **1993**, *12* (6), 2213-2220.
- (78) Makarem, A.; Berg, R.; Rominger, F.; Straub, B. F., *Angew. Chem., Int. Ed.* **2015**, *54* (25), 7431-7435.
- (79) Nolte, C.; Mayer, P.; Straub, B. F., *Angew. Chem., Int. Ed.* **2007**, *46* (12), 2101-2103.
- (80) Winn, J.; Pinczewska, A.; Goldup, S. M., *J. Am. Chem. Soc.* **2013**, *135* (36), 13318-13321.
- (81) Ito, M.; Hashizume, D.; Fukunaga, T.; Matsuo, T.; Tamao, K., *J. Am. Chem. Soc.* **2009**, *131* (50), 18024-18025.
- (82) Iacobucci, C.; Reale, S.; De Angelis, F., *Angew. Chem., Int. Ed.* **2016**, *55* (9), 2980-2993.
- (83) Keith-Roach, M. J., *Anal. Chim. Acta* **2010**, *678* (2), 140-148.
- (84) Schröder, D., *Acc. Chem. Res.* **2012**, *45* (9), 1521-1532.
- (85) Iacobucci, C.; Reale, S.; Gal, J.-F.; De Angelis, F., *Angew. Chem., Int. Ed.* **2015**, *54* (10), 3065-3068.

- (86) Iacobucci, C.; Lebon, A.; De Angelis, F.; Memboeuf, A., *Chem. Eur. J.* **2016**, n/a-n/a.
- (87) He, Q.; Xing, Z.; Wei, C.; Fang, X.; Zhang, S.; Zhang, X., *Chem. Commun.* **2016**, 52 (69), 10501-10504.
- (88) Sun, S.; Wu, P., *J. Phys. Chem. A* **2010**, 114 (32), 8331-8336.
- (89) Worrell, B. T.; Malik, J. A.; Fokin, V. V., *Science* **2013**, 340 (6131), 457-460.
- (90) Díaz-Torres, R.; Alvarez, S., *Dalton Trans.* **2011**, 40 (40), 10742-10750.
- (91) Buckley, B. R.; Dann, S. E.; Heaney, H., *Chem. Eur. J.* **2010**, 16 (21), 6278-6284.
- (92) Gutmann, V., Certain Donor Solvents. In *Coordination Chemistry in Non-Aqueous Solutions*, Springer Vienna: Vienna, 1968; pp 126-160.
- (93) Himo, F.; Lovell, T.; Hilgraf, R.; Rostovtsev, V. V.; Noodleman, L.; Sharpless, K. B.; Fokin, V. V., *J. Am. Chem. Soc.* **2005**, 127 (1), 210-216.
- (94) Meng, J.-c.; Fokin, V. V.; Finn, M., *Tetrahedron Lett.* **2005**, 46 (27), 4543-4546.
- (95) Proulx, G.; Bergman, R. G., *J. Am. Chem. Soc.* **1995**, 117 (23), 6382-6383.
- (96) Yuan, Z.; Kuang, G.-C.; Clark, R. J.; Zhu, L., *Org. Lett.* **2012**, 14 (10), 2590-2593.
- (97) Barz, M.; Herdtweck, E.; Thiel, W. R., *Angew. Chem., Int. Ed.* **1998**, 37 (16), 2262-2265.
- (98) Brotherton, W. S.; Michaels, H. A.; Simmons, J. T.; Clark, R. J.; Dalal, N. S.; Zhu, L., *Org. Lett.* **2009**, 11 (21), 4954-4957.
- (99) Escobar, L. B.; Guedes, G. P.; Soriano, S. p.; Speziali, N. L.; Jordão, A. K.; Cunha, A. C.; Ferreira, V. F.; Maxim, C.; Novak, M. A.; Andruh, M., *Inorg. Chem.* **2014**, 53 (14), 7508-7517.
- (100) Zhu, L.; Brassard, C. J.; Zhang, X.; Guha, P. M.; Clark, R. J., *Chem. Rec.* **2016**, 16 (3), 1501-1517.
- (101) Uttamapinant, C.; Tangpeerachaikul, A.; Grecian, S.; Clarke, S.; Singh, U.; Slade, P.; Gee, K. R.; Ting, A. Y., *Angew. Chem., Int. Ed.* **2012**, 51 (24), 5852-5856.
- (102) Li, Z.; Seo, T. S.; Ju, J., *Tetrahedron Lett.* **2004**, 45 (15), 3143-3146.
- (103) Kislukhin, A. A.; Hong, V. P.; Breitenkamp, K. E.; Finn, M., *Bioconjugate Chem.* **2013**, 24 (4), 684-689.
- (104) Collman, J. P.; Devaraj, N. K.; Chidsey, C. E., *Langmuir* **2004**, 20 (4), 1051-1053.
- (105) Zhang, W.-B.; Tu, Y.; Ranjan, R.; Van Horn, R. M.; Leng, S.; Wang, J.; Polce, M. J.; Wesdemiotis, C.; Quirk, R. P.; Newkome, G. R., *Macromolecules* **2008**, 41 (3), 515-517.
- (106) Jin, L.; Romero, E. A.; Melaimi, M.; Bertrand, G., *J. Am. Chem. Soc.* **2015**, 137 (50), 15696-15698.
- (107) Díez-González, S., *Catal. Sci. Tech.* **2011**, 1 (2), 166-178.

- (108) Crowley, J. D.; McMorran, D. A., "Click-Triazole" Coordination Chemistry: Exploiting 1,4-Disubstituted-1,2,3-Triazoles as Ligands. In *Click Triazoles*, Košmrlj, J., Ed. Springer Berlin Heidelberg: Berlin, Heidelberg, 2012; pp 31-83.
- (109) Wang, Q.; Chan, T. R.; Hilgraf, R.; Fokin, V. V.; Sharpless, K. B.; Finn, M., *J. Am. Chem. Soc.* **2003**, *125* (11), 3192-3193.
- (110) Chan, T. R.; Hilgraf, R.; Sharpless, K. B.; Fokin, V. V., *Org. Lett.* **2004**, *6* (17), 2853-2855.
- (111) Hong, V.; Presolski, S. I.; Ma, C.; Finn, M., *Angew. Chem., Int. Ed.* **2009**, *48* (52), 9879-9883.
- (112) Hong, V.; Steinmetz, N. F.; Manchester, M.; Finn, M., *Bioconjugate Chem.* **2010**, *21* (10), 1912-1916.
- (113) Besanceney - Webler, C.; Jiang, H.; Zheng, T.; Feng, L.; Soriano del Amo, D.; Wang, W.; Klivansky, L. M.; Marlow, F. L.; Liu, Y.; Wu, P., *Angew. Chem., Int. Ed.* **2011**, *50* (35), 8051-8056.
- (114) Soriano del Amo, D.; Wang, W.; Jiang, H.; Besanceney, C.; Yan, A. C.; Levy, M.; Liu, Y.; Marlow, F. L.; Wu, P., *J. Am. Chem. Soc.* **2010**, *132* (47), 16893-16899.
- (115) Wang, W.; Hong, S.; Tran, A.; Jiang, H.; Triano, R.; Liu, Y.; Chen, X.; Wu, P., *Chem. Asian J.* **2011**, *6* (10), 2796-2802.
- (116) Yang, M.; Jalloh, A. S.; Wei, W.; Zhao, J.; Wu, P.; Chen, P. R., *Nat. Commun.* **2014**, *5*.
- (117) Kumar, A.; Li, K.; Cai, C., *Chem. Commun.* **2011**, *47* (11), 3186-3188.
- (118) Özçubukçu, S.; Ozkal, E.; Jimeno, C.; Pericas, M. A., *Org. Lett.* **2009**, *11* (20), 4680-4683.
- (119) Ozkal, E.; Özçubukçu, S.; Jimeno, C.; Pericas, M. A., *Catal. Sci. Tech.* **2012**, *2* (1), 195-200.
- (120) Ozkal, E.; Llanes, P.; Bravo, F.; Ferrali, A.; Pericas, M. A., *Adv. Synth. Catal.* **2014**, *356* (4), 857-869.
- (121) Rodionov, V. O.; Presolski, S. I.; Gardinier, S.; Lim, Y.-H.; Finn, M., *J. Am. Chem. Soc.* **2007**, *129* (42), 12696-12704.
- (122) Gupta, S. S.; Kuzelka, J.; Singh, P.; Lewis, W. G.; Manchester, M.; Finn, M. G., *Bioconjugate Chem.* **2005**, *16* (6), 1572-1579.
- (123) Hong, V.; Udit, A. K.; Evans, R. A.; Finn, M., *ChemBioChem* **2008**, *9* (9), 1481-1486.
- (124) Candelon, N.; Lastécouères, D.; Diallo, A. K.; Aranzaes, J. R.; Astruc, D.; Vincent, J.-M., *Chem. Commun.* **2008**, (6), 741-743.
- (125) Liang, L.; Ruiz, J.; Astruc, D., *Adv. Synth. Catal.* **2011**, *353* (18), 3434-3450.
- (126) Díez - González, S.; Correa, A.; Cavallo, L.; Nolan, S. P., *Chem. Eur. J.* **2006**, *12* (29), 7558-7564.

- (127) Díez-González, S.; Escudero-Adán, E. C.; Benet-Buchholz, J.; Stevens, E. D.; Slawin, A. M.; Nolan, S. P., *Dalton Trans.* **2010**, 39 (32), 7595-7606.
- (128) Díez - González, S.; Nolan, S. P., *Angew. Chem.* **2008**, 120 (46), 9013-9016.
- (129) Velázquez, H. D.; García, Y. R.; Vandichel, M.; Madder, A.; Verpoort, F., *Org. Biomol. Chem.* **2014**, 12 (46), 9350-9356.
- (130) Gu, S.; Du, J.; Huang, J.; Xia, H.; Yang, L.; Xu, W.; Lu, C., *Beilstein J. Org. Chem.* **2016**, 12 (1), 863-873.
- (131) Gu, S.; Huang, J.; Liu, X.; Liu, H.; Zhou, Y.; Xu, W., *Inorg. Chem. Commun.* **2012**, 21, 168-172.
- (132) Liu, B.; Chen, C.; Zhang, Y.; Liu, X.; Chen, W., *Organometallics* **2013**, 32 (19), 5451-5460.
- (133) Pérez-Balderas, F.; Ortega-Munoz, M.; Morales-Sanfrutos, J.; Hernández-Mateo, F.; Calvo-Flores, F. G.; Calvo-Asín, J. A.; Isac-García, J.; Santoyo-González, F., *Org. Lett.* **2003**, 5 (11), 1951-1954.
- (134) Lal, S.; Díez-González, S., *J. Org. Chem.* **2011**, 76 (7), 2367-2373.
- (135) Lal, S.; McNally, J.; White, A. J.; Díez-González, S., *Organometallics* **2011**, 30 (22), 6225-6232.
- (136) Wang, D.; Zhao, M.; Liu, X.; Chen, Y.; Li, N.; Chen, B., *Org. Biomol. Chem.* **2012**, 10 (2), 229-231.
- (137) Gonda, Z.; Novák, Z., *Dalton Trans.* **2010**, 39 (3), 726-729.
- (138) Wang, F.; Fu, H.; Jiang, Y.; Zhao, Y., *Green Chem.* **2008**, 10 (4), 452-456.
- (139) Fabbrizzi, P.; Cicchi, S.; Brandi, A.; Sperotto, E.; van Koten, G., *Eur. J. Org. Chem.* **2009**, 2009 (31), 5423-5430.
- (140) Bai, S.-Q.; Koh, L. L.; Hor, T. A., *Inorg. Chem.* **2009**, 48 (3), 1207-1213.
- (141) Wang, C.; Ciganda, R.; Salmon, L.; Gregurec, D.; Irigoyen, J.; Moya, S.; Ruiz, J.; Astruc, D., *Angew. Chem., Int. Ed.* **2016**, 55 (9), 3091-3095.
- (142) Brown, I.; Dunitz, J., *Acta Crystallogr.* **1961**, 14 (5), 480-485.
- (143) Bondi, A., *J. Phys. Chem.* **1964**, 68 (3), 441-451.
- (144) Greenwood, N. N.; Earnshaw, A., *Chemistry of the Elements*. Elsevier: 2012.
- (145) Gray, T. G.; Sadighi, J. P., Group 11 Metal–Metal Bonds. In *Molecular Metal–Metal Bonds*, Wiley-VCH Verlag GmbH & Co. KGaA: 2015; pp 397-428.
- (146) Merz Jr, K. M.; Hoffmann, R., *Inorg. Chem.* **1988**, 27 (12), 2120-2127.
- (147) Hermann, H. L.; Boche, G.; Schwerdtfeger, P., *Chem. Eur. J.* **2001**, 7 (24), 5333-5342.
- (148) Beck, J.; Strähle, J., *Angew. Chem. Int. Ed. Engl.* **1985**, 24 (5), 409-410.
- (149) Cotton, F. A.; Feng, X.; Timmons, D. J., *Inorg. Chem.* **1998**, 37 (16), 4066-4069.

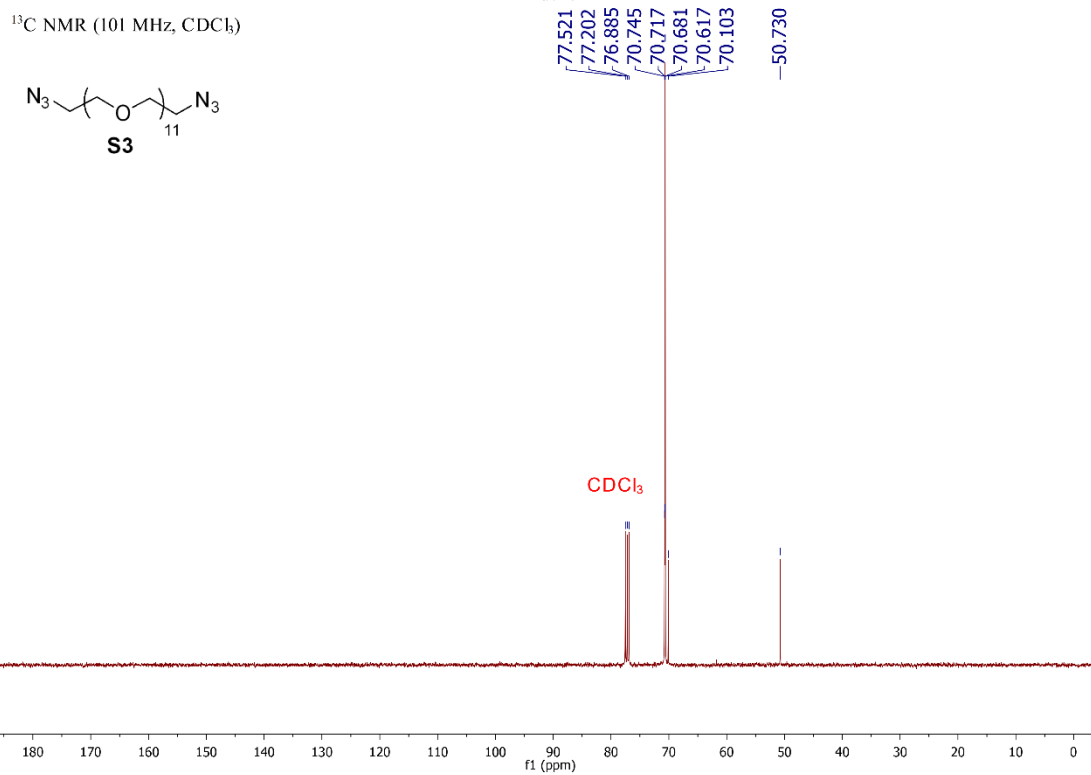
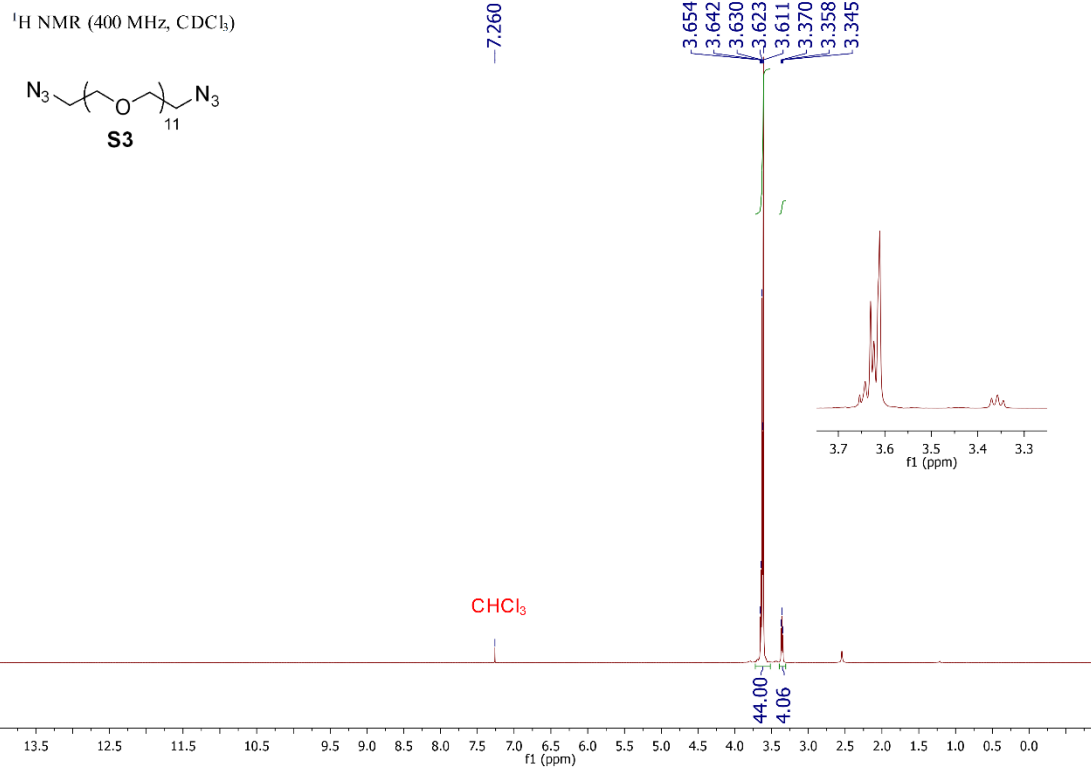
- (150) Mankad, N. P.; Laitar, D. S.; Sadighi, J. P., *Organometallics* **2004**, *23* (14), 3369-3371.
- (151) Frey, G. D.; Donnadiou, B.; Soleilhavoup, M.; Bertrand, G., *Chem. Asian J.* **2011**, *6* (2), 402-405.
- (152) Wyss, C. M.; Tate, B. K.; Bacsa, J.; Gray, T. G.; Sadighi, J. P., *Angew. Chem., Int. Ed.* **2013**, *52* (49), 12920-12923.
- (153) Frenking, G.; Fröhlich, N., *Chem. Rev.* **2000**, *100* (2), 717-774.
- (154) Thompson, J. S.; Bradley, A. Z.; Park, K.-H.; Dobbs, K. D.; Marshall, W., *Organometallics* **2006**, *25* (11), 2712-2714.
- (155) Srebro, M.; Mitoraj, M., *Organometallics* **2009**, *28* (13), 3650-3655.
- (156) Dias, H. V. R.; Flores, J. A.; Wu, J.; Kroll, P., *J. Am. Chem. Soc.* **2009**, *131* (31), 11249-11255.
- (157) Mealli, C.; Godinho, S. S.; Calhorda, M. J., *Organometallics* **2001**, *20* (9), 1734-1742.
- (158) Zhu, D.; Budzelaar, P. H., *Organometallics* **2008**, *27* (12), 2699-2705.
- (159) Leysens, T.; Peeters, D.; Orpen, A. G.; Harvey, J. N., *Organometallics* **2007**, *26* (10), 2637-2645.
- (160) Mitoraj, M. P.; Michalak, A., *Inorg. Chem.* **2009**, *49* (2), 578-582.
- (161) Ardizzoia, G. A.; Bea, M.; Brenna, S.; Therrien, B., *Eur. J. Inorg. Chem.* **2016**.
- (162) Rodgers, M.; Stanley, J.; Amunugama, R., *J. Am. Chem. Soc.* **2000**, *122* (44), 10969-10978.
- (163) Urankar, D.; Pinter, B.; Pevec, A.; De Proft, F.; Turel, I.; Košmrlj, J., *Inorg. Chem.* **2010**, *49* (11), 4820-4829.
- (164) Su, P.; Li, H., *J. Chem. Phys.* **2009**, *131* (1), 014102.
- (165) Ostermeier, M.; Berlin, M. A.; Meudtner, R. M.; Demeshko, S.; Meyer, F.; Limberg, C.; Hecht, S., *Chem. Eur. J.* **2010**, *16* (33), 10202-10213.
- (166) Colasson, B.; Le Poul, N.; Le Mest, Y.; Reinaud, O., *Inorg. Chem.* **2011**, *50* (21), 10985-10993.
- (167) Hopkinson, M. N.; Richter, C.; Schedler, M.; Glorius, F., *Nature* **2014**, *510* (7506), 485-496.
- (168) Hu, X.; Castro-Rodriguez, I.; Olsen, K.; Meyer, K., *Organometallics* **2004**, *23* (4), 755-764.
- (169) Nemcsok, D.; Wichmann, K.; Frenking, G., *Organometallics* **2004**, *23* (15), 3640-3646.
- (170) Comas - Vives, A.; Harvey, J. N., *Eur. J. Inorg. Chem.* **2011**, *2011* (32), 5025-5035.
- (171) Solomon, E. I.; Sundaram, U. M.; Machonkin, T. E., *Chem. Rev.* **1996**, *96* (7), 2563-2606.
- (172) Lewis, E. A.; Tolman, W. B., *Chem. Rev.* **2004**, *104* (2), 1047-1076.

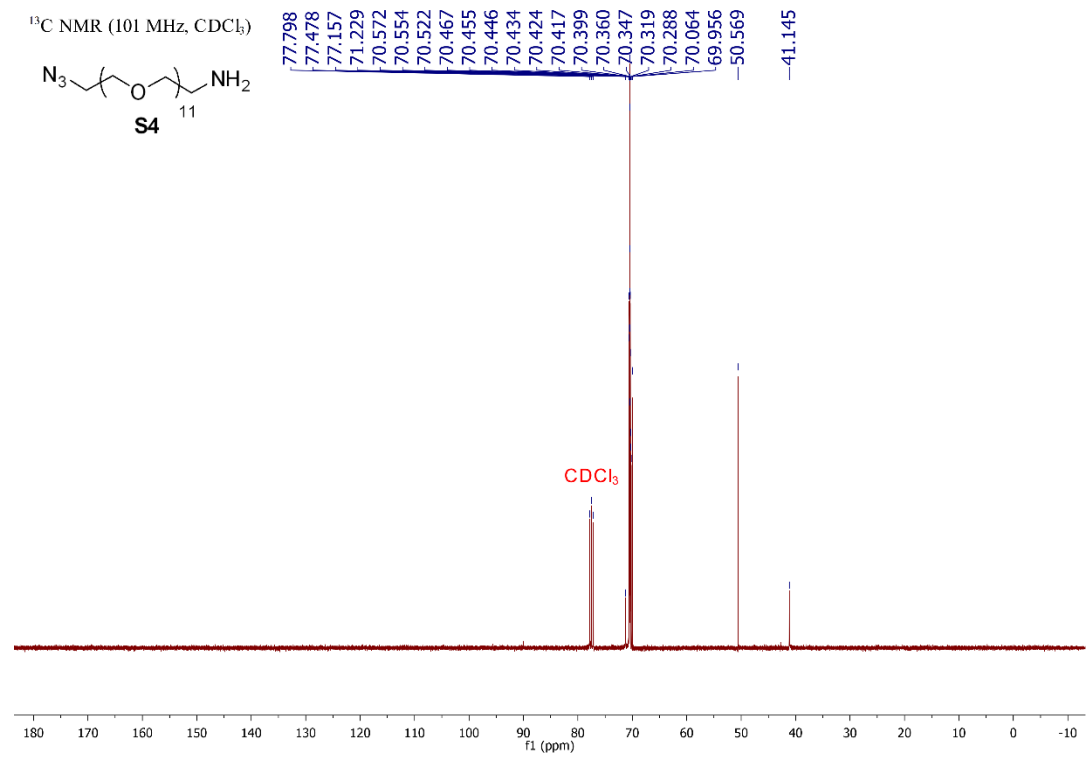
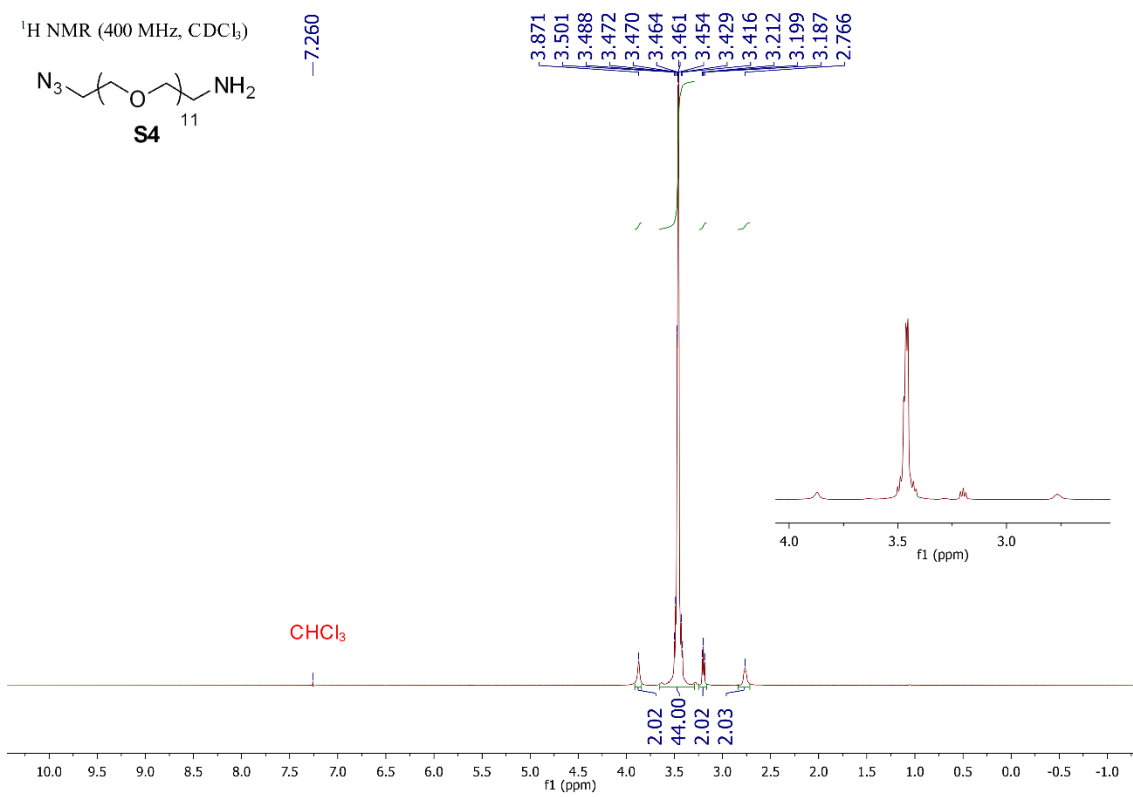
- (173) Mirica, L. M.; Ottenwaelder, X.; Stack, T. D. P., *Chem. Rev.* **2004**, *104* (2), 1013-1046.
- (174) Schatz, M.; Becker, M.; Thaler, F.; Hampel, F.; Schindler, S.; Jacobson, R. R.; Tyeklár, Z.; Murthy, N. N.; Ghosh, P.; Chen, Q., *Inorg. Chem.* **2001**, *40* (10), 2312-2322.
- (175) Zhang, C. X.; Kaderli, S.; Costas, M.; Kim, E.-i.; Neuhold, Y.-M.; Karlin, K. D.; Zuberbühler, A. D., *Inorg. Chem.* **2003**, *42* (6), 1807-1824.
- (176) Hatcher, L. Q.; Karlin, K. D., *Adv. Inorg. Chem.* **2006**, *58*, 131-184.
- (177) Osako, T.; Tachi, Y.; Taki, M.; Fukuzumi, S.; Itoh, S., *Inorg. Chem.* **2001**, *40* (26), 6604-6609.
- (178) Hinderling, C.; Adlhart, C.; Chen, P., *Angew. Chem., Int. Ed.* **1998**, *37* (19), 2685-2689.
- (179) Di Marco, V. B.; Bombi, G. G., *Mass Spectrom. Rev.* **2006**, *25* (3), 347-379.
- (180) Santos, L. S., *Eur. J. Org. Chem.* **2008**, *2008* (2), 235-253.
- (181) Wells, J. M.; Plass, W. R.; Patterson, G. E.; Ouyang, Z.; Badman, E. R.; Cooks, R. G., *Anal. Chem.* **1999**, *71* (16), 3405-3415.
- (182) Murphy, J. P.; Yost, R. A., *Rapid Commun. Mass Spectrom.* **2000**, *14* (4), 270-273.
- (183) Santos, L. S.; Padilha, M. C.; de Aquino Neto, F. R.; Santos Pereira, A. d.; Menegatti, R.; Manssour Fraga, C. A.; Barreiro, E. J.; Eberlin, M. N., *J. Mass Spectrom.* **2005**, *40* (6), 815-820.
- (184) Stollenz, M.; Meyer, F., *Organometallics* **2012**, *31* (22), 7708-7727.
- (185) Berg, R.; Straub, B. F., *Beilstein J. Org. Chem.* **2013**, *9*, 2715-2750.
- (186) Rae, M.; Berberan-Santos, M. N., *J. Chem. Educ.* **2004**, *81* (3), 436.
- (187) Bevilacqua, V.; King, M.; Chaumontet, M.; Nothisen, M.; Gabillet, S.; Buisson, D.; Puente, C.; Wagner, A.; Taran, F., *Angew. Chem., Int. Ed.* **2014**, *53* (23), 5872-5876.
- (188) Bonger, K. M.; van den Berg, R. J.; Heitman, L. H.; IJzerman, A. P.; Oosterom, J.; Timmers, C. M.; Overkleeft, H. S.; van der Marel, G. A., *Bioorg. Med. Chem.* **2007**, *15* (14), 4841-4856.
- (189) Sanders, B. C.; Friscourt, F.; Ledin, P. A.; Mbua, N. E.; Arumugam, S.; Guo, J.; Boltje, T. J.; Popik, V. V.; Boons, G.-J., *J. Am. Chem. Soc.* **2010**, *133* (4), 949-957.
- (190) Funder, E. D.; Jensen, A. B.; Tørring, T.; Kodal, A. L. B.; Azcargorta, A. R.; Gothelf, K. V., *J. Org. Chem.* **2012**, *77* (7), 3134-3142.
- (191) Kindahl, T.; Öhgren, J.; Lopes, C.; Eliasson, B., *Tetrahedron Lett.* **2013**, *54* (19), 2403-2408.
- (192) Li, J.; Cao, J. j.; Wei, J. f.; Shi, X. y.; Zhang, L. h.; Feng, J. j.; Chen, Z. g., *Eur. J. Org. Chem.* **2011**, *2011* (2), 229-233.
- (193) Donnelly, P. S.; Zanatta, S. D.; Zammit, S. C.; White, J. M.; Williams, S. J., *Chem. Commun.* **2008**, (21), 2459-2461.
- (194) Hu, X.; Castro-Rodriguez, I.; Meyer, K., *J. Am. Chem. Soc.* **2003**, *125* (40), 12237-12245.

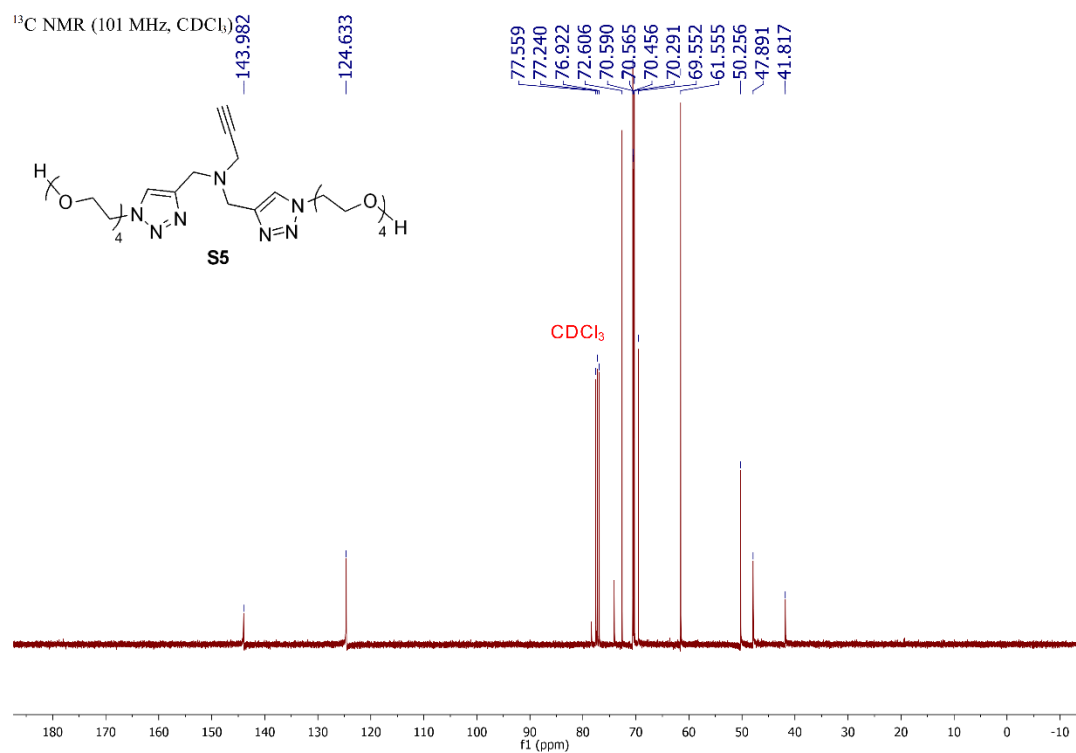
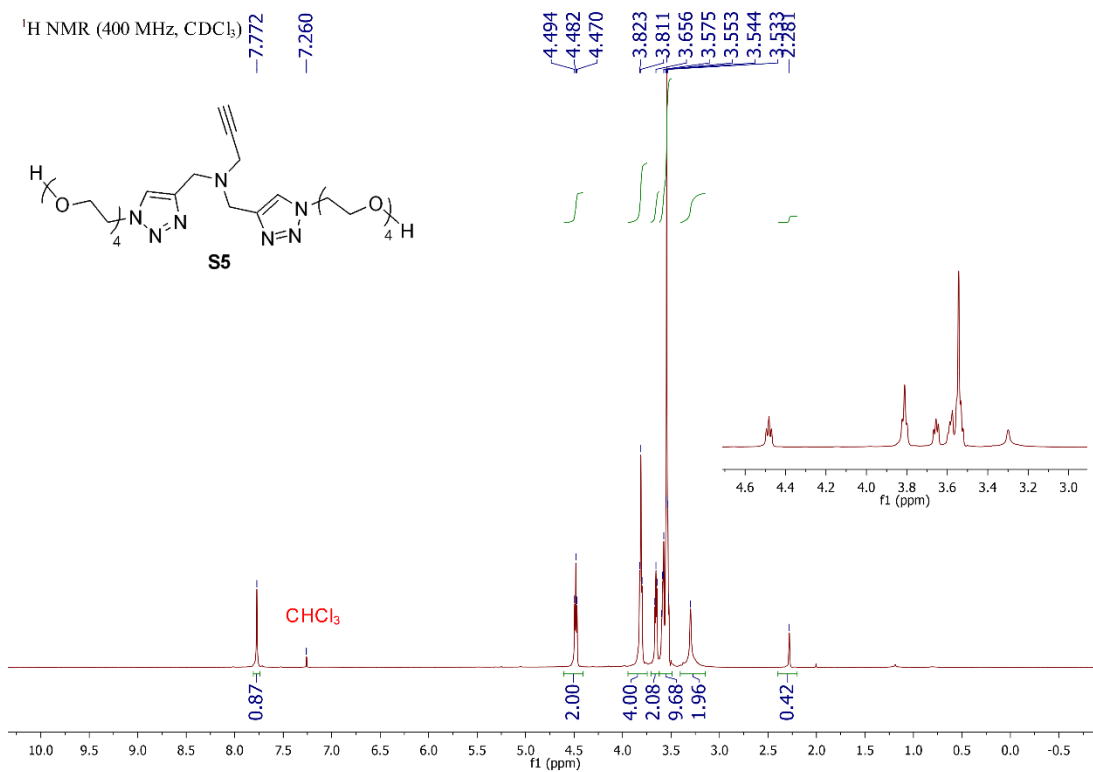
- (195) Ryu, E.-H.; Zhao, Y., *Org. Lett.* **2005**, 7 (6), 1035-1037.
- (196) Svensson, M.; Humbel, S.; Froese, R. D.; Matsubara, T.; Sieber, S.; Morokuma, K., *J. Phys. Chem.* **1996**, 100 (50), 19357-19363.
- (197) Steiner, T.; Starikov, E. B.; Amado, A. M.; Teixeira-Dias, J. J. C., *J. Chem. Soc., Perkin Trans. 2* **1995**, (7), 1321-1326.
- (198) Gebala, A. E.; Jones, M. M., *J. Inorg. Nucl. Chem.* **1969**, 31 (3), 771-776.
- (199) Ponikvar, M.; Žemva, B.; Liebman, J. F., *J. Fluor. Chem.* **2003**, 123 (2), 217-220.
- (200) Terborg, L.; Nowak, S.; Passerini, S.; Winter, M.; Karst, U.; Haddad, P. R.; Nesterenko, P. N., *Anal. Chim. Acta* **2012**, 714, 121-126.
- (201) Wiedemann, D.; Świątek, E.; Macyk, W.; Grohmann, A., *Z. Anorg. Allg. Chem.* **2013**, 639 (8-9), 1483-1490.
- (202) Keller, S.; Brunner, F.; Prescimone, A.; Constable, E. C.; Housecroft, C. E., *Inorg. Chem. Commun.* **2015**, 58, 64-66.
- (203) Guercio, G.; Manzo, A. M.; Goodyear, M.; Bacchi, S.; Curti, S.; Provera, S., *Org. Process Res. Dev.* **2009**, 13 (3), 489-493.
- (204) Shin, J. H.; Parkin, G., *Organometallics* **1998**, 17 (26), 5689-5696.
- (205) Radziszewski, J. G.; Downing, J. W.; Jawdosiuik, M.; Kovacic, P.; Michl, J., *J. Am. Chem. Soc.* **1985**, 107 (3), 594-603.
- (206) Cramer, C. J.; Truhlar, D. G., *Phys. Chem. Chem. Phys.* **2009**, 11 (46), 10757-10816.
- (207) Frisch, M. J.; Trucks, G. W.; Schlegel, H. B.; Scuseria, G. E.; Robb, M. A.; Cheeseman, J. R.; Scalmani, G.; Barone, V.; Mennucci, B.; Petersson, G. A.; Nakatsuji, H.; Caricato, M.; Li, X.; Hratchian, H. P.; Izmaylov, A. F.; Bloino, J.; Zheng, G.; Sonnenberg, J. L.; Hada, M.; Ehara, M.; Toyota, K.; Fukuda, R.; Hasegawa, J.; Ishida, M.; Nakajima, T.; Honda, Y.; Kitao, O.; Nakai, H.; Vreven, T.; Montgomery Jr., J. A.; Peralta, J. E.; Ogliaro, F.; Bearpark, M. J.; Heyd, J.; Brothers, E. N.; Kudin, K. N.; Staroverov, V. N.; Kobayashi, R.; Normand, J.; Raghavachari, K.; Rendell, A. P.; Burant, J. C.; Iyengar, S. S.; Tomasi, J.; Cossi, M.; Rega, N.; Millam, N. J.; Klene, M.; Knox, J. E.; Cross, J. B.; Bakken, V.; Adamo, C.; Jaramillo, J.; Gomperts, R.; Stratmann, R. E.; Yazyev, O.; Austin, A. J.; Cammi, R.; Pomelli, C.; Ochterski, J. W.; Martin, R. L.; Morokuma, K.; Zakrzewski, V. G.; Voth, G. A.; Salvador, P.; Dannenberg, J. J.; Dapprich, S.; Daniels, A. D.; Farkas, Ö.; Foresman, J. B.; Ortiz, J. V.; Cioslowski, J.; Fox, D. J. *Gaussian 09*, Gaussian, Inc.: Wallingford, CT, USA, 2009.
- (208) Zhao, Y.; Truhlar, D. G., *Theor. Chem. Acc.* **2008**, 120 (1-3), 215-241.
- (209) Lee, C.; Yang, W.; Parr, R. G., *Phys. Rev. B* **1988**, 37 (2), 785.
- (210) Krishnan, R.; Binkley, J. S.; Seeger, R.; Pople, J. A., *J. Chem. Phys.* **1980**, 72 (1), 650-654.
- (211) Boys, S. F.; Bernardi, F. d., *Mol. Phys.* **1970**, 19 (4), 553-566.
- (212) Rappé, A. K.; Casewit, C. J.; Colwell, K.; Goddard Iii, W.; Skiff, W., *J. Am. Chem. Soc.* **1992**, 114 (25), 10024-10035.

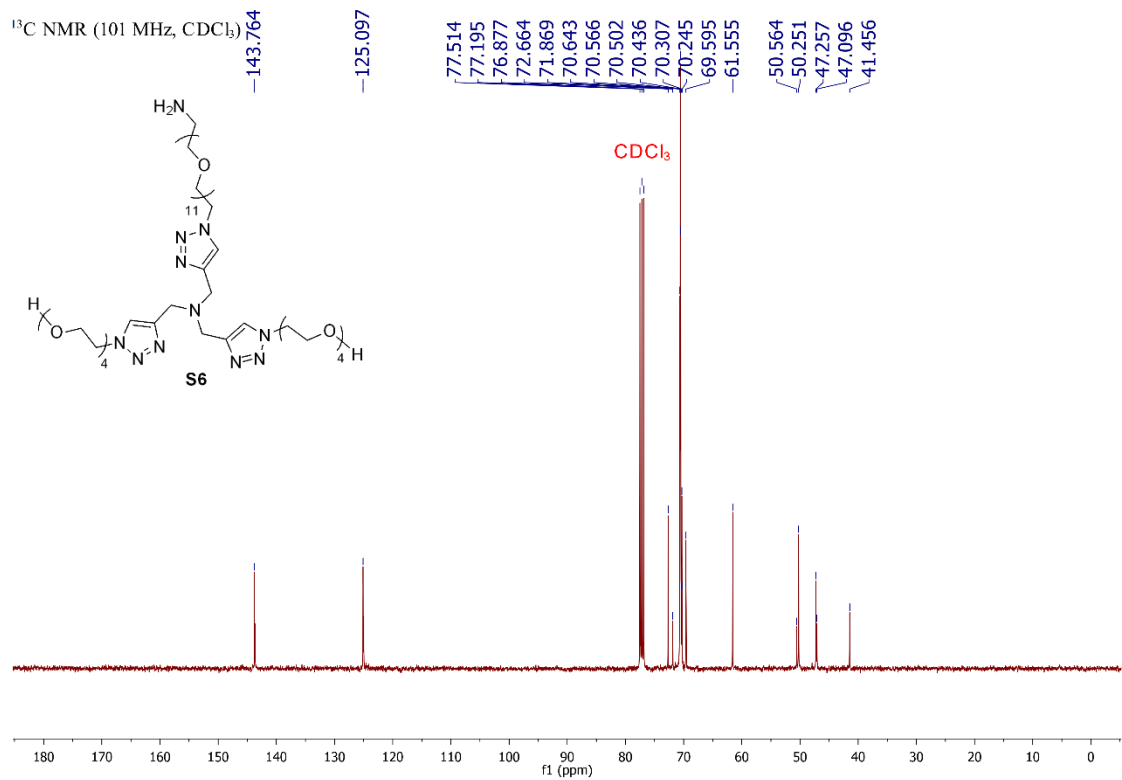
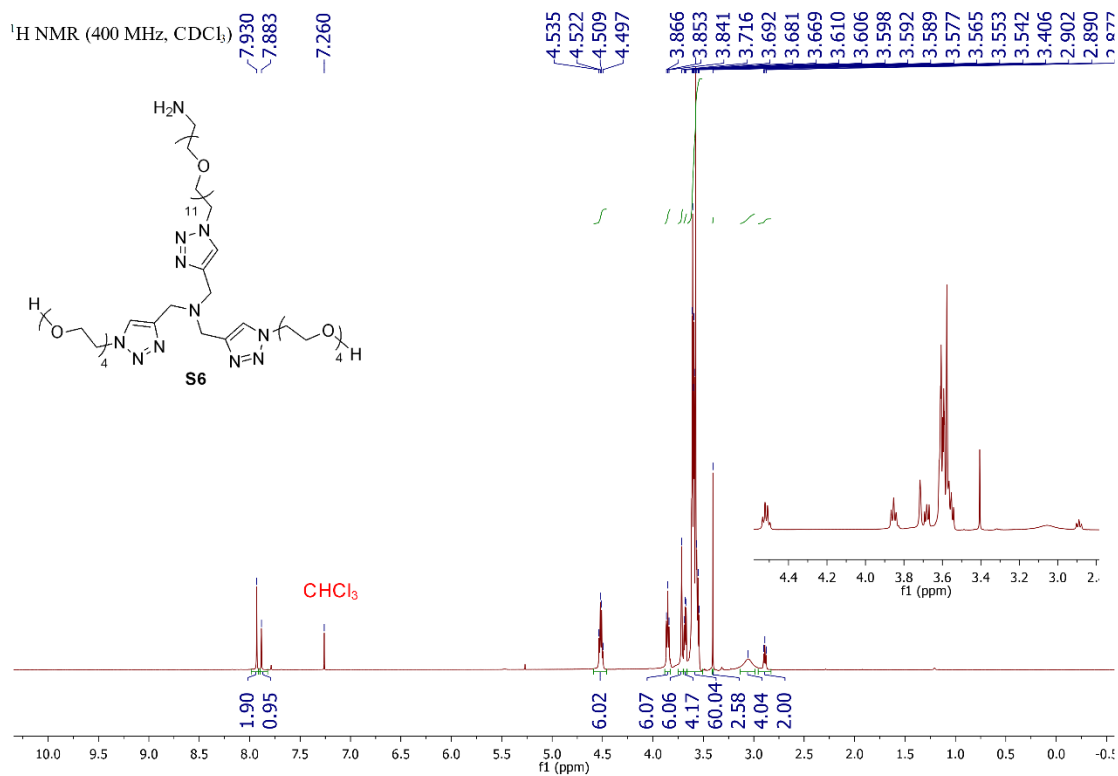
- (213) Pham, A. N.; Xing, G.; Miller, C. J.; Waite, T. D., *J. Catal.* **2013**, *301*, 54-64.
- (214) Kennedy, D. C.; McKay, C. S.; Legault, M. C.; Danielson, D. C.; Blake, J. A.; Pegoraro, A. F.; Stolow, A.; Mester, Z.; Pezacki, J. P., *J. Am. Chem. Soc.* **2011**, *133* (44), 17993-18001.
- (215) Abel Jr, G. R.; Calabrese, Z. A.; Ayco, J.; Hein, J. E.; Ye, T., *Bioconjugate Chem.* **2016**, *27* (3), 698-704.
- (216) Li, S.; Cai, H.; He, J.; Chen, H.; Lam, S.; Cai, T.; Zhu, Z.; Bark, S. J.; Cai, C., *Bioconjugate Chem.* **2016**, *27* (10), 2315-2322.
- (217) Becer, C. R.; Hoogenboom, R.; Schubert, U. S., *Angew. Chem., Int. Ed.* **2009**, *48* (27), 4900-4908.
- (218) Fitzwater, S. E.; Knauer, G. A.; Martin, J. H., *Limnol. Oceanogr.* **1982**, *27* (3), 544-551.
- (219) B. McKelvey, S. McIvor, and W. Wiltse, Polymer Comparisons for the Storage of Trace Metal Analysis of Ultrapure Water with the Agilent 7500cs ICP-MS, Agilent Technologies Application Note—5989-5782EN, 2006, <http://www.chem.agilent.com/Library/applications/5989-5782EN.pdf>
- (220) Thomas, R., *Practical Guide to Icp-MS: A Tutorial for Beginners*. CRC press: 2013.
- (221) Hart, J. R., *Ullmann's Encyclopedia of Industrial Chemistry* **2000**.
- (222) Baranyai, Z.; Pálinkás, Z.; Uggeri, F.; Brücher, E., *Eur. J. Inorg. Chem.* **2010**, *2010* (13), 1948-1956.

Appendix A: NMR Spectra

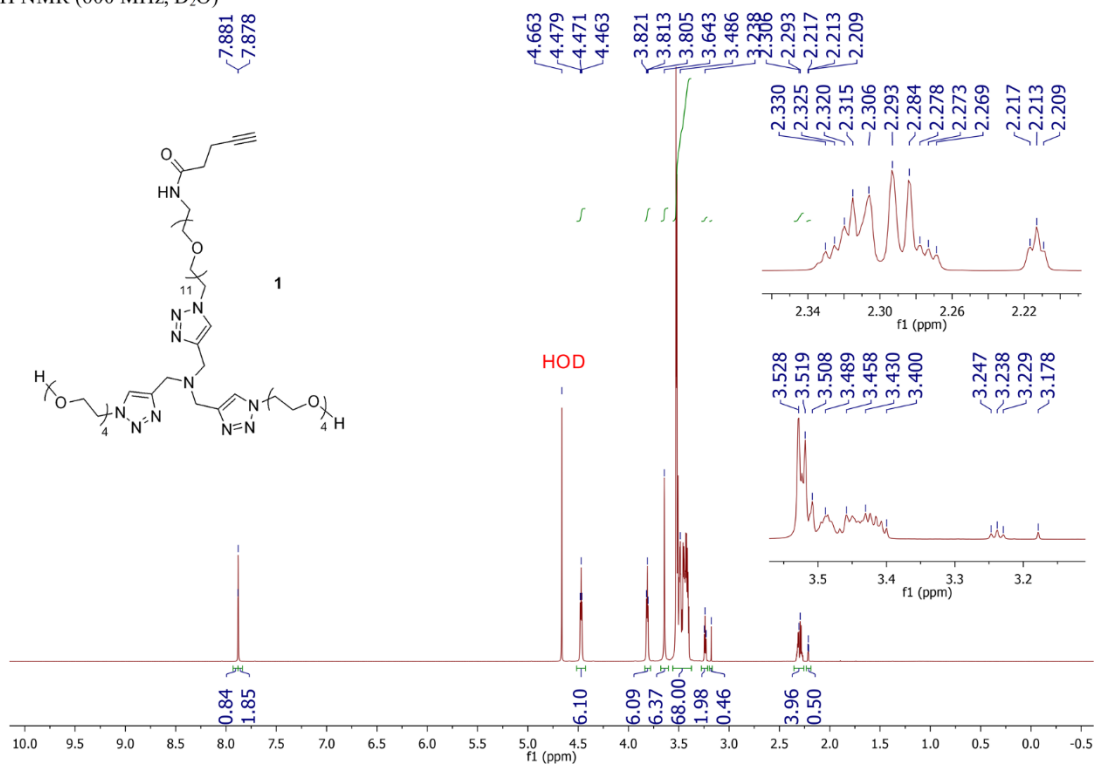




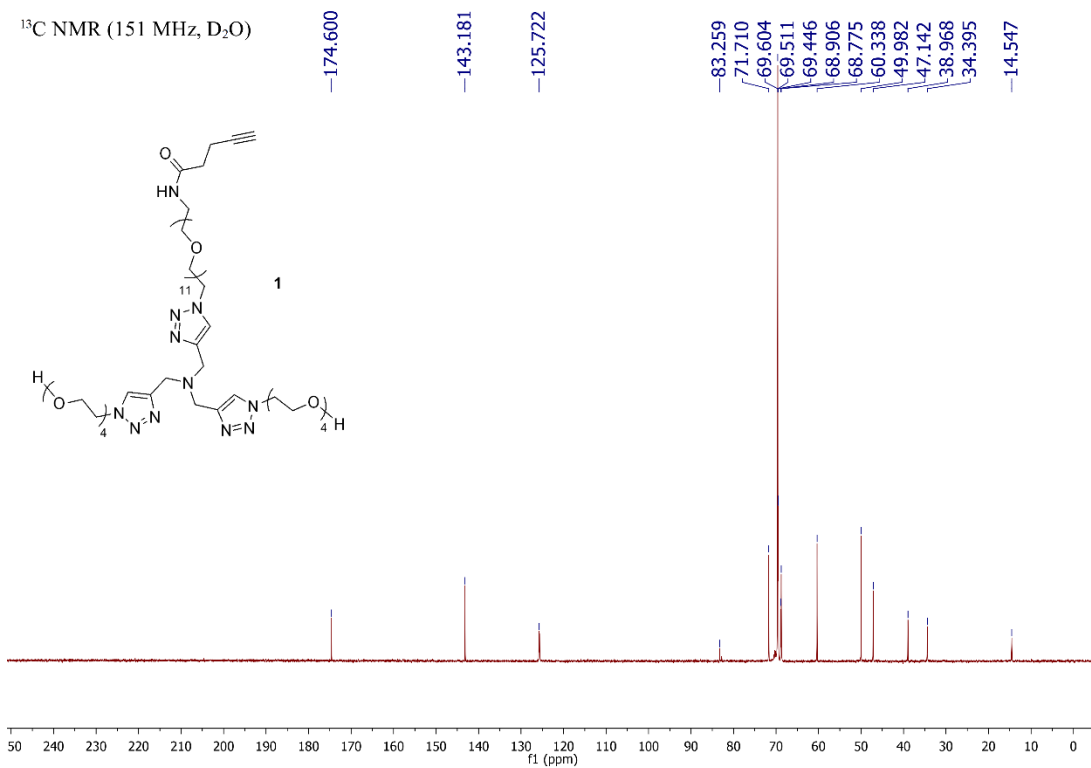




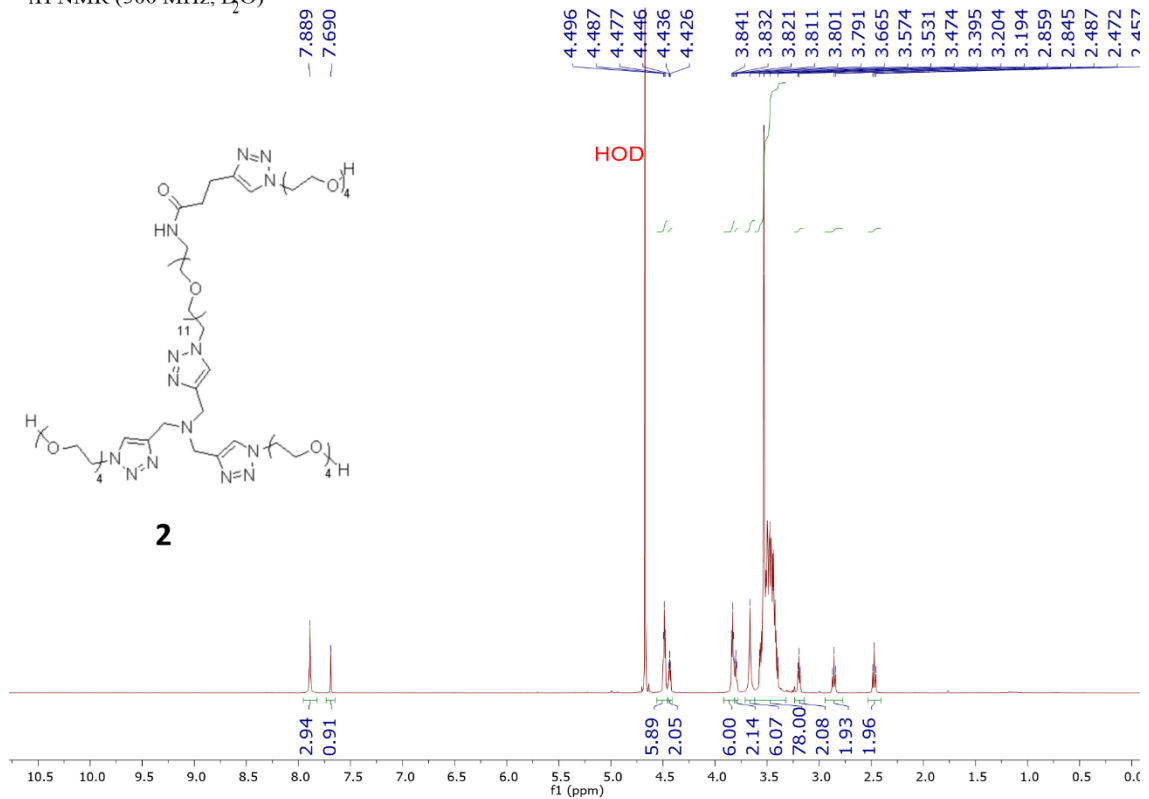
¹H NMR (600 MHz, D₂O)



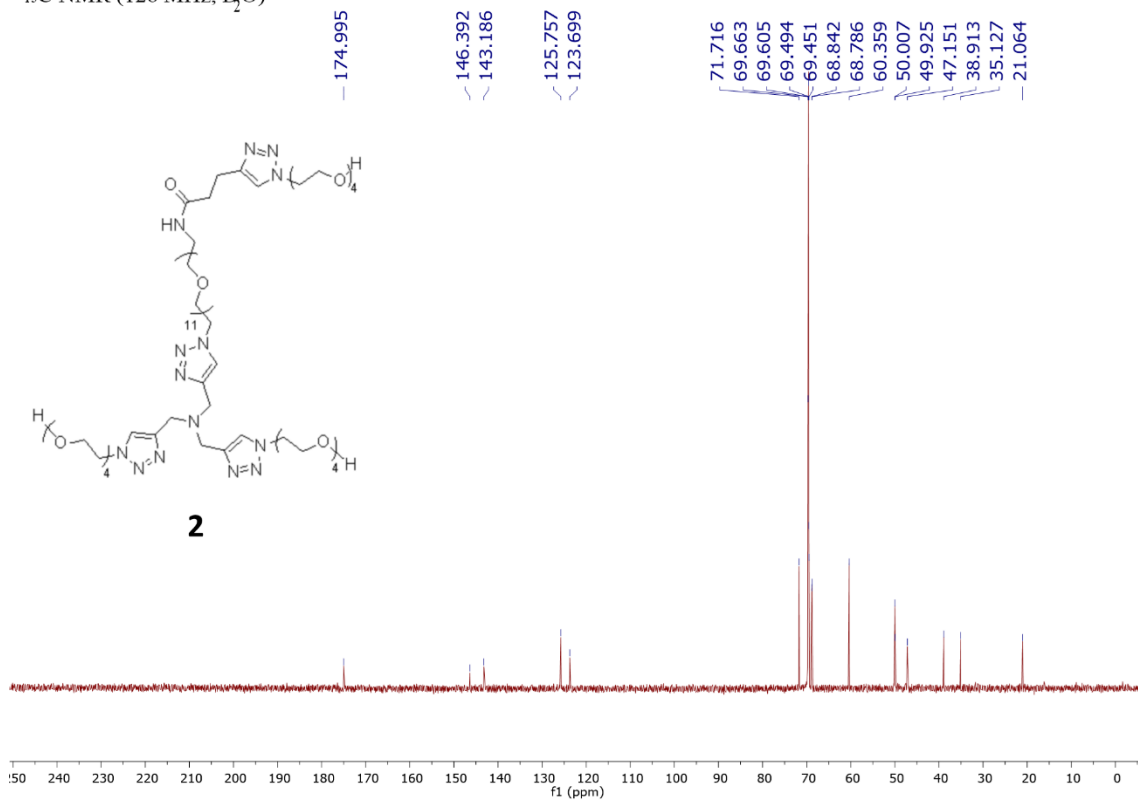
¹³C NMR (151 MHz, D₂O)



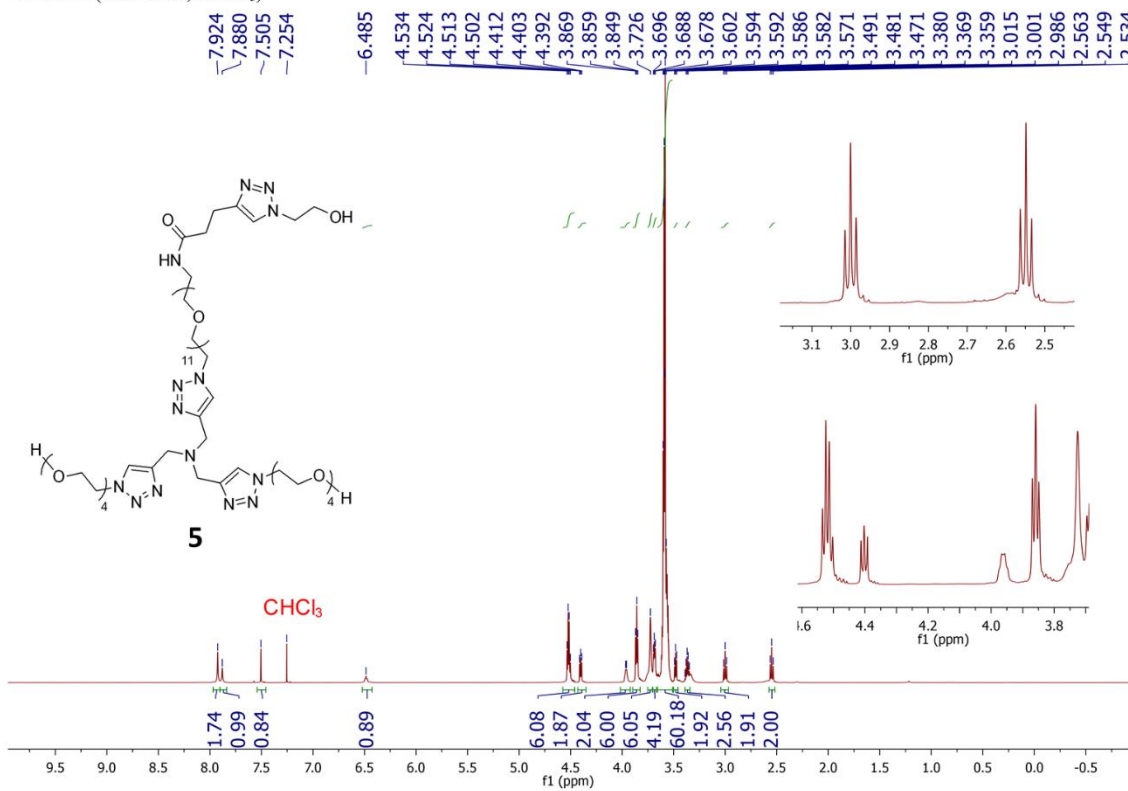
¹H NMR (500 MHz, D₂O)



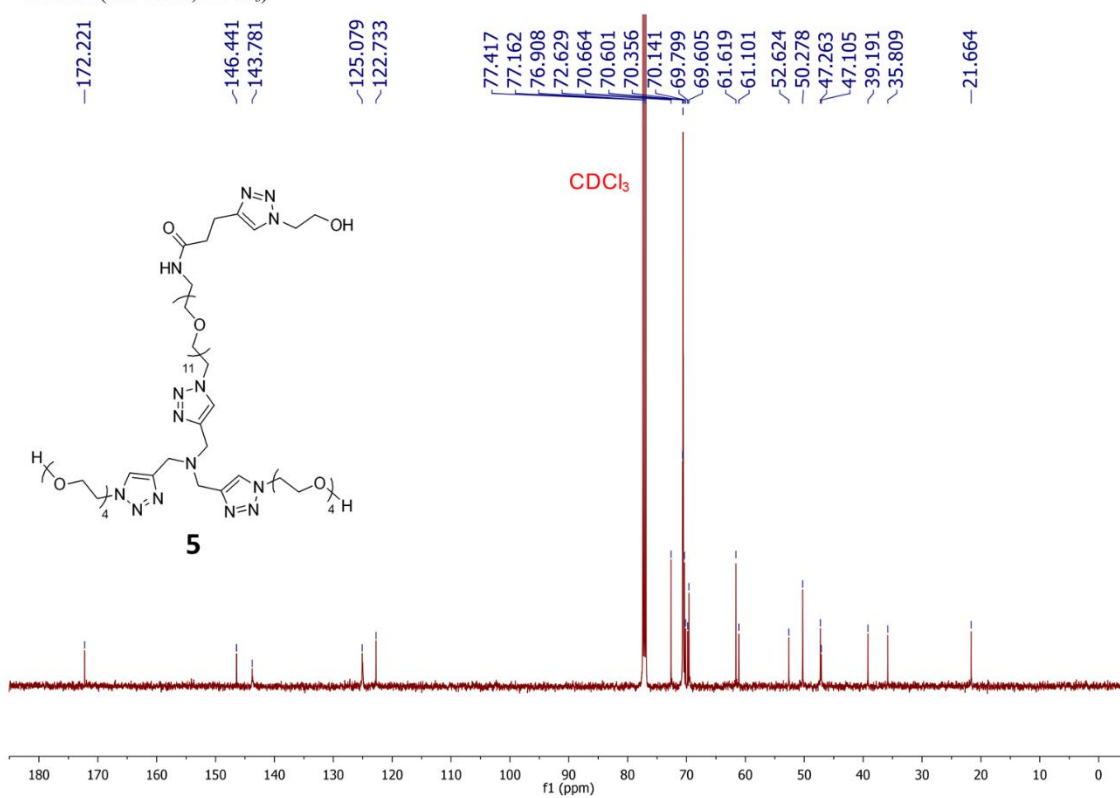
¹³C NMR (126 MHz, D₂O)



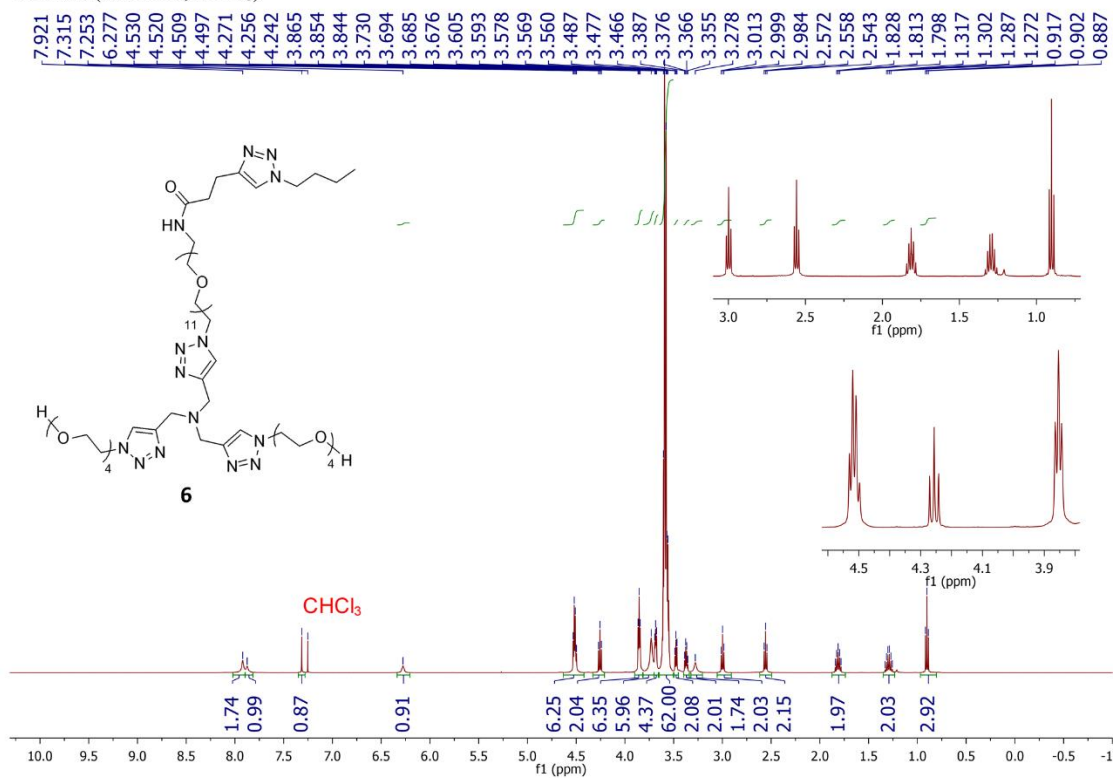
¹H NMR (500 MHz, CDCl₃)



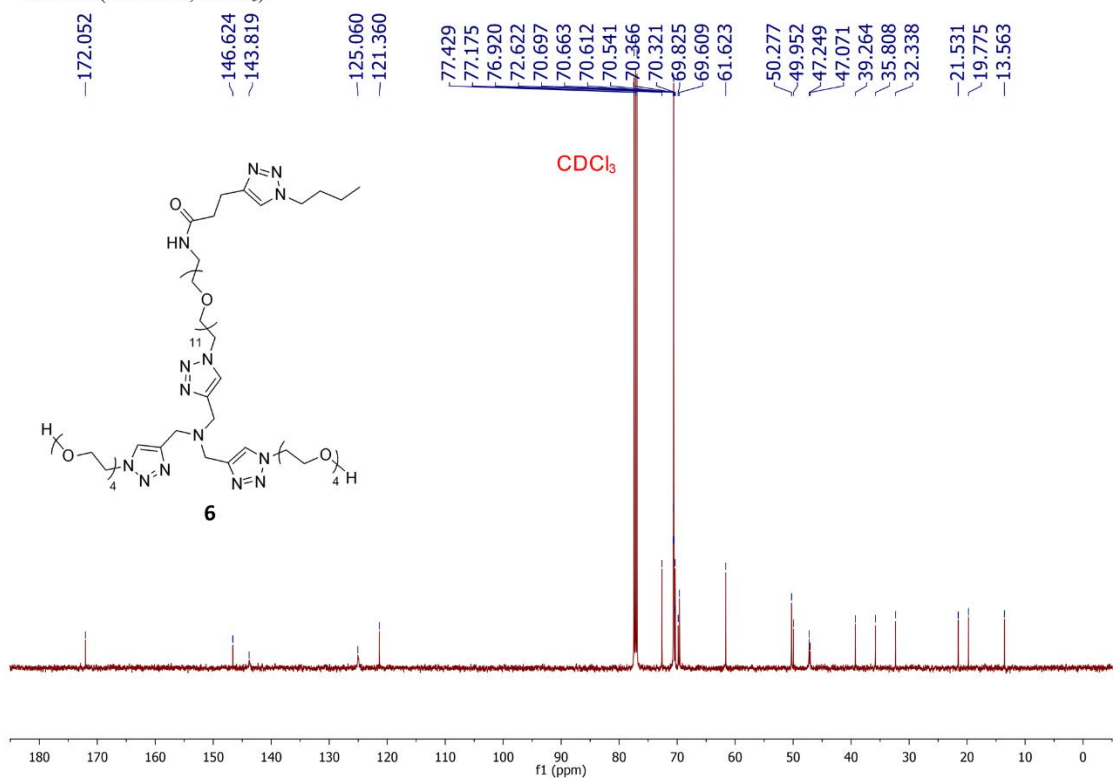
¹³C NMR (126 MHz, CDCl₃)



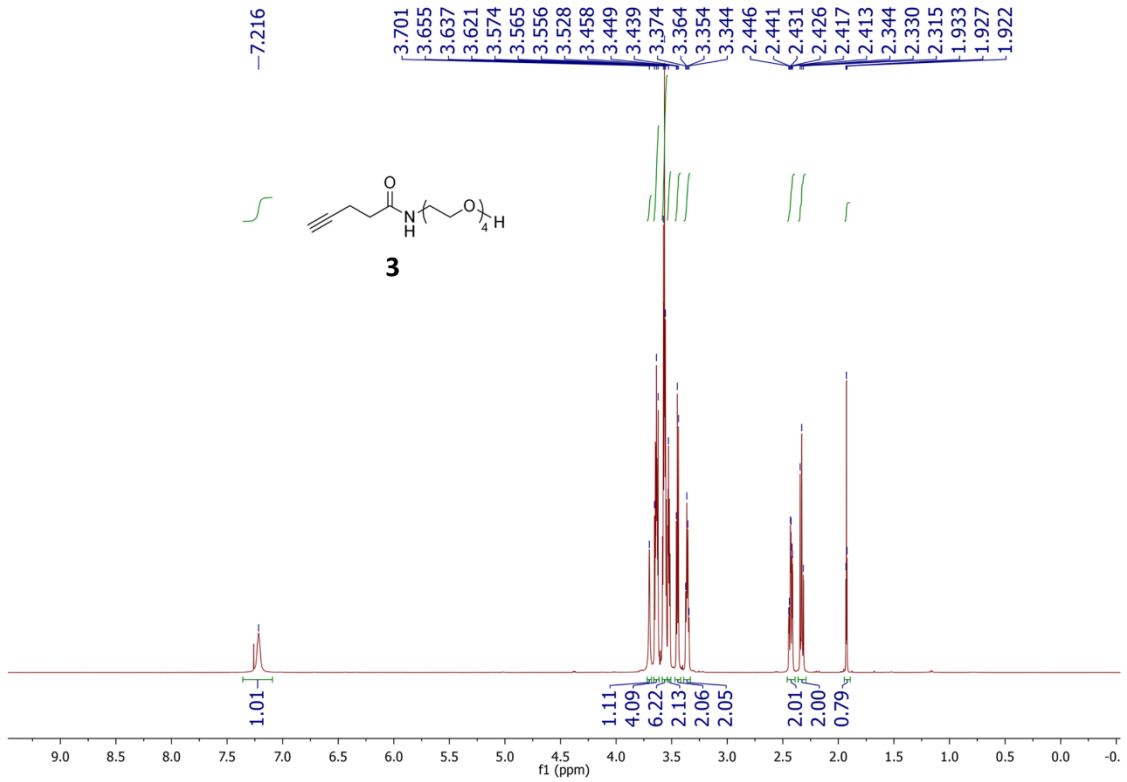
¹H NMR (500 MHz, CDCl₃)



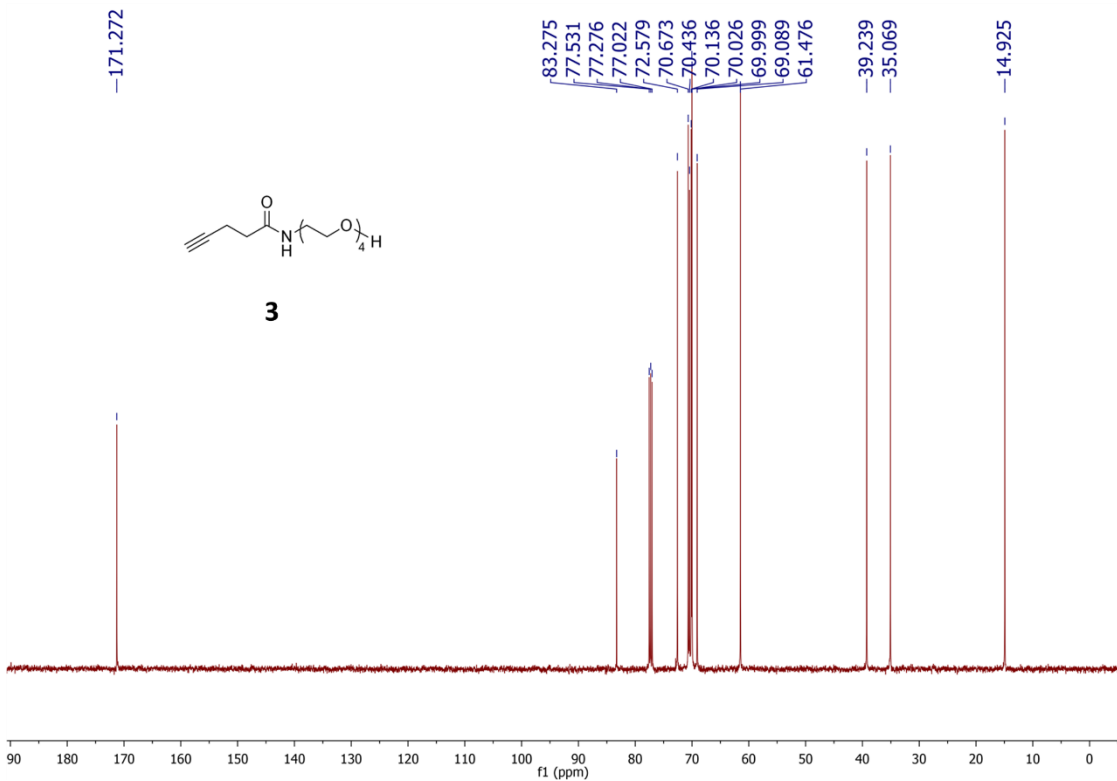
¹³C NMR (126 MHz, CDCl₃)



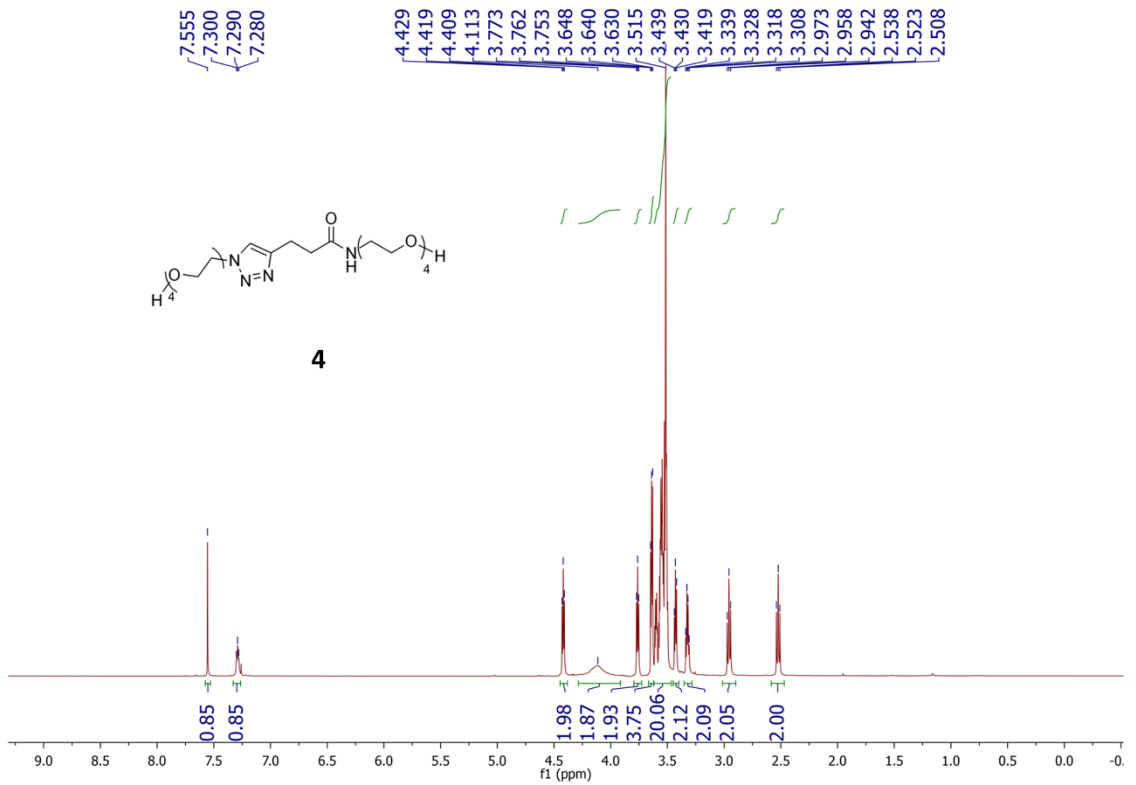
^1H NMR (500 MHz, CDCl_3)



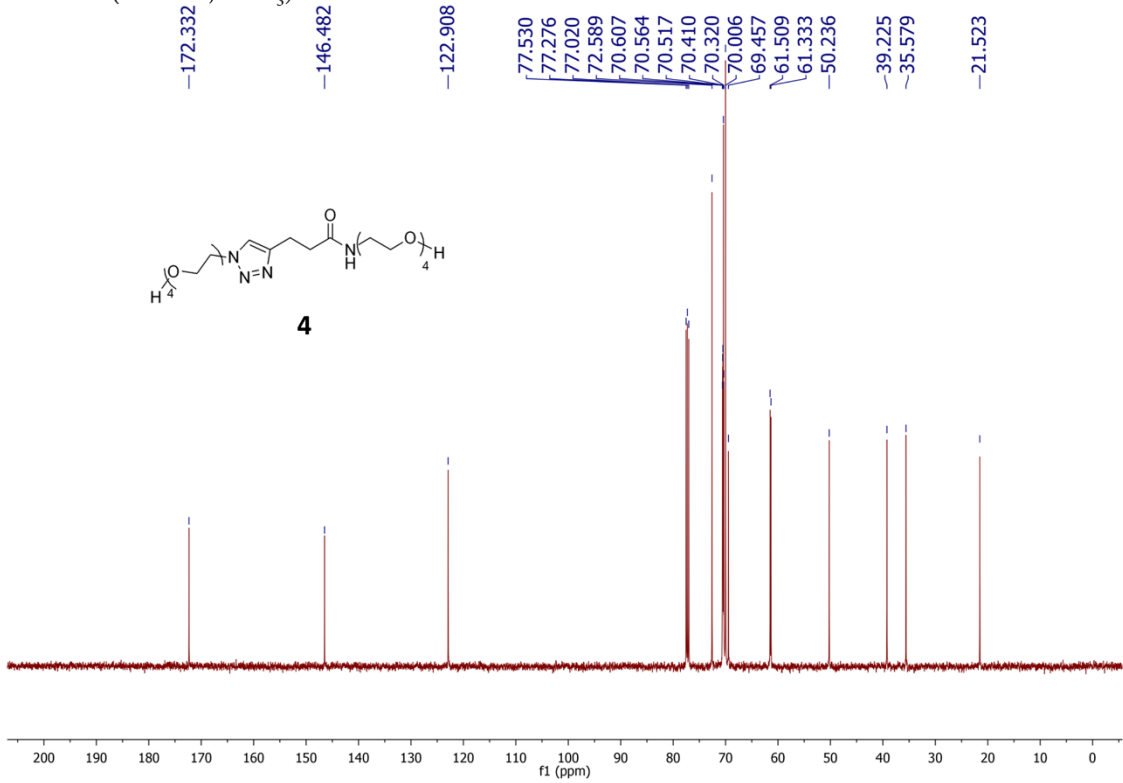
^{13}C NMR (126 MHz, CDCl_3)



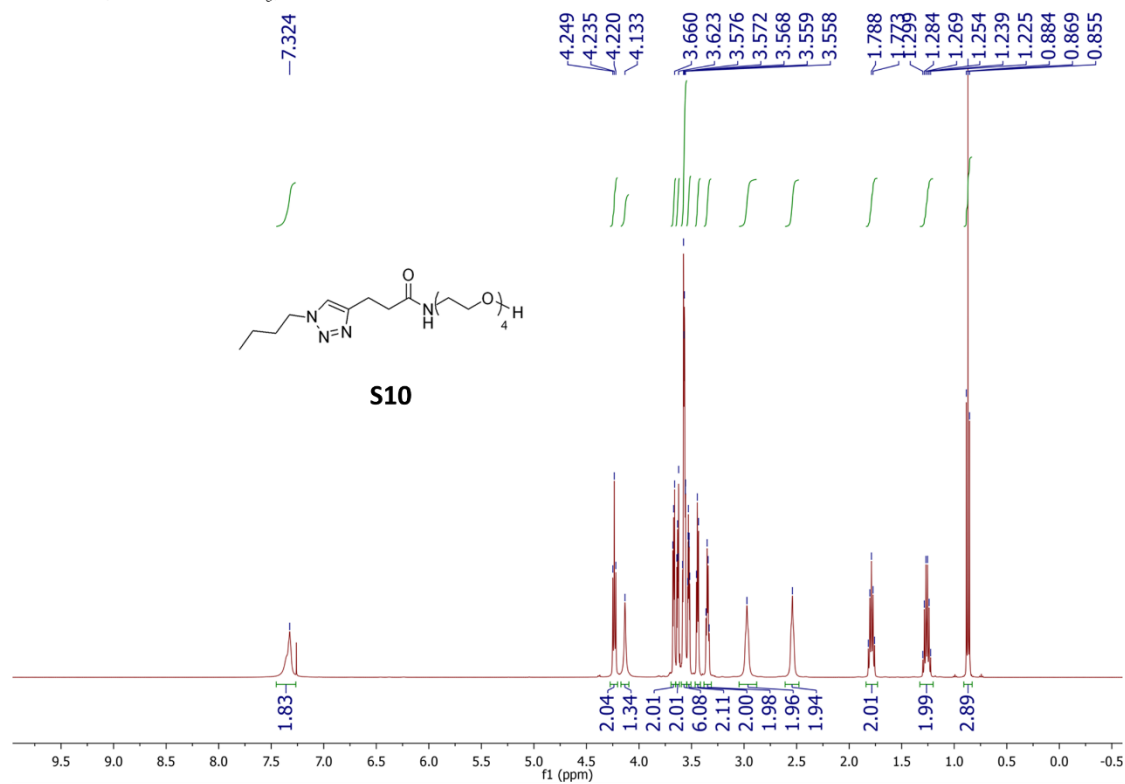
¹H NMR (500 MHz, CDCl₃)



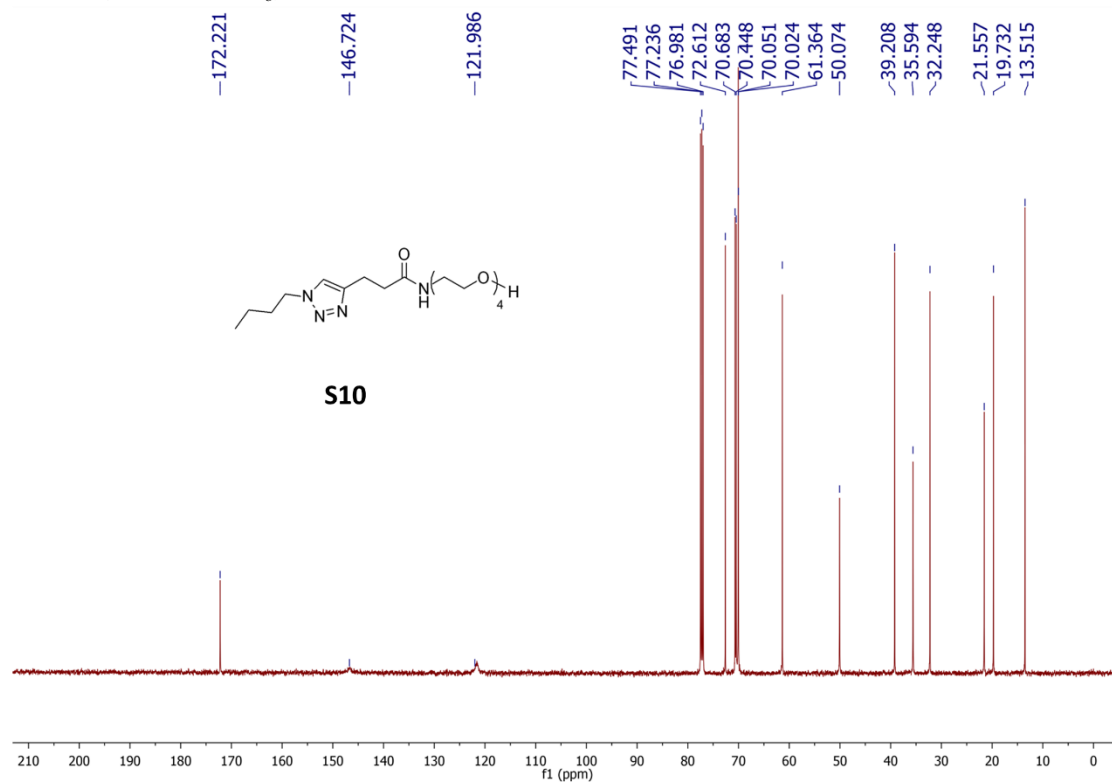
¹³C NMR (126 MHz, CDCl₃)



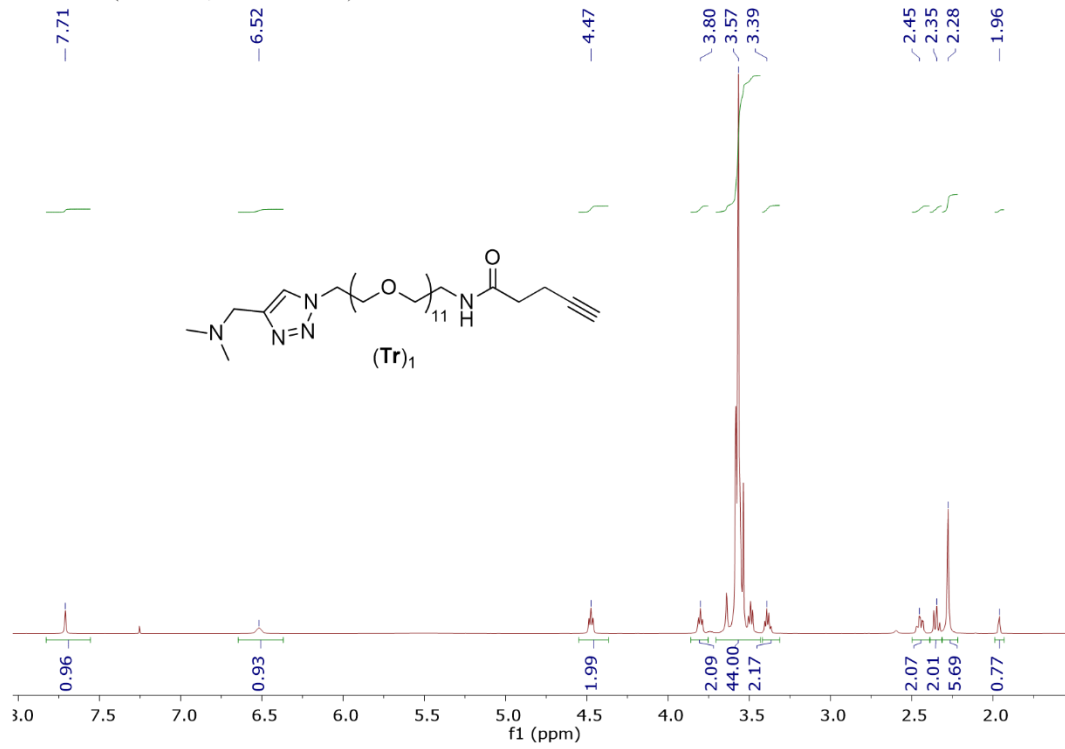
¹H NMR (500 MHz, CDCl₃)



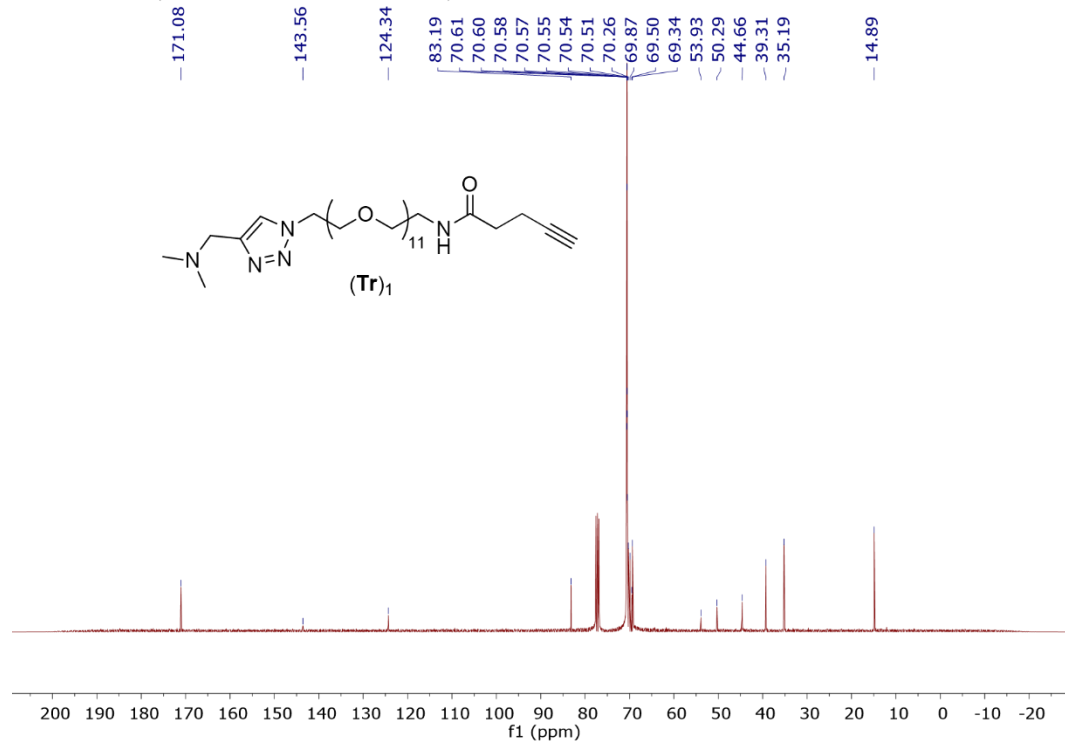
¹³C NMR (126 MHz, CDCl₃)



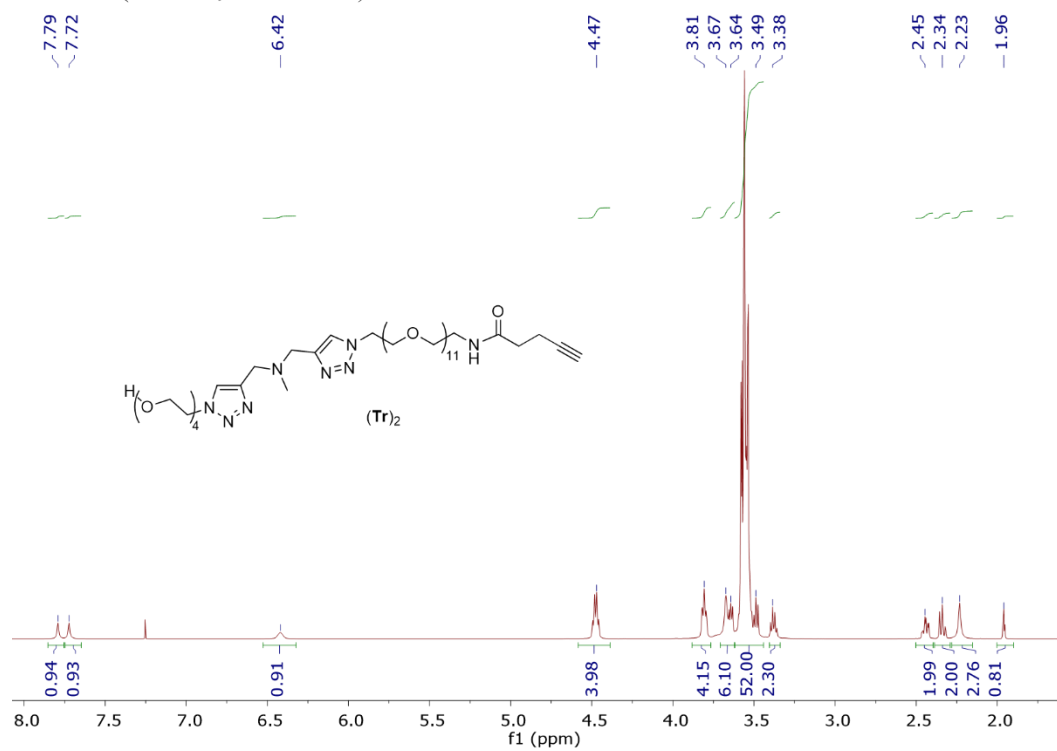
¹H NMR (400 MHz, Chloroform-*d*)



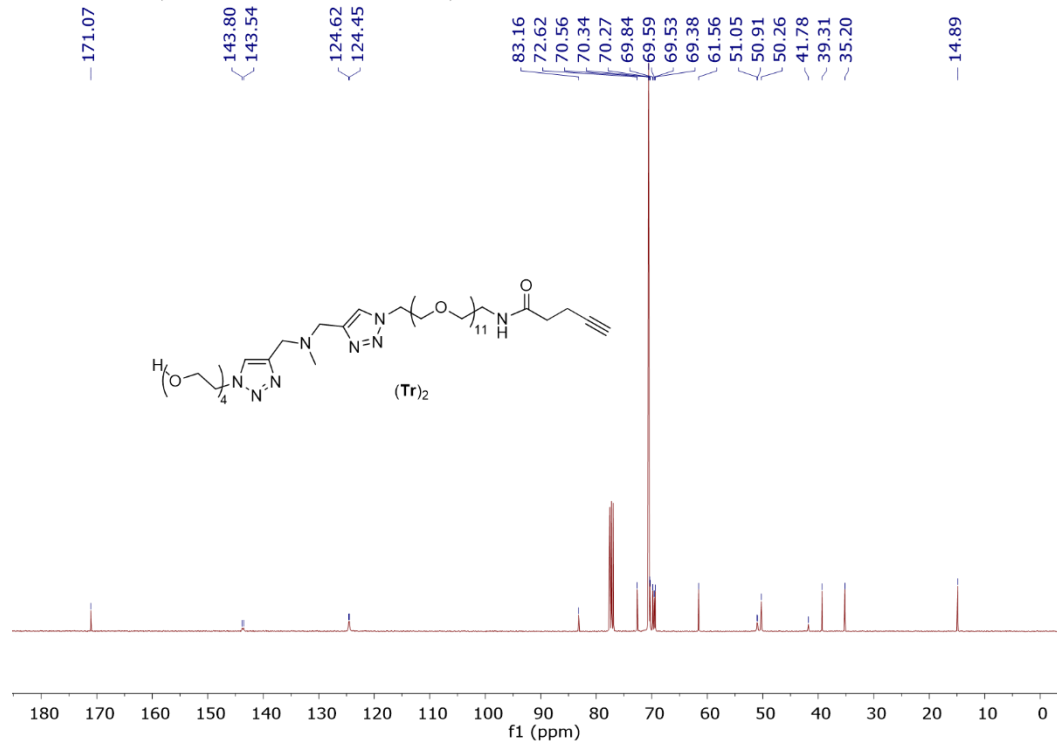
¹³C NMR (101 MHz, CHLOROFORM-*D*)



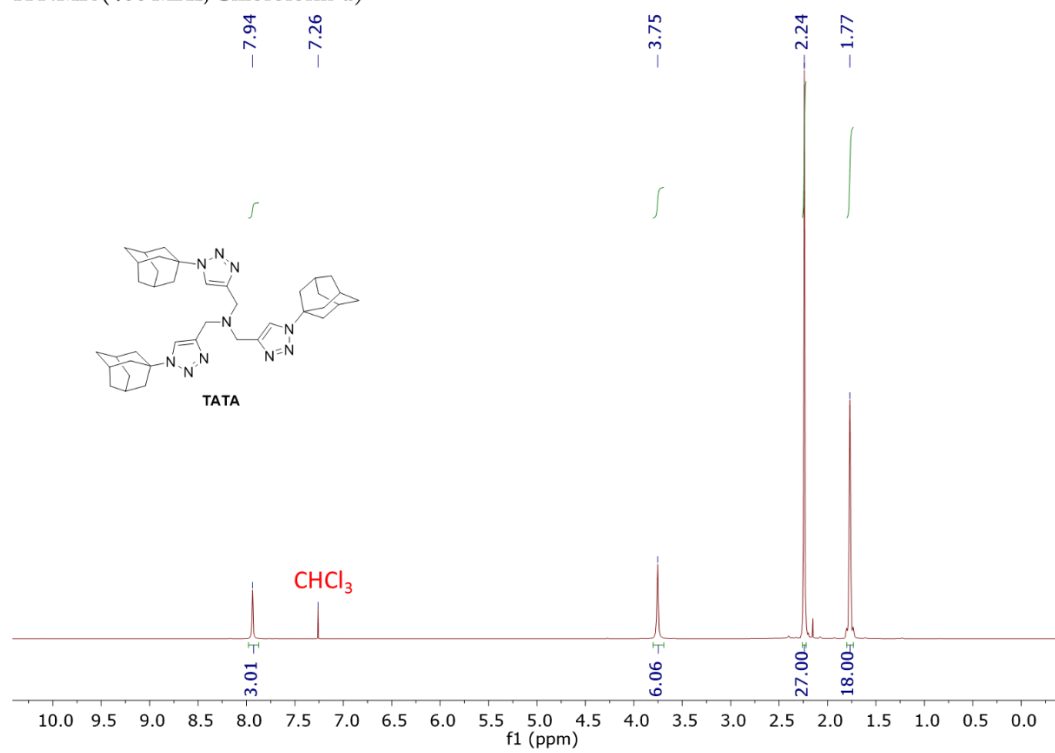
¹H NMR (400 MHz, Chloroform-d)



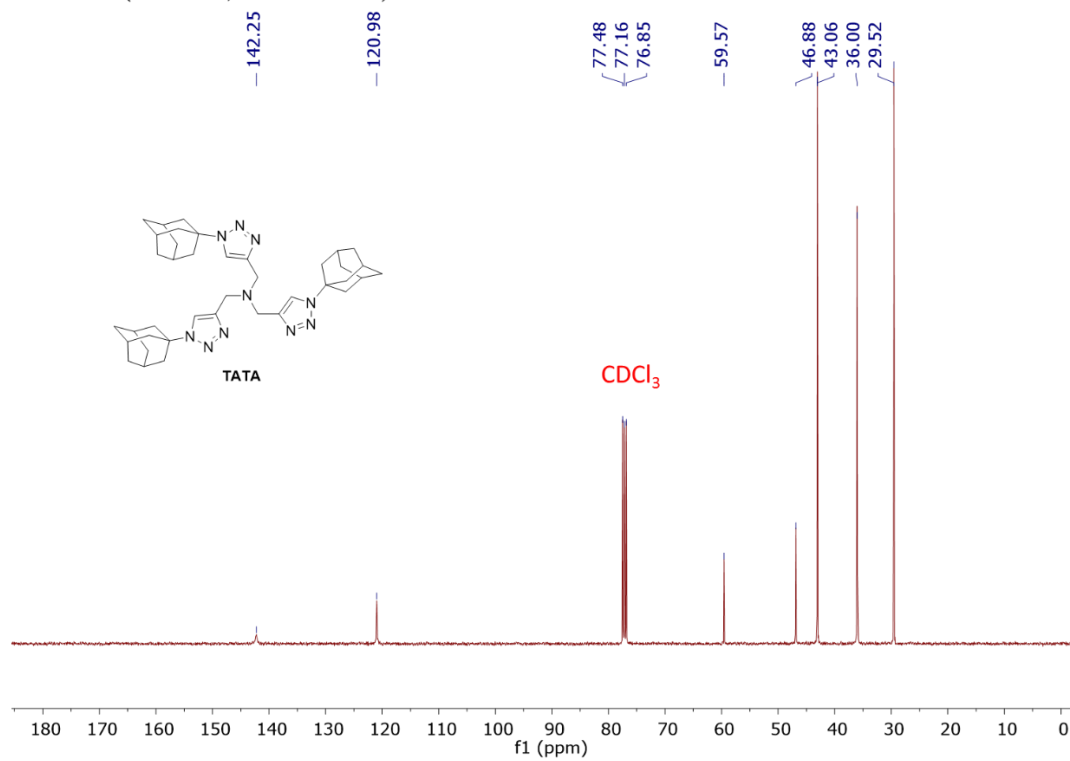
¹³C NMR (101 MHz, CHLOROFORM-D)



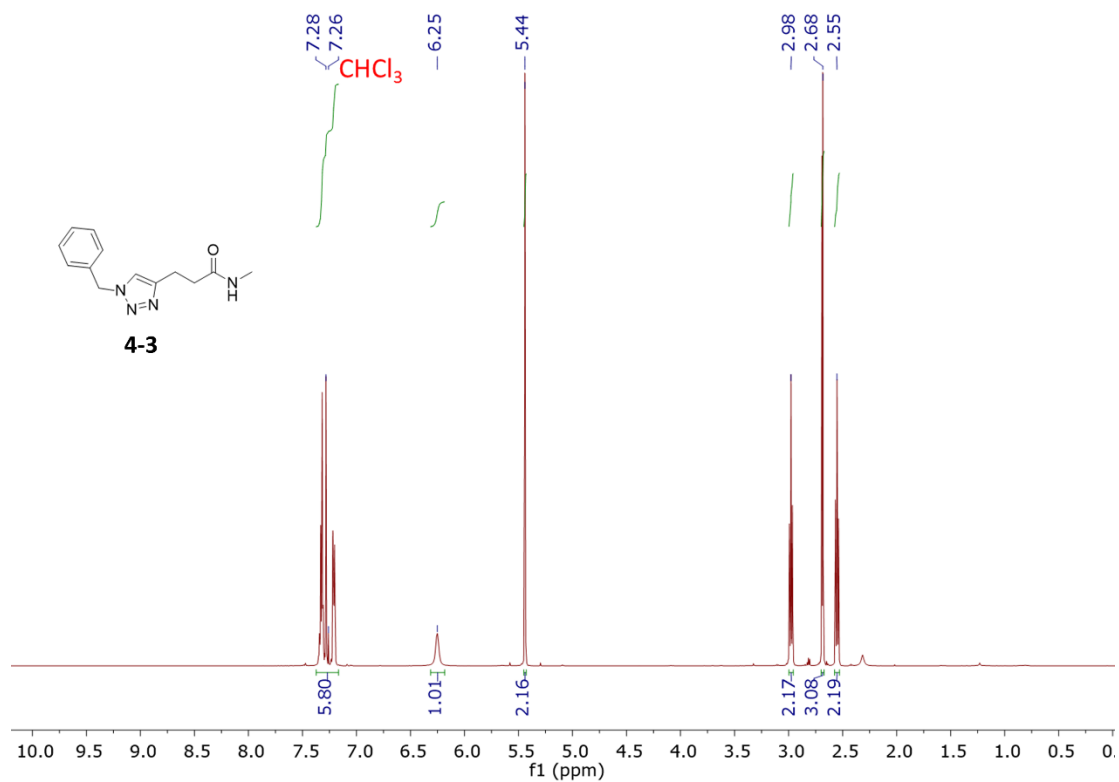
¹H NMR (400 MHz, Chloroform-*d*)



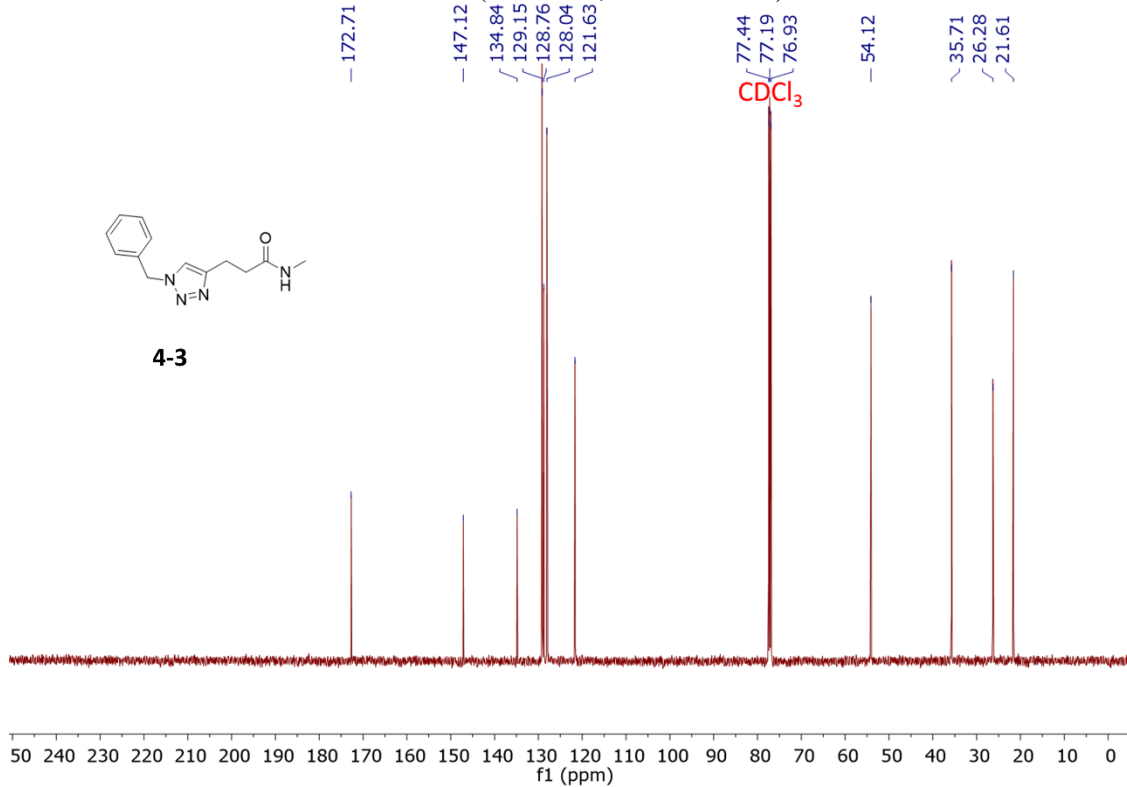
¹³C NMR (101 MHz, Chloroform-*d*)

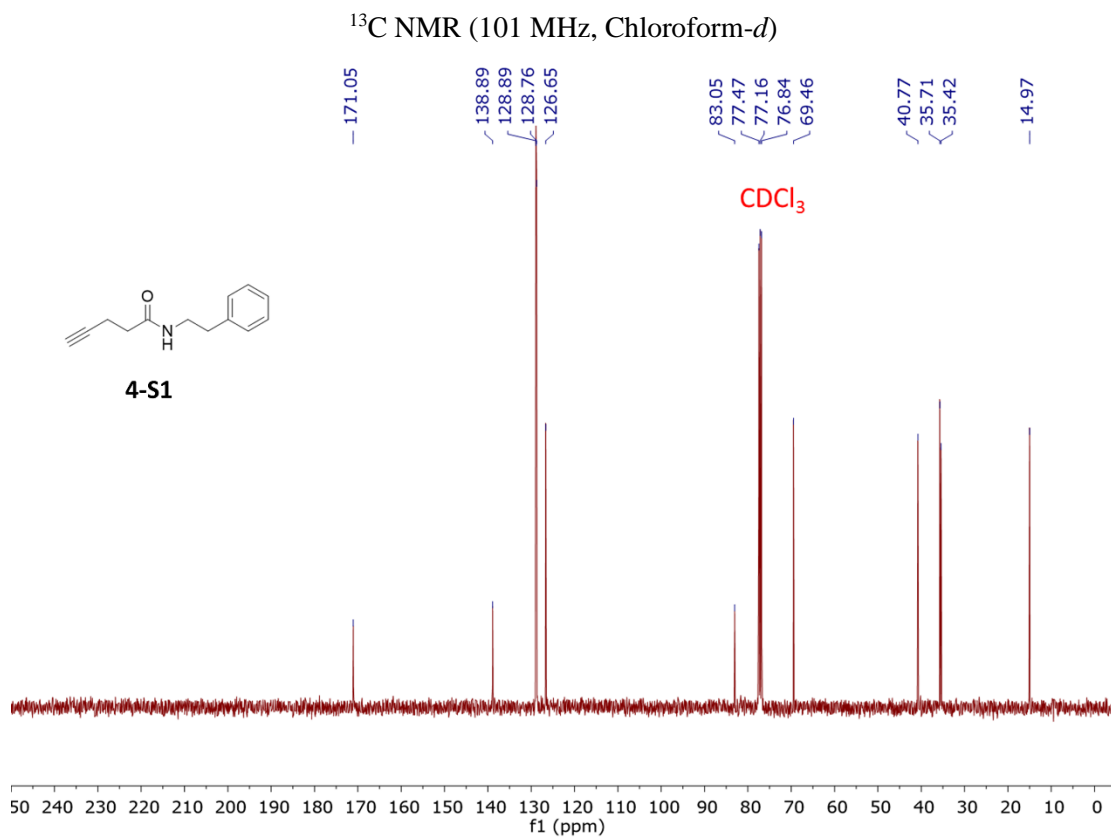
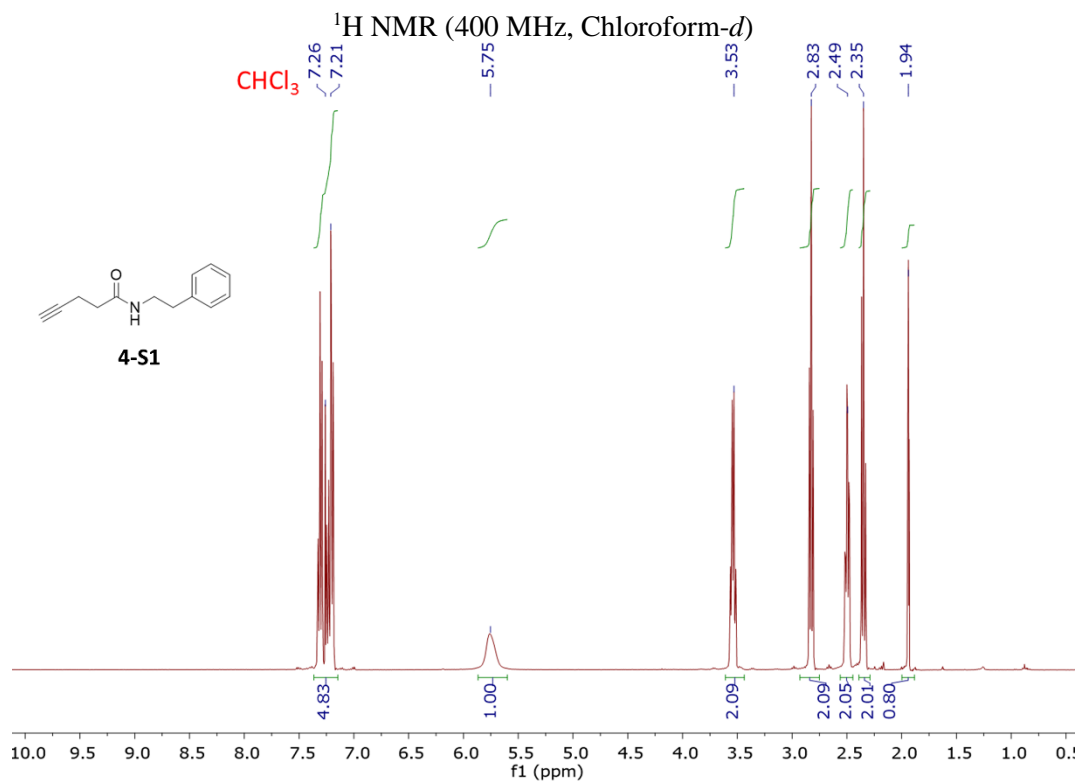


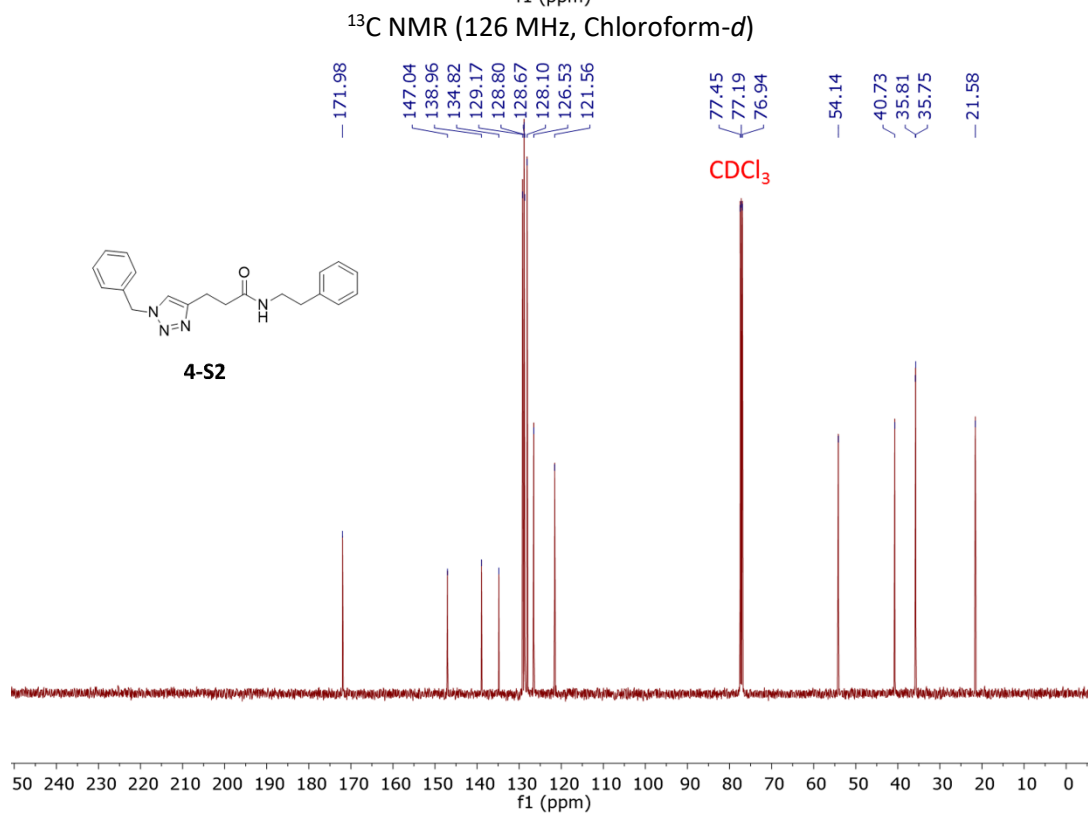
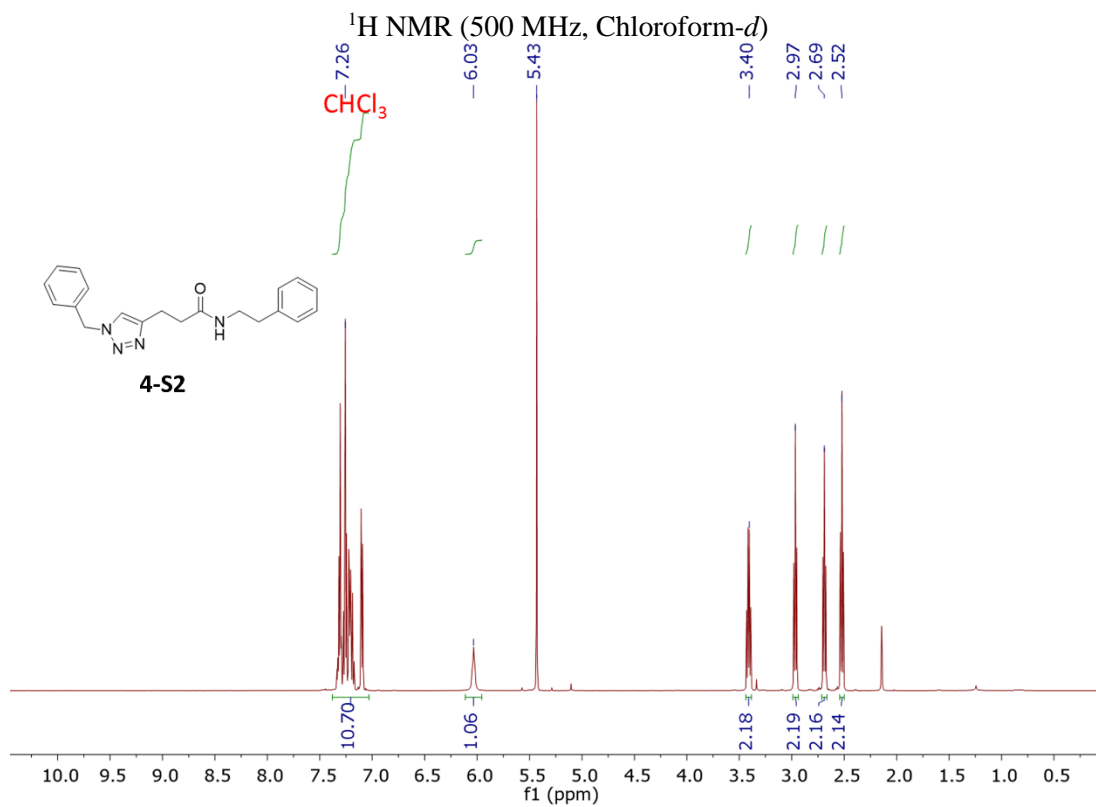
¹H NMR (500 MHz, Chloroform-*d*)

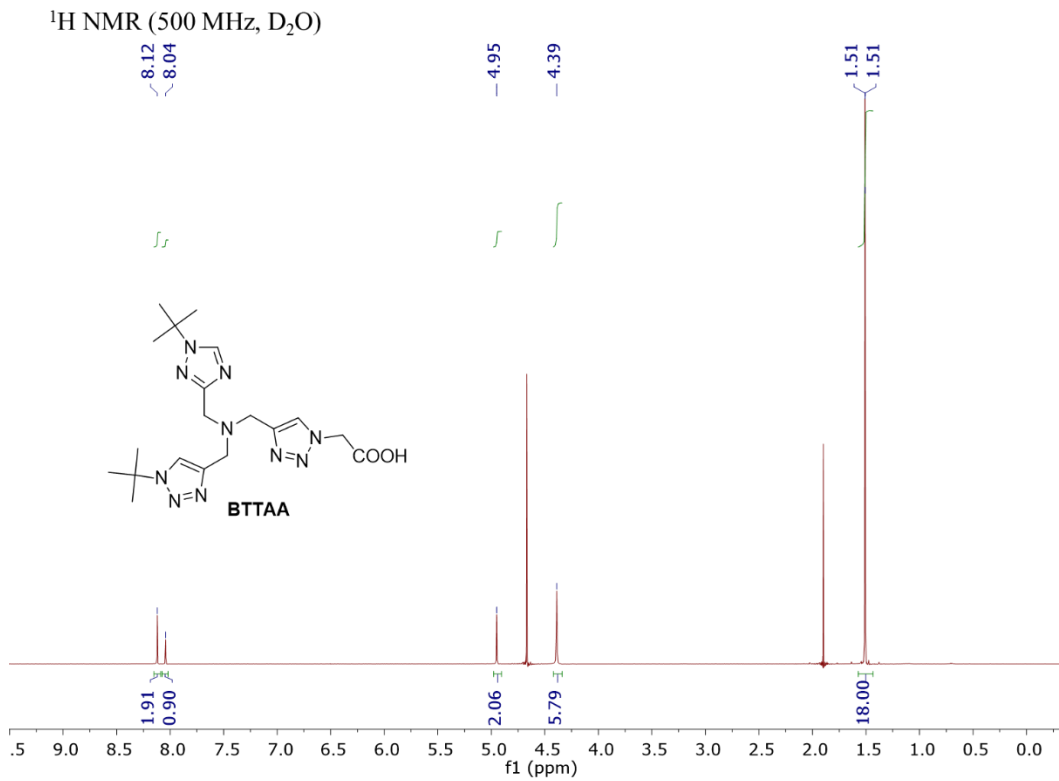
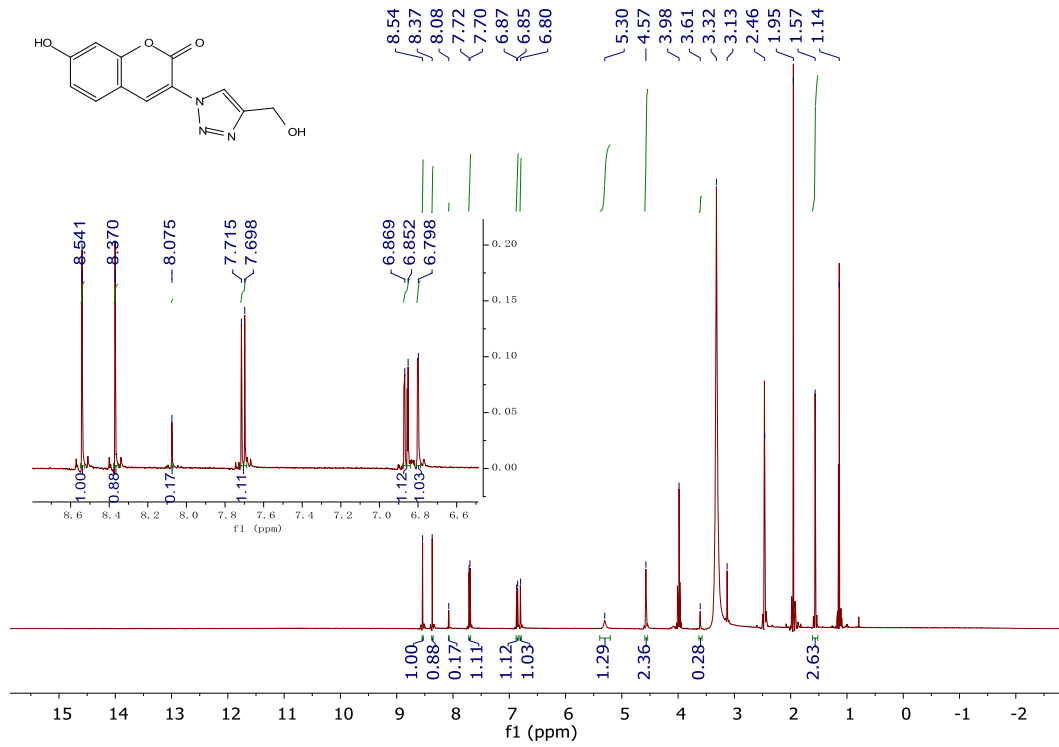


¹³C NMR (126 MHz, Chloroform-*d*)

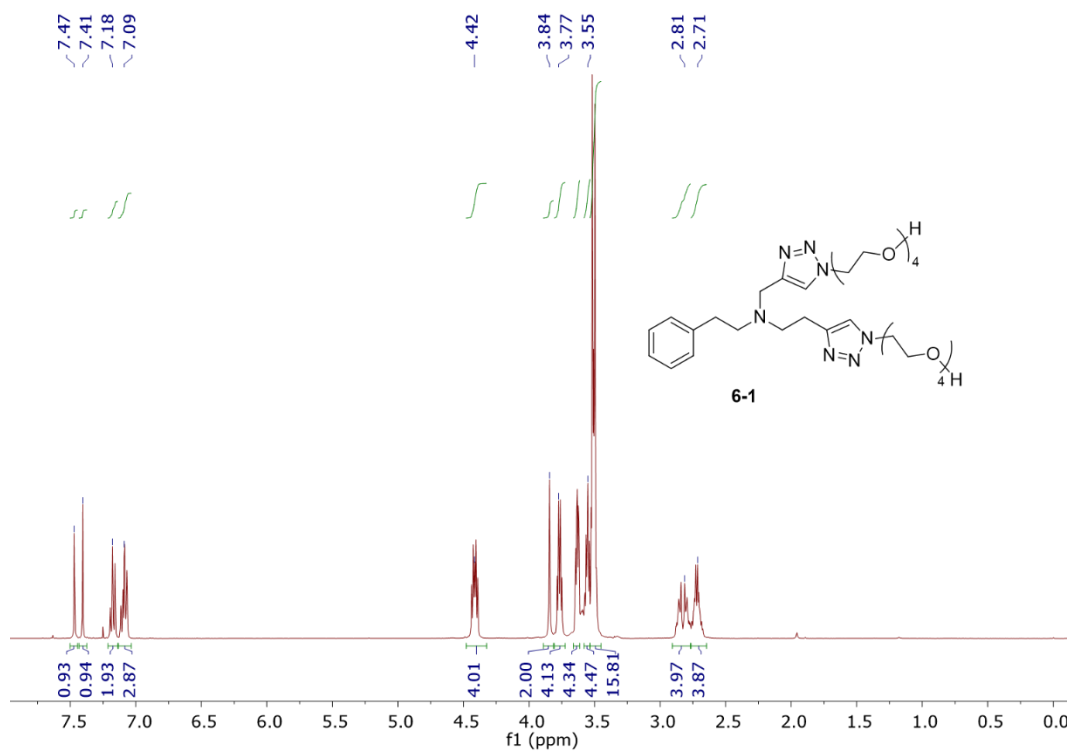




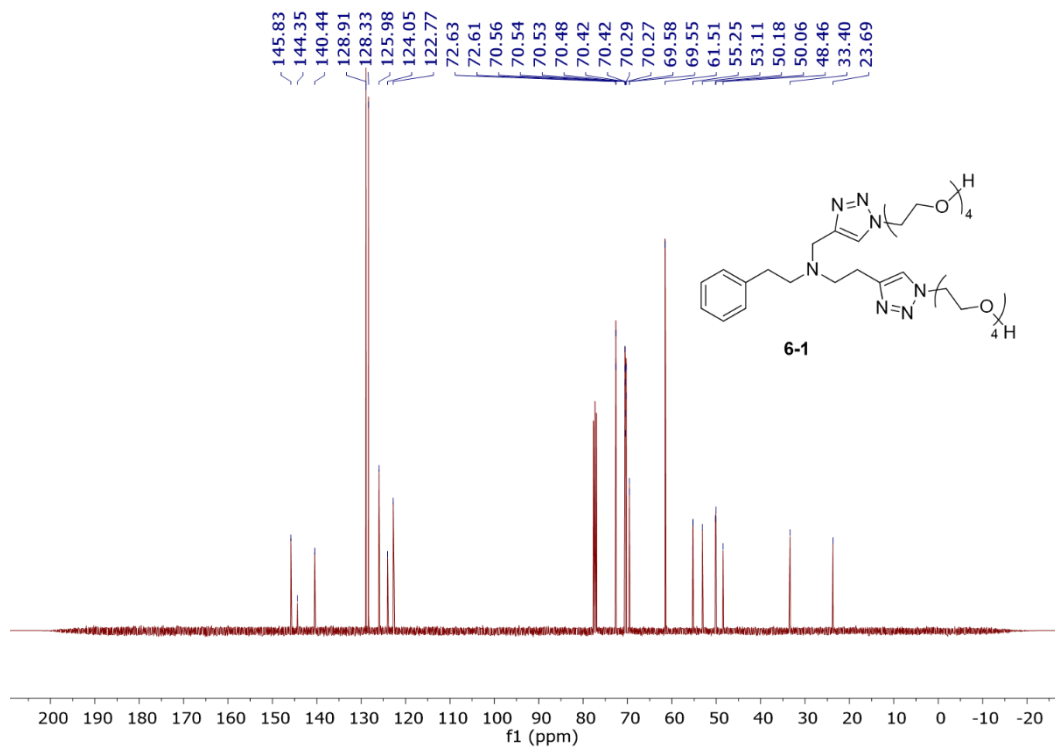




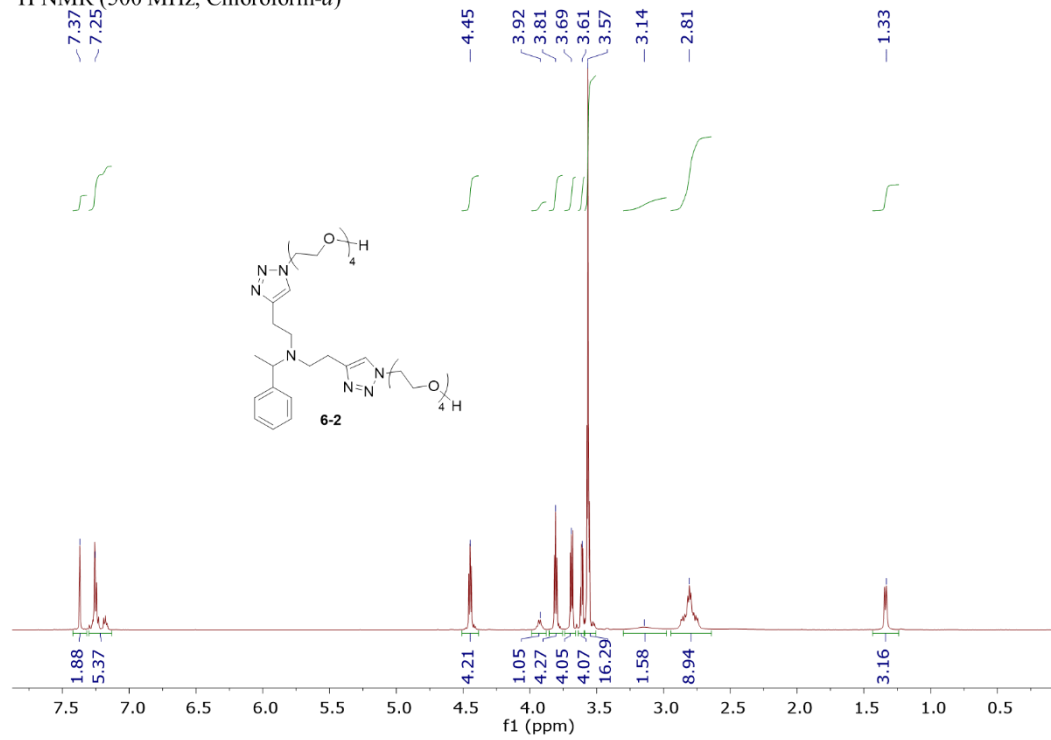
¹H NMR (400 MHz, CHLOROFORM-D)



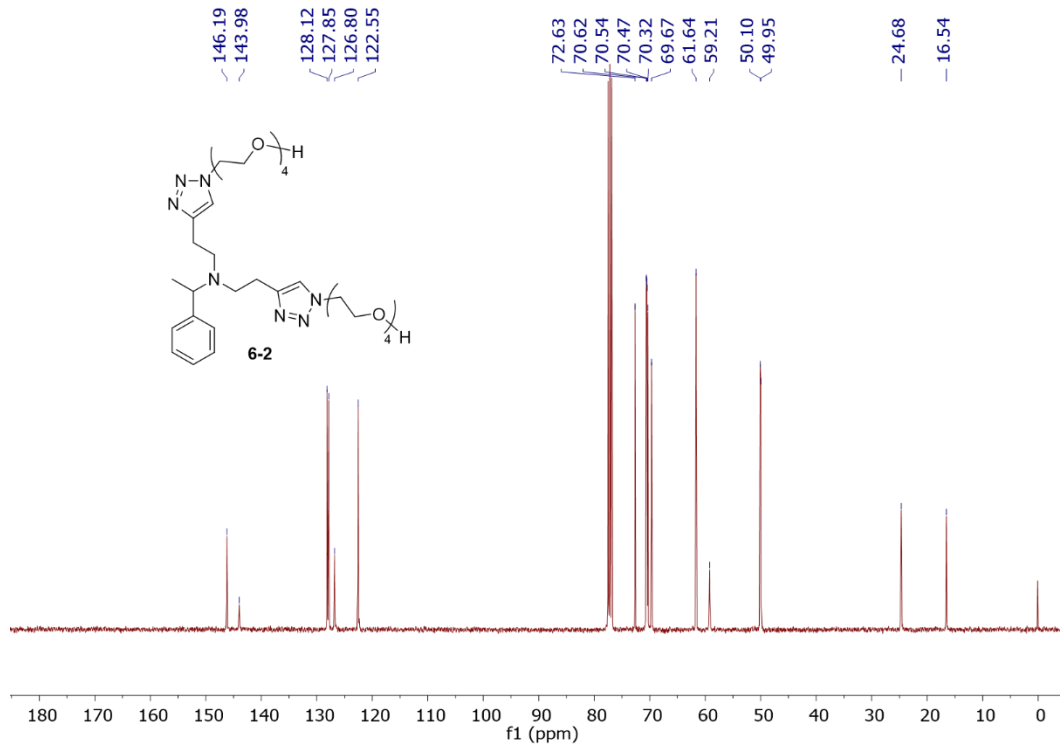
¹³C NMR (101 MHz, CHLOROFORM-D)



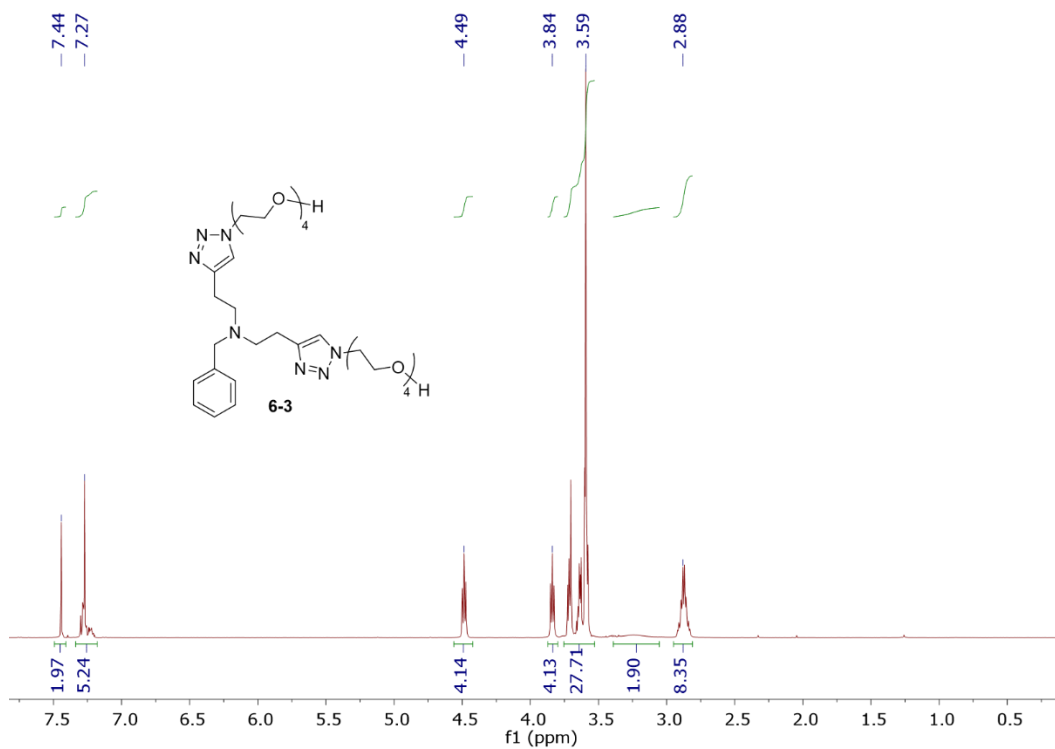
¹H NMR (500 MHz, Chloroform-*d*)



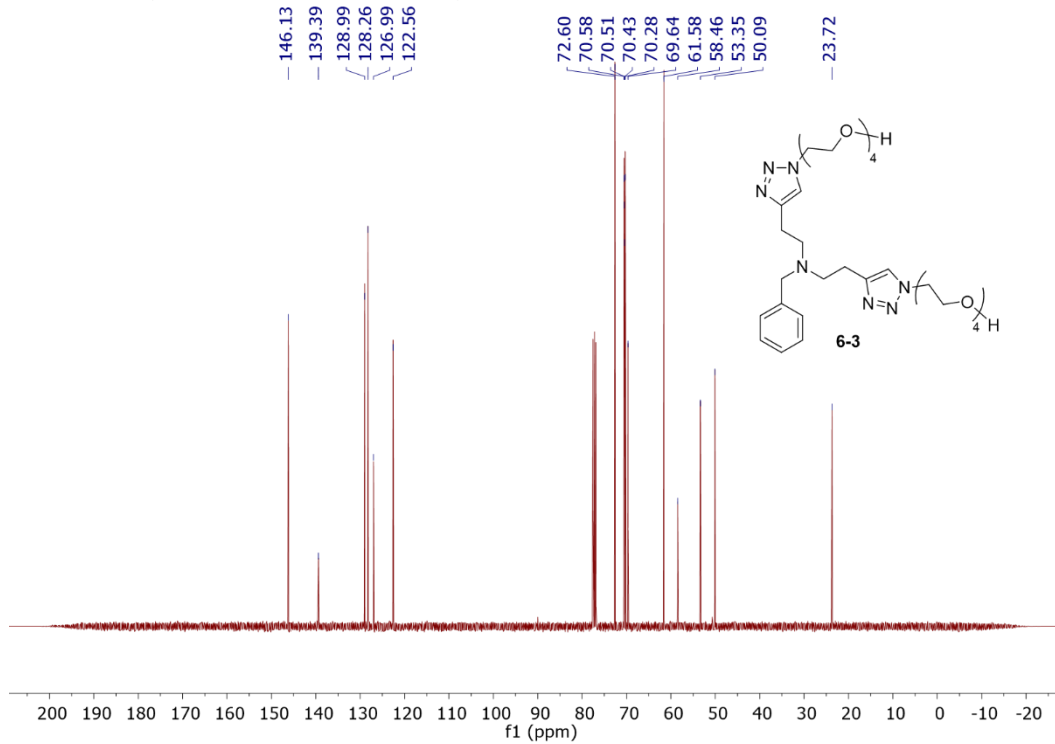
¹³C NMR (101 MHz, CHLOROFORM-*D*)



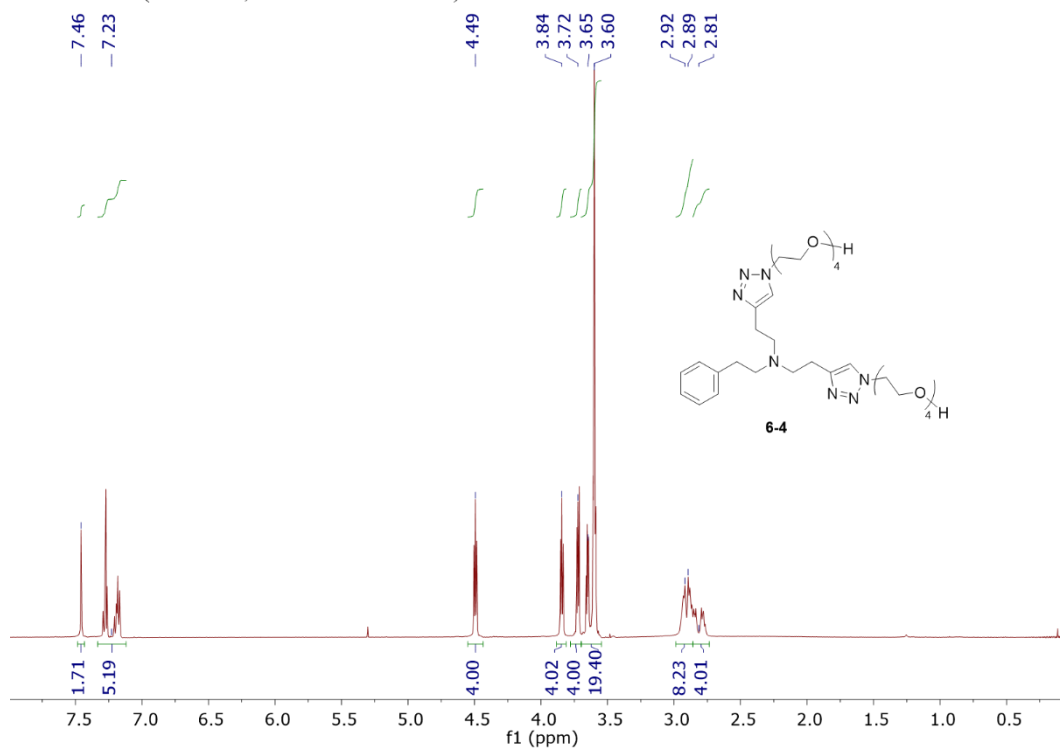
¹H NMR (400 MHz, CHLOROFORM-D)



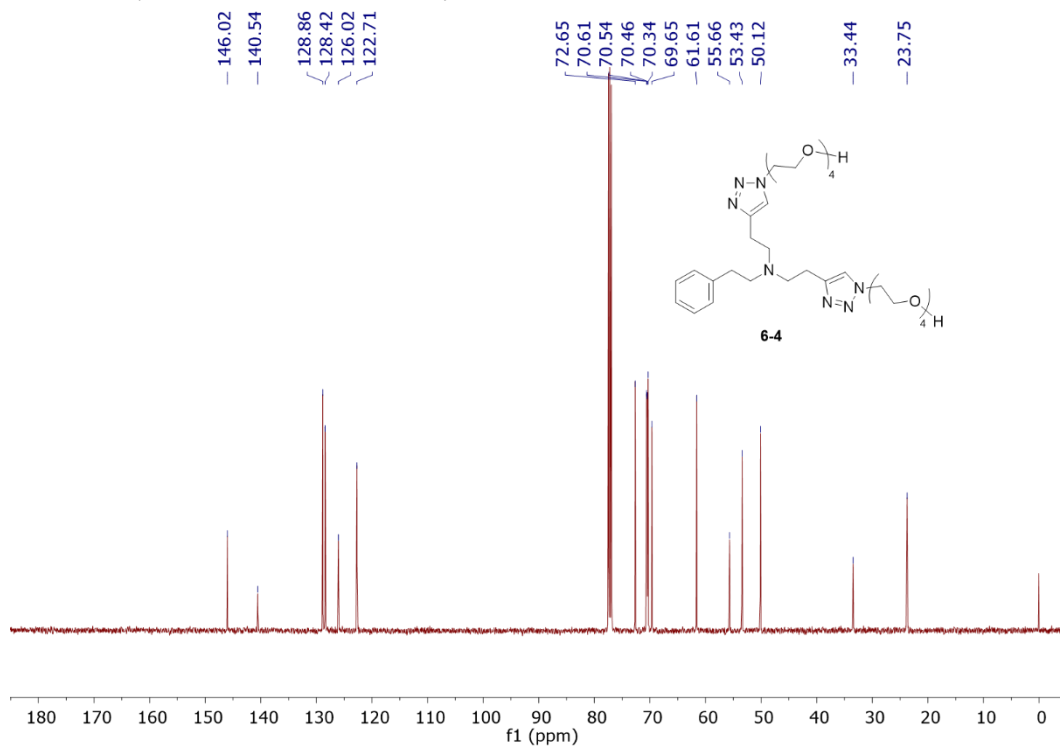
¹³C NMR (101 MHz, CHLOROFORM-D)

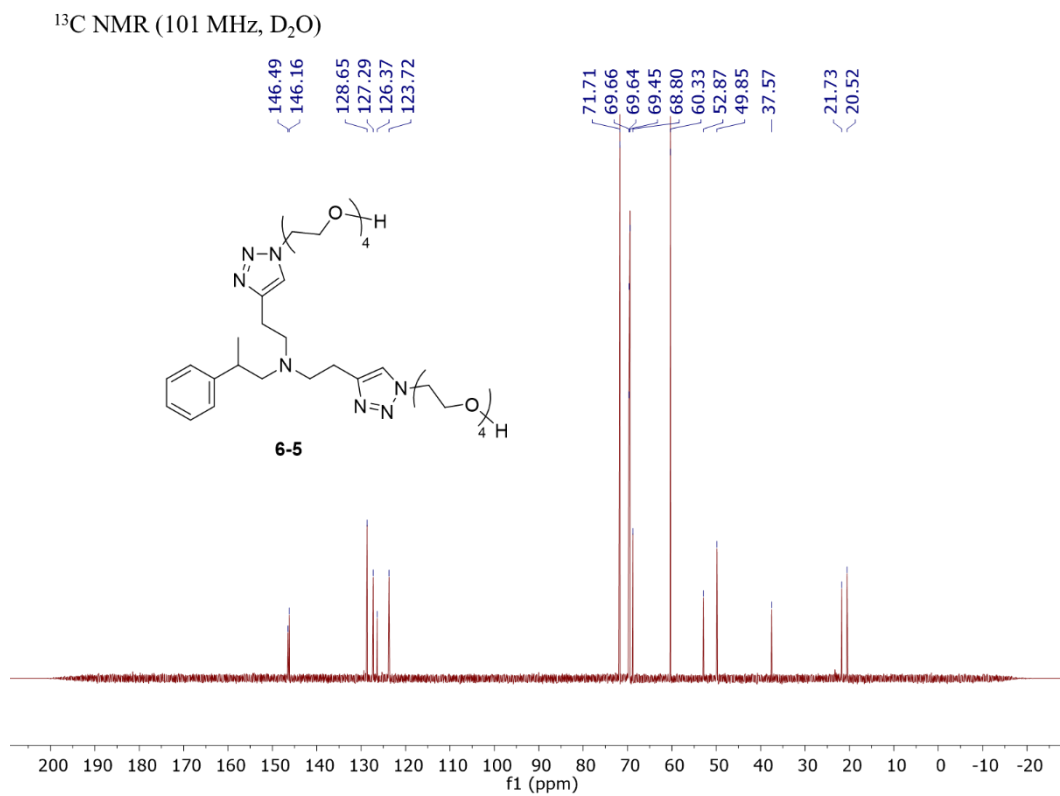
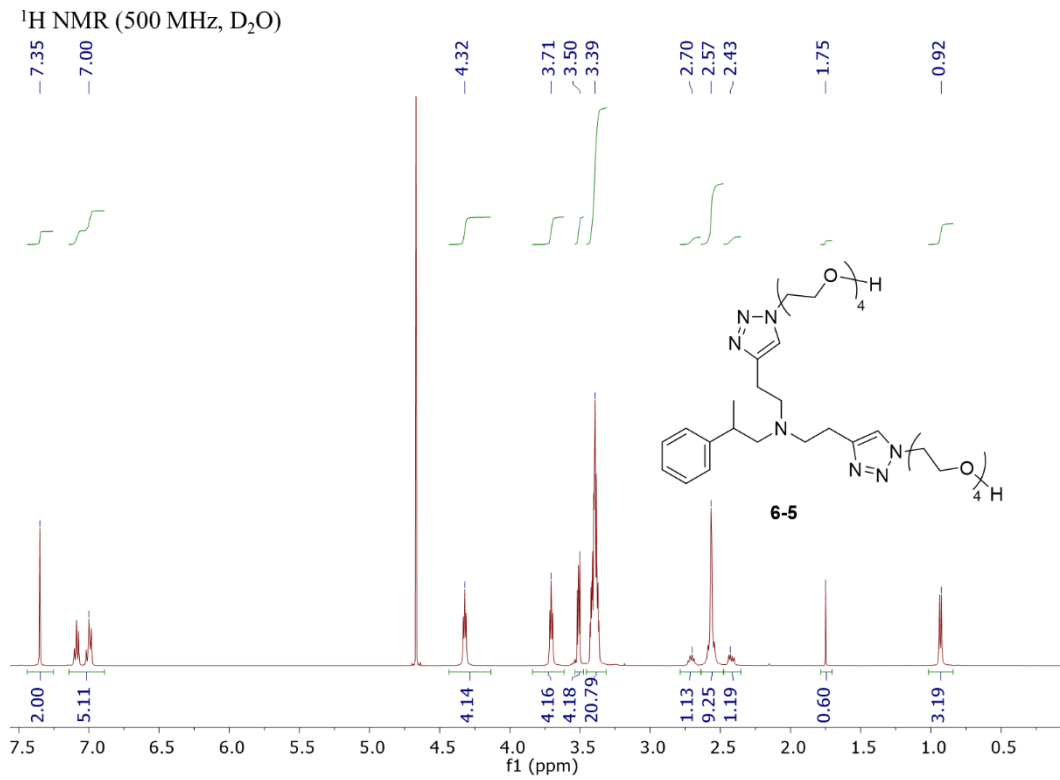


¹H NMR (500 MHz, CHLOROFORM-D)

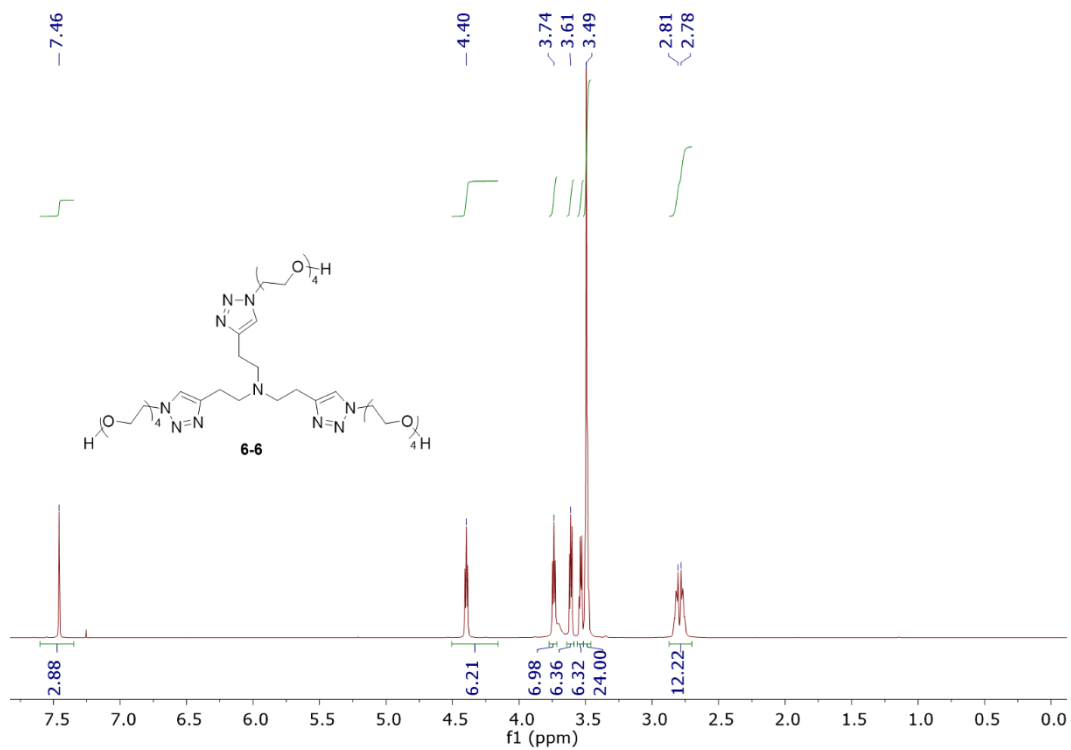


¹³C NMR (126 MHz, CHLOROFORM-D)

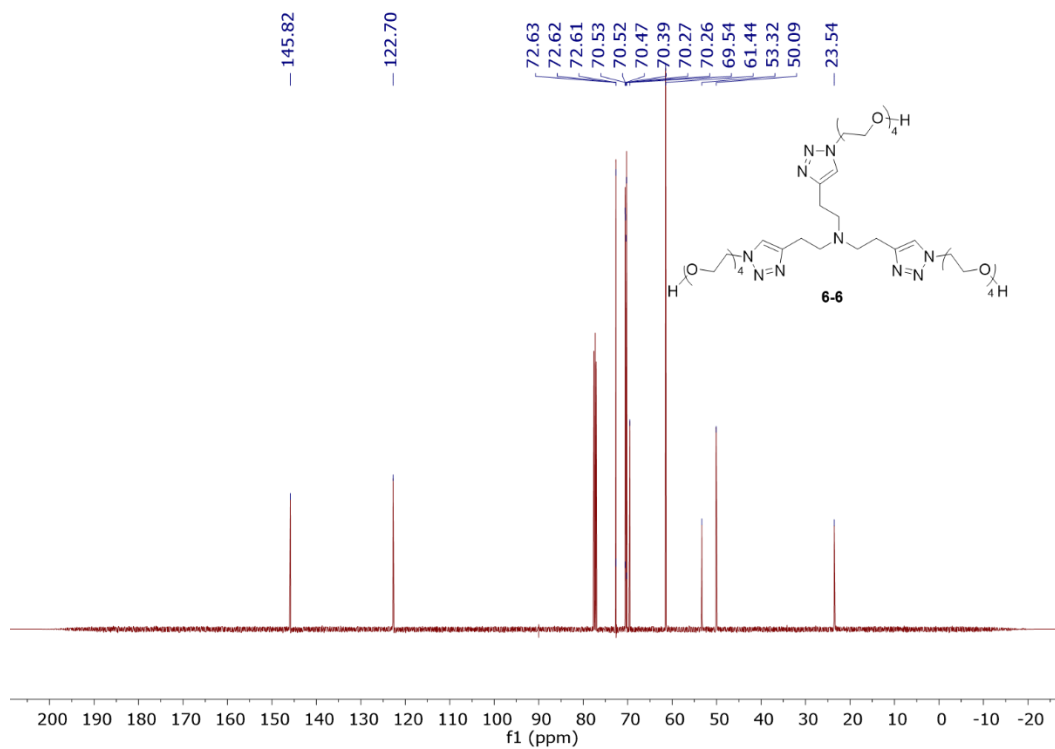




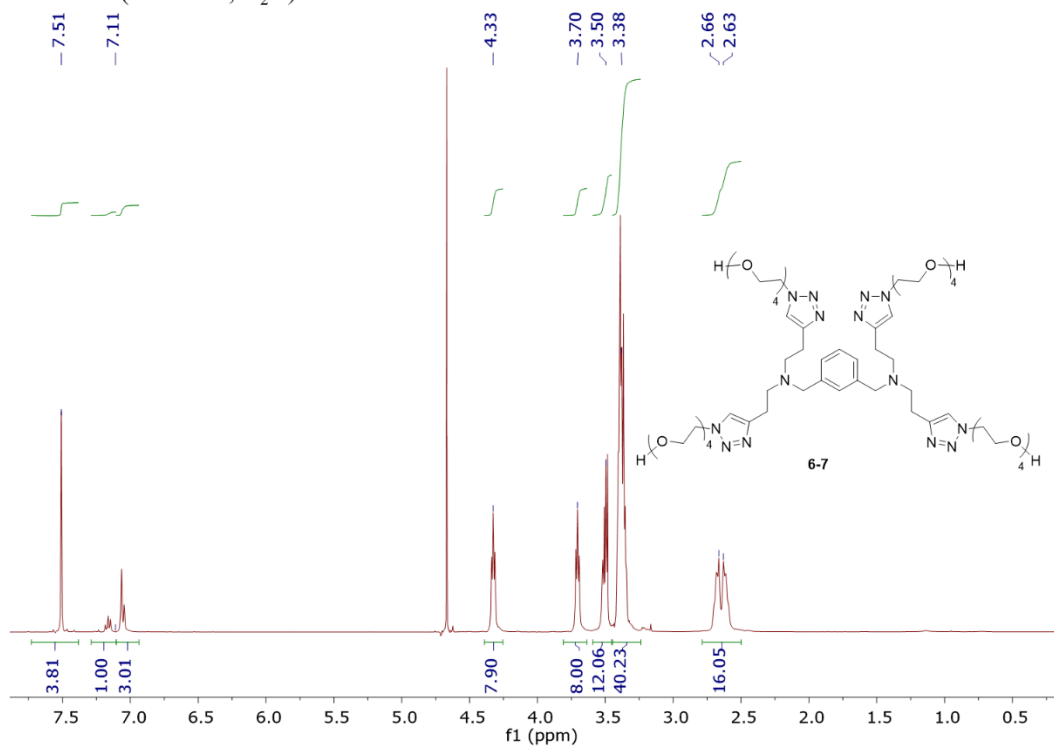
¹H NMR (500 MHz, CHLOROFORM-D)



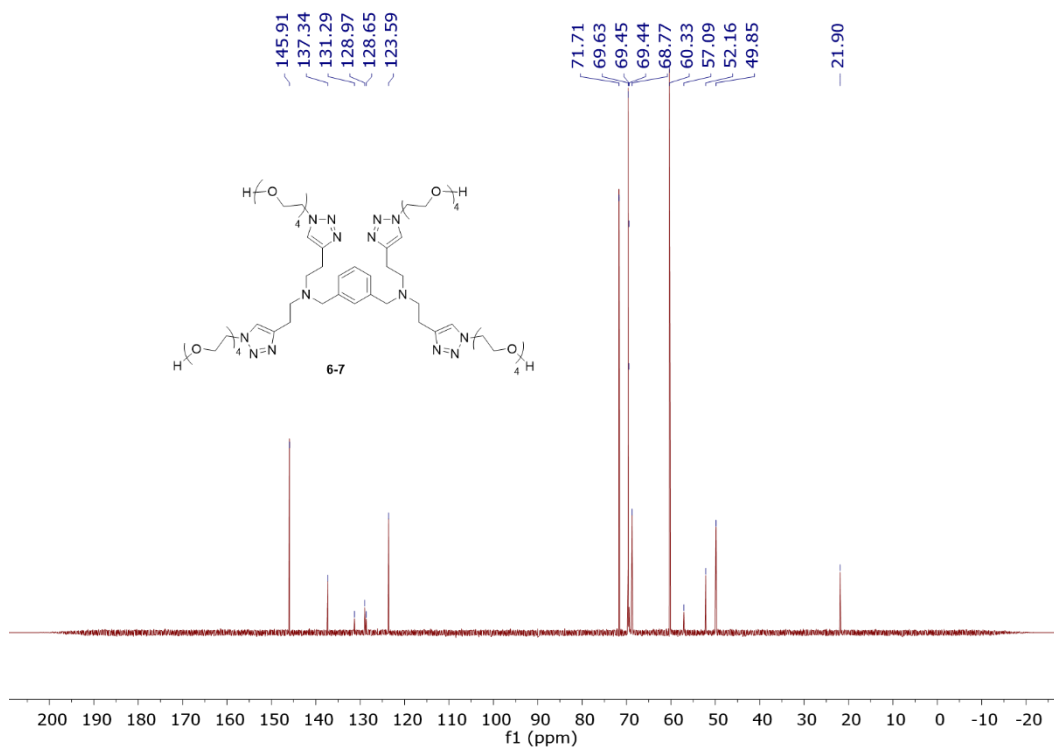
¹³C NMR (126 MHz, CHLOROFORM-D)



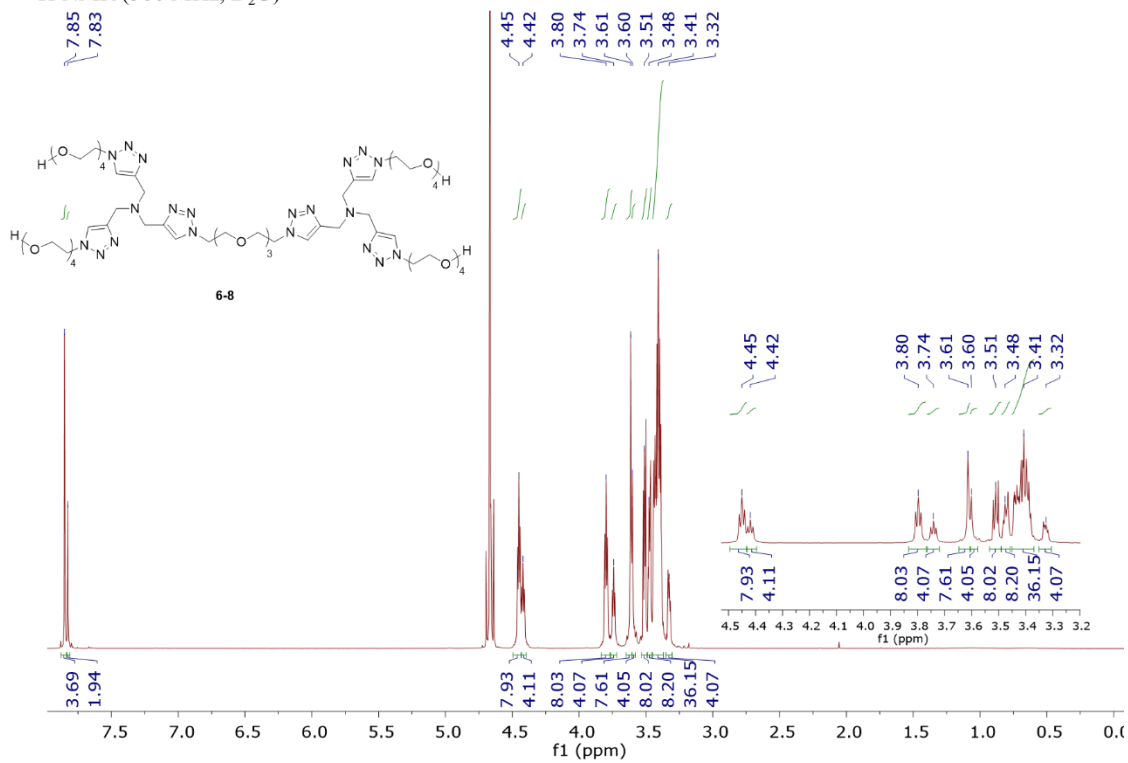
¹H NMR (400 MHz, D₂O)



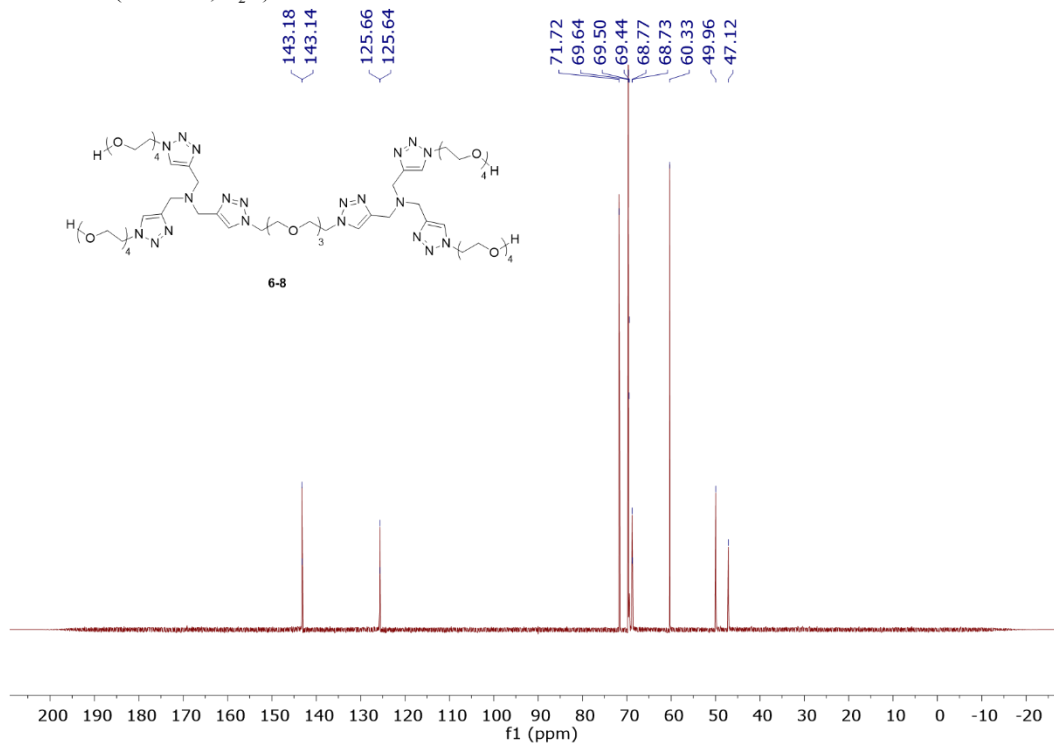
¹³C NMR (101 MHz, D₂O)



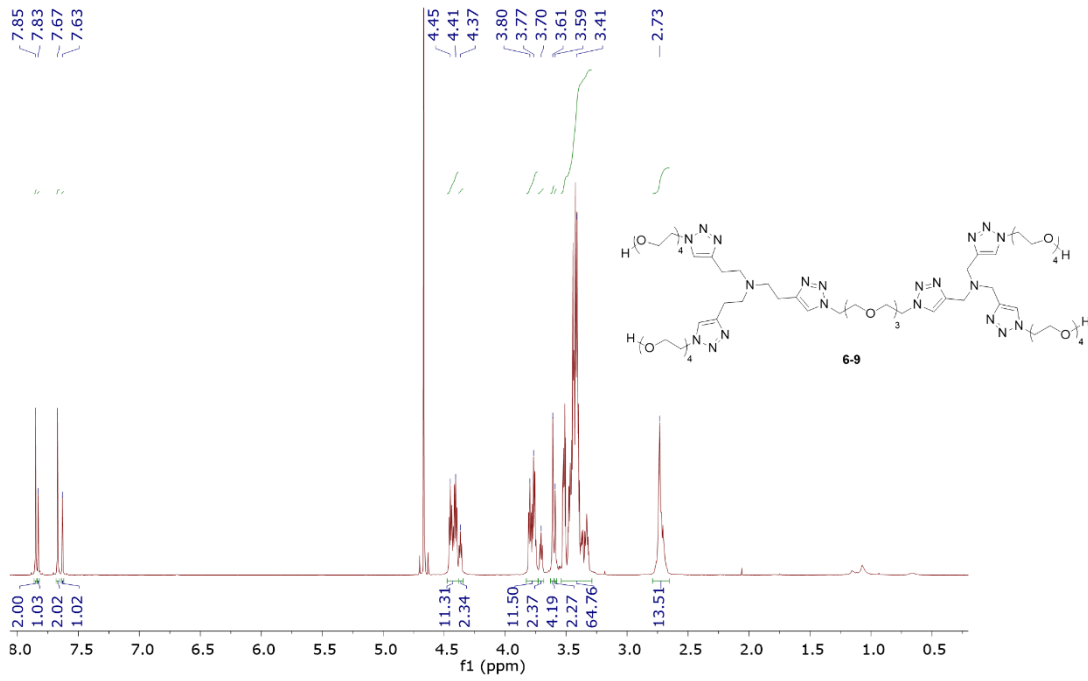
¹H NMR (500 MHz, D₂O)



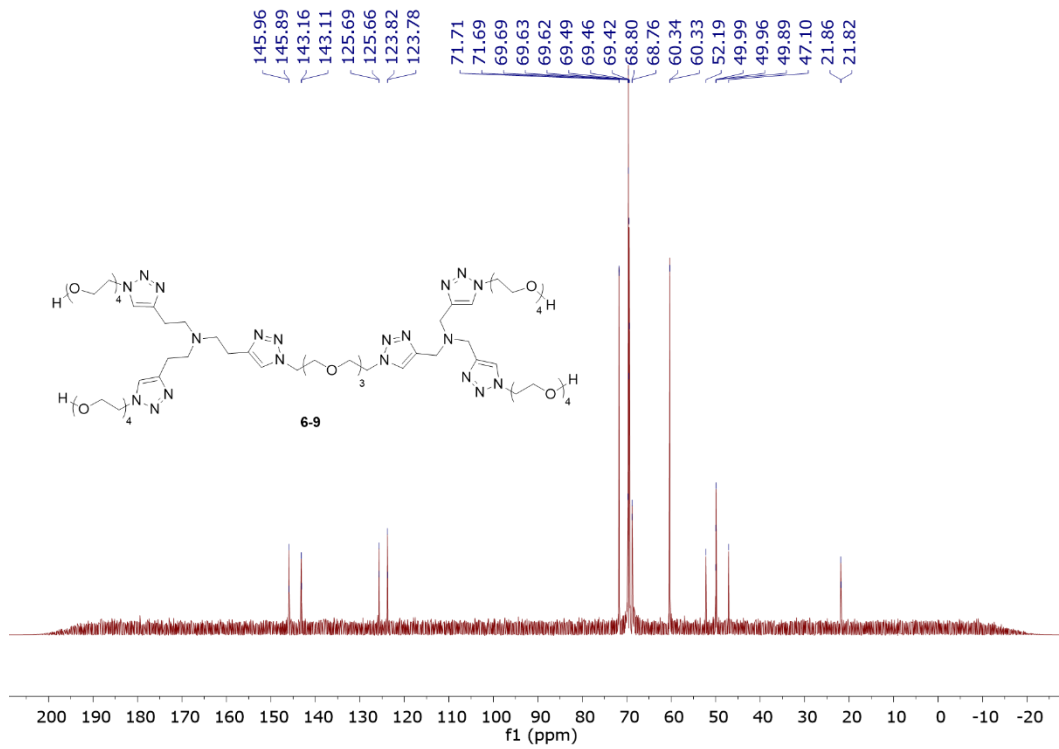
¹³C NMR (101 MHz, D₂O)



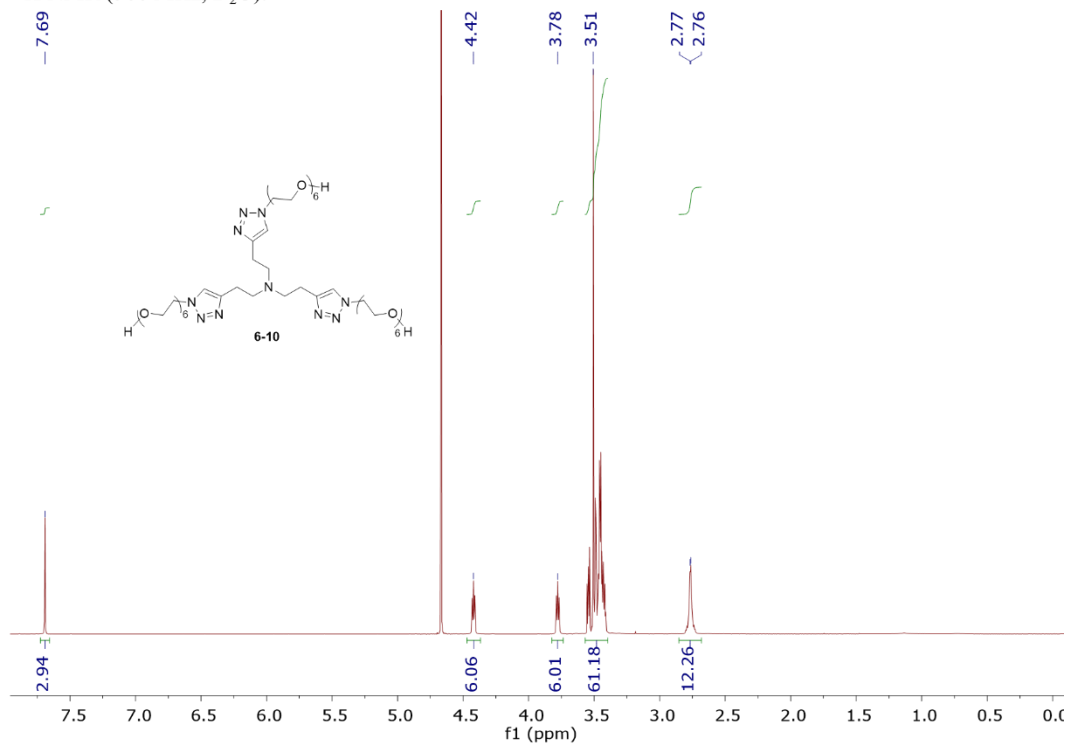
¹H-NMR (500 MHz, D₂O)



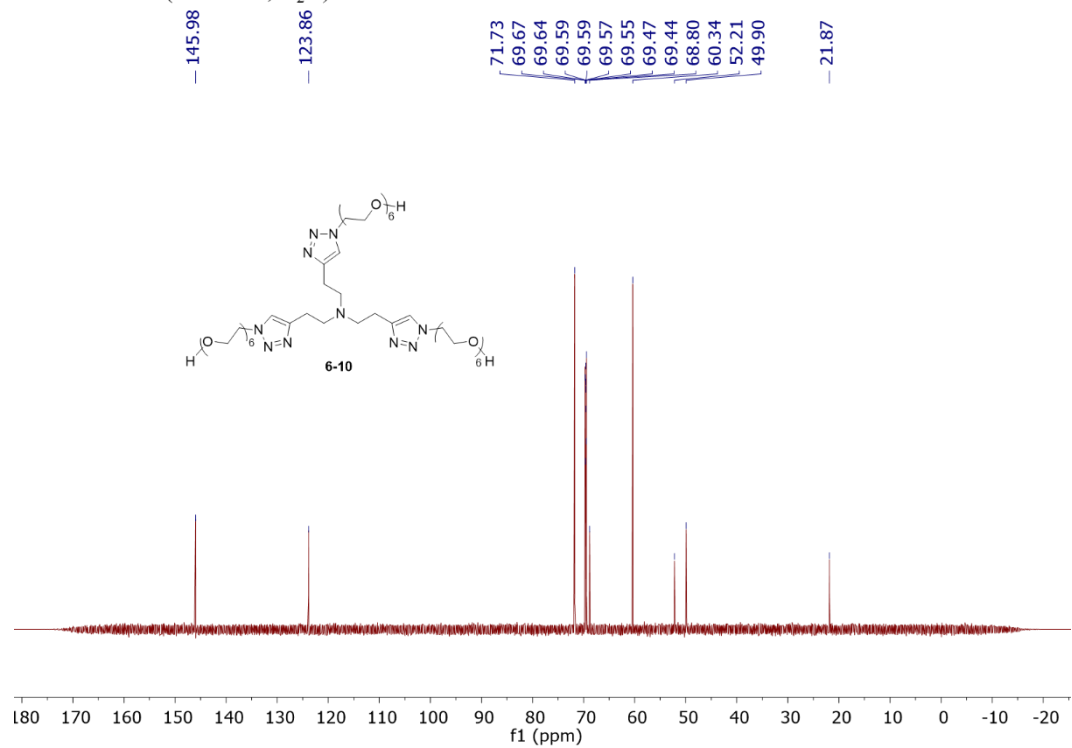
¹³C-NMR (126 MHz, D₂O)

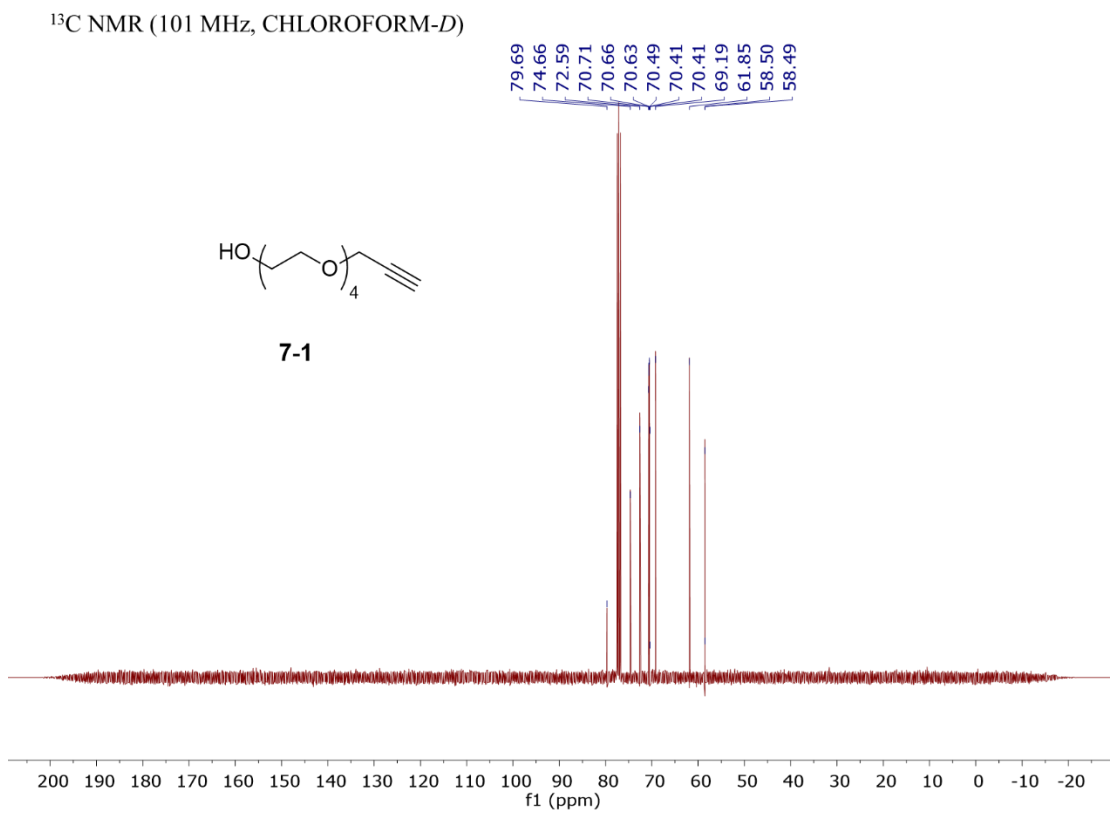
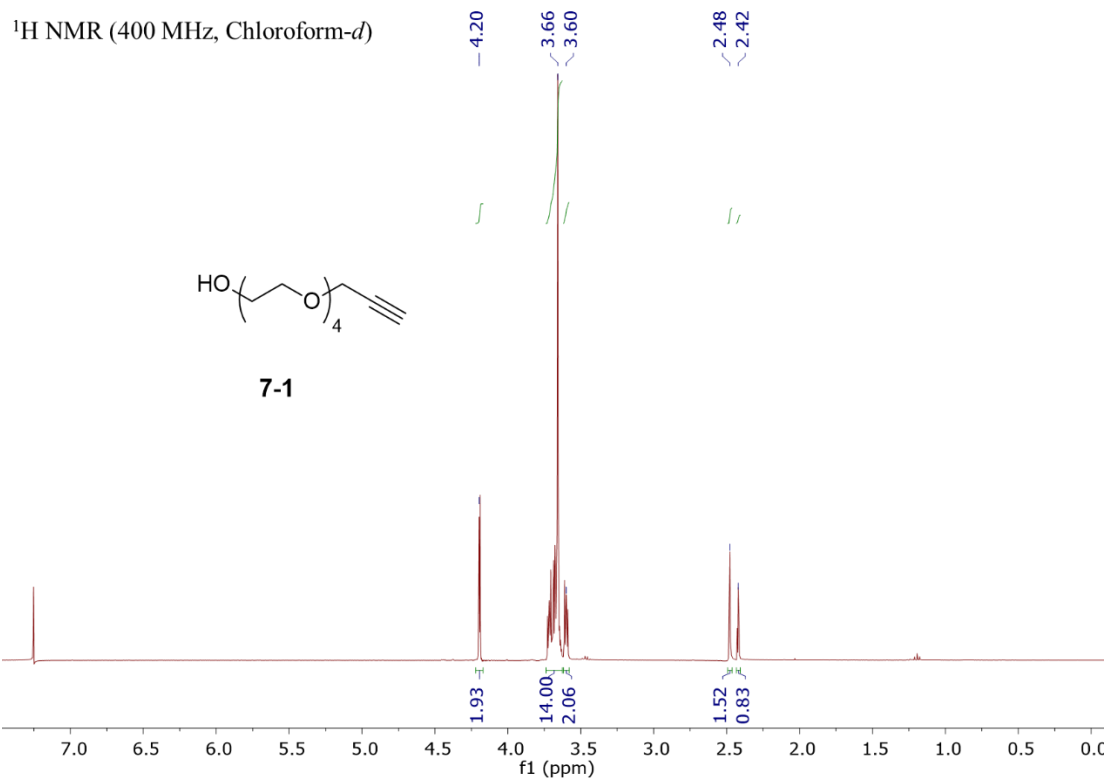


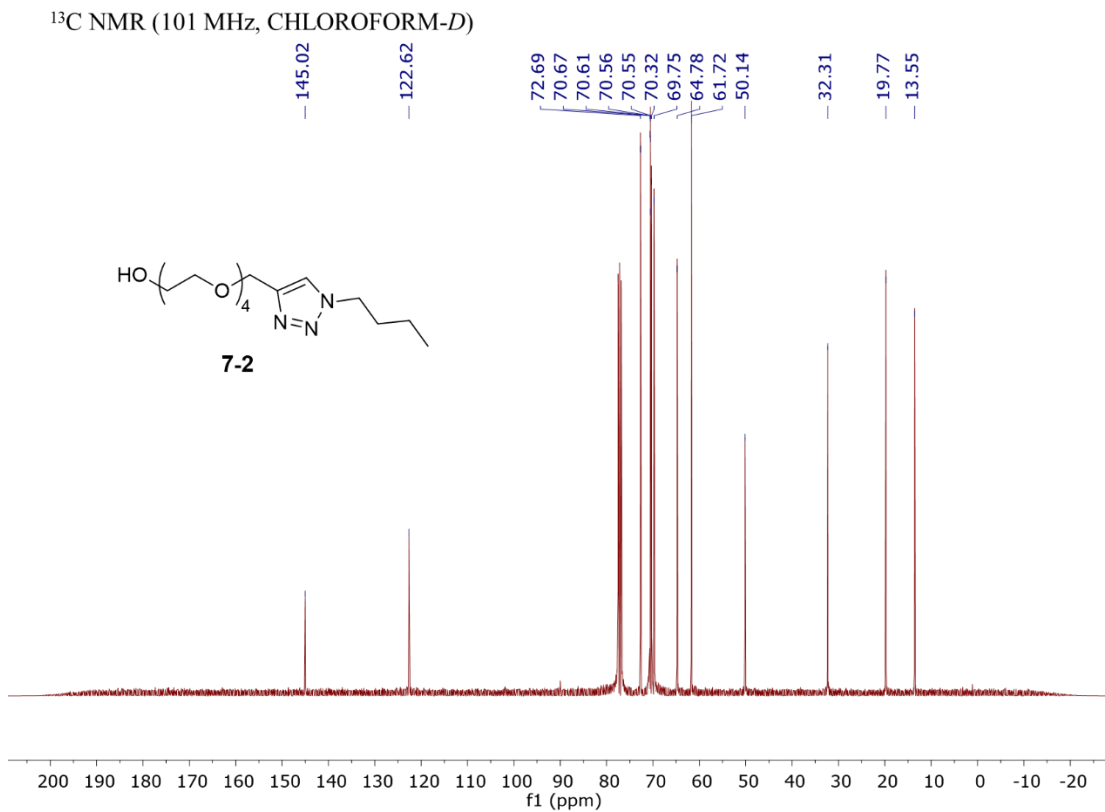
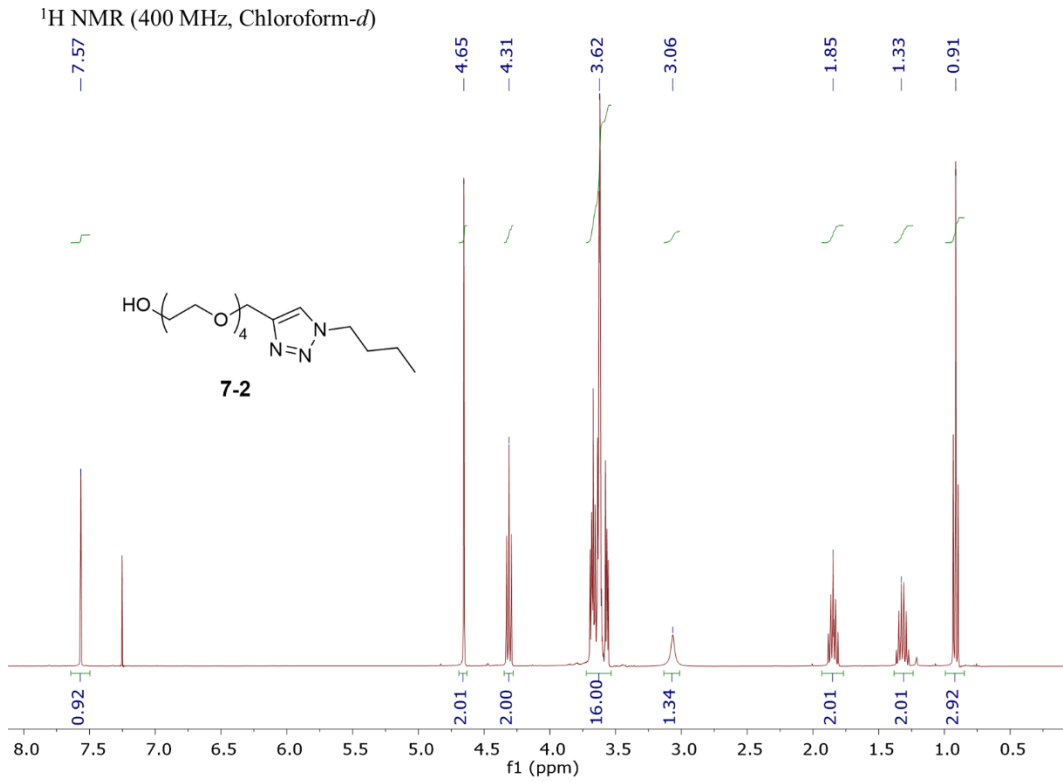
¹H NMR (500 MHz, D₂O).



¹³C NMR (126 MHz, D₂O)

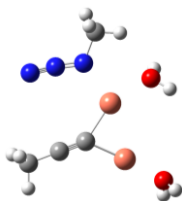






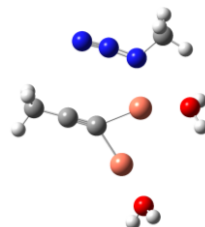
Appendix B: Coordinates and Energies for Ground State and Transition State Geometries (in Chapter 5)

Di-Cu Azide-acetylide Complex II'



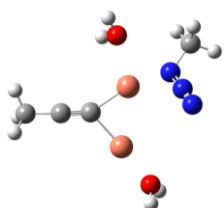
B3LYP (water)

Symbol	X	Y	Z
Cu	0.322839	-0.63176	-0.02577
O	0.276111	-2.71644	-0.09522
H	0.356987	-3.12284	-0.96761
H	-0.48464	-3.13846	0.322907
Cu	-2.10727	0.087303	0.009386
C	-0.24824	2.351531	0.04329
C	-0.50484	1.151295	0.021124
C	0.050999	3.777586	0.071373
H	-0.86949	4.359883	0.174982
H	0.700054	4.029745	0.914497
H	0.547046	4.098645	-0.84867
O	-3.83343	-0.87859	0.001336
H	-4.28288	-1.02444	0.843449
H	-4.5098	-0.60923	-0.63308
N	2.982013	0.587313	-0.09574
N	3.326764	1.657035	-0.21831
N	2.476834	-0.53381	0.024423
C	3.424689	-1.65138	0.272315
H	2.817662	-2.54483	0.383227
H	4.105043	-1.77086	-0.57312
H	3.992186	-1.47622	1.188392



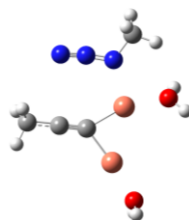
M06 (water)

Symbol	X	Y	Z
Cu	0.253362	-0.68587	-0.06452
O	0.194423	-2.72226	-0.18361
H	0.282149	-3.10923	-1.06167
H	-0.56218	-3.15724	0.223716
Cu	-2.05881	0.172477	0.037944
C	-0.03562	2.309493	-0.03661
C	-0.41608	1.145625	-0.01729
C	0.397859	3.691566	-0.06148
H	-0.4616	4.364247	0.023521
H	1.076138	3.912398	0.768283
H	0.915411	3.931501	-0.99542
O	-3.81809	-0.67468	0.083274
H	-4.11913	-1.06419	0.911459
H	-4.56908	-0.20301	-0.29338
N	2.848414	0.530826	0.0285
N	3.146539	1.618458	-0.00036
N	2.37447	-0.60253	0.043891
C	3.319232	-1.71801	0.227735
H	2.718238	-2.62446	0.264685
H	4.017671	-1.77667	-0.61085
H	3.871424	-1.60893	1.164538



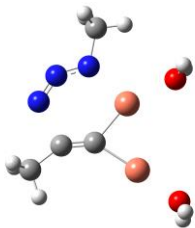
B3LYP (gas)

Symbol	X	Y	Z
Cu	0.477094	0.617224	0.007059
O	1.015904	2.655232	-0.92796
H	1.360239	3.395356	-0.41345
H	0.259022	3.004673	-1.41368
Cu	-1.40942	-1.17061	-0.241
C	-2.42389	1.378496	0.499773
C	-1.45338	0.690582	0.197341
C	-3.55564	2.213837	0.867844
H	-4.1041	1.785065	1.71087
H	-3.21068	3.207759	1.169177
H	-4.24741	2.338343	0.030429
O	-1.52222	-3.10607	-0.67894
H	-1.73247	-3.79164	-0.034
H	-1.72331	-3.45336	-1.55578
N	2.727406	-0.87603	0.885424
N	2.968321	-1.69434	1.620858
N	2.399059	0.029627	0.091633
C	3.517067	0.539956	-0.75586
H	3.090439	1.311828	-1.38905
H	4.303999	0.967726	-0.13111
H	3.923965	-0.26293	-1.37398



M06 (gas)

Symbol	X	Y	Z
Cu	0.312442	-0.73429	-0.0659
O	0.456155	-2.77219	-0.25896
H	0.838742	-3.16353	-1.05025
H	-0.17129	-3.40691	0.097789
Cu	-2.0784	0.081285	0.048284
C	-0.18552	2.237002	0.021796
C	-0.44887	1.041198	0.013908
C	0.123227	3.649612	0.032093
H	-0.79262	4.238984	0.1399
H	0.784661	3.904522	0.865409
H	0.611473	3.955983	-0.89784
O	-3.88233	-0.70567	0.09393
H	-4.45129	-0.64754	0.86785
H	-4.44724	-0.75613	-0.68336
N	2.773191	0.703683	-0.12925
N	2.935775	1.806197	-0.28568
N	2.443226	-0.47971	0.010362
C	3.50016	-1.38062	0.504643
H	3.035606	-2.3524	0.662294
H	4.305568	-1.48124	-0.22841
H	3.909222	-1.02619	1.454945



Di-Cu Transition State III'
B3LYP (water)

Symbol	X	Y	Z
C	0.247086	0.960879	0.000265
C	-0.31658	2.090215	-0.00126
C	-0.1478	3.561267	-0.00355
H	0.911609	3.81962	-0.00413
H	-0.62041	3.998802	-0.88616
H	-0.62013	4.001529	0.87786
N	-2.17743	1.945937	-0.00066
N	-2.6666	0.867798	-0.00031
N	-2.32713	-0.35259	0.000945
C	-3.4204	-1.34136	-0.00122
H	-4.04474	-1.23775	0.8892
H	-4.03752	-1.24196	-0.89717
H	-2.96307	-2.32799	0.002998
Cu	1.977992	0.137674	0.002443
Cu	-0.36867	-0.84353	0.000844
O	-0.20859	-2.87589	0.000615
H	-0.43622	-3.40232	-0.77537
H	-0.43044	-3.40156	0.77879
O	3.814662	-0.58378	0.003538
H	4.411071	-0.36055	0.729526
H	4.335125	-0.55473	-0.80939

B3LYP (gas)

Symbol	X	Y	Z
C	-0.28953	0.886973	0.000016
C	0.223066	2.05033	0.000019
C	-0.12009	3.496278	0.000021
H	-1.20029	3.637401	0.000084
H	0.307905	3.979752	0.881031
H	0.3078	3.979722	-0.88106
N	1.955175	2.059722	0.000052
N	2.577143	1.049903	0.000026
N	2.364283	-0.20093	0.000009
C	3.557397	-1.06927	-0.00014
H	4.164168	-0.90119	-0.89244
H	4.164433	-0.90113	0.891976
H	3.209894	-2.1008	-5.5E-05
Cu	-1.99138	0.036844	-0.00002
Cu	0.453411	-0.8553	0.000018
O	0.474971	-2.91473	0.000071
H	0.563093	-3.47567	0.779206
H	0.562386	-3.47571	-0.77912
O	-3.86513	-0.61198	-4.8E-05
H	-4.42939	-0.66942	-0.78035
H	-4.42891	-0.6709	0.780483

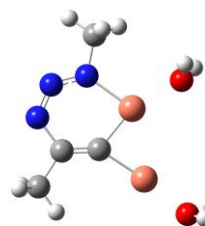
M06 (water)

Symbol	X	Y	Z
C	-0.21172	0.987004	-0.00145
C	0.40045	2.087312	-0.0007
C	0.30826	3.555269	-0.00125
H	-0.73595	3.871998	-0.00272
H	0.804725	3.969894	0.881032
H	0.806993	3.969318	-0.88253
N	2.215972	1.864203	0.002318
N	2.651545	0.769397	0.00329

N	2.277634	-0.42992	0.0015
C	3.320613	-1.45743	0.007384
H	3.958848	-1.3764	-0.87672
H	3.934339	-1.39131	0.91002
H	2.824056	-2.42692	-0.00758
Cu	-1.93986	0.183088	-0.00171
Cu	0.318422	-0.83471	-0.00224
O	0.082759	-2.83287	-0.00874
H	0.295919	-3.36657	0.763579
H	0.288448	-3.35861	-0.78851
O	-3.76294	-0.50495	0.002191
H	-4.35844	-0.2753	-0.71958
H	-4.27737	-0.4753	0.816252

M06 (gas)

Symbol	X	Y	Z
C	0.278921	0.920224	0.000004
C	-0.25748	2.066939	0.000006
C	0.015362	3.516009	0.000013
H	1.088492	3.709286	0.000018
H	-0.43633	3.980716	-0.88096
H	-0.43634	3.980709	0.880985
N	-1.9828	2.01396	-4E-06
N	-2.5531	0.982882	-8E-06
N	-2.31476	-0.2521	-0.00001
C	-3.46529	-1.15978	-1.4E-05
H	-4.07961	-1.01606	0.892877
H	-4.07961	-1.01604	-0.8929
H	-3.07737	-2.17823	-2.8E-05
Cu	1.960054	0.054415	-2E-06
Cu	-0.40528	-0.83856	0.000004
O	-0.48546	-2.87754	0.000016
H	-0.41768	-3.43942	0.777343
H	-0.41761	-3.43943	-0.77729
O	3.804816	-0.60305	-1.4E-05
H	4.36917	-0.6351	0.778747
H	4.369189	-0.635	-0.77876



Di-Cu Metallacycle Intermediate IV'

B3LYP (water)

Symbol	X	Y	Z
N	1.924377	2.094524	-0.02781
C	0.47635	2.002434	0.045035
C	-0.18134	0.867768	0.037207
Cu	0.423316	-0.88759	0.049968
Cu	-1.92412	0.111769	-0.03194
O	0.353472	-2.90745	0.163322
H	0.845438	-3.38016	0.846366
H	0.391855	-3.44477	-0.63796
C	-0.14791	3.37303	0.125688
H	-1.23381	3.323209	0.190173
H	0.23828	3.894359	1.005484
H	0.131068	3.951192	-0.75923
N	2.23415	-0.15406	-0.10579
N	2.636446	1.063565	-0.08338
O	-3.7952	-0.49097	-0.09968
H	-4.15281	-0.86782	-0.91373
H	-4.16734	-0.99411	0.6358
C	3.306621	-1.16853	-0.12285

H	3.034065	-1.96686	-0.81298
H	4.239357	-0.71099	-0.45205
H	3.443899	-1.59443	0.874457

B3LYP (gas)

Symbol	X	Y	Z
N	1.827	2.112872	-0.00034
C	0.324612	2.014746	0.000115
C	-0.25124	0.849856	0.000192
Cu	0.483591	-0.86993	0.000189
Cu	-1.96009	0.028659	-6.2E-05
O	0.525095	-2.92778	0.000133
H	0.598918	-3.49105	0.779446
H	0.598687	-3.49107	-0.77919
C	-0.24727	3.402248	0.000371
H	-1.33607	3.39418	0.00075
H	0.111663	3.938601	0.882219
H	0.111059	3.938684	-0.88167
N	2.303226	-0.11412	-0.00036
N	2.557684	1.136956	-0.00038
O	-3.83302	-0.61876	-0.00028
H	-4.39686	-0.68087	-0.78071
H	-4.39696	-0.68083	0.780092
C	3.484257	-1.00173	-2.1E-05
H	3.132111	-2.0318	-0.00061
H	4.091339	-0.83342	-0.89168
H	4.090409	-0.83409	0.892403

M06 (water)

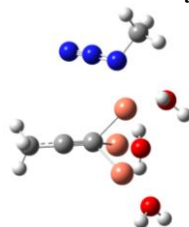
Symbol	X	Y	Z
N	2.019144	2.017051	0.001659
C	0.570466	1.994793	-0.01372
C	-0.13494	0.896209	-0.00492
Cu	0.363313	-0.88827	-0.0106
Cu	-1.88576	0.175149	0.012607
O	0.190534	-2.8797	-0.05636
H	0.538689	-3.42587	0.656656
H	0.335103	-3.35781	-0.87991
C	0.016022	3.382742	-0.04311
H	-1.07449	3.389037	-0.05064
H	0.372246	3.933282	0.833
H	0.383794	3.899525	-0.93488
N	2.194504	-0.23378	0.020636
N	2.663648	0.949232	0.017493
O	-3.74321	-0.3948	0.034328
H	-4.11615	-0.84678	-0.73065
H	-4.10671	-0.81462	0.821846
C	3.182936	-1.31589	0.052454
H	3.000003	-2.00614	-0.77483
H	4.18802	-0.90051	-0.03862
H	3.103958	-1.8684	0.993276

M06 (gas)

Symbol	X	Y	Z
N	-1.87973	2.058048	-0.08434
C	-0.37186	2.021318	0.062652
C	0.230562	0.878545	0.065023
Cu	-0.43094	-0.8655	0.056804
Cu	1.927515	0.062226	-0.0355
O	-0.4438	-2.89036	0.174038
H	-0.39456	-3.50785	-0.56149
H	-0.58548	-3.39651	0.979554
C	0.115777	3.420775	0.179029
H	1.200887	3.467686	0.272064
H	-0.20164	3.988719	-0.70055
H	-0.34333	3.891414	1.053634
N	-2.26141	-0.17825	-0.13915
N	-2.55265	1.053696	-0.12962
O	3.77835	-0.5709	-0.141

H	4.350431	-0.72608	0.617102
H	4.331139	-0.50705	-0.92626
C	-3.39804	-1.10592	-0.10998
H	-3.01963	-2.11404	-0.28077
H	-3.9074	-1.07435	0.857555
H	-4.10962	-0.8598	-0.90149

Tri-Cu Azide-acetylide Complex II



M06 (gas)

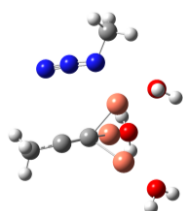
Symbol	X	Y	Z
C	-0.46398	-1.22639	-1.89678
C	-0.49616	-0.61978	-0.8204
C	-0.41191	-1.9308	-3.15998
H	-1.25706	-2.618	-3.25327
H	-0.44913	-1.22247	-3.99228
H	0.514423	-2.5061	-3.23991
Cu	-2.02265	0.511215	-0.36475
N	3.176555	-0.53318	-0.43362
N	3.487923	-1.54171	-0.83496
Cu	-0.49504	-1.32859	0.989087
Cu	0.640122	0.872923	-0.10115
O	0.654211	2.870491	0.517109
H	-0.01135	3.129996	1.166702
O	-0.5003	-2.09013	2.809762
H	0.30511	-2.51107	3.137149
O	-3.60234	1.624563	0.053871
H	-4.25937	1.778874	-0.63712
H	0.614201	3.534585	-0.18309
H	-1.23846	-2.65469	3.073126
H	-4.08902	1.442329	0.867871
N	2.731935	0.545101	-0.01957
C	3.742381	1.4928	0.5248
H	4.457256	1.773139	-0.25083
H	3.189941	2.369106	0.850187
H	4.263362	1.047434	1.374232



B3LYP (gas)

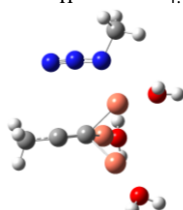
Symbol	X	Y	Z
C	1.678258	0.075438	1.653378
C	0.931568	0.341418	0.689686
C	2.478667	-0.07011	2.85993
H	3.544083	-0.12674	2.62052
H	2.318765	0.794512	3.511278
H	2.201974	-0.97313	3.411114
Cu	0.924189	1.615463	-0.76277
N	-2.81422	-1.29035	-1.15387
N	-2.82534	-1.79111	-2.16097
Cu	1.640963	-1.39369	-0.06907
Cu	-1.05626	0.254883	0.505623

O	-2.00756	1.86696	1.682539
H	-2.79636	2.369241	1.442504
O	2.208978	-3.02296	-1.01269
H	2.989588	-3.09915	-1.57723
O	1.076296	2.9759	-2.17208
H	1.523403	3.827003	-2.0739
H	-1.68681	2.248001	2.509208
H	1.878134	-3.91627	-0.85094
H	0.769376	2.909654	-3.08535
N	-2.74471	-0.70989	-0.04659
C	-3.96811	-0.87391	0.804403
H	-4.13973	-1.92898	1.023839
H	-3.77565	-0.33761	1.729157
H	-4.83864	-0.44645	0.303809



M06 (water)

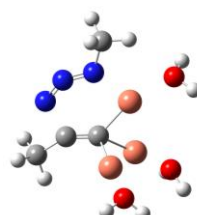
Symbol	X	Y	Z
C	0.140596	-1.6592	1.55436
C	0.330613	-0.79302	0.699104
C	-0.08455	-2.66213	2.559365
H	0.782103	-3.3229	2.65026
H	-0.26356	-2.19226	3.53112
H	-0.9595	-3.26952	2.309238
Cu	1.907439	0.329805	0.569294
N	-2.97196	-0.57125	0.309762
N	-3.18158	-1.64952	0.560243
Cu	0.502973	-1.01992	-1.20996
Cu	-0.55149	0.917502	0.194262
O	-0.5036	2.926286	-0.12495
H	0.150287	3.250583	-0.75387
O	0.684613	-1.3343	-3.12488
H	-0.07419	-1.675	-3.61193
O	3.552377	1.382044	0.546813
H	4.231743	1.196953	1.204844
H	-0.42228	3.484626	0.656426
H	1.460436	-1.81028	-3.44211
H	4.003189	1.519593	-0.29366
N	-2.60708	0.578036	0.06073
C	-3.66082	1.54133	-0.31057
H	-4.38165	1.656871	0.502209
H	-3.1606	2.49071	-0.49009
H	-4.17255	1.221367	-1.22133



M06 (gas)

Symbol	X	Y	Z
C	0.280072	-1.34849	1.69566
C	0.402512	-0.54694	0.758487
C	0.123652	-2.2478	2.80302
H	1.038143	-2.82279	2.979246
H	-0.10972	-1.68336	3.712857
H	-0.69974	-2.94735	2.623624

Cu	1.942803	0.569297	0.429814
N	-2.90318	-0.47589	0.583725
N	-3.04431	-1.45911	1.110446
Cu	0.454376	-1.36511	-0.98828
Cu	-0.58206	0.984279	-0.035
O	-0.56355	2.936103	-0.66051
H	-0.39995	3.283184	-1.54351
O	0.519765	-2.27819	-2.70785
H	-0.24738	-2.57681	-3.20937
O	3.63039	1.537534	0.326644
H	4.193783	1.724448	1.086625
H	-0.73738	3.689682	-0.08586
H	1.295846	-2.72037	-3.07081
H	4.090831	1.841715	-0.46291
N	-2.61365	0.584511	0.00955
C	-3.76241	1.426838	-0.40311
H	-4.3283	1.763658	0.468764
H	-3.34492	2.289345	-0.91869
H	-4.41755	0.881372	-1.08619



Tri-Cu Transition State III

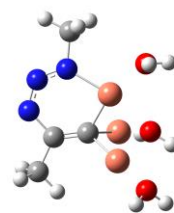
B3LYP (water)

Symbol	X	Y	Z
C	-0.21234	-1.47866	-1.33367
C	0.172342	-0.4615	-0.65675
C	0.234675	-2.57793	-2.21493
H	1.321893	-2.63856	-2.23194
H	-0.1866	-3.52635	-1.87725
H	-0.13427	-2.39593	-3.22801
Cu	0.737236	-1.18099	1.083376
N	-2.69034	-0.90465	-0.78706
N	-2.02412	-1.71146	-1.34093
Cu	1.691909	0.738385	-0.73645
Cu	-0.78021	1.007642	0.138104
O	-1.13969	2.77951	1.045926
H	-1.26387	3.558056	0.487461
O	3.264931	1.918647	-0.89196
H	3.682984	2.040473	-1.75421
O	1.295441	-1.85546	2.853701
H	1.272558	-2.80572	3.024938
H	-0.55495	3.047931	1.766324
H	3.974501	1.843895	-0.24094
H	2.108491	-1.51633	3.249371
N	-2.59425	0.163221	-0.13165
C	-3.83633	0.783411	0.370552
H	-4.37387	0.092589	1.022225
H	-3.54497	1.661766	0.940944
H	-4.47569	1.088858	-0.45992

B3LYP (gas)

Symbol	X	Y	Z
C	-0.00734	1.10763	1.549138
C	0.277295	0.281922	0.58422
C	0.647296	1.928931	2.598515
H	1.727932	1.959561	2.470902
H	0.2347	2.940255	2.592383
H	0.405624	1.499273	3.576327
Cu	0.658586	1.467975	-0.93465
N	-2.47263	0.738247	1.233478

N	-1.65968	1.352777	1.838332
Cu	1.748322	-0.97181	0.465325
Cu	-0.86227	-0.95084	-0.37116
O	-1.34836	-2.54572	-1.54262
H	-1.584	-3.42398	-1.21567
O	3.285186	-2.20103	0.538275
H	3.942037	-2.36153	-0.1516
O	1.042496	2.689496	-2.43519
H	0.462574	3.404552	-2.72948
H	-1.37379	-2.58208	-2.50749
H	3.563882	-2.68795	1.32551
H	1.893534	2.804977	-2.87772
N	-2.58047	-0.13767	0.348797
C	-3.93906	-0.57263	-0.06658
H	-4.51563	0.281779	-0.42234
H	-3.81514	-1.28809	-0.87563
H	-4.45055	-1.05194	0.769284



Tri-Cu Metallacycle Intermediate IV

B3LYP (water)

Symbol	X	Y	Z
C	0.351601	1.360373	1.450675
C	-0.12	0.475132	0.548127
C	-0.54285	2.233796	2.292235
H	-1.59008	2.153558	2.007826
H	-0.43072	1.939574	3.339167
H	-0.21312	3.270323	2.19505
Cu	-1.54556	-0.80625	0.77973
N	2.622333	0.936734	1.118377
N	1.708336	1.5861	1.727644
Cu	-0.764	1.168929	-1.13576
Cu	0.821166	-0.90458	-0.31877
O	1.245312	-2.55141	-1.39751
H	0.835949	-2.66238	-2.2654
O	-1.44349	1.876481	-2.84481
H	-2.27695	1.542717	-3.20063
O	-3.00216	-2.0989	1.068672
H	-3.2426	-2.37206	1.963129
H	1.22484	-3.41476	-0.96469
H	-1.41985	2.826825	-3.01557
H	-3.81747	-2.04729	0.553743
N	2.456072	0.001326	0.284309
C	3.685807	-0.55563	-0.31791
H	3.756198	-1.61649	-0.0756
H	3.633424	-0.44213	-1.40112
H	4.551887	-0.02323	0.071656

M06 (water)

Symbol	X	Y	Z
C	0.303031	1.534592	-1.2691
C	-0.16648	0.466977	-0.74327
C	-0.03553	2.746043	-2.02652
H	-1.11625	2.873311	-2.08898
H	0.419943	3.622302	-1.55869
H	0.38122	2.662719	-3.03523
Cu	-0.54154	1.18944	1.026435
N	2.669595	0.759379	-0.6789
N	2.09017	1.651849	-1.18335
Cu	-1.75919	-0.60036	-0.67122
Cu	0.641562	-1.09053	0.007552
O	0.891369	-2.89936	0.816627
H	0.751955	-3.67127	0.256334
O	-3.4734	-1.51788	-0.68653
H	-3.90717	-1.71932	0.150184
O	-0.97734	1.798799	2.824851
H	-0.2825	2.191404	3.365203
H	0.452306	-3.08482	1.654424
H	-3.60072	-2.27933	-1.26355
H	-1.77213	2.327716	2.956911
N	2.49938	-0.34359	-0.1268
C	3.667734	-1.08906	0.354222
H	4.205284	-0.51432	1.111755
H	3.2965	-2.01147	0.798209
H	4.335798	-1.33237	-0.47524

M06 (gas)

Symbol	X	Y	Z
C	0.121177	-1.33834	-1.45322
C	-0.2533	-0.40769	-0.63472
C	-0.41211	-2.34857	-2.37822
H	-1.49731	-2.42215	-2.31186
H	-0.12105	-2.07783	-3.39989
H	0.049536	-3.31981	-2.17638
Cu	-1.82163	0.685415	-0.53279
N	2.503976	-0.74554	-1.06352
N	1.788675	-1.49399	-1.6244
Cu	-0.47608	-1.2423	1.091672
Cu	0.714258	1.041812	0.166195
O	1.099909	2.811988	1.029048
H	0.907524	3.080294	1.934117
O	-0.72131	-2.14714	2.80176
H	-0.0193	-2.57136	3.308594
O	-3.47907	1.70429	-0.62744
H	-3.80027	2.148125	-1.42133
H	1.387508	3.598297	0.550871
H	-1.56347	-2.43982	3.168491
H	-4.17372	1.755716	0.038438
N	2.516855	0.239364	-0.31204

B3LYP (gas)

Symbol	X	Y	Z
C	0.054019	0.835582	1.732845
C	-0.27683	0.271807	0.554175
C	-0.84005	1.522251	2.721984
H	-1.85526	1.657447	2.353916
H	-0.85788	0.928833	3.64201
H	-0.40266	2.489663	2.982565
Cu	-1.81835	-0.86774	0.30275
N	2.346662	0.300191	1.619455
N	1.408022	0.821908	2.230235
Cu	-0.35779	1.607071	-0.85904
Cu	0.788202	-0.92031	-0.48577
O	1.22045	-2.33888	-1.87787
H	1.295105	-2.22711	-2.8347
O	-0.47168	3.045842	-2.20012
H	-1.1713	3.178312	-2.85324
O	-3.44279	-1.97559	0.193507
H	-3.74061	-2.5867	0.881053
H	1.390083	-3.27067	-1.68398
H	0.089483	3.833052	-2.21114
H	-4.13452	-1.93521	-0.4799
N	2.389109	-0.38469	0.568976

C	3.733618	-0.80982	0.09636
H	4.157303	-1.52321	0.805198
H	3.614588	-1.28594	-0.87395
H	4.386774	0.058054	0.004901

M06 (water)

Symbol	X	Y	Z
C	0.470149	-1.36402	-1.47383
C	-0.09237	-0.50663	-0.60337
C	-0.32187	-2.34486	-2.27077
H	-1.36422	-2.39463	-1.95604
H	-0.27999	-2.04933	-3.324
H	0.141907	-3.33062	-2.18125
Cu	-1.81953	0.322539	-0.4794
N	2.615573	-0.68833	-1.0563
N	1.840934	-1.44613	-1.72025
Cu	-0.17616	-1.09477	1.211347
Cu	0.523283	1.197566	-0.10127
O	0.741669	3.069793	0.507241
H	0.176715	3.398024	1.215969
O	-0.28115	-1.68432	3.063315
H	-1.10298	-1.55846	3.550666
O	-3.59442	1.103956	-0.42924
H	-4.04816	1.332572	-1.24823
H	0.785239	3.763754	-0.16038
H	0.063674	-2.55161	3.304108
H	-4.25782	0.773721	0.186749
N	2.245948	0.235856	-0.28951
C	3.294751	0.935676	0.463911
H	3.428434	1.939152	0.051742
H	2.97996	1.023028	1.505456
H	4.227001	0.373471	0.40188

M06 (gas)

Symbol	X	Y	Z
C	0.134031	1.106249	1.629443
C	-0.25952	0.379106	0.580253
C	-0.66713	1.967362	2.533317
H	-1.69653	2.090705	2.197662
H	-0.65553	1.520589	3.534656
H	-0.17784	2.94199	2.627102
Cu	-1.87687	-0.61735	0.370583
N	2.378372	0.458399	1.468057
N	1.522297	1.109695	2.051245
Cu	-0.19209	1.381866	-1.05558
Cu	0.647187	-1.05262	-0.27038
O	0.998933	-2.72252	-1.3178
H	0.889246	-2.86682	-2.26428
O	-0.1653	2.498017	-2.65574
H	-0.90361	2.660934	-3.25371
O	-3.58814	-1.54041	0.325889
H	-3.96345	-2.03031	1.067365
H	1.231539	-3.57089	-0.92216
H	0.527553	3.135016	-2.86673
H	-4.25478	-1.50529	-0.36944
N	2.332259	-0.38426	0.552558
C	3.608355	-0.94243	0.060577
H	3.95933	-1.71296	0.751934
H	3.431308	-1.38564	-0.91881
H	4.355189	-0.15147	-0.02098



**Tri-Cu Triazolide V
B3LYP (water)**

Symbol	X	Y	Z
C	0.013008	-1.58295	-0.81915
C	0.001688	-0.53085	0.15325
C	-0.00089	-1.50765	-2.31405
H	-0.01252	-0.47477	-2.66053
H	0.880279	-2.00583	-2.72446
H	-0.88177	-2.01943	-2.70825
Cu	1.998339	-0.02991	-0.20013
N	0.043203	-2.57781	1.112794
N	0.037499	-2.78295	-0.18386
Cu	-0.01611	1.463612	0.130441
O	-0.0859	3.426309	0.067977
H	0.612231	3.906907	-0.39571
O	3.923312	0.301024	-0.46672
H	4.501686	0.303218	0.307227
H	-0.2755	3.916177	0.878738
H	4.383721	-0.18911	-1.16034
N	0.023737	-1.28269	1.345921
C	0.019635	-0.79311	2.726786
H	0.890096	-0.16153	2.895843
H	-0.89095	-0.22619	2.914054
H	0.057797	-1.6618	3.379169
Cu	-2.00295	-0.06624	-0.18134
O	-3.94441	0.207726	-0.38887
H	-4.48633	-0.52991	-0.69784
H	-4.25355	0.997019	-0.85217

B3LYP (gas)

Symbol	X	Y	Z
C	-0.12826	-1.53237	-0.77581
C	0.016961	-0.45359	0.176748
C	-0.13065	-1.51896	-2.27438
H	-0.06356	-0.51032	-2.68486
H	0.706183	-2.11112	-2.65425
H	-1.03521	-1.99859	-2.65617
Cu	2.030992	-0.14513	-0.20735
N	-0.17604	-2.4763	1.179222
N	-0.2396	-2.70517	-0.10705
Cu	0.079084	1.525152	0.108407
O	0.119579	3.489553	0.072098
H	0.396444	4.043279	-0.67044
O	3.969839	-0.08849	-0.52268
H	4.646932	0.112332	0.137361
H	-0.11099	4.078063	0.80381
H	4.421049	-0.42473	-1.30895
N	-0.02755	-1.18433	1.393482
C	0.05888	-0.69818	2.778186
H	0.993971	-0.15969	2.93157
H	-0.78765	-0.05004	3.006484
H	0.031633	-1.57276	3.42501
Cu	-2.00891	-0.01797	-0.20759
O	-3.95245	0.167451	-0.43151
H	-4.61398	-0.36975	0.025874
H	-4.41369	0.694655	-1.09726

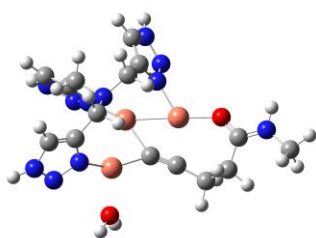
M06 (water)

Symbol	X	Y	Z
C	-0.00084	-1.5655	-0.81218
C	0.004667	-0.51569	0.154082
C	-0.02637	-1.47624	-2.29319
H	-0.03126	-0.43698	-2.62944
H	0.847	-1.97946	-2.71746
H	-0.91595	-1.97663	-2.68624
Cu	1.94701	-0.03948	-0.20298
N	0.03898	-2.55209	1.111776
N	0.020423	-2.76037	-0.17869
Cu	-0.01222	1.461817	0.130893
O	-0.08176	3.39682	0.045895
H	0.647703	3.877391	-0.36152
O	3.846131	0.257285	-0.50139
H	4.380172	0.579603	0.233662
H	-0.35647	3.898391	0.821881
H	4.354913	-0.43517	-0.93828
N	0.03041	-1.26555	1.342381
C	0.044198	-0.76013	2.707136
H	0.922143	-0.12982	2.856307
H	-0.86131	-0.18096	2.894639
H	0.082783	-1.61792	3.37638
Cu	-1.95	-0.07021	-0.16977
O	-3.86619	0.184257	-0.38794
H	-4.39237	-0.54929	-0.7261
H	-4.18026	0.983589	-0.82573

M06 (gas)

Symbol	X	Y	Z
C	-0.04064	-1.5366	-0.7704
C	0.002134	-0.44897	0.172292
C	-0.04775	-1.50667	-2.25431
H	-0.00414	-0.48793	-2.64934
H	0.797568	-2.07915	-2.64866
H	-0.94609	-1.99893	-2.64011
Cu	1.968229	-0.10613	-0.20149
N	-0.0553	-2.46582	1.179587
N	-0.07403	-2.70663	-0.10117
Cu	0.027003	1.515433	0.104192
O	0.044204	3.455546	0.062308
H	0.343353	4.006637	-0.67056
O	3.882566	-0.00337	-0.49845
H	4.54771	0.208318	0.167109
H	-0.23124	4.041976	0.777038
H	4.343728	-0.32761	-1.28133
N	-0.01128	-1.17446	1.386963
C	0.017577	-0.66112	2.753302
H	0.924699	-0.07512	2.916608
H	-0.8637	-0.04461	2.944264
H	0.01315	-1.52068	3.423398
Cu	-1.96187	-0.05331	-0.19992
O	-3.87978	0.07273	-0.46634
H	-4.53668	-0.45921	-0.0009
H	-4.3354	0.561721	-1.16119

Symbol	X	Y	Z
C	0.862516	-0.94657	-1.08879
C	2.067	-1.26745	-1.08327
C	3.412027	-1.80786	-1.24118
H	3.318955	-2.8667	-1.5114
H	3.879173	-1.31873	-2.10647
Cu	-0.38971	0.594233	-0.94735
Cu	1.925087	0.609374	-0.1406
Cu	-0.79843	-1.90331	-0.63582
O	-0.66537	-3.61195	-1.9397
H	-1.01041	-4.49601	-1.7763
H	-0.39322	-3.5879	-2.86266
N	-2.25407	-2.26865	0.492441
N	0.82742	2.110646	0.141811
O	3.801844	0.657067	0.259482
N	0.942927	3.2568	-0.54381
N	0.126977	4.235056	0.019928
C	-0.50374	1.395992	2.181751
H	0.01225	5.214016	-0.32307
N	-3.30876	-3.13621	0.223024
N	-4.21688	-3.12799	1.279956
H	-5.10965	-3.66657	1.3222
C	-0.04028	2.399448	1.166795
C	-0.45938	3.660701	1.08177
H	-1.16555	4.15239	1.738254
C	-3.7003	-2.21006	2.230028
C	-2.55567	-1.71837	1.762492
H	-4.17531	-1.95307	3.167793
C	-1.70034	-0.69187	2.449491
N	-2.08857	1.315315	-1.06974
N	-2.68269	1.780786	-2.17998
C	-3.01398	1.531711	-0.02006
N	-3.95136	2.279643	-1.88679
C	-4.11506	2.104409	-0.48873
H	-4.60785	2.722859	-2.56612
H	-4.98668	2.396396	0.082329
C	-2.77139	1.185551	1.416674
N	-1.4924	0.479721	1.579513
H	0.394719	0.835961	2.523316
H	-0.9319	1.912598	3.072234
H	-2.15346	-0.38899	3.422197
H	-0.725	-1.17997	2.666198
C	4.639215	-0.27318	0.37367
N	5.831139	0.003024	0.86888
H	5.960035	0.976421	1.128694
C	4.316833	-1.69112	-0.01245
C	6.943747	-0.91802	1.084178
H	7.343148	-1.28935	0.13687
H	7.737185	-0.37498	1.594957
H	6.646724	-1.7561	1.718374
H	5.235083	-2.25032	-0.20511
H	3.845187	-2.16832	0.857826



Ligand-stabilized tri-Cu acetylide